

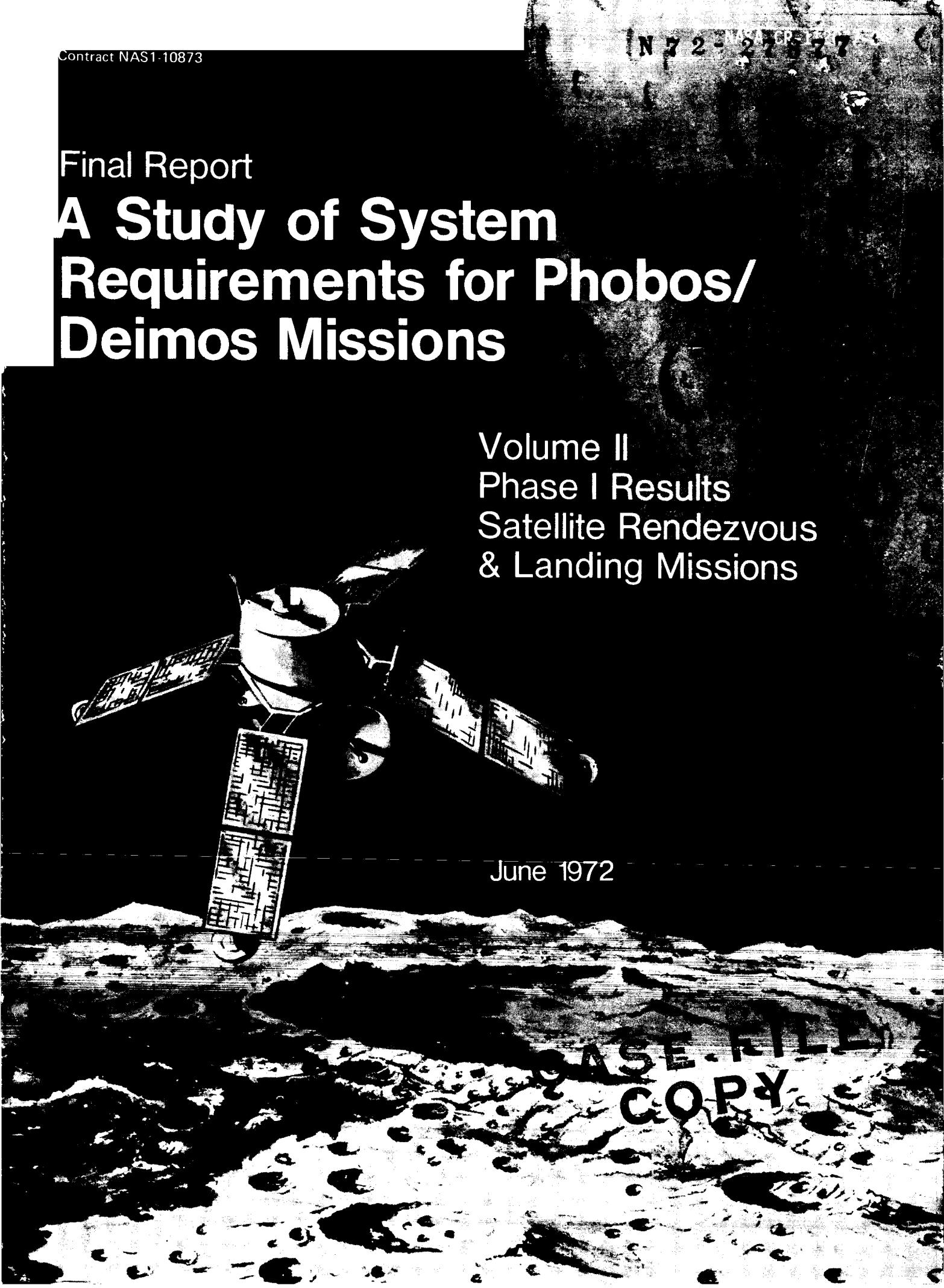
Final Report

A Study of System Requirements for Phobos/ Deimos Missions

Volume II
Phase I Results
Satellite Rendezvous
& Landing Missions

June 1972

USE FILE
COPY

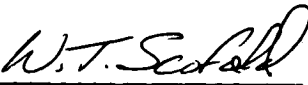


Contract NAS1-10873

A STUDY OF SYSTEMS REQUIREMENTS
FOR PHOBOS/DEIMOS MISSIONS
FINAL REPORT

Volume II
Phase I Results - Satellite Rendezvous
and Landing Missions

Approved


William T. Scofield
Program Manager

MARTIN MARIETTA CORPORATION
DENVER DIVISION
Denver, Colorado 80201

FOREWORD

This is Volume II of the Final Report on A Study of Systems Requirements for Phobos/Deimos Missions, conducted by the Martin Marietta Corporation.

This study was performed for the Langley Research Center, NASA, under Contract NAS1-10873, and was conducted during the period 4 June 1971 to 4 June 1972. Mr. Edwin F. Harrison of Langley Research Center, NASA, was the Technical Representative of the Contracting Officer. The study was jointly sponsored by the Advanced Concepts and Mission Division of the Office of Aeronautics and Space Technology (OAST) and the Planetary Programs Division of the Office of Space Sciences (OSS) in NASA Headquarters.

This Final Report, which summarizes the results and conclusions of the three-phase study, consists of four volumes as follows:

- Volume I - Summary
- Volume II - Phase I Results - Satellite
Rendezvous and Landing Missions
- Volume III - Phase II Results - Satellite Sample
Return Missions and Satellite Mobility
Concepts
- Volume IV - Phase III Results - Combined Missions
to Mars and Its Satellites

ACKNOWLEDGEMENT

Martin Marietta wishes to recognize the contributions of the following NASA individuals to this study:

Edwin F. Harrison of the NASA Langley Research Center, Technical Representative of the Contracting Officer, for NASA management and direction.

E. Brian Pritchard of the NASA Langley Research Center, for general guidance and direction.

James J. Taylor and Nickolas L. Faust of the NASA Manned Spacecraft Center, for information on broken-plane trajectory performance characteristics.

George F. Lawrence of OSS, NASA Headquarters, for technical monitoring and general guidance.

Robert H. Rollins, II of OAST, NASA Headquarters, for technical monitoring and general guidance.

Donald L. Young of the Jet Propulsion Laboratory, (JPL) for supplying data on JPL's space storable propulsion studies.

CONTENTS

	<u>Page</u>
Foreword	ii
Acknowledgements	iii
Contents	iv
Abbreviations and Symbols	vi
I. Background	I-1 thru I-7
II. Objectives and Study Results	II-1
A. Introduction	II-1
B. Phase I Study Objectives and Guidelines	II-3
C. Study Approach	II-5
D. Study Results	II-7 thru II-12
III. Mission Analysis and Design	III-1
A. Performance Analysis	III-1
B. Navigation Analysis	III-31 thru III-62
IV. System Description	IV-1
A. System Overview	IV-1
B. Guidance and Control	IV-17
C. Structural Design	IV-55
D. Thermal Control	IV-64
E. Propulsion	IV-73
F. Telecommunications	IV-91
G. Power	IV-103
H. Rover Concepts	IV-117 thru IV-126

	<u>Page</u>
V. Program Costs	V-1 thru V-4
VI. Program Schedule	VI-1 thru VI-2
VII. Conclusions	VII-1 thru VII-9
Appendix A	A-1 thru A-10
Appendix B	B-1 thru B-2
Appendix C	C-1 thru C-38
Appendix D	D-1 thru D-7
Appendix E , , , , ,	E-1 thru E-5

LIST OF FIGURES

<u>Figure</u>		<u>Page</u>
II-1	Study Methodology	II-6
III-1	Overview of Mission Profile	III-3
III-2	Mars Orbital Operations	III-5
III-3	Lander/Orbiter Relative Motion	III-7
III-4	Baseline Launch Vehicle Payload Capability	III-12
III-5	ΔV to Match Phobos Orbit vs Altitude of Initial Periapse	III-18
III-6	MOI ΔV vs VHE	III-19
III-7	ΔV Required for Plane Change vs Argument of Periapse	III-20
III-8	Resultant Inclinations vs Argument of Periapse	III-22
III-9	1977 VHE Contours	III-23
III-10	1979 VHE Contours	III-24
III-11	1981 VHE Contours	III-25
III-12	1983/84 VHE Contours	III-26
III-13	1977 Payload Capability	III-27
III-14	1979 Payload Capability	III-28
III-15	1981 Payload Capability	III-29
III-16	1983/84 Payload Capability	III-30
III-17	Schematic for Rendezvous to Deimos	III-34
III-18	Schematic for Rendezvous to Phobos	III-35
III-19	TV Tracking Intervals for Rendezvous to Deimos	III-40
III-20	Schematic for Alternate Mode of Rendezvous to Phobos	III-60
IV-1	Phobos/Deimos Lander/Rover Baseline Configuration	IV-4
IV-2	Lander/Rover External Configuration	IV-7
IV-3	Wheeled Lander/Rover	IV-9
IV-4	Lander/Rover Landed Configuration	IV-10
IV-5	Alternate Lander/Rover Configuration	IV-11

<u>Figure</u>		<u>Page</u>
IV-6	Phobos/Deimos Landed Orbiter (Alternate Configuration)	IV-16
IV-7	Phobos/Deimos Landed Orbiter on Surface	IV-18
IV-8	Phobos/Deimos Four Tank Concept	IV-20
IV-9	Phobos/Deimos Staged Concept	IV-21
IV-10	Combined Mars Lander and Phobos/Deimos Mission Concept	IV-22
IV-11	Terminal Rendezvous and Landing Phases	IV-28
IV-12	Rendezvous G & C System Mechanization	IV-31
IV-13	Suggested Rendezvous Radar	IV-34
IV-14	Interferometer Tracking System	IV-36
IV-15	Landing Site Selection System	IV-37
IV-16	Typical Closure - Long Range	IV-44
IV-17	Typical Closure - Short Range	IV-45
IV-18	Rendezvous Trajectory	IV-46
IV-19	Rendezvous Time Profile	IV-47
IV-20	Rendezvous Propellant Efficiency	IV-49
IV-21	Relative Closing Velocity Vs Range - Long Range	IV-51
IV-22	Relative closing Velocity Vs Range - Short Range	IV-52
IV-23	Typical Closure - Long Range	IV-53
IV-24	Typical Closure - Short Range	IV-54
IV-25	Predicted Satellite Surface Temperatures	IV-66
IV-26	Thermal Control Schematic/ Alternate Configuration	IV-74
IV-27	Phobos/Deimos Orbiter Propulsion System Schematic	IV-81
IV-28	Phobos/Deimos Orbiter Attitude Control System	IV-86
IV-29	Thrust Chamber Assembly	IV-90
IV-30	Performance of Lander Thruster	IV-92

<u>Figure</u>		<u>Page</u>
IV-31	Lander/Rover Terminal Descent System Schematic	IV-93
IV-32	Lander to Orbiter - View Time	IV-97
IV-33	Orbiter to Earth Occultation - No Date	IV-98
IV-34	Lander to Earth View Times	IV-100
IV-35	Propagation of Anomalies of X-Band Transmission	IV-101
IV-36	Orbiter Power Profile	IV-107
IV-37	Lander/Rover Profile	IV-111
IV-38	Solar Array Power System	IV-112
IV-39	RTG Power System	IV-113
IV-40	Solar Panel Output - Landed Orbiter	IV-118
IV-41	Wheeled Lander/Rover	IV-121
IV-42	ΔV , Altitude and Flight Duration - Phobos/Deimos Rovers	IV-123
IV-43	Gas Propelled Orbiter/Lander/Rover	IV-124
IV-44	Boom Deployed Instruments	IV-126
VI-1	Phase I Program Schedule	VI-2

LIST OF TABLES

<u>Table</u>	<u>Page</u>
I-1 Characteristics of the Satellites of Mars	I-2
I-2 Phobos/Deimos Science Objectives - First Mission . . .	I-6
II-1 Study Milestones	II-2
II-2 Phase I Study Tasks	II-4
II-3 LRC Directed Study Ground Rules	II-4
II-4 MMC Derived Study Ground Rules	II-5
III-1 Summary of Studies and Trades	III-2
III-2 Baseline ΔV Budget	III-10
III-3 Baseline Weight Profile	III-11
III-4 Typical Event Sequences and Timing	III-13
III-5 Phobos Payload Capability	III-15
III-6 Spacecraft Propulsion Alternatives	III-16
III-7 Maneuver Sequence	III-33
III-8 Errors Limiting DSN Accuracy During Encounter	III-38
III-9 Errors Limiting DSN Accuracy In-Orbit	III-39
III-10 Satellite Ephemeris Errors	III-44
III-11 Execution Error Statistics	III-48
III-12 Encounter Control and Knowledge Dispersions Based on DSN Tracking Only	III-51
III-13 In-Orbit Knowledge Dispersions Based on DSN Tracking Only	III-51
III-14 Navigation Accuracy in Observation Orbit with Noisy TV Data and Perfect DSN	III-54
III-15 Navigation Accuracy in Observation Orbit with Noisy TV Data and Corrupt DSN	III-55
III-16 Summary of Results for Rendezvous to Deimos	III-56
III-17 Maneuver ΔV_{STAT} for Rendezvous to Deimos	
III-18 ΔV_{STAT} for ΔV Combinations	III-58
IV-1 Spacecraft Options Considered	IV-2
IV-2 Nominal Science Payload	IV-12
IV-3 Baseline Spacecraft System Weight Summary (kg)	IV-13

<u>Table</u>		<u>Page</u>
IV-4	Lander/Rover Weight Summary (kg)	IV-14
IV-5	Phobos/Deimos Landed Orbiter System Weight Summary (kg)	IV-19
IV-6	Phobos/Deimos Four Tank System Weight Summary (kg) . .	IV-23
IV-7	Phobos/Deimos Staged Concept System Weight Summary (kg)	IV-24
IV-8	Combined Mars Lander and Phobos/Deimos Mission System Weight Summary (kg)	IV-25
IV-9	Rendezvous Radar Maximum Range	IV-39
IV-10	G & C Subsystem Hardware for a Phobos/Deimos Mission	IV-40
IV-11	Scale Height of Thermally Stirred Dust Atmospheres	IV-68
IV-12	Thermal Control Areas of Concern	IV-70
IV-13	Landed Thermal Performance, Baseline Configuration	IV-72
IV-14	Landed Thermal Performance/ Alternate Configuration	IV-75
IV-15	Phase I Conclusions - Thermal Analysis	IV-76
IV-16	Phobos/Deimos Orbiter Propulsion System Weight Statement	IV-83
IV-17	Phobos/Deimos ΔV Capability and Weight Sequence	IV-84
IV-18	Phobos/Deimos Orbiter Attitude Control System Weight Statement	IV-87
IV-19	Attitude Control System Requirements	IV-88
IV-20	Lander/Rover Terminal Descent Weight Statement	IV-94
IV-21	Relay Link Lander/Rover to Orbiter	IV-96
IV-22	Power Source Matrix	IV-104
IV-23	Orbiter Power Summary (Watts)	IV-105
IV-23	(Concluded) Orbiter Power Summary (Watts)	IV-106
IV-24	Orbiter Solar Panel Performance	IV-108

<u>Table</u>		<u>Page</u>
IV-25	Lander/Rover Power Summary (Watts)	IV-110
IV-26	Power Source Tradeoffs	IV-115
IV-27	Landed Orbiter Loads - Transmitting Mode	IV-116
IV-28	Rover Operating Environment	IV-120
IV-29	Surface Transport Constraints/Characteristics	IV-122
V-1	Baseline Mission Cost Summary - Phase I	V-2
V-2	Alternate Mission Cost Summary - Phase I	V-4
VII-1	Recommendations for Further Study and Technology Requirements.	VII-2

ABBREVIATIONS AND SYMBOLS

a	orbit semi-major axis
ACS	attitude control system
ARU	attitude reference system
Ax,Ay,Az	body acceleration
Az	azimuth angle
bps	bits per second
CC&S	control computer and sequencer
cg	center of gravity
db	decibel
DLA	declination of launch asymptote
DSN	Deep Space Net
DSS	Deep Space System
EL	elevation angle
ETC	engineering test capsule
$F1_c, F2_c, F3_c, FN_c$	lander engine thrust command
FOV	field of view
g	acceleration due to gravity, earth
G&C	guidance and control
GCSC	guidance, control and sequencing computer
grms	gravity (rms)
HZ	hertz
i	orbit inclination
IRU	inertial reference unit
JPL	Jet Propulsion Laboratory
kbps	kilobits per second
km	kilometers
L/E	launch/encounter

LOS	line-of-sight
LPCA	lander pyrotechnic control assembly
LRC	Langley Research Center
mbps	megabits per second
MCC	midcourse correction
MLI	multilayer insulation
MMC	Martin Marietta Corporation
MOI	Mars orbit insertion
NASA	National Aeronautics and Space Administration
NW	net load factor times weight
OSR	optical solar reflector
p,q,r	body attitude rates
PTC	proof test capsule
PTO	proof test orbiter
R	range
\dot{R}	range rate
RCS	reaction control system
RF	radio frequency
RSS	root-sum-of-squares
RTG	radioisotope thermoelectric generator
R99	99 percentile closest approach radius
S/C	spacecraft
TA	orbit true anomaly
TEI	trans-Earth injection
T/M	thrust-to-mass
TMI	trans-Mars injection
TWTA	traveling wave tube amplifier
UHF	ultra-high frequency
UV	ultraviolet
VHE	hyperbolic excess velocity

VM	velocity meter
VO	Viking Orbiter
VRU	velocity reference unit
W	weight
α	solar absorptivity
ΔV	delta velocity
ΔV_{STAT}	navigation uncertainty delta velocity
ϵ	orbit eccentricity
θ	pitch attitude angle
π	3.1416
ρ	density
σ	standard deviation
ϕ	roll attitude angle
ψ	yaw attitude angle
μ_{MARS}	Mars central gravity potential constant
Ω	Mars longitude of ascending node
ω	Mars argument of periapsis
\sim	approximately

I. Background

I. BACKGROUND

What is the origin of Phobos and Deimos?

What has happened to them since their formation?

What can they teach us about the origin and evolution of the solar system?

These are the fundamental scientific questions concerning the two tiny moons of Mars. Asteroid capture has been proposed as a theory of origin, but it is also possible that the moons are left over planetesimals from the episode of Mars accretion. Other mechanisms of formation and evolution can be envisioned, limited only by one's imagination. In any event, a detailed study of these two bodies would add immensely to our present knowledge of the solar system.

Of the thirty-one known satellites in the solar system, Phobos and Deimos were the 19th and 20th to be discovered. They were found in 1877 by A. Hall, who observed them visually using a 26-inch refractor. All subsequent satellites, with the exception of Jupiter V, were discovered with the aid of photographic plates. Indeed, Phobos and Deimos are so small that they appear as objects of the 11th or 12th magnitude; and the brilliance of Mars, plus the proximity of the satellites to Mars, renders observation from Earth very difficult.

For almost a century following their discovery, we knew very little about these small bodies other than their orbital characteristics. This vacuum of knowledge led understandably to interesting, if far fetched, conjecture about Phobos and Deimos. While some of the more romantic explanations for them have been dispelled, most of the questions about their origin, evolution, and relationship to the rest of the solar system remain unanswered.

Data on Phobos and Deimos are given in Table I-1. As shown, Phobos has an orbital period of only about 7.6 hours, while Deimos' orbital period is approximately 30.3 hours. It is interesting to note that the ratio of the orbital period of Deimos to that of Phobos is almost exactly four (actually, 3.96). This might be an example of orbit-orbit resonance between satellites, a phenomenon that also occurs with certain satellites of Saturn and Jupiter.

Table I-1 Characteristics of the Satellites of Mars

Property	Phobos	Deimos
Semi-Major Axis, km	9382	23480
Orbital Period, hr	7.654	30.298
Inclination to Mars Equator, deg	0.95	1.3
Eccentricity	0.0170	0.0028
Velocity in Orbit, km/sec	2.1	1.3
Size, km	21 x 25	12 x 13.5
Albedo	0.065	0.05
Surface Gravity, Earth g	0.001	0.0005

The diameters and shapes of the satellites of Mars cannot be determined directly from Earth observations, but have been inferred from television images obtained by the Mariner 7 spacecraft in 1969 and Mariner 9 in 1971. Although seen at poor resolution by Mariner 7, Phobos was determined to be irregularly shaped (18 x 22 km), with the elongation along its orbital plane. The cross-sectional area was larger than predicted, and the geometric albedo was found to be only 0.065, lower than that known for any other body in the solar system.

The Mariner 9 spacecraft that went into orbit about Mars in November of 1971 was able to observe the Martian satellites as

predicted by Harrison and Campbell (Ref. I-1)* and obtained some reasonably high-resolution photographs of these bodies. These photographs provided details of the rugged surface of Phobos and the first glimpse of the smaller Deimos. Preliminary analyses of these photographs indicate that Phobos is 21 by 25 km, which is slightly larger than the values obtained from the Mariner 7 mission. By comparing the two photographs taken by Mariner 9, it was determined that Phobos is in synchronous rotation about Mars. Furthermore, the estimate of geometric albedo from Mariner 7 appears to be confirmed by Mariner 9, that is, that the albedo of Phobos is quite low, about 0.065 and Deimos is about 0.05.

Although the results from the Mariner 7 and 9 missions have provided new information about the Martian satellites, most of the questions concerning the mass and density of these bodies, as well as their origin, evolution, and relationship to the rest of the solar system, remain unanswered. Thus, a mission dedicated to the exploration of these bodies would be of considerable scientific value. Moreover, many of the same reasons suggested by Alfven and Arrhenius for a mission to an asteroid (Ref. I-2) also apply to Phobos/Deimos missions. For example, such missions would contribute to the establishment of the range of variation in elemental abundance in the solar system.

The original concept for a spacecraft mission to rendezvous with and land on Phobos and Deimos was developed by E. B. Pritchard and E. F. Harrison at the NASA Langley Research Center (Ref. I-3). In June of 1971, the Denver Division of the Martin Marietta Corporation was awarded a contract by the NASA Langley

* References cited in each chapter appear in the last section of each chapter.

Research Center to define science objectives for such missions and to perform a detail study of the necessary spacecraft systems and mission designs.

There are many important scientific objectives or questions which may be answered by future Phobos/Deimos missions. The first priority science measurements are of the geochemical (elemental abundances and mineralogy) and geochronological (ages) constitution of the bodies. From the geochemical data, we can classify these bodies as Mars-like, Earth-like, Lunar-like, meteorite-like (six or more subclasses), or unique. Obviously, the classification derived will infer a great deal about possible formation mechanisms. Also, the mineral assemblages may provide important clues as to the thermal history of the bodies. Determination of the various ages (crystallization, gas retention, cosmic ray exposure, solar wind exposure) will provide a time history which may also contribute greatly to an understanding of the formation of these bodies. Unfortunately, age dating techniques are highly sophisticated and not readily amenable to miniaturization and automation. On the other hand, several powerful experimental techniques are available for remote geochemical analyses. These include x-ray diffraction and fluorescence, alpha particle chemical analysis, light microscopy, gamma-ray spectroscopy, and neutron activation analysis. These techniques are excellent candidates for missions to Phobos and Deimos.

What are the preferred missions? In answering this question, one must reckon with limitations in resources. A well-balanced program of solar system exploration must weigh the allocation of these resources against the probable scientific return of each proposed mission. Thus, although missions to small bodies, such as Phobos and Deimos, may prove to be of high scientific value, our present lack of knowledge dictates a very rudimentary

approach. The first mission is thus preferably a minimal science, low cost mission of a highly exploratory nature. A list of typical investigations with representative instrumentation requirements which could be conducted by Phobos/Deimos orbiter/lander missions is given in Table I-2. A more detailed evaluation of these satellites (including age dating) will require a sample return mission. The mass of the satellites can, perhaps, be determined from perturbations of the spacecraft motions as it passes close to the satellite. Size, shape, and volume can be deduced from orbital imagery data. The imagery system is envisioned to be similar to the Viking Orbiter (VO) television system. It will not only provide the capability for obtaining high-resolution photographs of the surface of the satellite, but will also be used for approach navigation to the satellites. The other instruments listed in Table I-2 will be used to determine the elemental composition, minerals, and radioactive elements of the satellites. These instruments are also all strong candidates for follow-on Viking missions as well as for the satellite missions. Thus, the development cost of the instruments can be amortized over several missions. The final selection of the instrumentation for a Phobos/Deimos mission will, of course, be made by the scientific community; but the list given in Table I-2 can serve as a model to be used as an input when studying spacecraft systems requirements, mission modes, and program costs.

Table I-2 Phobos/Deimos Science Objectives - First Mission

	<u>Science Objective</u>	<u>Candidate Instrumentation</u>
Orbiter	Mineralogy	Visible and IR Spectrometry
	Elemental Composition	X-Ray Fluorescence (Solar-Stimulated)
	Radioactive Elements	Gamma-Ray Spectrometer
	Imagery	Television Camera
Lander	Mineralogy	X-Ray Diffraction; Optical Microscopy
	Elemental Composition	Alpha Backscatter; X-Ray Fluorescence
	Radioactive Elements	Gamma-Ray Spectrometer
	Imagery	Facsimile Camera

REFERENCES

- I-1 Harrison, E. F., and J. W. Campbell: "Reconnaissance of Mars Satellites." *J. of Spacecraft and Rockets*, Vol 7, October 1970, p 1188.
- I-2 Alfven, H., and G. Arrhenius: "Mission to an Asteroid." *Science*, January 1970.
- I-3 Pritchard, E. B., and E. F. Harrison: *Phobos/Deimos Missions*. Paper presented at the AIAA Systems Meeting, Denver, Colorado, July 19-20, 1971

II. Objectives and Study Results

II. OBJECTIVES AND STUDY RESULTS

A. INTRODUCTION

This report, in four volumes, contains the results of a nine-month, three-phase study conducted for the Langley Research Center to evaluate the systems requirements to accomplish Phobos/Deimos missions in the 1977-1983 time period.

The study was initiated in June 1971, under NASA Contract NAS1-10873. The study milestones are summarized in Table II-1. The study was based on a succession of three phases that allowed a logical progression from a straight-forward rendezvous and landing satellite mission conducted during Phase I, to a more meaningful sample return mission performed during Phase II, and finally culminating in a highly cost effective combined Mars landing and Phobos/Deimos mission studied during Phase III. Each succeeding phase effort built upon the results of the previous phase to a large degree. For example, the original concept of missions to the Martian satellites was developed by Messrs. Pritchard and Harrison of the NASA Langley Research Center. They demonstrated the technical feasibility of such space missions in a preliminary mission design that became the basis for the system study performed during Phase I. Using this basic knowledge then, we generated basic data on mission analysis and spacecraft system requirements during Phase I which we applied to alternate mission concepts during Phases II and III in a search for the most cost effective Phobos/Deimos exploration approach.

Throughout the study phases, numerous trade studies and analyses were performed to progress through the mission and system options available. These studies and analyses are documented in the appropriate study phases in which they were performed.

Each of the study phases is treated in a separate volume of this report. A brief summary of the study ground rules and guidelines applicable to that particular study effort is presented at the beginning of each of the study phases.

Overall program schedules and cost estimates based on detailed equipment lists, were derived for each of the study phases.

Table II-1 Study Milestones

Preliminary Mission Design by NASA/LRC-MAAB	January 1971
Systems Definition Study Contract to MMC	June 4, 1971
Phase I - Landing Roving Mission	June 4, 1971 thru September 9, 1971
First Presentation	September 9 & 10, 1971
Phase II - Sample Return Mission	September 13, 1971 thru December 9, 1971
Second Presentation	December 9 & 10, 1971
Phase III - Combined Mars and Phobos/Deimos Missions	December 13, 1971 thru April 6, 1972
Third Presentation	April 6 & 7, 1972
Final Report	May 5, 1972

B. PHASE I STUDY OBJECTIVES AND GUIDELINES

The overall objective of this phase of the study effort was to provide the answer to the question: Is a Phobos/Deimos rendezvous and landing mission feasible and practicable?

In order to answer this question it was necessary to perform several major categories of study effort. First, a mission mode trade study was conducted in which a large number of candidate mission modes were evaluated. From this study the most promising approach was selected from which a nominal mission profile was developed. Once the baseline mission profile was identified a systems analysis study was performed to define supporting subsystem tradeoffs, develop subsystem requirements, and to isolate areas where existing technology would provide greatest gains in the areas of weight, cost and reliability. Configuration and subsystem optimization analysis were then conducted from which a baseline program(s) was selected. Program schedules and cost estimates were then prepared for the recommended baseline program(s). Some of the more detailed study tasks that were performed in meeting the study objectives are summarized in Table II-2.

Throughout the Phase I study a series of ground rules was supplied to the study team by the Langley Research Center. These ground rules are summarized in Table II-3. Also, as preliminary results of the study were derived, a series of study generated ground rules evolved. These ground rules are shown in Table II-4.

Table II-2 Phase I Study Tasks

- Augment original NASA mission concept and design developed by Messrs. Pritchard and Harrison of the Langley Research Center.
- Develop preliminary science objectives and define a nominal science payload.
- Select a nominal baseline mission profile.
- Define systems and subsystems required to accomplish the nominal baseline mission.
- Explore mission and system options and perform trade studies to develop spacecraft systems and subsystem designs to perform the selected baseline mission with predictable reliability and cost effectiveness.
- Produce a baseline spacecraft design and attractive alternate designs to accommodate the nominal mission.
- Provide program costs and develop program schedules.

Table II-3 LRC Directed Study Ground Rules

- Launch vehicles considered: Titan IIIC, Titan IIIE/Centaur and Shuttle Centaur.
- Launch opportunities shall be from 1977 to 1981.
- Type I, II and Broken Plane trans-Mars trajectories.
- Landing operations to consider landing entire vehicle vs separable lander package.
- Autonomous rover to be considered for landed mission.
- Design mission around realistic science objectives.
- Minimize program costs.
- Apply proven hardware and technology (Mariner, Viking, Pioneer).

Table II-4 MMC Derived Study Ground Rules

- Titan IIIIE/Centaur launch vehicle.
- 1979 opportunity.
- Type II trajectory to Mars.
- Orbital operations to consist of: Mars elliptical capture orbit (4 day period), phasing orbit (~2 day period), observation orbit (15.1 hour period).
- "Stretched" Viking '75 orbiter (38% propellant increase).
- Phobos landing.
- Separable lander module with "hopping" mobility.

C. STUDY APPROACH

The Phobos/Deimos rendezvous and landing mission is one of the more complex unmanned planetary missions considered to date. The large array of mission mode and system options available for consideration produce a very large number of potential mission/system approaches worthy of investigation.

The overall study plan is shown in block diagram form in Figure II-1. The general approach in performing the study was to first establish a nominal baseline mission profile that was relatively simple but that still embodied all of the basic mission sequences. This approach allowed us to test the sensitivity of the critical parameters; such as landed weight, mission risk, and systems cost and complexity, to the various mission options that were available to us. Detailed analyses were then made of the individual elements of the mission design to preliminarily identify subsystem configurations. In configuring the individual subsystems, our approach was to use existing qualified

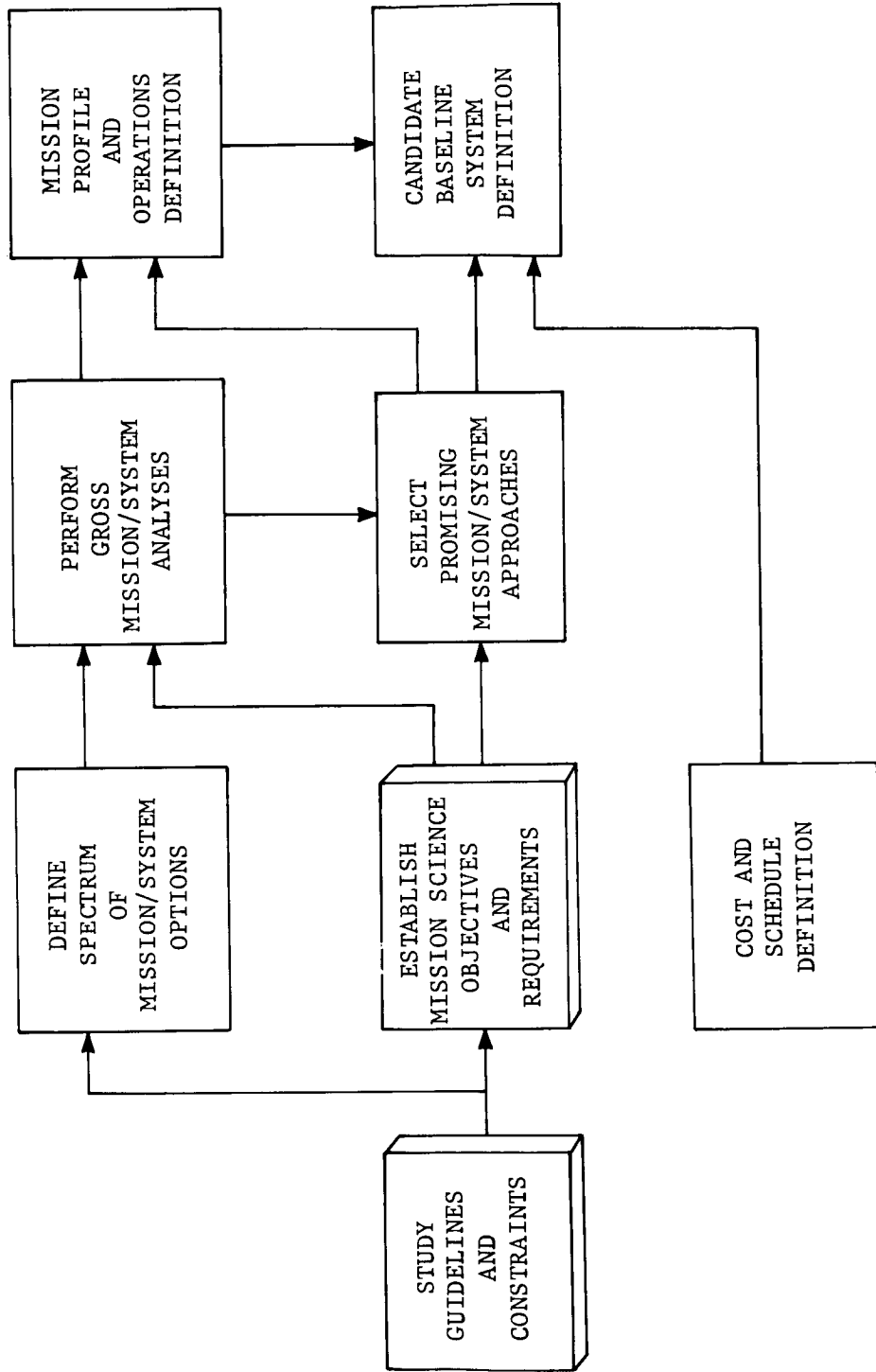


Figure II-1 Study Methodology

systems and hardware from programs already in being or in the planning stage, wherever feasible, and the Viking systems in particular. Completion of the individual detailed analyses, then, allowed a baseline spacecraft and several alternate designs to be identified, all of which were capable of accommodating the nominal mission. Associated cost and schedule data were then formulated around the baseline design.

The definition of the mission scientific objectives and their impact on system requirements also had prime emphasis during the first study phase. A representative science instrument complement was selected for use in our systems studies that employed recognized experimental techniques applicable to the science objectives.

Environmental criteria unique to the mission that affect the mission/system design were developed and made available to the study team in the form of a design criteria document, Phobos/Deimos Engineering Model (Ref. Appendix A).

D. STUDY RESULTS

Studies conducted during Phase I were concentrated principally in three general categories: mission-oriented analysis, system analysis and conceptual design studies. The studies resulted in the definition of a baseline mission concept and an alternate mission configuration.

1. Baseline Mission/System Concept Description

In developing the launch vehicle requirements for the baseline, the energy requirements of the 1977, 1979 and 1981 Mars opportunities were compared with the Titan IIIC, Titan IIIE/Centaur, Titan IIIF/Centaur and Shuttle/Centaur launch vehicle performance capabilities.

The selected baseline launch opportunity is a 1979 launch from Earth with a 1980 arrival at the vicinity of Mars. The launch vehicle is the Titan IIIE/Centaur which is the basic Viking '75 launch vehicle. The launch is from Cape Kennedy. The spacecraft is placed into a 185 km Earth parking orbit by the first burn of the Centaur stage. After coasting in this Earth parking orbit for a maximum of 30 minutes, the Centaur stage is again ignited providing the injection velocity required to place the spacecraft into the proper Earth-Mars trajectory. Type II trajectories were selected for the trans-Mars phase of the mission.

After injection, the spacecraft, which weighs 3392 kg, is separated from the launch vehicle, extends its solar panels, and automatically acquires the Sun and Canopus to provide external references for three-axis stabilization.

The Phobos/Deimos spacecraft is comprised of two major components, a modified Viking '75 Orbiter, and a separable lander/rover vehicle. The orbiter dry weight is approximately 983 kg. This, together with 1928 kg of fuel, gives a total landed weight of 2911 kg. The lander/rover loaded weight is 482 kg.

The orbiter configuration is essentially the same as that presently conceived for the Viking '75 Orbiter. The most significant modification is the growth of the propulsion system to provide the delta velocity requirements for the Phobos/Deimos mission.

The trans-Mars coast trajectory is deliberately biased to guarantee missing Mars and the mid-course maneuvers have the additional function of removing this bias. The normal trip time from Earth launch to Mars encounter is 11 months.

The spacecraft will arrive at Mars about September 1980 at which time the orbiter propulsion system will insert the spacecraft into a highly elliptical orbit about Mars, having a periapsis of 2660 km and an apoapsis of 95,000 km. A delta velocity requirement of 980 mps is required to perform this maneuver. A plane change maneuver is then performed at apoapsis so that the line of apsides is in the desired plane of Deimos. After adequate time is allowed for tracking, a phasing orbit is established by performing a retro-burn at periapsis.

An observation orbit is then established by performing another retro maneuver at periapsis, thereby reducing the orbital period to one-half of Deimos' period. This observation orbit with a period of 15 hours allows close encounters with Deimos every other revolution and repeated close crossings of Phobos. The decision to land at either Phobos or Deimos is made while in the observation orbit. If the decision is made to land on Deimos, the orbiter is circularized at apoapsis on a revolution when Deimos is also there. At this point, the orbiter and Deimos co-

orbit Mars with a separation distance between the spacecraft and Deimos of less than 100 km. If the choice is made to land on Phobos, a similar sequence of events occur. The periapsis of the observation orbit is raised to that of Phobos and the orbit is then circularized. The total delta velocity budget to accomplish the Phobos mission maneuvers just described is 2375 mps, all of which is supplied by the orbiter's propulsion system.

The delta velocity budget of 2375 mps includes 175 mps to correct for navigation uncertainties (ΔV_{STAT}). The uncertainties considered were:

- 1) Mars orbit insertion uncertainties,
- 2) DSN tracking uncertainties,
- 3) Satellite ephemeris uncertainties,
- 4) Spacecraft execution errors and
- 5) TV camera pointing errors.

(Later navigation analyses indicated that 175 mps is a conservative allocation for ΔV_{STAT} and that 100 mps could be used.)

After the spacecraft has attained the co-orbit with the chosen satellite at an altitude of 100 km, the lander/rover is separated from the orbiter and initiates the terminal rendezvous and landing phase of the mission. After separation of the lander/rover the orbiter remains in the stationkeeping orbit, performing its science mission and acting as a communication relay between the lander on the surface of the satellite and Earth. Using its 147 cm (58 inch) high gain S-band antenna, the orbiter has the capability to transmit 95.76 mega bits of data to Earth per Phobos orbital period.

After separation from the orbiter, the lander performs the terminal rendezvous and landing phase. This phase consists of four subphases:

- 1) Closing ΔV phase,
- 2) Terminal rendezvous phase,
- 3) Constant velocity and attitude phase,
- 4) Landing phase

During the closing ΔV phase, a closing ΔV of 50 mps is imparted to the vehicle along the line-of-sight vector by the body mounted RCS thrusters. This phase is terminated when the axial accelerometer indicates the additional velocity (velocity to be gained) is reached. The vehicle rendezvous to within 30 meters of the satellite during the terminal rendezvous phase. During the terminal rendezvous phase, the vehicle's thrust is controlled to point along the LOS vector. During the constant velocity and attitude phase, the spacecraft descends at a constant velocity of .36 km/sec (1.5 ft/sec) to within 2 meters of the surface. The RCS engines facing upward are fired continuously during the landing phase to produce an artificial g-level and damping to the touchdown, thereby settling the spacecraft into a smooth landing.

The weight of the baseline lander without propellants is 482 kg of which 82 kg is allocated to the science payload. Landing stability simulations were run using a modified version of the Viking landing stability computer program. The results of this study indicated that the lander was 100% stable for surface slopes of 25° or less. Once the lander has settled on the surface, science operations are carried out and data transmitted back to the orbiter or direct to Earth. The lander has the capability to transmit at a data rate up to 784 kbps to the orbiter via the 1-watt UHF relay system or 2.43 mega bits per Phobos revolution direct to Earth via its 20-watt S-band system. Mobility capability has also been provided by means of "hopping" or a wheeled concept. Mobility thus provided gives access to virtually any point on the satellite's surface during a 90-day lander mission.

2. Alternative Concept

The alternate mission/system that was studied during Phase I involved landing the entire orbiter delivery system. The mission sequence is identical to that described for the baseline mission. The concept can land much greater usable payloads, 498.9 kgs (versus 82 kg for the baseline configuration). This is possible because the same orbiter subsystems, such as communications and power, can support both the orbiting and landed functions. Several hardware modifications are required in order to adapt the orbiter to a lander role. Some of the more important modifications are:

- 1) Addition of four landing legs,
- 2) Addition of a terminal descent propulsion system,
- 3) Addition of a rendezvous radar to assist in landing operations,
- 4) Addition of flip covers mounted over the existing Viking Orbiter temperature control louver system. These flip covers serve to de-activate the louvers during surface operations. Also required are the addition of heaters and phase change material to equalize the diurnal variations,
- 5) Adding provisions to enable the outboard panels of the solar array to droop 32° below the horizontal after landing. This optimizes the Sun incidence on the panels during the landed sequence of the mission.

III. Mission Analysis and Design

III. MISSION ANALYSIS AND DESIGN

A. PERFORMANCE ANALYSES

1. Mission Profile

Several trade studies were performed to substantiate the selection of a baseline mission profile for the Phobos rendezvous and landing. Table III-1 indicates the major areas in which these trades were made. All but the communications geometry study will be discussed in this section. The result of these studies is a mission profile briefly described in Figure III-1. This overview indicates the major events of the mission to Phobos from Earth launch to the Mars observation orbit. The baseline launch opportunity is a 1979 launch and 1980 arrival and the launch vehicle is the Titan IIIE/Centaur as scheduled for use on Viking '75 mission to Mars. The launch is from Cape Kennedy and has a launch azimuth determined by the required departure declination (DLA). The trans-Mars injection is done with the second burn of the Centaur upper stage which currently has a coast time constraint in the 185 km circular parking orbit of 30 minutes. (The first Centaur burn is used to establish the circular parking orbit.) The coast time in the parking orbit and injection velocity are selected so the desired departure conditions are obtained for the trans-Mars trajectory. The trans-Mars coast trajectory is deliberately biased to guarantee missing Mars and the second and final midcourse maneuver has the additional function of removing this bias. The nominal trip time from Earth launch to Mars encounter is 11 months and approximately 30 days are needed for the various phases from the Mars orbit insertion (MOI) to the landing on Phobos. This trajectory to Mars is a type II tra-

Table III-1 Summary of Studies and Trades

LAUNCH VEHICLE PAYLOAD CAPABILITIES

MISSION OPPORTUNITY CHARACTERISTICS (1977 - 1984)

MARS ORBITAL STRATEGY

PLANE CHANGE STRATEGY

PROPULSION ALTERNATES

COMMUNICATION GEOMETRY

DIRECT MARS ENTRY OPTION

1. Mars Orbit Insertion

2. Coast In Capture Ellipse

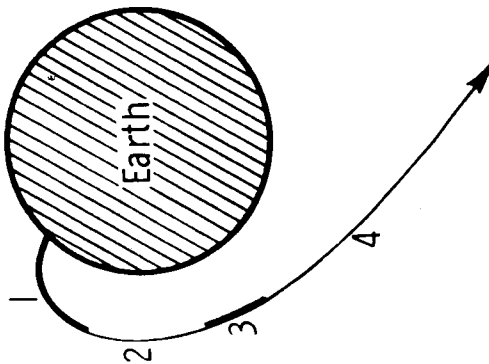
3. Plane Change Maneuver

4. Capture-To-Phasing Maneuver

5. Phasing Orbit

6. Phasing-To-Observation Maneuver

7. Observation Orbit

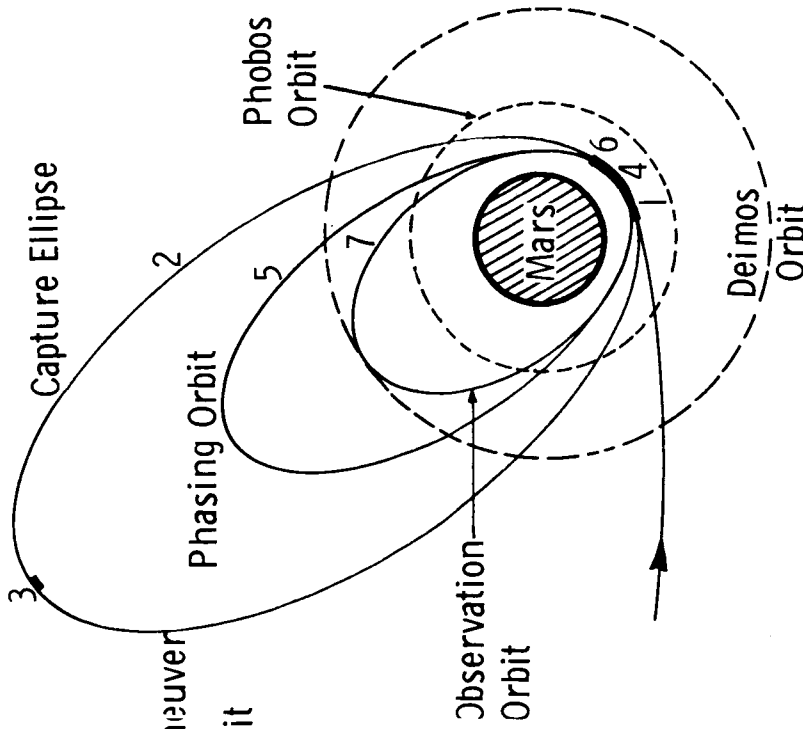


1. Launch to Circular Park

2. Coast In Circular Park

3. Trans Mars Injection

4. Trans Mars Coast



Not To Scale

Figure III-1 Overview of Mission Profile

jectory (greater than 180° heliocentric transfer angle) and was selected because of the greater payload capability over the type I trajectory (less than 180°). The Mars orbital events are shown in Figure III-2. The MOI maneuver inserts the spacecraft into an orbit with an altitude of periapsis of 2660 km and altitude of apoapsis of 95,000 km which yields an orbital period of 97 hours. This initial capture ellipse allows the required plane change of approximately 15° to be accomplished at a relatively low velocity at apoapsis. This reduces the ΔV required for the plane change significantly since the velocity there is only 230 meters per second. In order to perform this maneuver at apoapsis the approach angle to Mars (θ_{aim}) is selected so the resultant line of apsides is in the desired plane of Deimos' orbit. After one and a half revolutions for tracking, a phasing orbit is established by lowering apoapsis a predetermined amount by performing a retro-burn at periapsis. The phasing orbit period is between 30 and 60 hours (nominally 47 hours) to allow the desired relative geometry between Deimos and the spacecraft to be established for the observation orbit. The desired phasing orbit is selected in real time using the latest tracking data and the satellite ephemeris data.

The observation orbit is established by doing another retro maneuver at periapsis reducing the orbital period to half of Deimos' period (15.149 hours). The spacecraft in the observation orbit makes a close passage to Deimos (200 km) every other revolution and makes periodic observations of Phobos since Phobos' relative geometry with the orbiting spacecraft changes approximately 7.5° per spacecraft orbit. Since the orbital paths of the spacecraft and Phobos cross at two places, there are two opportunities for very close observation when the phasing lines up. A small change to the orbiter spacecraft's orbital period of 0.16

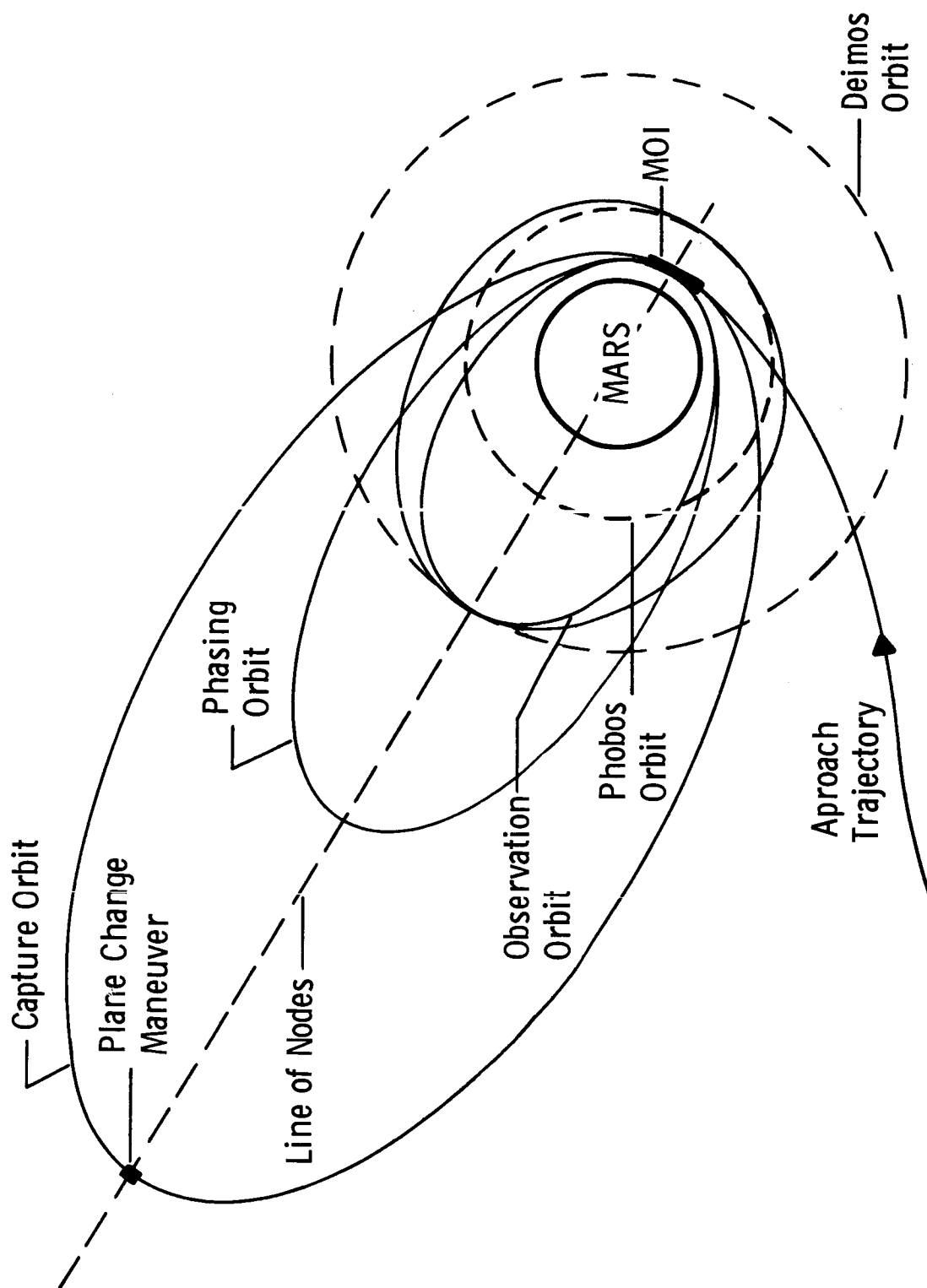


Figure III-2 Mars Orbital Operations

hours applied at the proper time would allow repeated observation of Phobos while Deimos moves relative to the orbit of the spacecraft. If the decision is made to rendezvous and land on Deimos, the orbiter is circularized at apoapsis on a revolution when Deimos is also there. At this point the orbiter and Deimos can be expected to co-orbit Mars with a separation distance between the spacecraft and Deimos of less than 100 km. After allowing an appropriate amount of time for tracking the landing sequence is started. A small closing velocity is imposed and shortly before touchdown the closing velocity is reduced to allow a very low impact velocity touchdown. This landing sequence is described in Section IV-B.

If the choice is to land on Phobos rather than Deimos, a similar sequence of events occur from the observation orbit. A phasing orbit is established by raising the periapsis of the observation orbit a portion of the way between the 2660 km original periapsis and the 6000 km altitude of Phobos, depending on the required phasing needs. This allows the desired relative geometry to be obtained. The periapsis is then raised to that of Phobos and the orbit is then circularized and proceeds the same as with a Deimos landing.

The baseline mission employs a separable satellite lander which uses the orbiter for a communication relay link to Earth. The orbiter co-orbits with the satellite with a range from the center of the satellite that can vary from 50 km to 100 km as shown in Figure III-3. The figure also indicates the viewing time from the lander on Phobos to the orbiter. The communication time for Deimos would be ~8 hours per 30.3 hour cycle. This co-orbit is not an actual orbit about the satellite but is a relative motion caused by the slight difference in eccentricity of the two Mars orbiting objects. The effective period of this

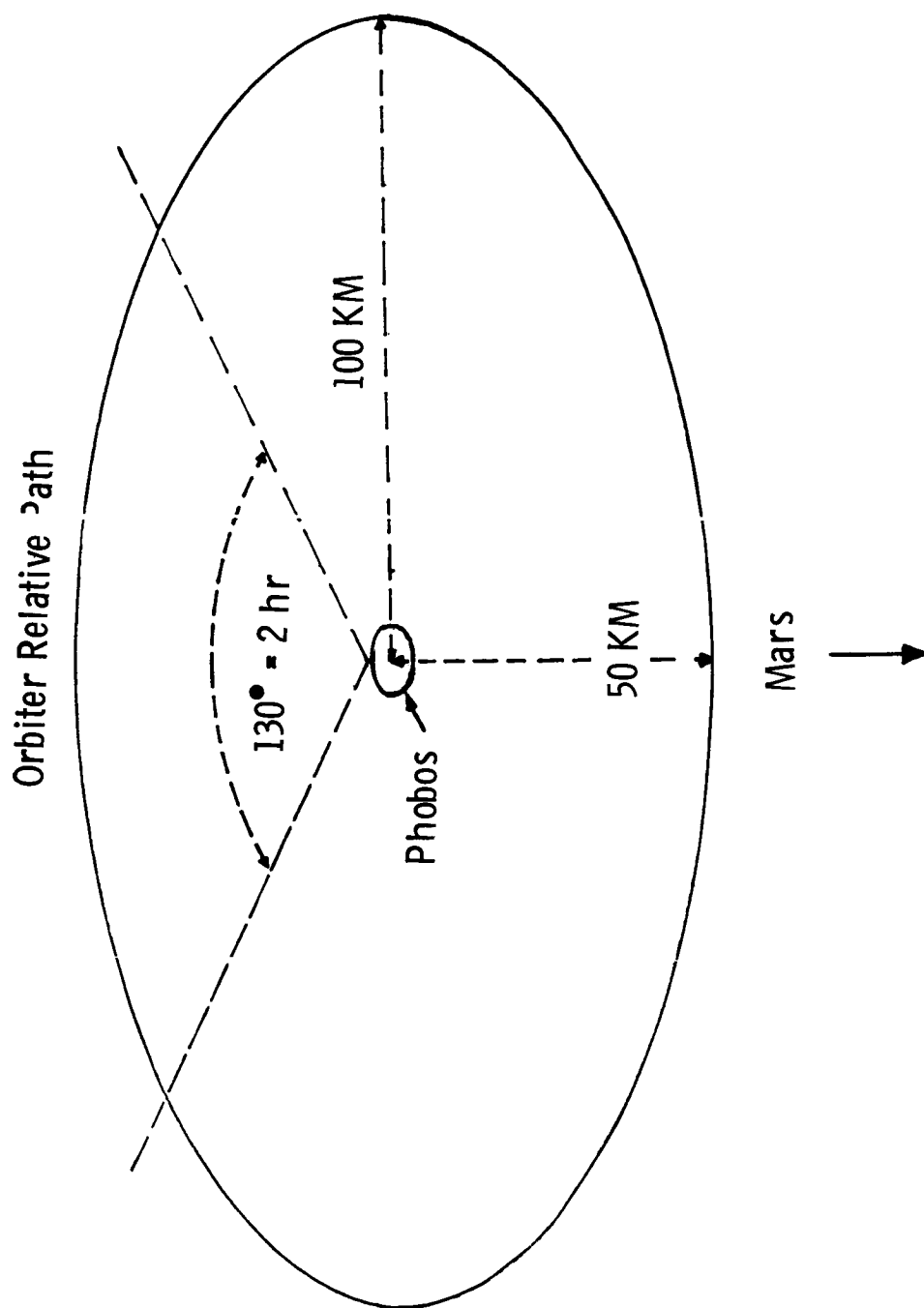


Figure III-3 Lander/Orbiter Relative Motion

relative motion orbit is the same as the period about Mars of the satellite (7.6 hours for Phobos and 30.3 hours for Deimos).

2. Performance Characteristics

The baseline launch vehicle is the Titan IIIE/Centaur which has the capability of injecting 4157 kg to Mars during a 30-day launch period in 1979. This weight includes the Centaur spacecraft adapter, launch vehicle mission peculiar items (LVMP) and Project reserves. The total for these items is 216 kg. The maximum spacecraft weight is then 3941 kg. The comparable maximum injected weight using the Titan IIIE/Centaur for the 1977, 1981, and 1983/84 opportunities are 4131, 4153, and 3882, respectively. In each case these weights include the 216 kg for the adapters, LVMP and Project reserves. The baseline spacecraft for this phase does not utilize the full launch vehicle capability in 1979. The actual total weight is 3608 kg including the adapter, LVMP and Project reserves. The actual spacecraft loaded weight is 3392 kg. This weight is limited by the ΔV capability of the 38% stretched orbiter.

The Mars orbit insertion (MOI) maneuver varies in magnitude as a function of the hyperbolic approach velocity (VHE) which, in turn, varies with the launch and encounter date. In order to minimize the orbiter propellants required, a minimum VHE encounter region is selected that still provides for a 30-day launch period within the injected weight capability of the launch vehicle. The baseline mission has a maximum impulsive MOI ΔV requirement of 980 meters per second for the 30-day launch window. In order to convert this impulsive ΔV requirement to actual ΔV , 100 mps is allocated for gravity and steering losses. This

maneuver leaves the spacecraft in the 97 hour capture orbit with periapsis altitude of 2660 km and apoapsis altitude of 95,000 km. The equivalent impulsive MOI ΔV requirements for 1977, 1981 and 1983/84 launch opportunities are 870, 1250, and 1560 meters per second respectively. These data were determined using the TRACK program described in Appendix B.

The ΔV budget for the baseline mission to Phobos is shown on Table III-2. Later navigation analysis has shown a 75 mps reduction in navigation uncertainties. These results are used in Phases II and III of this study. All the ΔV allocations except for the MOI and plane change maneuvers remain the same regardless of launch opportunity. The total ΔV for the baseline mission would be 2200, 2670, and 2910 mps for a mission to Phobos in 1977, 1981, and 1983/84, respectively, compared to the 2375 mps for 1979. The higher ΔV requirements (a result of the higher MOI requirements) for a Phobos mission in 1981 and 1983/84 requires significantly more orbiter propellant than for the 1979 baseline. Using the Titan IIIE/Centaur the baseline separable lander could not be delivered to Phobos in these more difficult years. This would require a new lander design or the use of a landed orbiter concept. The baseline weight profile is shown in Table III-3. This table shows the total spacecraft weight after each major phase of the mission. The actual launch encounter space available for this weight profile is shown in Figure III-4. The payload capability of 1160 kg shown does not include the orbiter propulsion inerts and, if included, would be the 1465 kg indicated in the previous table for the 38% stretched orbiter propulsion system. The event sequences and timing are shown in Table III-4 for a typical launch and encounter date. A nominal amount of time (15 days) is spent in the observation orbit to allow for multiple viewings of both Deimos and Phobos before

Table III-2 Baseline ΔV Budget

EVENT	ΔV (MPS)
Midcourse Corrections	25
Mars Orbit Insertion	980
Plane Change	65
Transfer to Phasing Orbit	300
Transfer to Observation Orbit	
Raise Periapse to Phobos	200
Circularize at Phobos	430
Gravity and Steering Losses	100
Navigation Uncertainties	175
Orbit Trims	50
Rendezvous and Landing	50
Total	<u>2375</u>

Table III-3 Baseline Weight Profile

EVENT	WEIGHT (Kg)
Injected Weight	3608
Spacecraft Loaded Weight (Inj. wt - 216 Kg)	3392
After Midcourse Corrections	3362
After Mars Orbit Insertion	2260
After Plane Change Maneuver	2208
After Transfer to Phasing Orbit	1980
After Transfer to Observation Orbit	1957
After Maneuver to Raise Periapse to Phobos	1806
After Orbit Match with Phobos	1519
After Rendezvous, Landing, and Orbit Trims	1465 (Lander - 482, Orbiter - 983)

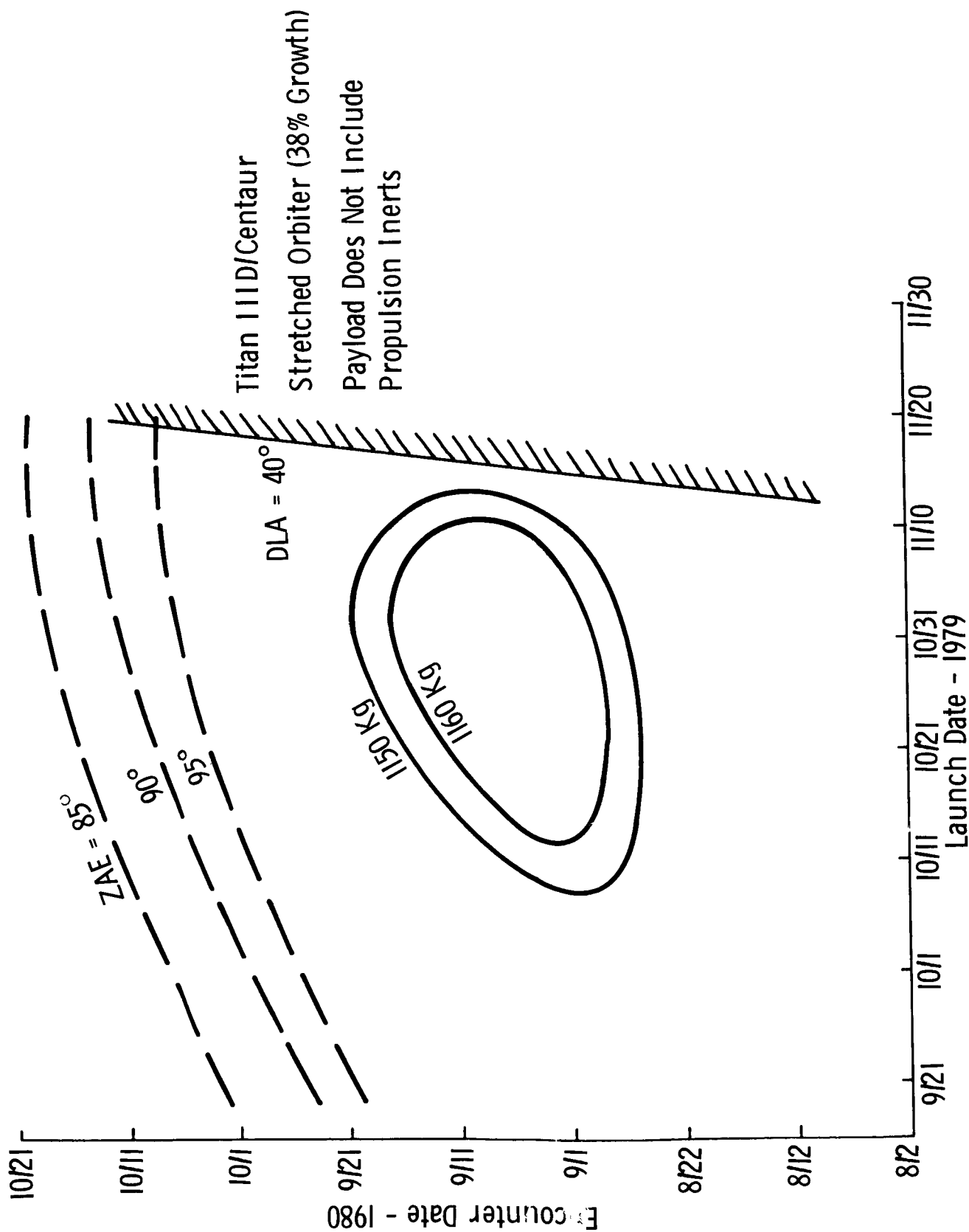


Figure III-4 Baseline Launch Vehicle Payload Capability

Table III-4 Typical Event Sequences and Timing

EVENT	TIME
Launch	Oct 9 1979
Midcourse Correction #1	Oct 19 1979
Midcourse Correction #2	Aug 22 1980
Mars Orbit Insertion	Sept 1 1980
Plane Change (MOI + 1 1/2 Rev)	Sept 7 1980
Transfer to Phasing Orbit (MOI + 3 Rev)	Sept 13 1980
Transfer to Observation Orbit	Sept 15 1980
Transfer to Phasing Orbit for Phobos	Oct 1 1980 (Typical)
Raise Periapse to Phobos Altitude	Oct 2 1980
Transfer to Orbit with Phobos	Oct 3 1980
Rendezvous and Landing	Oct 3 1980

deciding which satellite to investigate with a rendezvous and landing. If at this phase of the mission it is decided to rendezvous with Deimos rather than Phobos, on October 1, 1980 the spacecraft would be circularized at Deimos with rendezvous and landing taking place on October 2.

3. Trade Studies

Table III-5 indicates the maximum capabilities over a 30-day launch window of the Titan IIIC, Titan IIIE/Centaur, Titan IIIE7/Centaur and the Shuttle/Centaur launch systems for opportunities between 1977 and 1984. In all cases the propulsion system is excluded in order to indicate payload potential more accurately. For comparison the baseline spacecraft weight without the propulsion system is 1160 kg. The orbiter's weight is 679 kg without the propulsion. This would be minimum weight for a landing mission utilizing Viking Orbiter hardware. The Titan IIIC cannot accommodate this type weight for any of the launch opportunities while the Titan IIIE/Centaur can for each of the launch opportunities considered. The propulsion system inert weights used for this table are based on a formula using a base weight (41 or 91 kg) plus a percentage (15%) of the propellant as indicated. The base weight changes from 41 kg to 91 kg when the required propellant exceeds a 60% increase over the Viking '75 propellant load. This is to accommodate a heavier four tank, two engine configuration for these higher propellant requirements.

Table III-6 indicates the different potential Deimos/Phobos payloads for several propulsion designs. The difference in the orbiter weight is in the different weight of the propulsion system design needed to accommodate the different propellant loads.

Table III-5 Phobos Payload Capacity

<u>Launch Opportunity</u> (Year)	<u>Launch Vehicle</u>		
	<u>TIIC</u>	<u>TIID/Centaur</u>	<u>TIIF/Centaur</u>
1977	560 Kg	1375 Kg	1850 Kg
1979	495	1280	1710
1981	435	1058	1420
1983/4	314	813	1112
			2640 Kg
			2435
			2030
			1540

- Notes:
1. Payload is weight at Phobos less the propulsion system weight.
 2. Inert propulsion weight is 15% of propellant plus 41 Kg (prop. to 2220 Kg) or 91 Kg (prop. over 2220 Kg).
 3. Payload capabilities are calculated for a Phobos mission (highest ΔV).
 4. 30-day launch window.

Table III-6 Spacecraft Propulsion Alternatives

<u>Configuration</u>	Payload at Phobos (Kg)	
	<u>Lander</u>	<u>Orbiter</u>
Orbiter/Lander With 1928 Kg Propellant (38% Growth)	482	983
Orbiter/Lander With 2236 Kg Propellant (60% Growth)	635	1072
Orbiter/Lander With 2 Stage Orbiter (1408 Kg 1st stage & 750 Kg 2nd stage)	658	1129
Direct Entry Option 1550 Kg propellant and a 1210 Kg Direct Entry Lander	214	966

Also shown is a direct entry option where a Mars lander is separated from the spacecraft prior to MOI and the orbit then is used to propel the remainder of the spacecraft to its Phobos landing. The study of combined Mars landers and Deimos/Phobos missions using the direct entry option is discussed in detail in Phase III.

Another trade study involved the effects of periapsis altitude on the MOI ΔV required to achieve a usable capture orbit. Figure III-5 indicates the ΔV required to go directly to a Phobos landing using different initial periapsis altitudes. The baseline case uses the periapsis altitude of the desired observation orbit rather than add another maneuver to change the periapsis back to the periapsis altitude of the observation orbit. As indicated further savings in ΔV can be obtained by lowering the periapsis altitude. This is more fully indicated in Figure III-6 which shows the impulsive MOI ΔV for getting into a capture orbit versus VHE magnitude with all apoapsis altitudes at 95,000 km. The ΔV savings indicated are about three times greater than the cost of raising periapsis back up to the observation orbit periapsis altitude if this is done at apoapsis. This saving is not utilized in this phase of the study since an adequate payload is available without it.

The ΔV required to match the capture orbit to the orbit plane of Deimos is a function of the inclination mismatch, the height of apoapsis, and also the position in the orbit where the plane change maneuver is accomplished. The plane change maneuver may be done at either of the two intersections of the two planes. It is therefore desirable to minimize the total effects of both velocity and angular change on the plane change ΔV . Figure III-7 indicates the required plane change ΔV for various VHE declinations as a function of the argument of periapsis (Ω). The argument of peri-

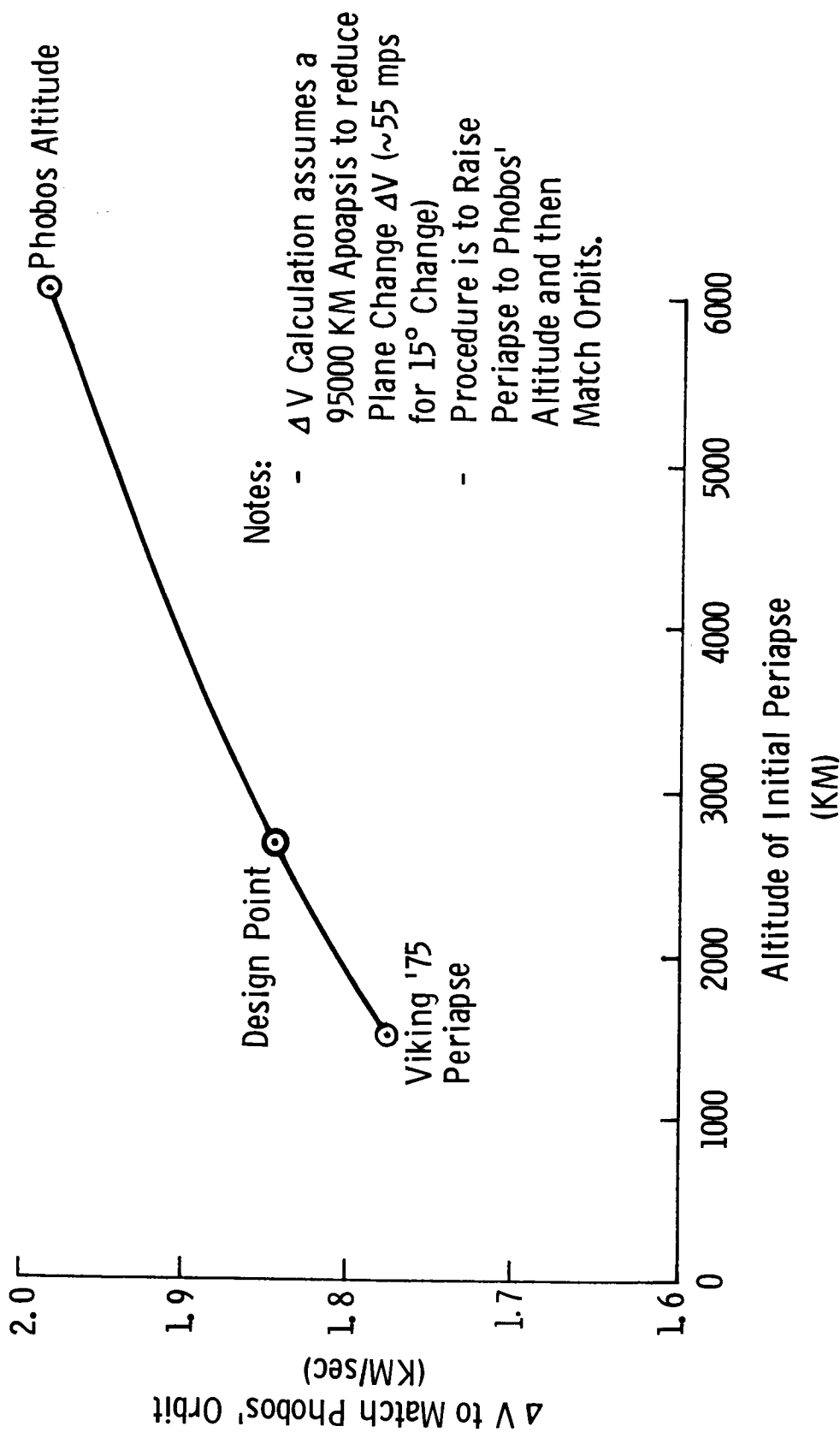
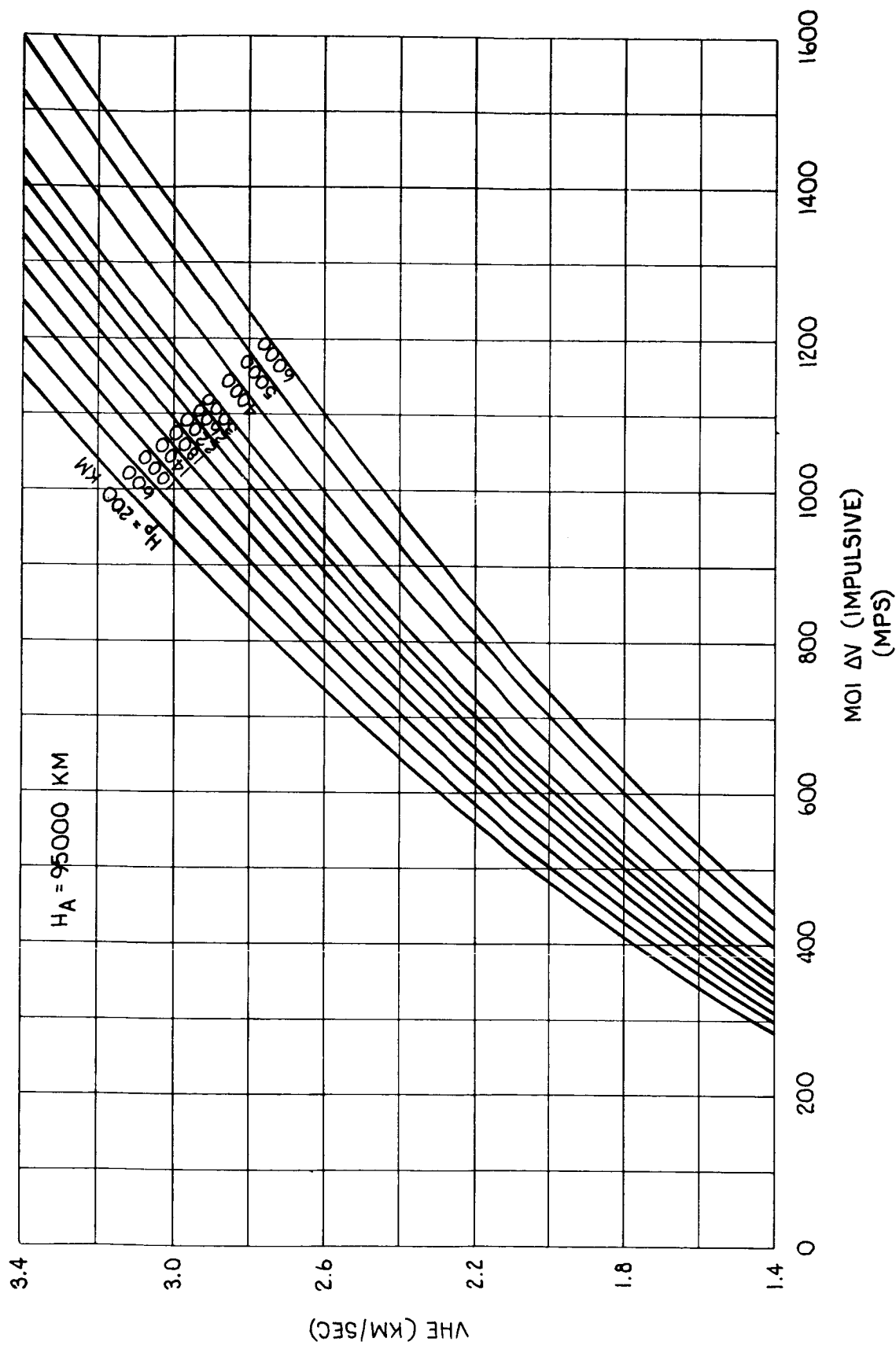
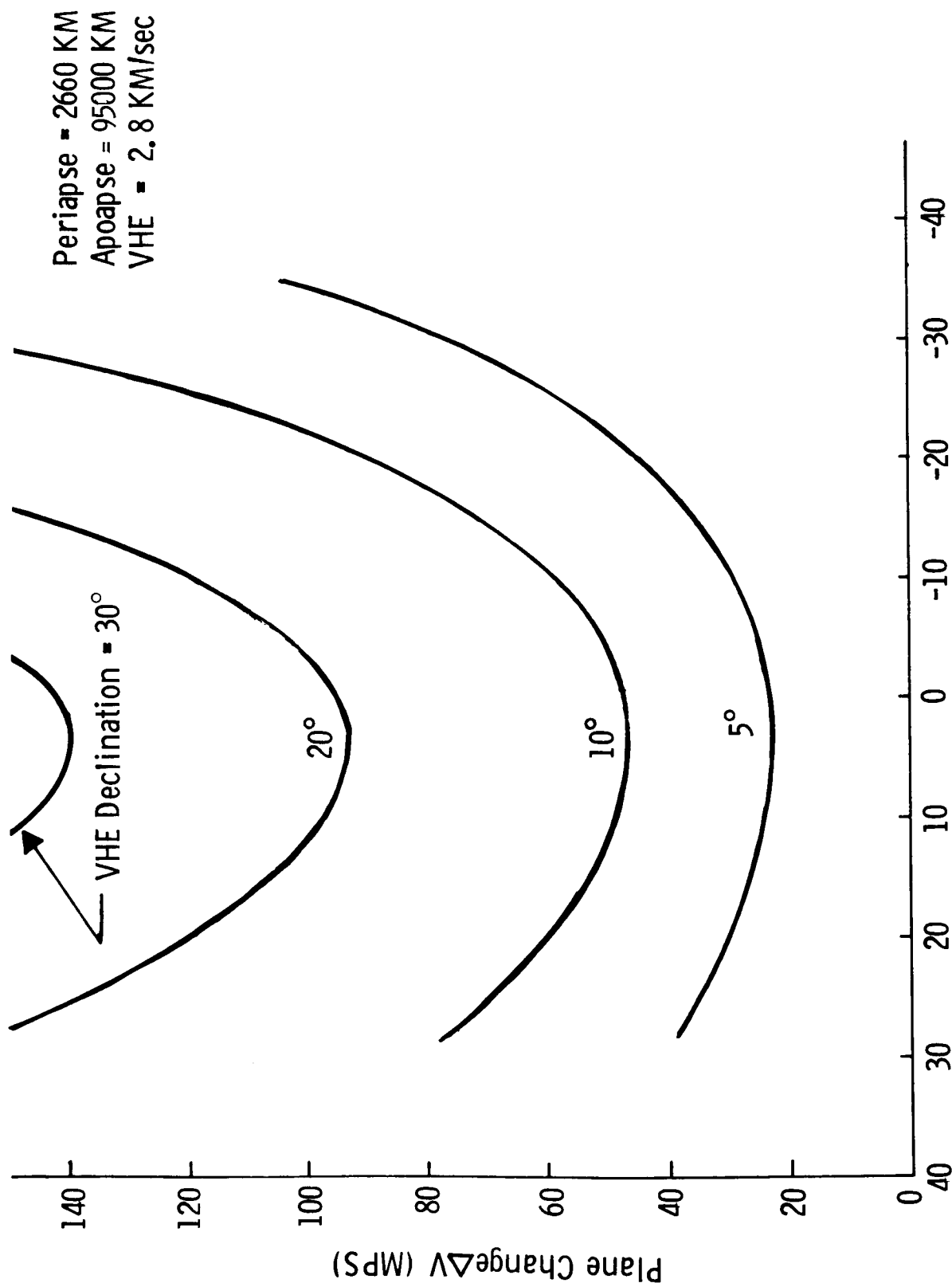


Figure III-5 ΔV to Match Phobos Orbit vs Altitude of Initial Periapse





Argument of Periapsis - Degree

Figure III-7 ΔV Required for Plane Change vs Argument of Periapse

apsis determines the position in the orbit where the maneuver can be performed. The VHE declination combined with the argument of periapsis determines the required plane change angle as indicated in Figure III-8. This analysis indicates that for a minimum ΔV maneuver, the plane change should be performed near apoapsis in an orbit with the argument of periapsis near zero. The height of apoapsis determines the velocity at apoapsis and the higher the apoapsis the lower the plane change ΔV . The baseline mission therefore does the plane change at apoapsis (line of apsides is placed in Deimos' orbit plane) at an altitude of 95,000 km.

The VHE magnitude and declination determine the ΔV required for the MOI and plane change maneuvers. This information is shown as a function of launch and encounter dates for launch opportunities between 1977 and 1984 in Figures III-9 through III-12. The combination of VHE magnitude and declination and the launch vehicle capabilities yield the payload capabilities. Figures III-13 through III-16 indicate the payload capability of the Titan IIIE/Centaur for each of these opportunities. Also shown is the comparable capabilities of the Titan IIIC, Titan IIIE7/Centaur and the Shuttle/Centaur.

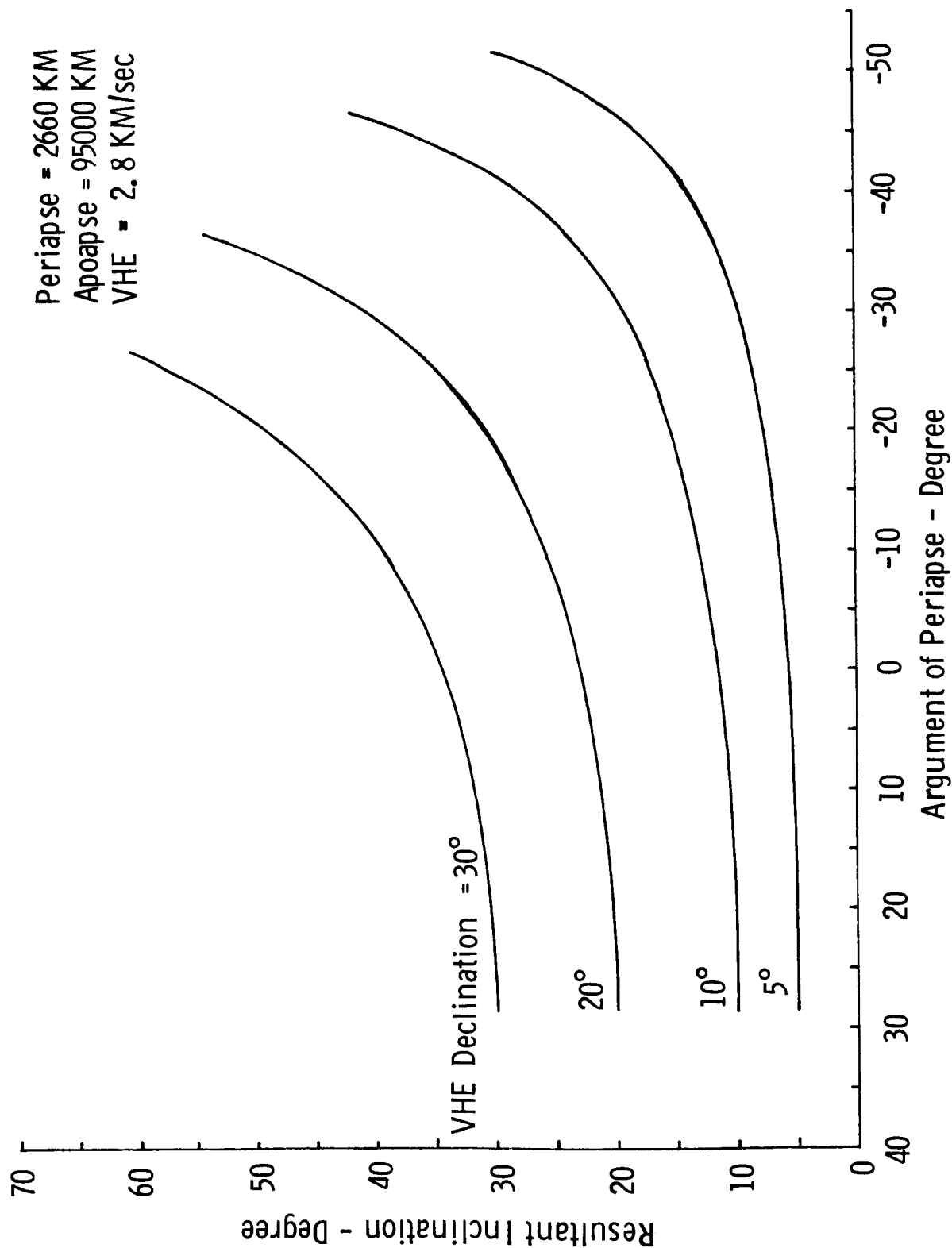


Figure III-8 Resultant Inclinations vs Argument of Periapse

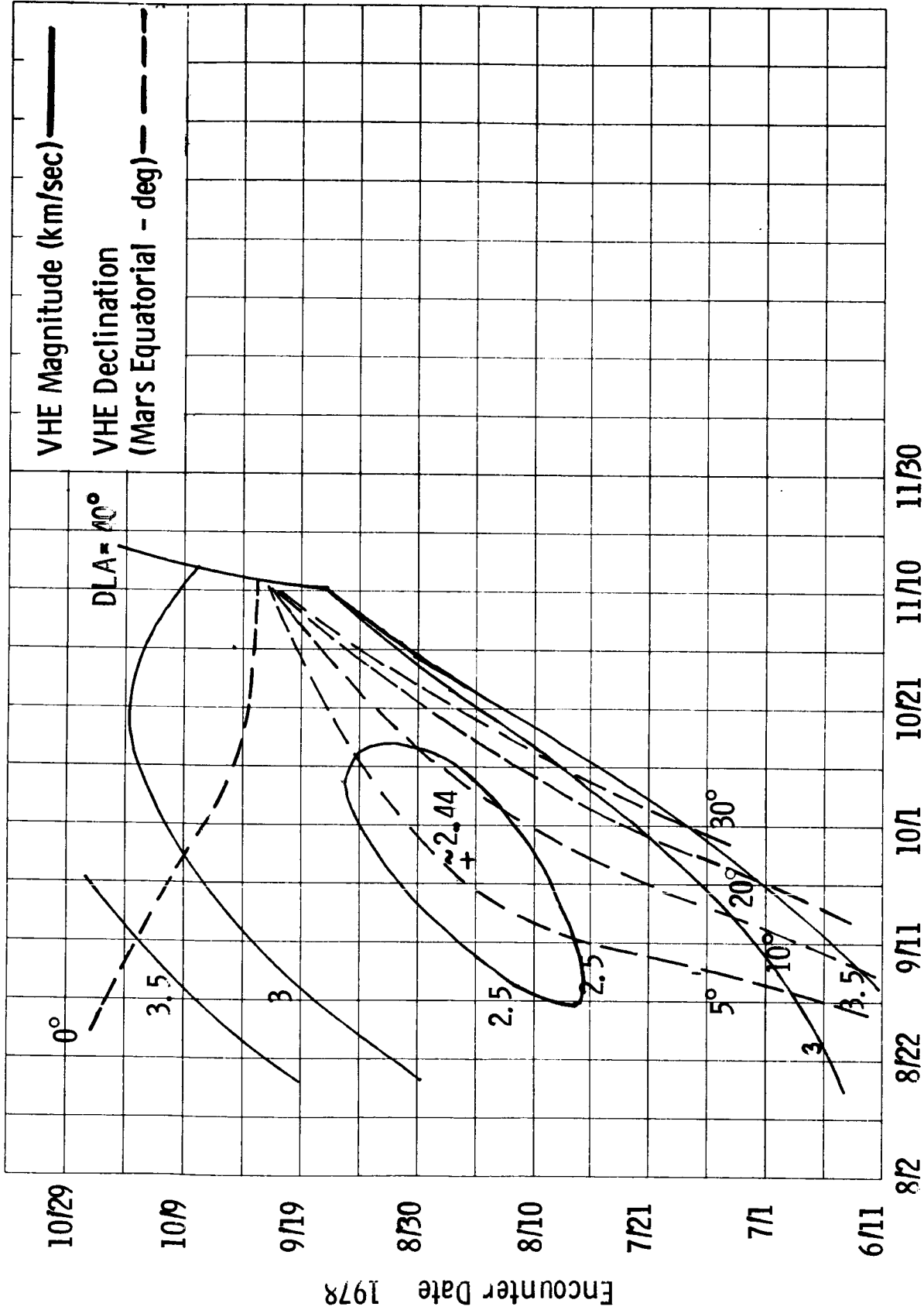
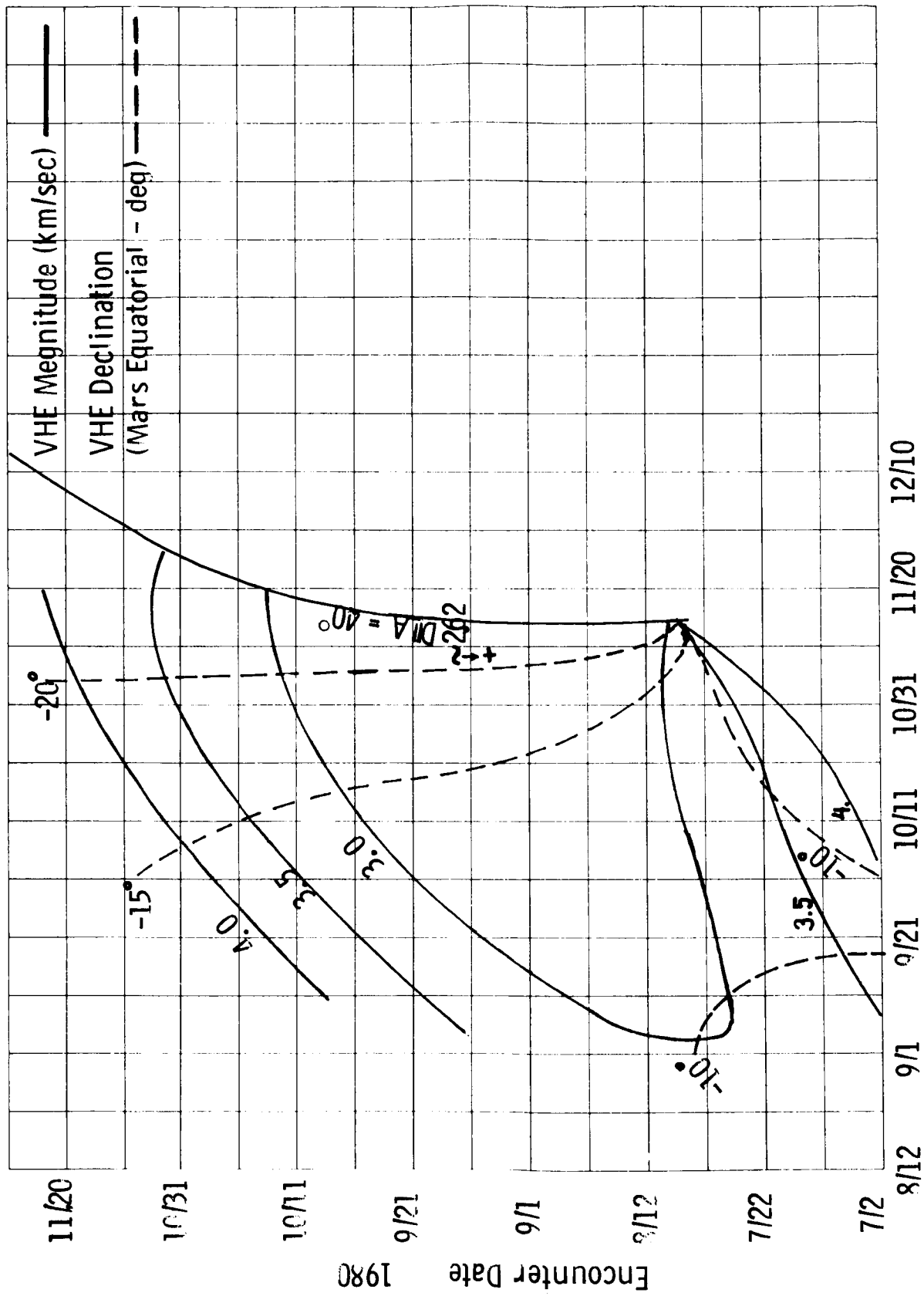
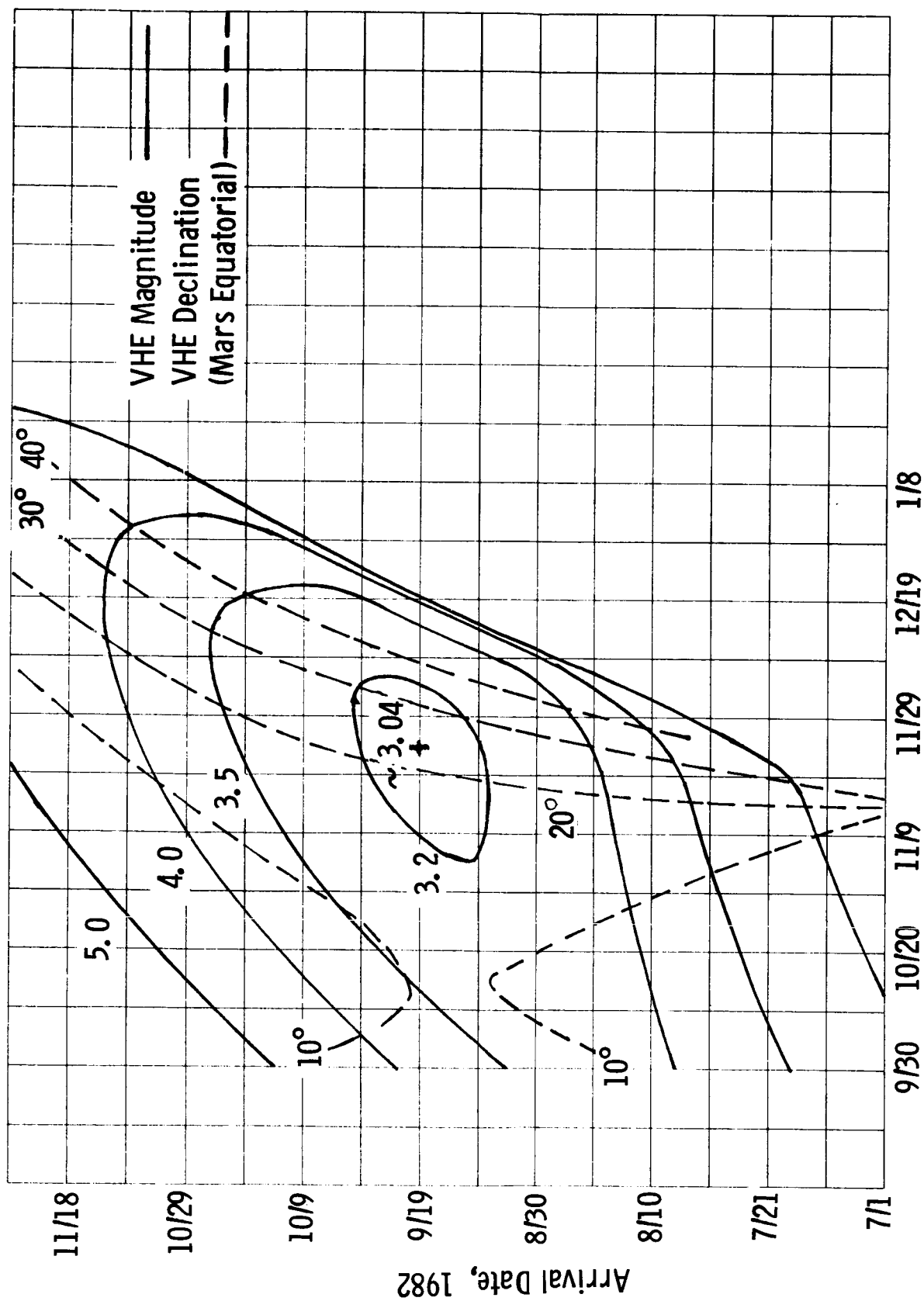


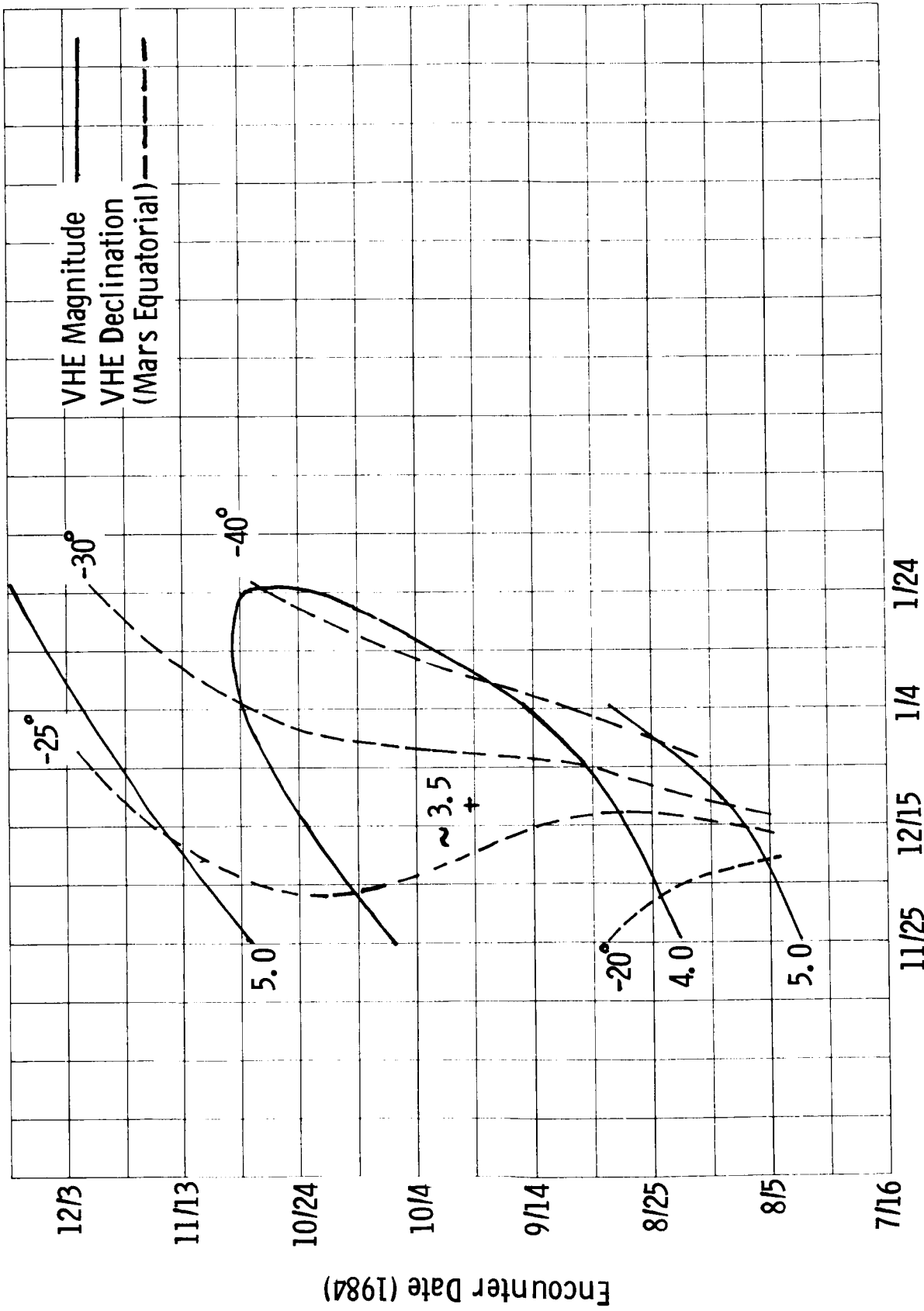
Figure III-9 1977 VHE Contours



Launch Date - 1979
Figure III-10 1979 VHE Contours

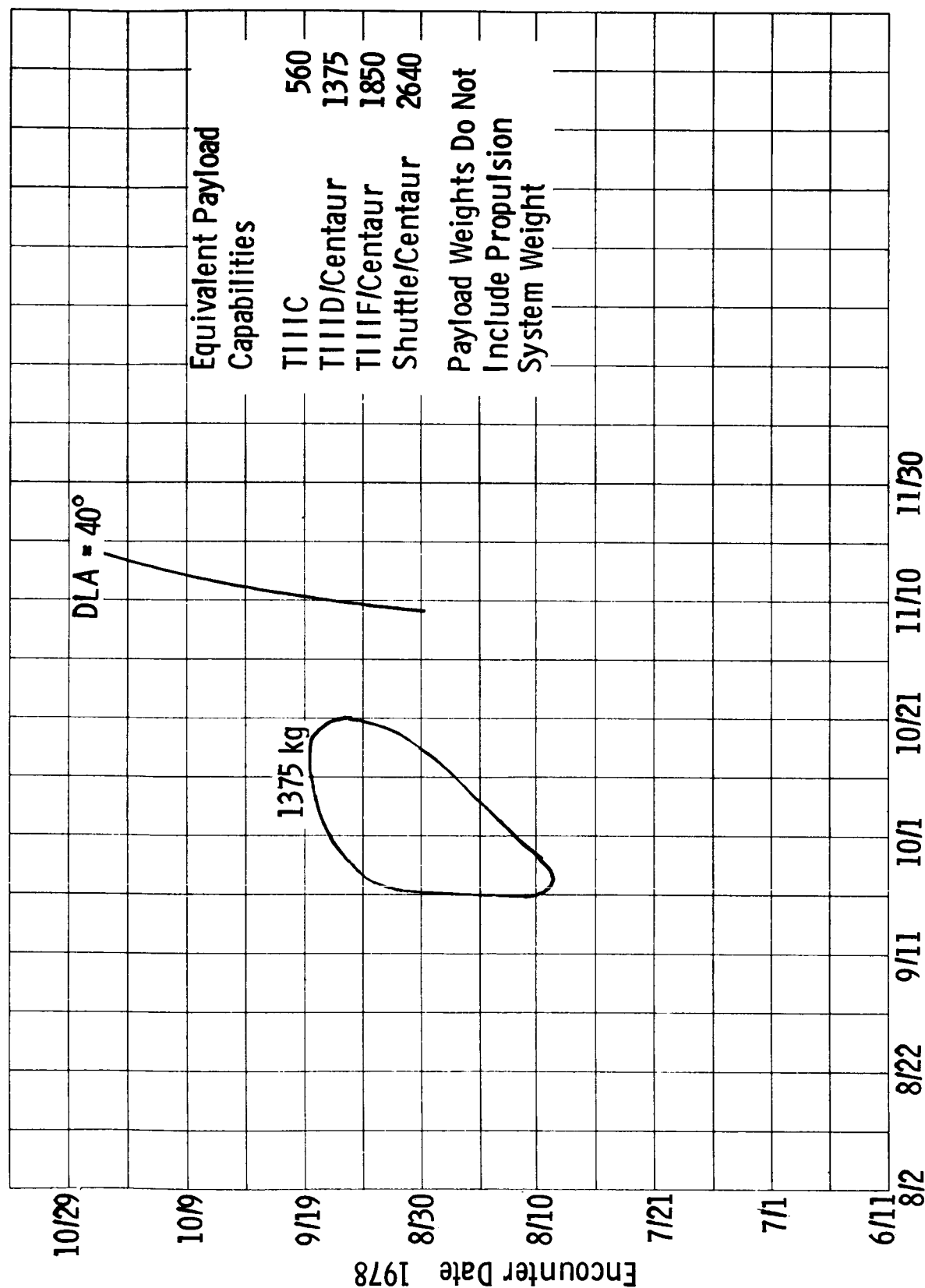


Launch Date, 1981
Figure III-11 1981 VHE Contours



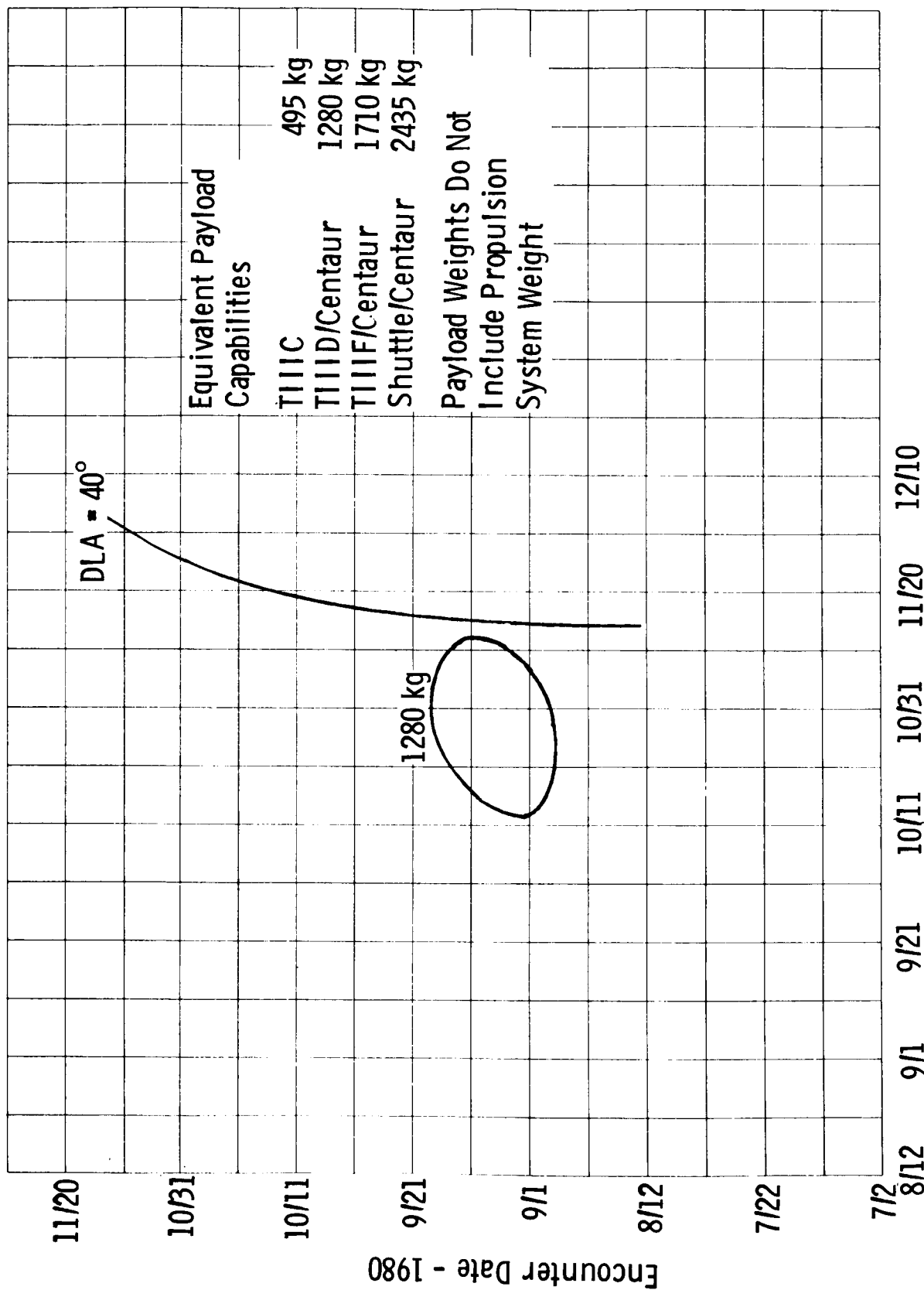
Launch Date (1983/1984)

Figure III-12 1983/84 VHE Contours

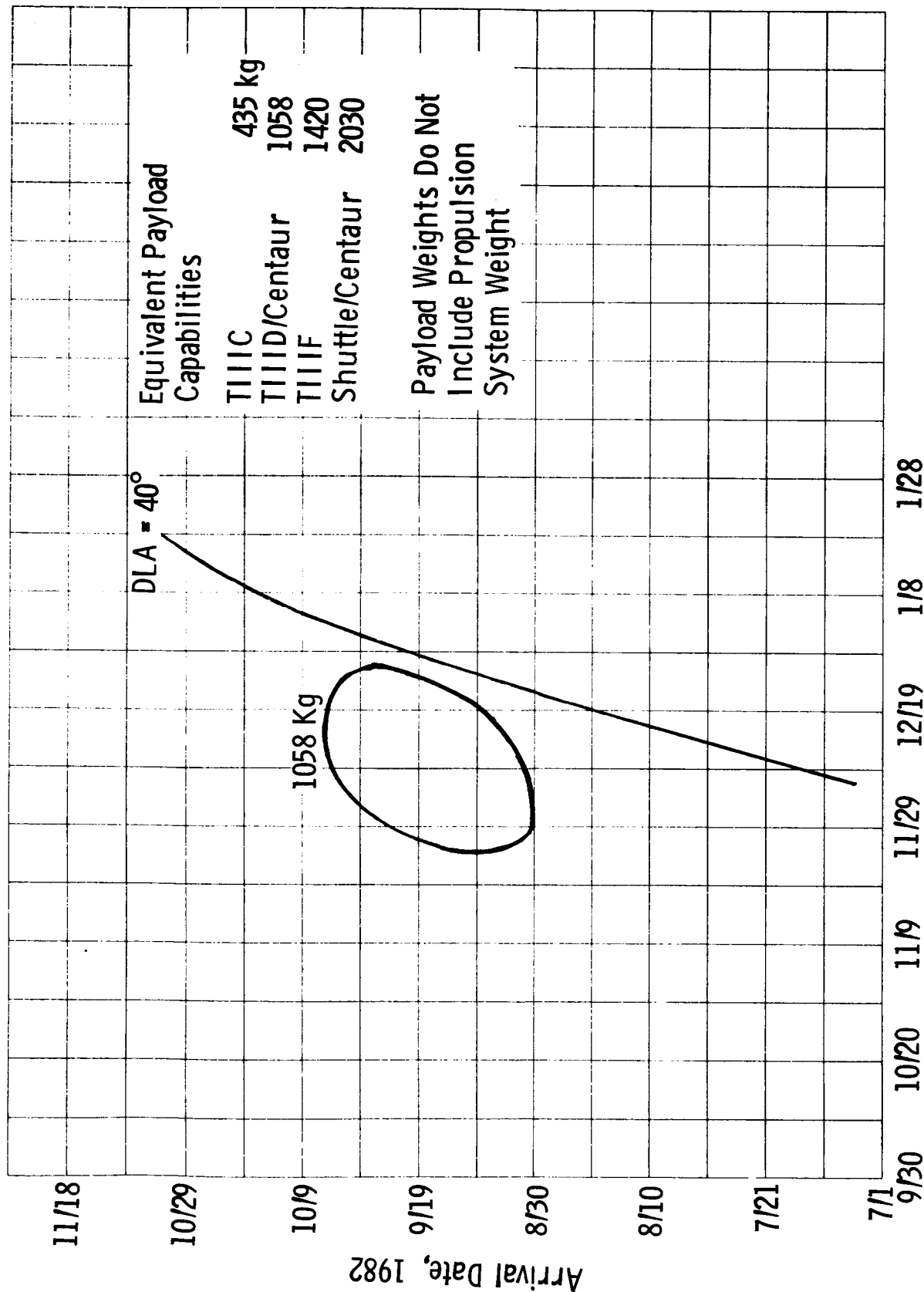


Launch Date 1977

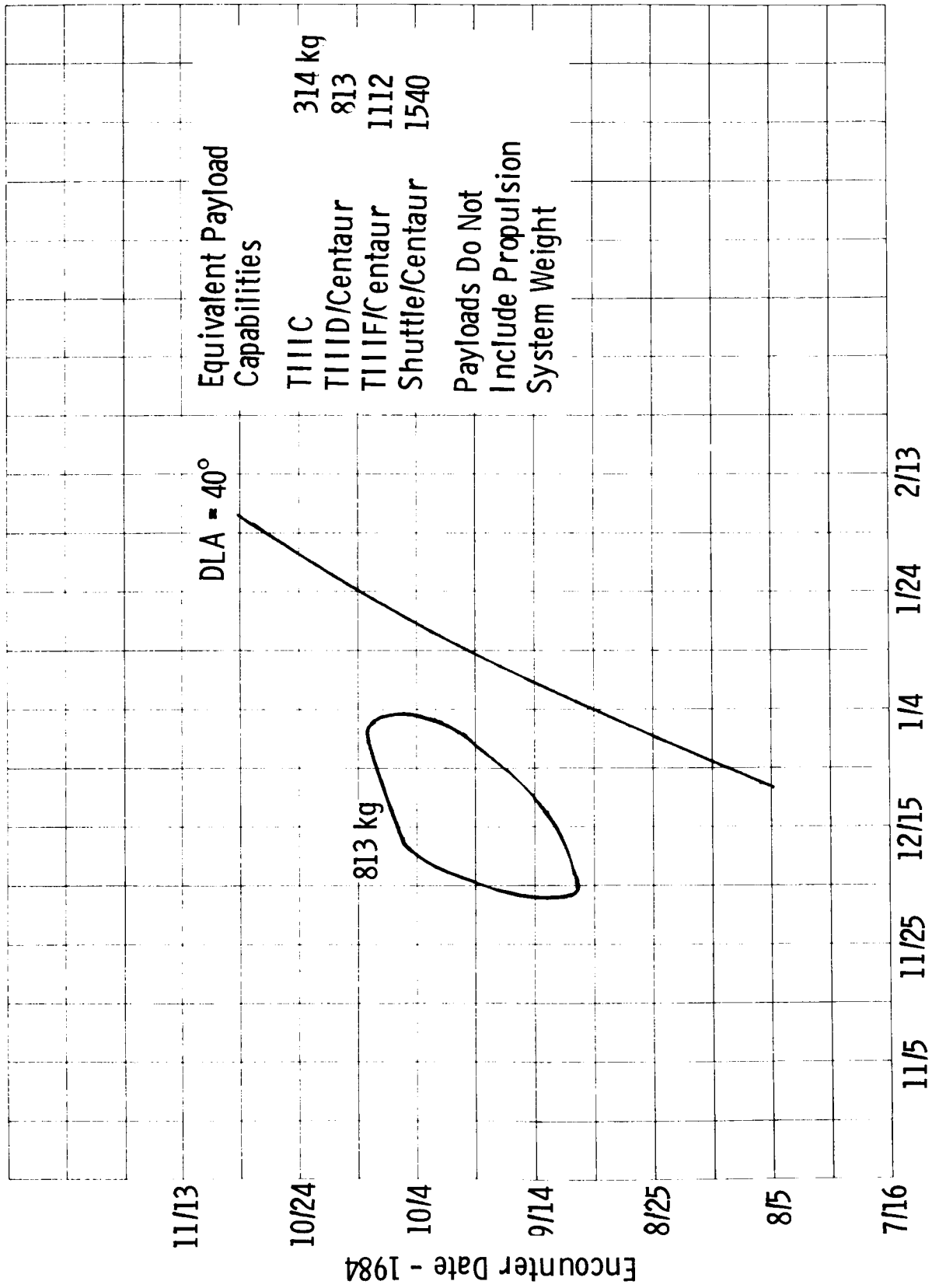
Figure III-13 1977 Payload Capability



Launch Date - 1979
 Figure III-14 1979 Payload Capability



Launch Date, 1981
Figure III-15 1981 Payload Capability



Launch Date - 1983/84
Figure III-16 1983/84 Payload Capability

B. NAVIGATION ANALYSIS

1. Introduction and Summary

The Phase I study deals with the description of the baseline mission for rendezvous with the satellite Phobos (the inner satellite of Mars). The navigation part of this effort consists of a detailed statistical analysis of: 1) the ΔV budget that must be allocated to correct navigation errors; and 2) the predicted closest approach radius to the satellite at rendezvous. The statistical nature of these quantities results from uncertainties in the encounter and rendezvous navigation and in maneuver execution. (Navigation accuracy was limited by DSN and TV measurement errors, Mars gravity field uncertainty and satellite ephemeris error.) A Monte Carlo program was used to simulate the effect of all these error sources in the following mission maneuver sequence:

<u>Maneuver</u>	<u>Nominal Magnitude</u>
1. Insertion into loose Mars capture orbit (MOI)	1027.6 m/s
2. Plane change maneuver (PCM)	53.6 m/s
3. Phasing orbit maneuver (POM)	54.8 m/s
4. Observation orbit maneuver (OOM)	233.2 m/s
5. Lambert intercept maneuver (LIM)	6.1 m/s
6. Midcourse correction maneuver (MCCM)	0.0 m/s
7. Velocity matching maneuver (VMM)	504.1 m/s

The above sequence is for a rendezvous mission to Deimos. These data were extrapolated to the Phobos rendezvous case. In the above sequence, navigation updates based on DSN tracking occur at the last MCCM prior to MOI, at MOI and prior to the PCM, POM, OOM and LIM. DSN and TV sightings of Deimos against a star back-

ground taken before the LIM were used simultaneously to update the vehicle and the Deimos state vector and another batch taken after LIM was used to update the vehicle state vector prior to the MCC. The Monte Carlo program calculates the statistical ΔV (defined as the 99 percentile total ΔV less the nominal ΔV) for the rendezvous and the 99 percentile distance of closest approach radius, R99. Results for the baseline rendezvous (LD = 10/9/79, ED = 9/1/80) show that a TV imaging system is required to achieve an R99 less than the range of the terminal rendezvous radar (100 km). With the noisy TV system an R99 of 20.9 km can be achieved with a corresponding statistical ΔV (denoted ΔV_{STAT}) of 103.0 m/s. Without the TV, R99 is 213.5 km. These results will vary slightly over the performance window due to variations in the encounter control and knowledge statistics and in the Mars orbit knowledge statistics. (Knowledge uncertainty is the difference between the actual state and the reference state.) The effect of these variations on R99 and ΔV_{STAT} were determined as part of the Phase II effort. (Results presented here are for the baseline case only.)

2. Assumptions and Techniques

a. Baseline Mission Simulation - The key assumption in analyzing the baseline mission to Phobos was that the R99 and the ΔV_{STAT} could be inferred (estimated) by analyzing the mission to Deimos. Since R99 seems to depend solely on the characteristics of the TV system and on the geometry of the TV tracking arc it will be the same for a rendezvous to Phobos or Deimos. The maneuver sequence for a rendezvous to Phobos is essentially the same as for a rendezvous to Deimos with the addition of a Phobos phasing burn and a burn to raise periapsis to the radius of

Phobos. A comparison of these sequences is shown in Table III-7 and is illustrated in Figures III-17 and III-18.

Table III-7 Maneuver Sequence

Rendezvous to Deimos	Rendezvous to Phobos
Mars Orbit Insertion (MOI)	MOI
Plane Change Maneuver (PCM)	PCM
Phasing Orbit Maneuver (POM)	POM
Observation Orbit Maneuver (OOM)	OOM
Lambert Intercept Maneuver (LIM)	Phasing to Phobos (PPM)
Midcourse Correction Maneuver (MCCM)	Raise Periapsis to Phobos (RPM)
Velocity Match to Deimos (VMM)	LIM
	MCCM
	VMM (Phobos)

The ΔV_{STAT} for rendezvous to Phobos is estimated as

$$\Delta V_{\text{STAT}}(\text{Phobos}) = \left[\Delta V_{\text{STAT}}^2 (\text{MOI} + \text{PCM} + \text{POM} + \text{OOM}) + \Delta V_{\text{STAT}}^2 (\text{PPM} + \text{RPM}) + \Delta V_{\text{STAT}}^2 (\text{LIM} + \text{MCCM} + \text{VMM}) \right]^{\frac{1}{2}}$$

b. Rendezvous Philosophy - The MOI maneuver is targeted to yield a high elliptical capture orbit with period of 97.1 hours and argument of periapsis $\sim 0^\circ$ (i.e., line of apsides in Mars equator). To accomplish this without an apsidal shift during MOI it is necessary that the Mars approach angle (θ_{AIM}) be near 0° . The capture orbit, with approach periapsis radius of 6050 km (altitude of the observation orbit) has an apoapsis altitude of 95250 km. With the line of apsides in the Mars equatorial plane,

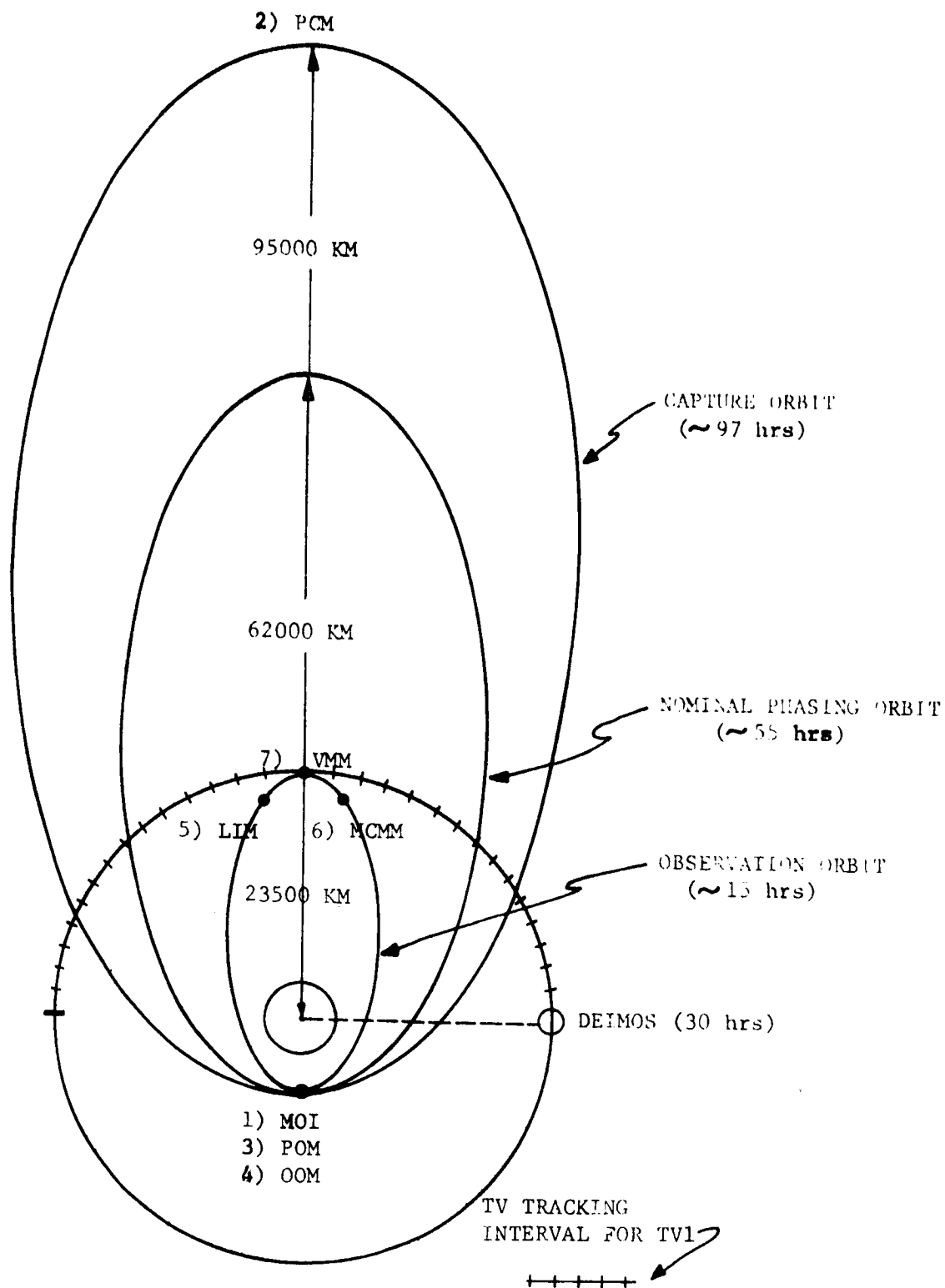


Figure III-17 Schematic for Rendezvous to Deimos

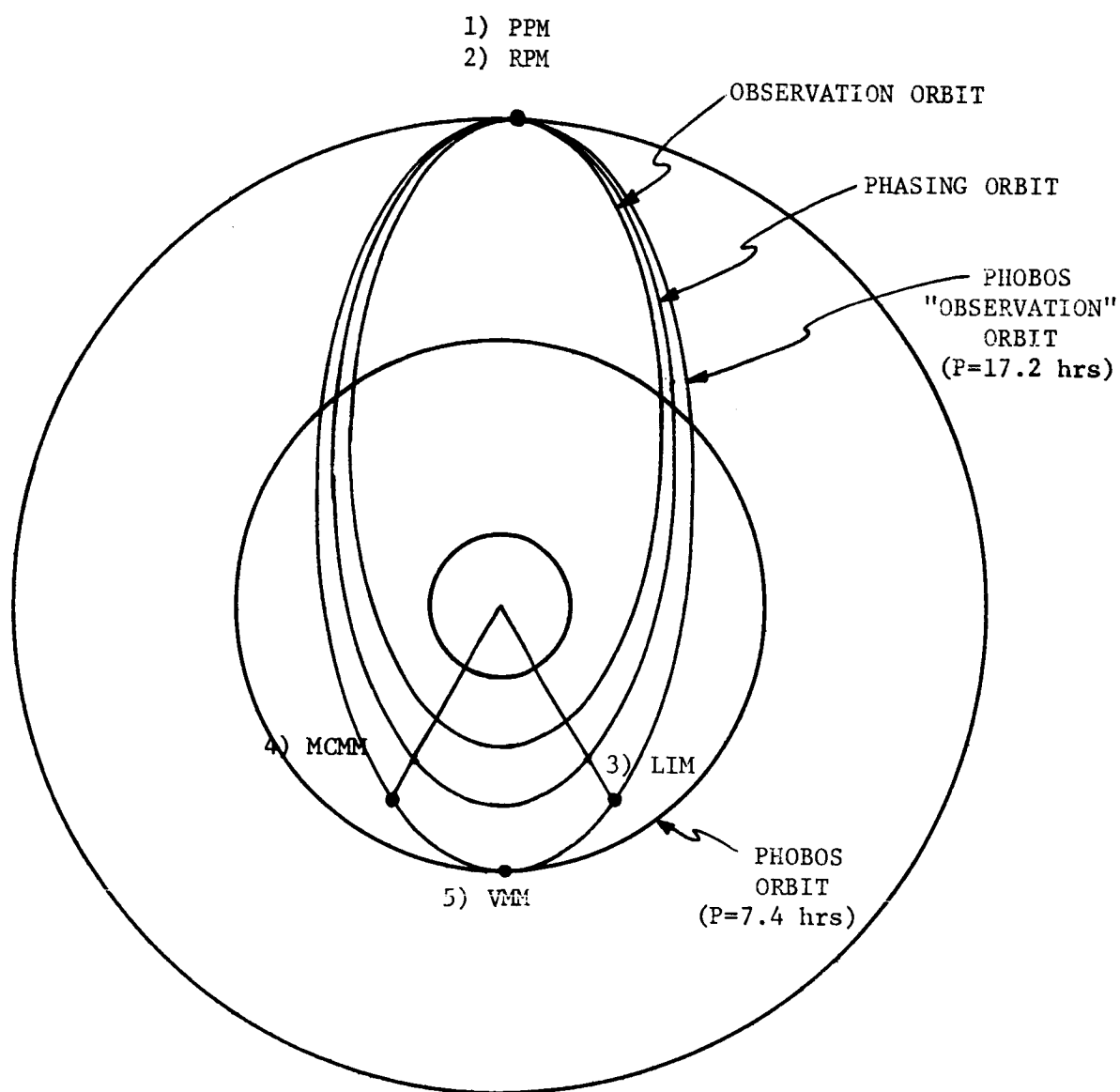


Figure III-18 Schematic for Rendezvous to Phobos

a minimum ΔV plane change maneuver can be performed at apoapsis to rotate the orbit to make it coplanar with the satellites. Once this is accomplished, a phasing orbit burn (performed at periapsis) is required to set up the satellite-vehicle phasing for the observation orbit. The phasing orbit period is calculated from Eq (1)

$$P_{\text{phas}} + 5/2 P_{\text{OBS}} = \text{DTP} + 2 P_{\text{DEIMOS}} \quad (1)$$

where P_{phas} = period of phasing orbit,

P_{OBS} = period of observation orbit (15.1 hours),

P_{DEIMOS} = period of Deimos orbit (30 hours),

DTP = time it takes Deimos to go from true anomaly TA to true anomaly of vehicle apoapsis vector with respect to satellite line of apsides.

The time to rendezvous, measured from the time of the phasing orbit burn, is then given by

$$\Delta t_{\text{REND}} = P_{\text{phas}} + 5/2 P_{\text{OBS}} \quad (2)$$

The phasing orbit burn occurs at the 3rd periapsis passage (MOI is the 0th). This method of computing the phasing orbit period guarantees that the period is never less than the observation orbit period, and what is more important it guarantees that at the time of the observation orbit burn (which occurs at the 4th periapsis passage, i.e., after one phasing orbit period) the satellite true anomaly (with respect to the vehicle line of apsides) will be 270° . This sets up the optimal closing geometry for TV sightings. The observation orbit has the property that it affords a closest approach to Deimos on every other apoapsis passage, and that the satellite Phobos will walk into it within a period of at most 15 days. Once a revolution of TV and

DSN sightings have been made in the observation orbit, a Lambert Intercept Maneuver is performed a half a revolution later to take out any inclination dispersion which may exist between the orbits of the vehicle and Deimos. This maneuver is nominally about 6 m/s. It is computed from an estimate of the vehicle state based on DSN tracking and estimate of the satellite ephemeris based on TV data. A nominally zero midcourse maneuver is performed at 150° true anomaly on the Lambert intercept trajectory. (Rendezvous occurs at 180° TA.) After the final MCC the actual vehicle/Deimos closest approach radius is computed. At the time of closest approach velocity matching ΔV is computed and the actual ΔV performed is tabulated.

c. DSN Tracking During Encounter - The control characteristics of the post-MOI orbits are primarily a function of the control and knowledge errors at the time of the MOI burn. Control is the ability to keep the actual trajectory state equal to the reference state whereas knowledge is how closely the estimated state (the output of some data filter) matches the actual state. The statistics of pre-MOI control (actual dispersions from reference) and knowledge (deviations of estimate from actual) are represented as covariance matrices and are computed by linear error analysis of the DSN tracking capability during the encounter (pre-MOI) phase. DSN tracking for this phase begins at E-30 days. The state estimate based on tracking from E-30 days to E-10 days is used to target the last MCC scheduled at E-10 days. The estimate based on DSN tracking from E-30 days to E-12 hours is used to target the MOI maneuver. The control covariance matrix at E-12 hours is the knowledge covariance at E-10 days mapped to E-12 hours, i.e., any control error at MOI is due to a knowledge error at the last MCC. The 6 x 6 control and knowledge covariance matrices at E-12 hours are mapped into the B-plane or

\hat{R} , \hat{S} , \hat{T} coordinate frame. The \hat{R} , \hat{T} plane or B-plane is perpendicular to the \hat{S} vector, (\hat{S} is the unit hyperbolic excess velocity vector) and the \hat{T} axis is the intersection of the B-plane with the ecliptic. \hat{R} completes a right-handed system with \hat{S} and \hat{T} . The parameters of interest in this system are the semi-major (SMAA), semi-minor (SMIA) axes of the dispersion ellipses in the \hat{R} , \hat{T} plane and the ellipse orientation angle θ_{MI} between the minor axis of the ellipse and the \hat{T} axis. The uncertainty along \hat{S} is the time-of-flight error and is neglected in this study. The error sources and their statistics, which limit the DSN accuracy during the encounter phase, are shown in Table III-8. DSN data is assumed to be processed at a 1 cnt/min rate using an optimal consider (or Kalman Schmidt) filter. This is a sequential filter, i.e., processes one data point at a time, which yields the same local state accuracy as would be obtained if all the measurement biases were solved for. In addition, it considers dynamic noise (down-weights the state covariance) in propagating the estimate from one observation time to the next. This type of filter is being considered for Viking '75 and so should certainly be available for a D/P type mission. It generally yields more accurate state estimates because it down-weights previous data and hence limits the effect of unmodeled dynamic noise.

Table III-8 Errors Limiting DSN Accuracy During Encounter

Station Location Errors	
Z - height	= 0.0 m
r - spin	= 1.5 m
Longitude	= 3 m
Longitude correlation	= .98
μ - Mars	= .1 km ³ /sec ²
Data Noise (range-rate) - 1 mm/sec for cnt/min rate	

d. DSN and TV Tracking During Orbital Operations - The maneuver sequence leading to establishment of the observation orbit is supported by DSN tracking only (i.e., PCM, POM, and OOM) whereas the LIM and MCCM are targeted based on estimates formed from both DSN and TV data (Figure III-19). The DSN tracking arcs for the PCM, POM and OOM consist of about a revolution and a half of data with exclusion of those data points within an hour of either side of periapsis. This procedure yields a good solution for the relatively stable elliptical orbit away from periapsis (near periapsis the orbit oscillates wildly). Error sources affecting in-orbit DSN accuracies are listed in Table III-9.

Table III-9 Errors Limiting DSN Accuracy In-Orbit

$\sigma_{\mu} = .1 \text{ km}^3/\text{sec}^2$	$\sigma_{C22} = \sigma_{S22} = .111 \times 10^{-4}$
$\sigma_{J2} = .22 \times 10^{-4}$	$\sigma_{C33} = \sigma_{S33} = .828 \times 10^{-5}$
$\sigma_{C21} = \sigma_{S21} = .233 \times 10^{-4}$	
Data noise (range-rate) - 1 mm/sec for 1 cnt/min rate	

Immediately after the OOM, TV sighting data and DSN data (range-rate only) are processed simultaneously to solve for both the vehicle state and the four satellite ephemeris parameters a , i , Ω , MA . (No uncertainties were assumed in e and ω .) The 10×10 covariance matrix representing the distribution of estimation error at the end of the first TV tracking arc was used to construct the 6×6 covariance matrix of relative state error between vehicle and satellite. Uncertainties in Mars gravity field harmonics (other than the central force term μ_{MARS}) were not considered in generation of relative state covariance matrices. These terms, however, were considered as limiting the DSN single vehicle accuracies. The approximation here is that the effect of

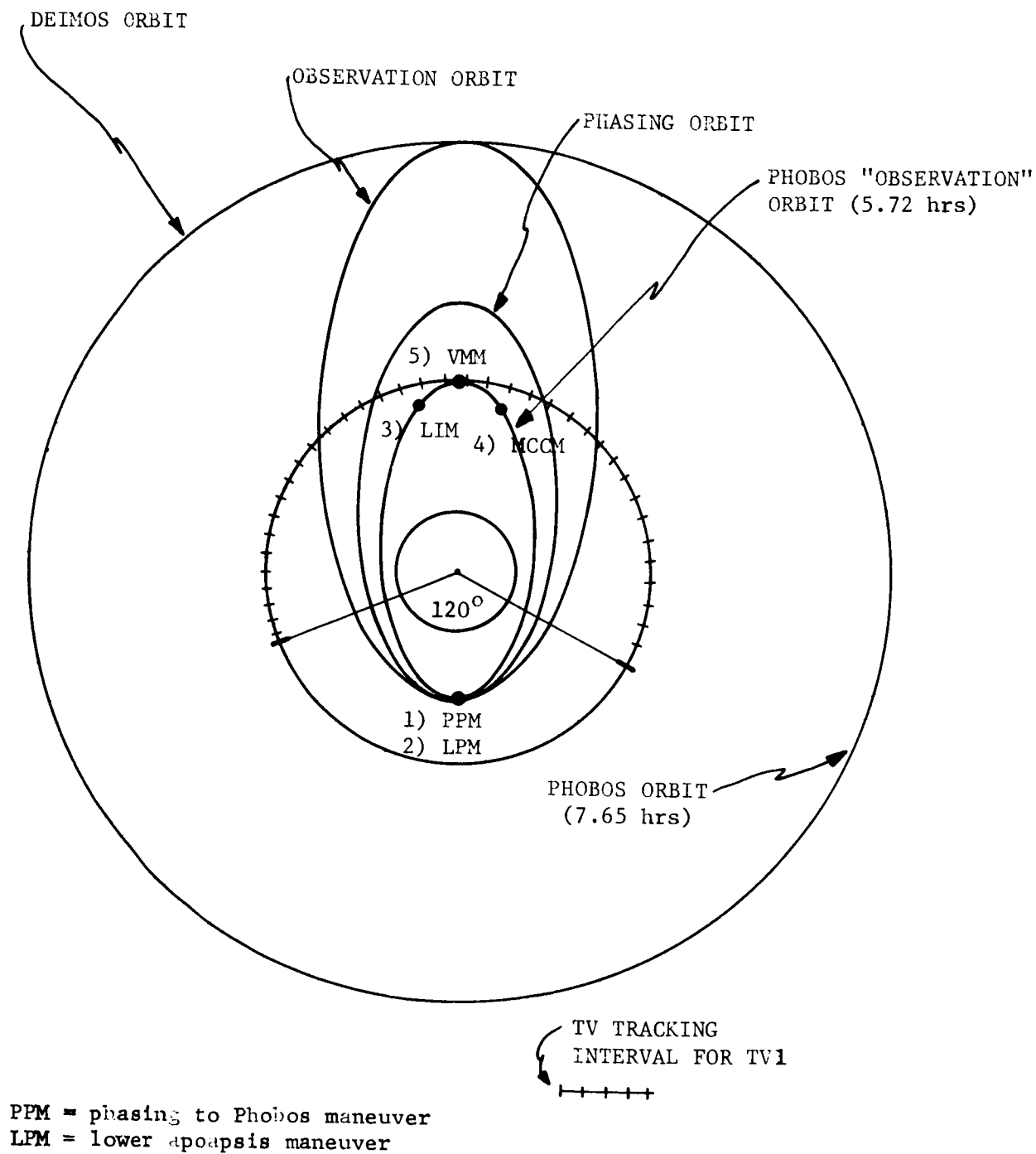


Figure III-19 TV Tracking Intervals for Rendezvous to Deimos

the gravity field would be about the same on vehicle and satellite and hence would cancel out in the relative state determination. During the second TV tracking arc only the vehicle state is solved-for using TV data alone. The statistics of satellite error resulting from the first TV arc are used to generate the statistics of relative state error for the second TV arc (e.g., the satellite estimate at the end of the first data arc is used in conjunction with TV data taken during the second arc to estimate the vehicle state).

Vehicle updates prior to the PCM, POM and OOM were performed in the Monte Carlo simulation by randomly drawing samples from the distributions of state error as represented by 6 x 6 covariance matrices. The sample (ΔX_E) is added to the actual state vector (X_A) to form the new estimate (X_E), i.e.,

$$X_E = X_A + \Delta X_E$$

The updates occurred at specified actual true anomalies corresponding to the ends of the data arcs, as follows:

<u>Update Prior To</u>	<u>Data Arc</u>
PCM	MOI to 150° on 2nd capture orbit revolution
POM	0° to 270° on 3rd capture orbit revolution
OOM	0° to 270° on phasing orbit

Although the phasing orbit period is variable for each cycle of the simulation it had to be assumed that the DSN accuracy at 270° TA would be the same for each cycle (i.e., the same covariance matrix was sampled regardless of phasing orbit period). Also, the DSN covariance matrix for the update prior to the POM was taken to be the DSN covariance for the update prior to the OOM.

The update prior to the LIM, based on DSN and TV tracking from 0° to 270° on the observation orbit, was computed as follows:

- 1) The vehicle state is first updated by sampling a 6 x 6 covariance matrix representative of DSN accuracy as limited by present knowledge of Mars gravity field harmonics, i.e.,

$$X_E^{Veh} = X_A^{Veh} + \Delta X_E^{Veh}$$

- 2) A sample of the relative state error, ΔX_E^{Rel} , is then drawn from a distribution characterized by the relative state covariance matrix. This matrix was generated with μ_{MARS} the only uncertain gravity term.

- 3) A relative state estimate, X_E^{Rel} , is formed from

$$X_E^{Rel} = X_A^{Rel} + \Delta X_E^{Rel}$$

where X_A^{Rel} is the actual relative state.

- 4) Since the estimated relative state is the difference between the satellite estimate, X_E^{SAT} , and the vehicle estimate, X_E^{Veh} , i.e.,

$$X_E^{Rel} = X_E^{SAT} - X_E^{Veh}$$

it follows that the satellite estimate is given by

$$X_E^{SAT} = X_E^{Veh} + X_A^{SAT} - X_A^{Veh} + \Delta X_E^{Rel}$$

The optimal procedure for simulating state vector updates when both vehicle and satellite are being solved-for is to sample a 12 x 12 covariance matrix representative of the state errors when all gravity harmonics are uncertain. Since the ability to consider general harmonic uncertainties does not exist when processing TV data, the optimal procedure could not be followed. The procedure used here considers the effect of gravity harmonic uncertainties on the vehicle state uncertainty and ignores their effect on the relative state uncertainty. As mentioned earlier this should be a good approximation because the relative state

accuracy is not strongly affected by gravity uncertainty when the two objects are in similar orbits. Also, sampling the vehicle covariance and the relative covariance separately is justified by the fact that the relative error and the vehicle error are largely uncorrelated.

TV images of the satellite against a star background are assumed processed every 10 minutes during the TV tracking periods. Measurements obtained from these images are of the included angle between the line-of-sight to the star and to the satellite (or equivalently of the separation, in the image plane, between the center of the satellite and the star). It can be shown that two independent measurements of this type (i.e., where the vehicle-star-satellite planes are not the same for each star) have the same information content as a single measurement of the vector line-of-sight to the satellite. This analysis simulates TV tracking as satellite line-of-sight tracking and therefore implicitly assumes that two independent star-satellite measurements can be obtained from each TV image. This assumption is conservative in that many measurements may be obtained from a single TV image depending on the available star background.

e. Satellite Ephemeris Errors - Errors (1σ) in the satellite ephemeris expressed in Kepler elements were obtained from References III-1 and III-2, and are shown in Table III-10. (Uncertainty in eccentricity was not readily available and was assumed zero for this study.) Other combinations of ephemeris error were studied in the Phase II effort. When the inclination of the satellite orbit is small, the longitude of the ascending node error and the argument of periapsis error will be highly correlated, i.e., these two errors cannot be distinguished by the data. This situation is simulated by assuming a relatively large standard deviation of ascending node error and small

standard deviation of periapsis error with no correlation. Also, since the eccentricity is small the same sort of assumption was made for true anomaly (TA) error, i.e., a small standard deviation of TA error and no correlation with ascending node and argument of periapsis was used.

Table III-10 Satellite Ephemeris Errors

	Deimos	Phobos
σ_a	7.5 km	7.5 km
σ_i	.02°	.1°
σ_Ω	1.5°	1.5°
σ_ω	.005°	.005°
σ_{TA}	.00001°	.0001°

As mentioned earlier, results for the baseline rendezvous to Phobos were extrapolated from Deimos rendezvous results. In order to make this procedure more justifiable, the Phobos ephemeris errors, which are larger than the Deimos errors, were used for the Deimos rendezvous case.

f. Simulation Techniques - A detailed description of the Monte Carlo simulation program is found in Appendix C. The functional steps in the computational logic are as follows:

- 1) Sample control and knowledge dispersions at encounter.
- 2) Obtain estimated and actual approach hyperbole pre-MOI.
- 3) Find optimal Mars orbit insertion (MOI) burn controls and insert vehicle into capture orbit.

- 4) Perform a DSN update of vehicle state at 120° TA on 2nd capture orbit revolution (DSN#1).
- 5) Compute and execute a minimum ΔV plane change maneuver (PCM) near apoapsis (180° TA) on the 2nd capture orbit revolution.
- 6) Perform a DSN update of the vehicle state at 270° TA on the 3rd revolution (DSN#2).
- 7) Obtain the reference state (cartesian) for Deimos at time of vehicle DSN#2 update. Convert to conic elements. Also sample distribution of actual dispersions in Deimos conic elements to obtain actual Deimos state.
- 8) Compute the phasing orbit period, observation orbit period, Julian date of rendezvous and phasing orbit maneuver based on the reference Deimos state.
- 9) Execute the phasing orbit burn (POM) at periapsis #3 on the capture orbit.
- 10) Perform DSN update at 270° TA on the phasing orbit (DSN#3).
- 11) Recompute the observation orbit period, Julian date of rendezvous and the Hohmann burn to establish the observation orbit based on the new vehicle estimate.
- 12) Execute Hohmann burn, OOM, at periapsis #4.
- 13) Sequentially process DSN and TV data from 0° to 270° TA on the 1st observation orbit to simultaneously solve for the vehicle and satellite states (TV1).
- 14) Compute and execute Lambert intercept maneuver (LIM) at 210° TA on 2nd observation orbit revolution.

- 15) Sequentially process TV data from 0° to 150° TA on the 3rd observation orbit revolution to solve for the vehicle state (TV2).
- 16) Compute and execute the midcourse correction maneuver (MCCM), another Lambert transfer maneuver, at 160° TA on the 3rd observation orbit revolution.
- 17) Calculate the actual distance of closest approach (DCA) to Deimos and the corresponding Julian date.
- 18) Compute and execute the required velocity matching maneuver (VMM) at DCA.
- 19) Complete all Monte Carlo cases? If no, return to step #1. If yes:
- 20) Compute 99 percentile total ΔV above nominal (ΔV_{STAT}) and distance of closest approach (R99).

1) B-Plane Sampling - As mentioned earlier the control covariance at encounter (E) is taken to be the state vector accuracy at the last midcourse correction time (E-10 days) mapped to encounter. This matrix and the knowledge matrix at encounter largely determine the distribution of actual spacecraft states post-MOI. In the simulation an actual and an estimated B-vector (impact plane vector) are constructed by adding samples of the B-plane control and knowledge dispersions to the nominal B-vector according to

$$B_{ACT} = B_{Ref} + \Delta B_C$$

$$B_{EST} = B_{ACT} + \Delta B_K$$

If the approach hyperbolic excess velocity vector, VHE, is assumed unperturbed and perfectly known, then a unique map exists between the B-plane system and the conic elements a , e , i , ω , Ω . In this way an actual and estimated approach hyperbola is generated for each Monte Carlo cycle. The optimal time to perform

MOI on the estimated approach hyperbola is computed initially as a true anomaly and is then converted to a Julian date by assuming that the Julian date of periapsis passage on any approach orbit is always the reference Julian date. The true anomaly of the burn on the actual trajectory is then computed by backing up the same ΔT from periapsis.

2) Minimum ΔV MOI - The burn controls which yield a minimum ΔV fixed attitude insertion maneuver are computed using a Lagrange multiplier (Newton-Raphson) technique (Reference III-3). These controls are: attitude angles α and δ in the Mars equatorial system, burn time t_B and initiation true anomaly TA_B . Maneuver execution is degraded by uncertainty in: burn attitude angles, burn time, thrust level, and burn initiation true anomaly. Statistics of these errors are found in Table III-11. Note that the 1σ pointing inaccuracy for MOI is larger than for the other maneuvers. This is because MOI pointing accuracy is largely limited by platform drift during the burn whereas the shorter in-orbit trims are not.

3) Minimum ΔV Plane Change - After DSN#1 at 120° TA, the impulsive targeting routine VITAP is called for the minimum ΔV plane change maneuver. This burn is targeted to 0° inclination to place the vehicle motion in the equator. Since the line of apsides is not exactly in the equator the burn will not occur exactly at 180° TA but will occur at the orbital TA corresponding to the intersection of the vehicle plane and the equatorial plane.

4) Phasing Orbit Computation - The phasing orbit period and the POM are computed based on the vehicle estimate at DSN#2 and the reference Deimos state. The conic Deimos state is obtained by calling the subroutine MARSAT with a specified Julian date. This routine contains empirical time series expansions for certain ephemeris elements from which the satellite position

Table III-11 Execution Error Statistics*

MOI:

$$\sigma_{\alpha} = \sigma_{\delta} = .476 \text{ degrees}$$

$$\sigma_{t_B} = 1.76 \text{ secs}$$

$$\sigma_{TA} = .158 \text{ degrees}$$

$$\sigma_{THR} = .445 \times 10^{-2} \text{ kgm} - \text{km/sec}^2$$

Other Maneuvers:

$$\sigma_{\alpha} = \sigma_{\delta} = (.3166)^2 + (.1/\Delta V)^2 \text{ }^{\frac{1}{2}}$$

$$\sigma_{t_B} = (.15/1000)^2 + (.005 \times \Delta V)^2 \text{ }^{\frac{1}{2}} \times M/T$$

$$\sigma_{TA} = .158 \text{ degrees}$$

$$\sigma_{THR} = .445 \times 10^{-2} \text{ kgm} - \text{km/sec}^2$$

* Compatible with Reference III-4.

vector may be calculated. The instantaneous velocity vector at time t , $V(t)$, is obtained from two MARSAT position vectors, $R(t)$ and $R(t+.001)$, according to:

$$V(t) = [R(t+.0001) - R(t)]/.001$$

$R(t)$ and $V(t)$ are then rotated to a Mars equatorial system and used to obtain a complete set of instantaneous Deimos conic elements. From this point on the simulation assumes a time invariant conic set for the Deimos ephemeris. The actual conic set is obtained by adding a random sample of actual dispersion to the reference conic.

Note that in general MARSAT will be called with a different time t for each pass through the simulation (t is the time of DSN#2). This means that no one "reference conic for Deimos used in the simulation" exists. The period of the phasing orbit is computed from Eq (1) where DTP is the time it takes Deimos to go from the TA it has at periapsis #4 (time of POM) to the TA of the vehicle apoapsis vector measured with respect to the satellite orbit. DTP is found from

$$DTP = \Delta t_{TA \rightarrow 0} + PHI \text{ where}$$

$\Delta t_{TA \rightarrow 0}$ is the time from TA to 0° in the satellite orbit and PHI is the true anomaly of the vehicle apoapsis vector in the satellite orbit. Once the phasing orbit period is known, the POM is computed to be a Hohmann transfer which lowers the apoapsis radius to r_a , where r_a is chosen to yield a phasing orbit semi-major axis a [$a = (r_a + r_p)/2$] satisfying

$$P_{phas} = 2\pi \left(\frac{a^3}{\mu} \right)^{1/2}$$

5) Propagating Estimated and Actual State Vectors - All maneuvers in the simulation (except the VMM) occur when the estimated orbital geometry is appropriate, e.g., MOI and the PCM

occur when the estimated TA is the TA corresponding to minimum ΔV , the POM and the OOM occur at periapsis and the LIM and MCCM occur at fixed true anomalies (210° and 150° respectively on the observation orbit). The cartesian state estimates at these maneuver true anomalies are obtained by taking the estimated conic elements at the previous maneuver, replacing the old TA_i with the desired TA_f and then transforming the conic set back to the cartesian frame. The time difference Δt may also be computed based on the estimated orbital elements and TA_i and TA_f . The time difference is used to propagate the actual cartesian state vector directly from time t_i (corresponding to TA_i) to time $t_i + \Delta t$ (corresponding to TA_f). The VMM is computed at the actual distance of closest approach. This is only valid strictly speaking if the DCA is less than the terminal rendezvous radar maximum range.

6) Distance of Closest Approach Computation - The DCA is found by a four level iterative search technique. Since closest approach nominally occurs at 180° TA on the vehicle orbit this value is used as an initial guess for the computation of the separation distance R. The vehicle orbit is stepped around in 1° TA increments until the minimum R is bounded. Then the TA increment is reduced to $.1^\circ$, $.01^\circ$ and finally to $.001^\circ$. The nominal miss for the case analyzed here was $\sim 60m$ at $TA = 180.001^\circ$.

3. Results

Navigation accuracies are presented for the DSN tracking arcs during the Mars encounter phase and for both the DSN and TV tracking arcs during the in-orbit (rendezvous) phase. DSN data fixes the vehicle state (position and velocity) relative to Mars whereas TV tracking is used to determine the relative state between satellite and vehicle. These accuracies were input to the

Monte Carlo simulation program to obtain statistics of total ΔV and distance of closest approach.

a. Navigation Accuracy - Table III-12 contains data characterizing the encounter control and knowledge uncertainties in the B-plane system. In this system the error distributions are represented as ellipses with semi-major axes SMAA and semi-minor axes SMIA. The ellipse orientation in the B-plane is specified by the angle Θ_{MI} . This angle is measured from the T axis counterclockwise to the minor axis of the ellipse. A small Θ_{MI} angle means that the major axis of the ellipse is along the R axis.

Table III-12 Encounter Control and Knowledge Dispersions
Based on DSN Tracking Only

	SMAA	SMIA	Θ_{MI}
Control	279.7 km	35.6 km	.47°
Knowledge	195.0 km	31.9 km	.69°

Accuracies for the 4 in-orbit O.D. (orbit determinations) computations are found in Table III-13. The RSS (root-sum-of-squares) of the cartesian ecliptic position and velocity error components are presented. Note that the phasing orbit accuracy (prior to OOM) is assumed the same as the observation orbit accuracy (prior to LIM).

Table III-13 In-Orbit Knowledge Dispersions
Based on DSN Tracking Only

DSN Update	Vehicle State Error	
	RSS Pos. (km)	RSS Vel. (m/s)
DSN1 (Prior to PCM)	.472	.045
DSN2 (Prior to POM)	.337	.041
DSN3 (Prior to OOM)	12.78	.814
DSN4 (Prior to LIM)	12.78	.814

The vehicle state knowledge uncertainty is much larger in the observation orbit than in the capture orbit. This is because in the former case the vehicle is closer to the planet for longer periods of time and hence is more affected by the uncertain Mars gravity field. Once in the observation orbit (during the 1st orbit) the vehicle and satellite states are simultaneously solved for using DSN and TV data acquired and the TV1 tracking arc extending from 0° to 270° true anomaly. The simultaneous solution yields the most accurate relative vehicle/satellite state with the Kalman/Schmidt filter. After the LIM at 210° , it is necessary to perform a midcourse correction maneuver (MCCM) on the 2nd observation orbit at 150° true anomaly. TV data acquired on the TV2 arc, extending from 0° to 150° , is used to re-solve for the vehicle state (whose estimate was corrupted by LIM execution error).

As mentioned earlier, samples of vehicle and satellite state errors representative of the simultaneous TV1 solution are generated in approximate fashion in the Monte Carlo simulation. Samples of vehicle state error are obtained from a 6×6 state covariance matrix representative of DSN tracking only (from 0° - 270° true anomaly) in the presence of Mars gravity harmonic uncertainty. The cartesian satellite estimates are formed from the vehicle estimates and samples of the relative vehicle/satellite errors generated from a relative state covariance matrix corresponding to the simultaneous solution (i.e., the relative covariance matrix was computed from the 10×10 covariance matrix of error in the 6 vehicle components and 4 satellite elements, a, i, Ω, MA). With perfect DSN tracking (i.e., perfect vehicle state estimates) the satellite state and relative state accuracies are as presented in Table III-13. These data represent the limiting accuracies obtainable with the TV

system for a 1/10 min data rate and 10 sec noise figure. (A priori error is the error before the data is processed and a posteriori error is the error after the data has been processed. Note that the epoch for the a priori error is at the beginning of the tracking interval and for the a posteriori error at the end of the interval.) Standard deviations of the 4 satellite ephemeris errors considered, i.e., semi-major axis, inclination, longitude of ascending node, and mean anomaly, are denoted as σ_a , σ_i , σ_Ω , and σ_{MA} , respectively. Note that when no DSN error is present (i.e., with a perfect vehicle estimate) only the satellite state need be solved-for from TV data only.

After the two TV tracking segments the RSS relative state error (or equivalently the RSS satellite state error) is reduced below .2 km and .02 m/s. When DSN noise and Mars gravity uncertainty are present, the accuracies of Table III-14 result. Here the relative state accuracies after the two intervals of tracking are also very good, i.e., RSS position error is less than 1 km and RSS velocity error less than .4 m/s. Note that the TV1 a posteriori error is the a priori error for TV2. The a posteriori vehicle error for TV1 is not representative of DSN accuracy in the presence of gravity uncertainty (presented as DSN3 in Table III-13). These are DSN noise-only results for the vehicle state when a simultaneous solution is performed. Only the relative state accuracies from Table III-15 are used in the Monte Carlo simulation.

b. Statistical ΔV and R99 - Table III-16 contains a summary of statistical results for the rendezvous to Deimos. Each successive case (1 through 5) contains an additional error source. The simulation is constructed so that the same sequence of random errors occurs for each error source regardless of what other

Table III-14 Navigation Accuracy in Observation Orbit with Noisy TV Data and Perfect DSN

Data Arc	Solve-for State	A Priori (km x km x km/mps x mps x mps)			A Posteriori (km x km x km/mps x mps x mps)		
		Vehicle	Satellite	Relative	Vehicle	Satellite	Relative
TV1: TV + Perfect DSN 0° - 270° (First Observation Orbit)	Satellite	0.0/0.0	$\sigma_a = 7.5 \text{ km},$ $\sigma_i = .1^\circ;$ $\sigma_\Omega = 1.5^\circ;$ $\sigma_{MA} = 1 \times 10^{-4}$	600x120x37 6.9x35x1.1	0.0/0.0	.30x.14x.14 .07x.003x.03	.30x.14x.14 .07x.003x.03
TV2: TV Only 0° - 150° (Second Observation Orbit)	Satellite	0.0/0.0	.30x.14x.14 .07x.003x.03	.30x.14x.14 .07x.003x.03	0.0/0.0	.16x.03x.07 .01x.01x.005	.16x.03x.07 .01x.01x.005

error sources are present (e.g., the same sequence of encounter errors occur whether encounter errors are considered by themselves, case #1, or whether considered in conjunction with execution error, case #2). Only in this way does it make sense to compare the 50 sample statistical results for the various cases.

Table III-16 Summary of Results for Rendezvous to Deimos

Case Number and Description	ΔV_{STAT}	R99
1. Encounter Errors Only	55.7 m/s	.9 km
2. Case 1 + Execution Error	82.7 m/s	12.2 km
3. Case 2 + Ephemeris Error	85.5 m/s	12.2 km
4. Case 3 + Noisy TV	86.4 m/s	11.9 km
5. Case 4 + DSN Error	98.3 m/s	20.9 km
6. Case 5 with No TV	85.6 m/s	213.5 km

With encounter errors only (i.e., with perfect execution, perfect knowledge of satellite ephemeris, and perfect TV and DSN tracking) as case #1 shows, the 99 percentile closest approach radius (R99) is minimal because targeting and execution are perfect. In case #2 targeting is perfect but inaccurate execution causes R99 to increase to 12.2 km. The major ΔV_{STAT} contributors are encounter error and execution error, while the source of DCA miss is largely execution error and DSN error (see case #5). Note from case #6 that an unacceptable R99 (i.e., an R99 greater than the maximum terminal radar range of 100 km) is obtained when realistic vehicle/satellite TV tracking is not used. ΔV_{STAT} in this case is reduced, however, because ΔV is not expended in taking our errors which are not known to exist.

Table III-17 shows the ΔV_{STAT} breakdown by maneuver. Note that ΔV_{STAT} for the first four maneuvers are set by encounter and execution error only. In-orbit DSN error has a negligible

effect on the PCM, POM and OOM. It does, however, affect the last three maneuvers. The strong dependence of one maneuver on the others is exhibited by the fact that the RSS of the individual maneuver ΔV_{STATs} greatly exceeds the ΔV_{STAT} for the total ΔV (as presented in Table III-16. As an example of how this comes about, consider the POM and the OOM. The energy expenditure required to go from the capture orbit to the observation orbit is constant (since the phasing orbit period is always less than the capture orbit period). For this to be truly independent of the phasing orbit period requires that the sum of the POM ΔV and OOM ΔV be constant and therefore equal to the nominal value of 288 m/s. Because of this, the POM ΔV excursions may be large but the sum of the POM ΔV and OOM ΔV will be near 288 m/s. In this way the POM ΔV_{STAT} may be 120.7 m/s while ΔV_{STAT} for the sum of POM and OOM ΔV s is only 7.4 m/s.

In Table III-18, ΔV_{STAT} is presented for various combinations of maneuver ΔV s. As case #2 shows, the ΔV_{STAT} to establish the observation orbit is 25.9 m/s. Also, since the total ΔV_{STAT} is nearly the RSS of case #2 (to establish the observation orbit) and case #4 (to rendezvous out of the observation orbit) these two events are largely uncorrelated. These data may be used to estimate the ΔV_{STAT} for the rendezvous to Phobos. This mission proceeds like the Deimos mission up to establishment of the observation orbit. After several revolutions in the observation orbit, a maneuver is performed at apoapsis to raise the periapsis altitude (by an amount less than the altitude of Phobos) so that the resultant orbital period allows for proper vehicle/Phobos phasing. The period is determined so that the proper phasing occurs at the time of a second maneuver at apoapsis passage. This maneuver raises the periapsis altitude to the altitude of Phobos. Since energy is being put in the observation

Table III-17 Maneuver ΔV_{STAT} for Rendezvous to Deimos

Case Number and Description	Maneuver ΔV_{STAT} s					
	MOI	PCM	POM	OOM	LIM	MCC
1. Encounter Errors Only	17.7	9.6	120.0	0.3	26.5	0.0
2. Case 1 + Execution Error	25.2	13.3	120.7	0.4	31.7	31.7
3. Case 2 + Ephemeris Error	25.2	13.3	120.7	0.4	36.0	39.8
4. Case 3 + Noisy TV	25.2	13.3	120.7	0.4	35.8	40.3
5. Case 4 + DSN Error	25.2	13.3	120.7	0.2	34.6	47.0
6. Case 5 with No TV	25.2	13.3	120.7	0.4	32.5	31.8
						20.4
						26.8
						26.9
						26.7
						27.7
						28.1

Table III-18 ΔV_{STAT} for ΔV Combinations

ΔV Combination	ΔV_{STAT}
1. POM + OOM	7.4 m/s
2. MOI + PCM + POM + OOM	25.9 m/s
3. LIM + MCC	87.7 m/s
4. LIM + MCC + VMM	100.7 m/s
5. Total ΔV	98.3 m/s

orbit with each of the apoapsis maneuvers, the sum of the two will tend to be constant just as it was for the POM and OOM in the Deimos rendezvous case.* The ΔV_{STAT} for the two maneuvers will therefore be small and probably in the order of ~ 10 m/s. After the second apoapsis maneuver, the rendezvous to Phobos proceeds like the rendezvous to Deimos, i.e., with an LIM on MCC and finally with the VMM. The ΔV_{STAT} for these last three maneuvers will be estimated as 100 m/s since the relative TV tracking geometry, the DSN accuracies, and the Phobos ephemeris errors will be similar to what they were for the Deimos rendezvous case. If these three ΔV_{STATs} are RSSed the resultant ΔV_{STAT} for the rendezvous is ~ 103 m/s. Essentially, then, the ΔV_{STAT} for rendezvous to Deimos or Phobos is about the same (i.e., 98.3 m/s to 103.0 m/s).

The R99 for rendezvous for Phobos also will be the same as the R99 for the Deimos rendezvous. This is because the same TV system, data types and data characteristics will be used. Also, the closing geometry for Phobos will be approximately the same as it is for Deimos.

4. Conclusions

a. Need for TV - The TV tracking system is required in order to reliably get within a closest approach radius (R99) of 100 km (i.e., within the terminal rendezvous radar range). With the TV system, approach radii of the order of 21 km are expected whereas without the TV the best that can be achieved is ~ 214 km. These

* A more costly mode for rendezvous to Phobos (~ 80 m/s more), proceeds out of the observation orbit exactly as the rendezvous to Deimos proceeds out of the capture orbit. This is illustrated in Figure III-20.

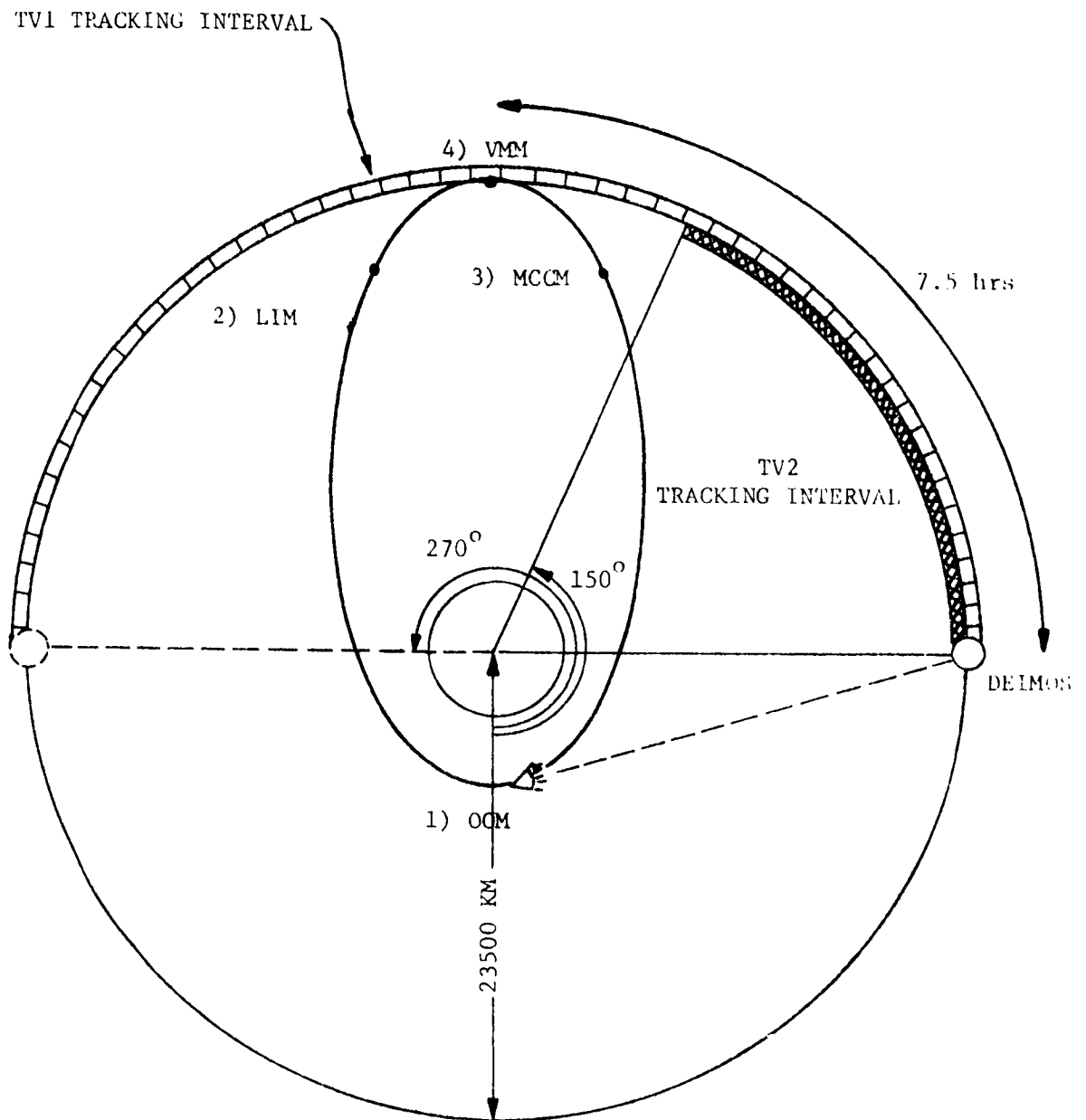


Figure III-20 Schematic for Alternate Mode of Rendezvous to Phobos

results depend on a TV "image" data rate of 1/10 min with the target satellite visible a good portion of the two orbits prior to rendezvous.

b. ΔV_{STAT} Budget Requirements - The ΔV_{STAT} budget for rendezvous to either Deimos or Phobos is 100 m/s. This is for the baseline mission only. The subject of the variation of this quantity with launch/encounter date is covered in Phase II.

c. Error Source Evaluation - Encounter and execution errors very nearly account for the entire ΔV_{STAT} requirement. The breakdown is as follows:

Encounter Error	56%
Execution Error	28%
Ephemeris Error	3%
TV Noise Error	1%
DSN Error	12%

Viking execution errors were assumed throughout. Uncertainty in the gravitational constant for Mars had a negligible effect on the rendezvous characteristics. R99 is determined primarily by the level of execution error and DSN error. It is not, however, sensitive to Mars ephemeris uncertainty. The question of the sensitivity of ΔV_{STAT} and R99 to the various error sources was explored in the Phase II study.

REFERENCES

- III-1 Wilkins, G. A.: "The Determination of the Mass and Oblateness of Mars from the Orbits of Its Satellites." Reprinted from *Mantles of the Earth and Terrestrial Planets*, Interscience Publishers, 1967.
- III-2 Garcia, H.: *The Mass and Figure of Saturn by Astrometry of Its Five Satellites*. Ph.D. Thesis, Georgetown University, 1970.
- III-3 Hoffmann, L. H.; Green, R. N.; Young, G. R.: *Thrusting Trajectory Minimization Program for Orbital Transfer Maneuvers*. NASA TN D-6120, 1971.
- III-4 Anon.: *Viking '75 Project Specification, Appendix A: Mission Requirements on System Design*. RS-3203001, 1971.

IV. System Descriptions

IV. SYSTEM DESCRIPTION

A. SYSTEM OVERVIEW

This section presents the overview of the baseline Phobos/Deimos rendezvous and landing spacecraft. Details of the subsystems are presented in the remaining sections of this chapter.

During the exploratory design phase of the study we investigated several alternate spacecraft designs with the basic goal of each design concept being, how do we maximize the spacecraft's payload capability while at the same time minimizing the spacecraft's structural weight. The incentive, of course, is the potential cost savings that may be achieved while still delivering adequate payloads. In keeping with this philosophy then, a baseline design was selected that provides adequate payload capability; flexibility of payload usage; i.e., in-situ science packages, or rover applications; minimum weight; minimum modifications required to be made to existing payload delivery system (Viking '75 Orbiter), and at the same time relatively low total program costs.

Table IV-1 presents the five basic design options that were identified during the systems study. Each of the design options presented meet all study objectives and guidelines, and are all capable of accommodating the described baseline mission profile.

Referring to the five basic design options A through E identified in Table IV-1, only Options B, C, and D utilize the full Titan IIIE/Centaur Launch vehicle capability for the 1979 opportunity (4157 kg). Option A, which is our baseline configuration, weighs 3608 kg (7955 lb) at injection, and is capable of delivering a 482 kg (1063 lb) lander to the surface of Phobos. Option E represents a configuration in which the entire orbiter

Table IV-1 Spacecraft Options Considered

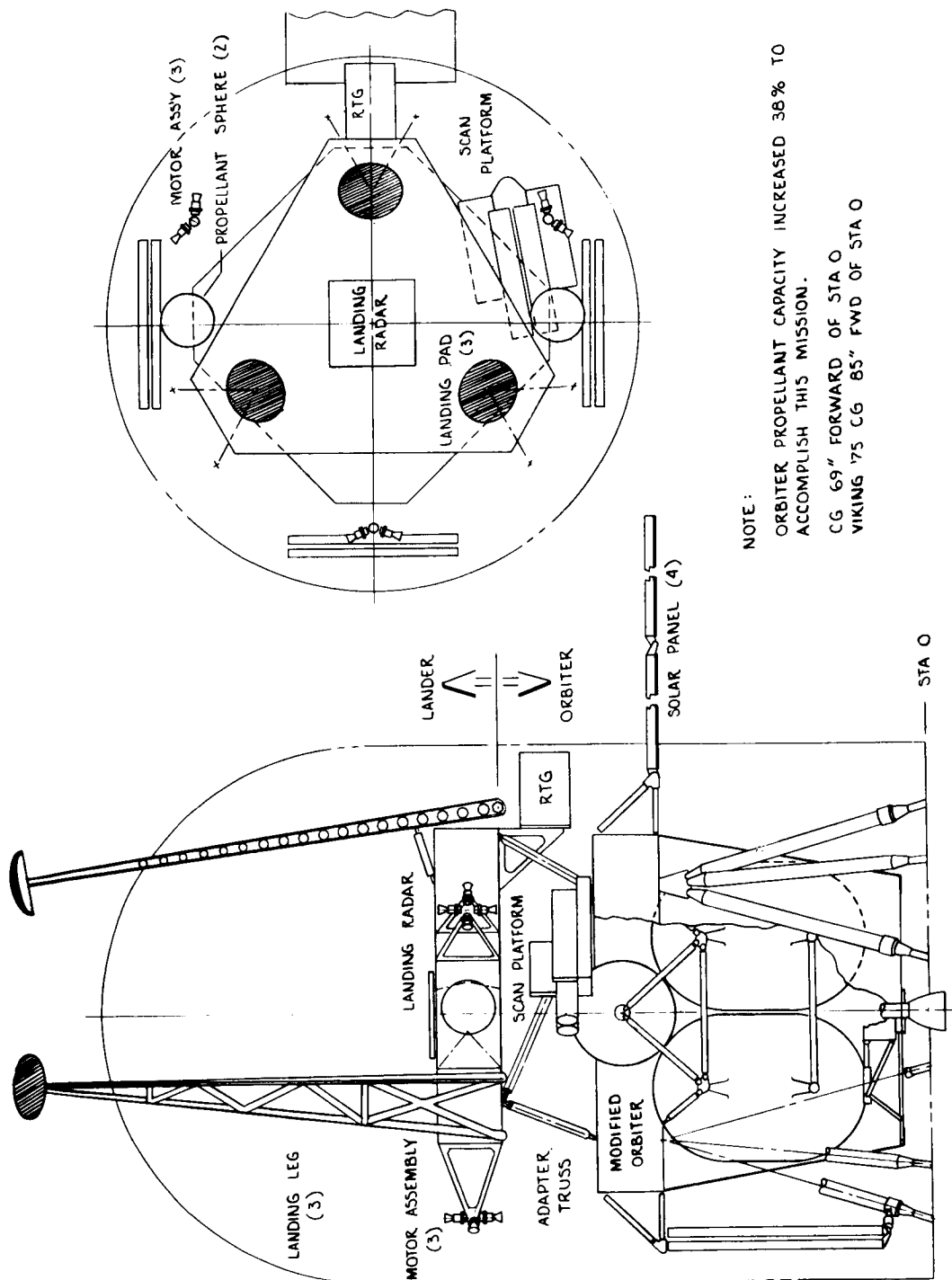
- A. Stretched Viking Orbiter (38% propellant increase) with separable landed payloads.
- B. Modified Viking Orbiter (60% propellant increase) with separable landed and sample return payloads.
- C. Staged orbiter concepts with separable landed and sample return payloads.
- D. Stretched Viking Orbiter with Direct Entry Mars Lander and Phobos/Deimos payloads.
- E. Landed orbiter with science packages.

delivery system is landed on the satellite surface rather than using the separable lander concept. Greater landed payloads and more efficient use of supporting subsystems can be achieved with this concept since certain subsystems such as the communication and power subsystems can be used to support payload landed operations as well as utilized during the cruise phase of the mission. Adapting an interplanetary cruise vehicle like the Viking Orbiter to a lander role does present added performance risk however. Option B represents an attempt to utilize the maximum launch capability of the Titan IIIE/Centaur launch vehicle. In order to accomplish this design, more extensive design changes are required to be made to the Viking '75 Orbiter. We must now employ a four-tank propellant system in lieu of the two-tank concept utilized in Option A. This change is required to maintain the spacecraft's c.g. location (in the launch configuration) within an acceptable envelope so that design launch dynamic loads are

not exceeded. This configuration has an injected weight of 4159 kg (9168 lb) and can deliver a 635 kg (1400 lb) payload to Phobos. A staged configuration was also investigated in an attempt to improve our spacecraft mass fraction efficiency. The resulting configuration, Option C, employs a two stage concept in which the first stage is the basic Viking '75 Orbiter propulsion system and the second stage is similar in concept to the Mariner '71 propulsion system. The first stage is jettisoned after performing the Mars orbit insertion (MOI) maneuver. Again this configuration weighs in at the full launch vehicle capability weight of about 4157 kg but yields a delta payload increase of only 23 kg compared to Option B, while at the same time requiring much more severe design changes to be made to the Viking Orbiter. Option D illustrates how a combination Mars landing and a Phobos/Deimos rendezvous vehicle might be configured. The Direct Entry Lander design was originally developed by the Martin Marietta Corporation's Viking Project in 1970 as an alternate design for the 1975 Mars mission. The lander design is separated from the orbiter some six hours before Mars encounter and enters the atmosphere directly from the approach trajectory to the surface. The orbiter then proceeds on through the baseline mission profile to Phobos and delivers a 214 kg (471 lb) payload to the satellite. The direct entry mode was studied during the Phase III study effort, and a detailed discussion of this concept is presented in Volume III of this report.

1. Selected Baseline Configuration

The 3608 kg baseline Phobos/Deimos spacecraft is shown in its launch configuration within the standard Viking fairing in Figure IV-1. As can be seen from the figure, this configuration is well within the allowable shroud dynamic envelope used for Viking '75. Only the landing gear of the separable lander protrude outside



NOTE:
 ORBITER PROPELLANT CAPACITY INCREASED 38% TO
 ACCOMPLISH THIS MISSION.
 CG 69" FORWARD OF STA O
 VIKING '75 CG 85" FWD OF STA O

Figure IV-1 Phobos/Deimos Lander/Rover Baseline Configuration

the envelope; however, this represents no problem since they merely extend into a void in the nose of the payload fairing. The Orbiter/Launch Vehicle adapter truss supports the Phobos/Deimos spacecraft at four symmetrical points and is attached to the modified Viking Orbiter with ordnance operated bolts and springs. This forms the Phobos/Deimos spacecraft-launch vehicle separation plane. The lander/orbiter adapter truss is a completely new design. The forward end of the truss attaches to the lander at three symmetrically located points. The aft end of the truss attaches to the orbiter, at four symmetrical points, mating with the same attachments on the orbiter as is presently utilized for the baseline Viking '75 Lander. Separation is provided by means of ordnance operated bolts and springs at the lander interface. The adapter truss remains attached to the orbiter after lander separation.

The Phobos/Deimos spacecraft is comprised of two major components, a modified Viking '75 Orbiter, and a separable lander/rover vehicle. The orbiter dry weight is approximately 983 kg. This together with 1928 kg of fuel gives a total loaded weight of 2911 kg. The lander/rover loaded weight is 482 kg.

The orbiter configuration is essentially the same as that presently conceived for the Viking '75 Orbiter with some modifications made to meet the 1979 Phobos/Deimos mission requirements. The most significant modification is the "growth" of the propulsion system to accommodate 1928 kg of expendable propellant. This represents a 38% increase in propellant loading when compared to the Viking '75 Orbiter. In order to handle this additional propellant the two main propellant tanks are increased 12.7 cm in diameter. The pressurant sphere was also increased by 5.6 cm. The truss members attaching the tanks to one another and to the orbiter octagon structural body have been

varied in length and in size to accommodate the increased tank size and loading.

Orbiter science instruments are mounted on a scan platform similar to the design used on the Viking '75 Orbiter. The two TV cameras (Camera A and B) have been retained. The IR thermal mapper and the Mars atmospheric water detector instruments currently on board the VO have been replaced by an IR spectrometer. Total science weight allocated to the baseline orbiter is 45 kg. The platform is mounted on the upper surface of the octagonal orbiter main structure in a manner which permits it to be deployed to the required cone and clock positions for scanning the satellites. Camera A serves a dual purpose, it not only provides the capability for obtaining wide-angle photographs of the surface of the satellite, but is also used for approach navigation to the satellites.

The baseline lander/rover vehicle is configured in much the same manner as that used for the baseline Mars Viking Lander. The external arrangement is shown in Figure IV-2. As can be seen, the enclosed web box body structure provides Mars satellite surface environmental protection for 81.5 kg (180.0 pounds) of science and supporting subsystems. Supporting subsystems which are attached to the lander body by means of an equipment mounting plate located on the lander upper surface are all identical to their Mars Viking counterparts with only one exception. This one exception is the rendezvous radar which is substituted for the Mars Viking radar altimeter. Design of the rendezvous radar is based on a modification to the Viking '75 Lander radar altimeter.

The three-legged landing gear configuration as shown in Figure IV-2 has a ratio of leg spread radius to CG height of two to provide suitable landing stability. The three-legged configuration was chosen based on a weight, cost, and complexity in

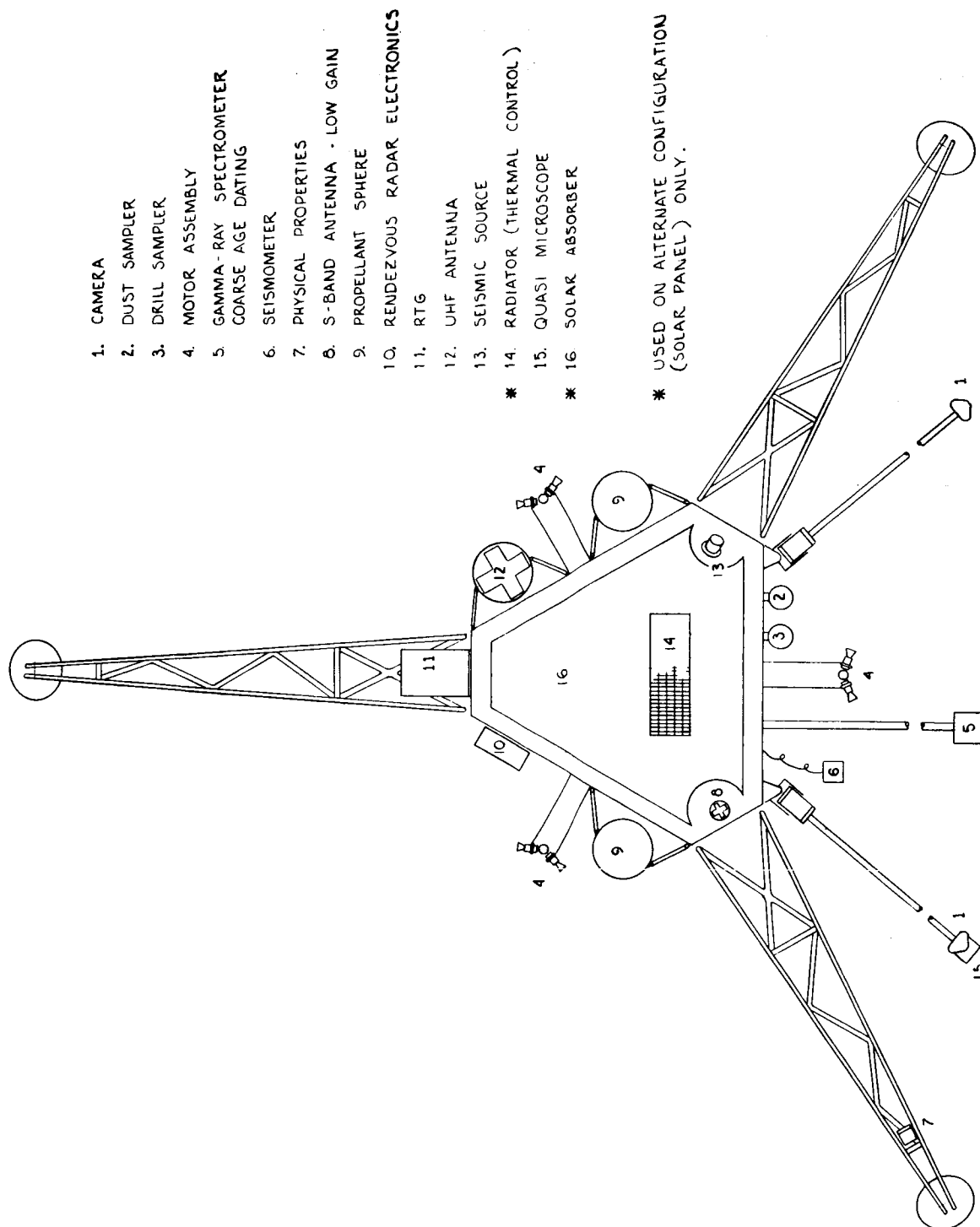


Figure IV-2 Lander/Rover External Configuration

comparison with four-legged and ring/disc configurations. Besides providing inherent post-landed stability, it also ensures consistent performance through predetermined load paths. The landing legs are based on proven design principles from Surveyor, Apollo Lunar Module and Viking '75.

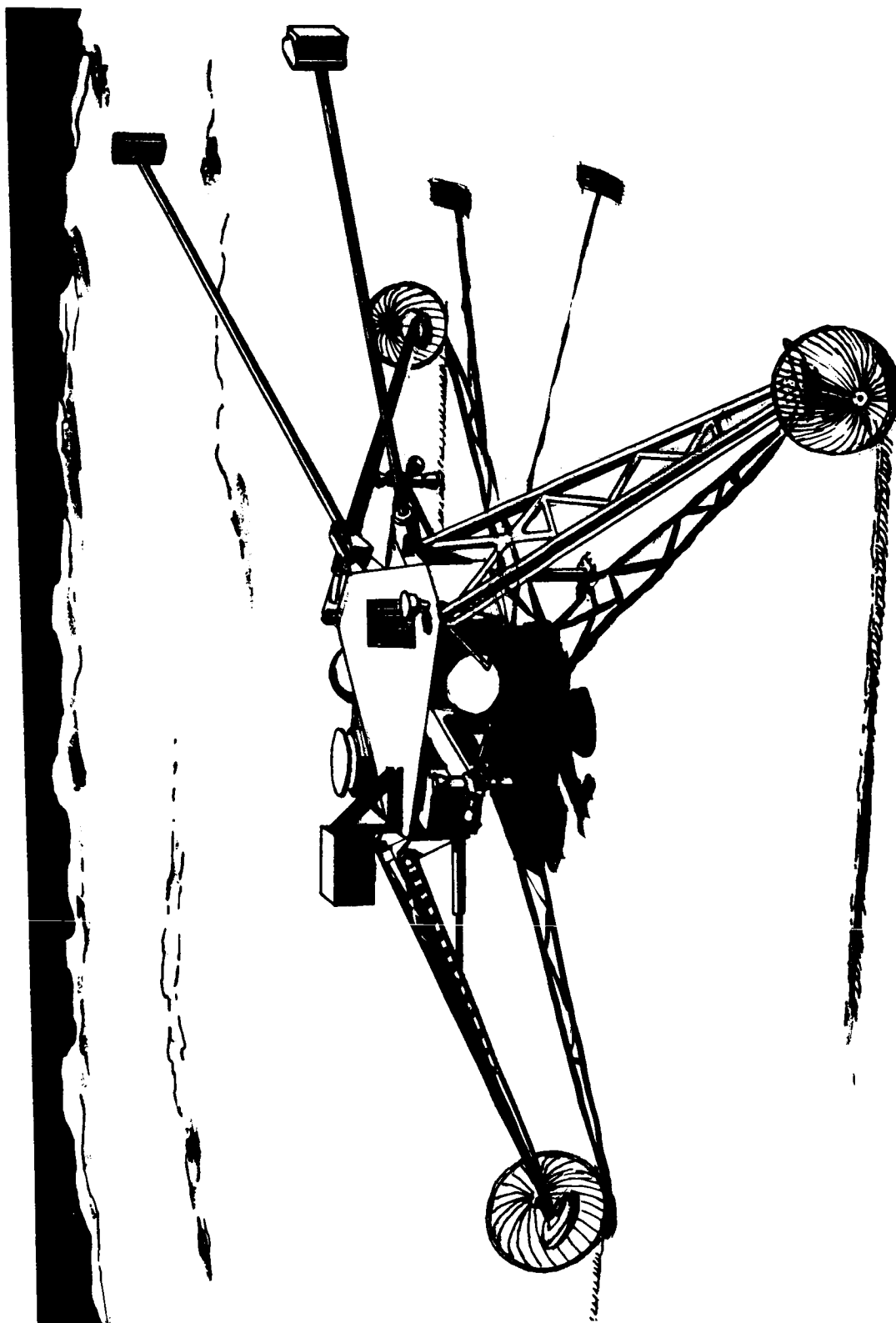
A wheeled roving concept for the lander vehicle was also studied as shown in Figure IV-3. This concept employs three 2.0 m diameter "umbrella-frame" wheels in lieu of the landing pads utilized on the baseline stationary lander.

The baseline lander/rover uses an RTG power source as shown in Figure IV-4. The mounting of the RTG was chosen to minimize radiation problems with science instruments on the lander/rover and to minimize "hot spot" effects on the orbiter during the time the lander/rover is mated to the orbiter. An alternate solar array power subsystem was also evaluated. This installation is shown in Figure IV-5 and consists of an articulated solar array of 3.9 square meters (42 square feet) and four eight ampere hour nickel cadmium batteries of the type used in the Viking '75 Lander. These batteries are required to provide the high peak power during landing and to provide power for landed operations during night periods. The solar array is stowed flush with the upper surface of the lander/rover during the descent and landing phase of the mission. Once the lander/rover has settled on the surface the solar array is deployed and aligned to the Sun line by means of a two degree of freedom motor driven boom.

The science payload carried by the lander/rover is shown in Table IV-2. Total weight of the science instruments is 81.5 kgs (180 pounds).

The weight breakdown for the baseline configuration is shown in Table IV-3 and IV-4 respectively.

Figure IV-3 Wheeled Lander/Rover



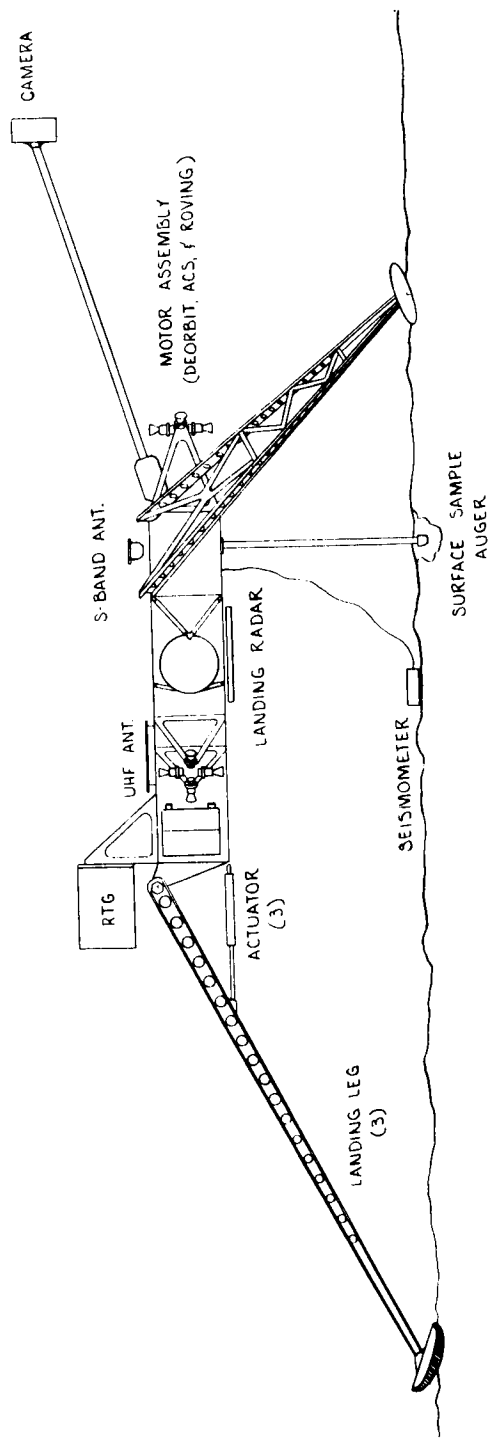
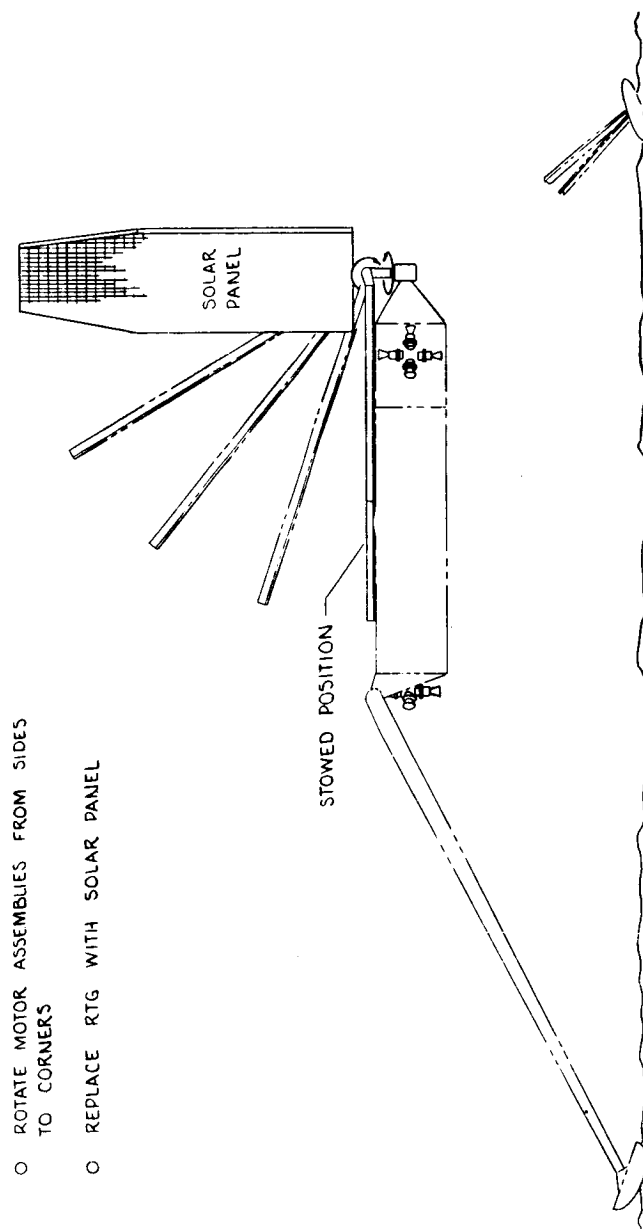


Figure IV-4 Lander/Rover Landed Configuration



- ROTATE MOTOR ASSEMBLIES FROM SIDES TO CORNERS
- REPLACE RTG WITH SOLAR PANEL

Figure IV-5 Alternate Lander/Rover Configuration

Table IV-2 Nominal Science Payload

<u>ORBITER</u>	<u>WEIGHT (KGS)</u>	<u>POWER(WATTS)</u>	
		<u>AVERAGE</u>	<u>PEAK</u>
1. Imagery	38.1	45	--
2. IR Spectrometer	<u>6.8</u>	<u>10</u>	<u>20</u>
Total Orbiter Science:	44.9 (99 lb)	55	20
<u>LANDER</u>			
1. Imagery	11.3	18	22
2. Quasi-Microscope	9.1	1	10
3. Drill Sampler	8.1	2	50
4. Dust Sampler	1.8	1	5
5. Integrated Geology (Alpha Backscatter, X-Ray Fluorescence, X-Ray Diffraction)	10.4	10	20
6. Seismometer	2.7	2	6
7. Seismic Source	7.7	1	2
8. Gamma-Ray Spectrometer	6.8	2	3
9. Coarse Age Dating	22.7	10	50
10. Physical Properties	<u>0.9</u>	<u>1</u>	<u>5</u>
Total Lander Science:	81.5 (180 lb)	48	173

Table IV-3 Baseline Spacecraft System Weight Summary (kgs)

Orbiter			
Structures & Mech. Devices	229.5		
Communication	46.1		
Modulation/Demodulation	9.3		
Power	129.2		
Computer Command	20.0		
Flight Data	13.8		
Attitude Control	47.6		
Pyrotechnics	5.0		
Cabling	54.4		
Data Storage	22.3		
Relay Telemetry	5.4		
Imaging & IR Spectrometer	44.9		
Propulsion - Inerts	304.1		
P/L - Orbiter Adapter	13.6		
Contingency (4%)	37.8		
Orbiter Dry Weight	983.0	(2167.1 lb)	
Expendable Propellant			
Orbiter Loaded Weight	2910.8	(6417.1 lb)	
Separable Payload Allocation	482.2	(1063 lb)	
Orbiter/Launch Vehicle Adapter			
Project Reserve	68 (150 lb)		
LVMP	56.7 (125 lb)		
	90.7 (200 lb)		
Injected Payload Weight	3608.4	(7955.1 lb)	

Table IV-4 Lander/Rover Weight Summary (kgs)

Structures	107.9 (237.9)	Guidance & Control (cont)	
Lander Body	25.0	Rendezvous Radar	10.4
Equip. Mtg Pit	22.6	GCSC	20.4
Bottom Pit	9.1	VDA	3.2
Landing Legs	31.8	Wire Harness	26.9 (59.3)
Equip. Sprt	10.0	Pyrotechnics	16.4 (36.1)
Mech	9.4	Propulsion	56.0 (123.5)
Thermal Control		Engines	11.6
Insulation	4.5	Tanks	5.4
Paint	4.5	Filters, Valves	0.9
Heaters	2.7	Plumbing	5.6
Power		Pressurant	1.2
Battery	6.3	Residual Prop.	0.9
RTG	32.0	Usable Prop.	30.4
Load Banks,	6.9	Communication	11.1 (24.6)
Control Logic		UHF Transmitter (1w)	0.9
PCDA	13.9	UHF Antenna	1.8
Telemetry		S-Band LGA	0.3
DAPU	9.1	S-Band Comm Rec (2)	4.5
Tape Recorder	8.6	S-Band Detector	3.6
DSM	3.6	Science	81.5 (180.0)
Transducers	1.8	Contingency	44.3 (97.5)
Guidance & Control		Lander/Rover Loaded Wt	482.0 (1063.0)
ARU	7.7		
VRU	2.3		

2. Alternate Spacecraft Configuration

As discussed earlier an attractive alternate spacecraft design, in which the entire orbiter delivery system is landed on the satellite surface was also evaluated (Option E of Table IV-1). This concept is shown in its launch configuration in Figure IV-6. Greater landed payloads are achievable (498.9 kg versus 82.2 kg for the baseline configuration) and more efficient use of supporting subsystems can be realized with this concept since certain subsystems, such as the communication and power subsystems, can be used to support payload landed operations as well as utilized during the cruise phase of the mission. Several hardware modifications are required in order to adapt the Viking Orbiter to a lander role. Some of the more important modifications are:

- 1) Addition of four landing legs;
- 2) Addition of a terminal descent propulsion system;
- 3) Addition of a rendezvous radar to assist in landing operations;
- 4) Addition of flip covers mounted over the existing Viking Orbiter temperature control louver system. These flip covers serve to de-activate the louvers during surface operations. Also required are the addition of heaters and phase change material to equalize the diurnal variations, and,
- 5) Adding provisions to enable the outboard panels of the solar array to be deployed so that they droop 32° below the horizontal during landed operations. This solar panel configurational arrangement optimizes the solar panel power output during the landed sequence of the mission.

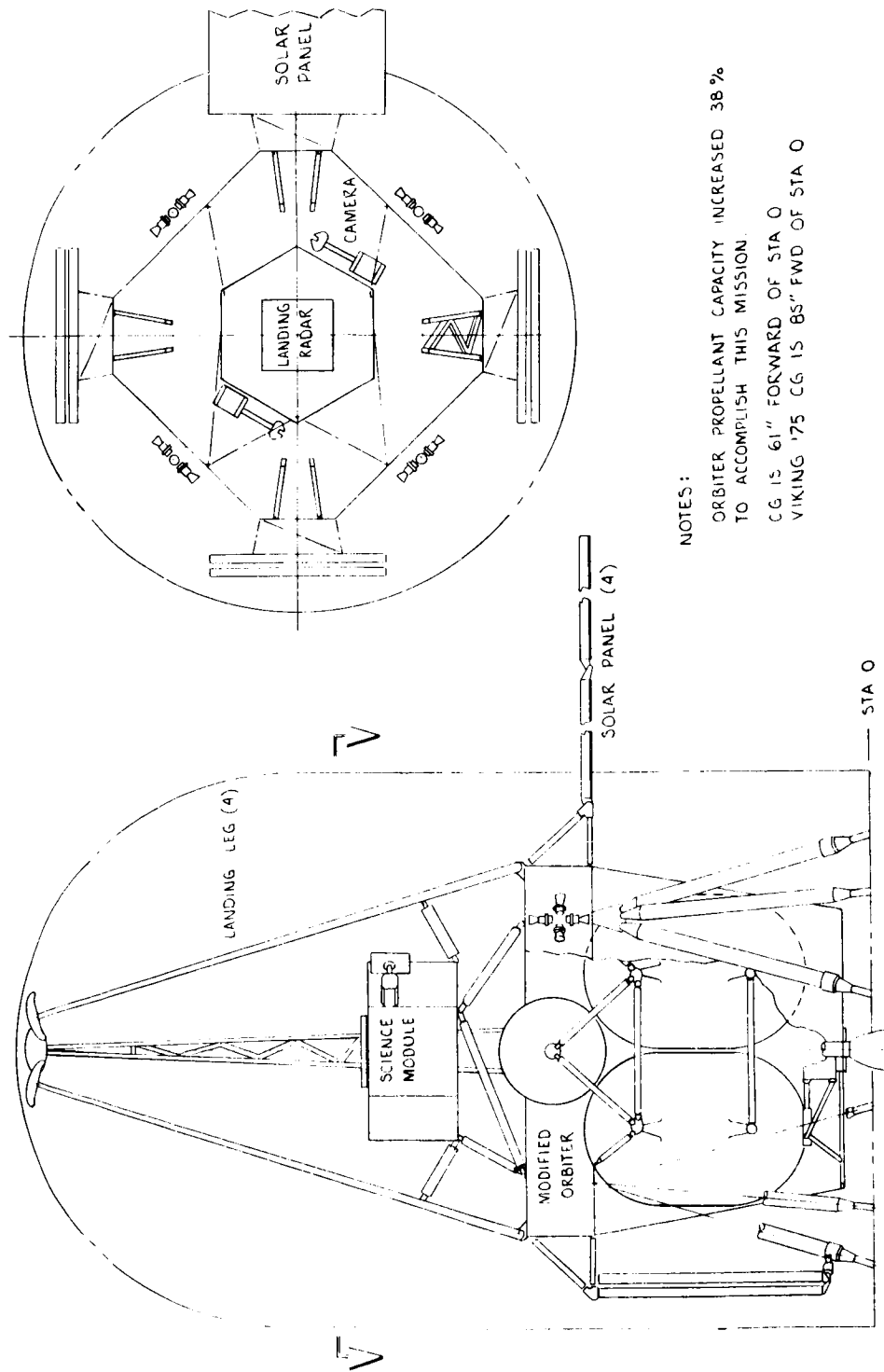


Figure IV-6 Phobos/Deimos Landed Orbiter (Alternate Configuration)

Figure IV-7 shows the landed Orbiter configuration on the surface of the satellite. A weight summary of the landed orbiter concept is given in Table IV-5.

3. Spacecraft Configurations for Alternate Missions

Several spacecraft system studies were evaluated to determine what alternate mission modes might be flown since neither the baseline or the alternate system concepts utilized the full launch vehicle capability for a 1979 launch opportunity.

Two alternate mission modes were identified; a sample return mission to the Martian satellites, and a combined Mars Lander and Phobos/Deimos mission. Spacecraft configurations that would support these missions are presented in Figures IV-8, IV-9, and IV-10. As can be seen in Tables IV-6, IV-7, and IV-8, the full injected capability of 4157 kg is utilized. The spacecraft configurations of Figures IV-8 and IV-9 can deliver payloads of 635 kgs (1400 pounds) and 657.7 kgs (1450 pounds), respectively. These payloads are adequate to handle sample return missions from either of the Martian satellites. The combined Mars Lander and Phobos/Deimos spacecraft configuration of Figure IV-10 can deliver a 1210 kg lander to Mars and a 214 kg payload to either Phobos or Deimos.

These preliminary systems studies formed the basis for the more comprehensive studies conducted during Phase II and III, and are reported on in detail in Volumes II and III of this report.

B. GUIDANCE AND CONTROL

This section describes the G&C subsystems used during the interplanetary transfer, orbital maneuver, rendezvous and satellite landing operations of the baseline Phobos/Deimos mission. A description of the mission timeline was given in the MA&D

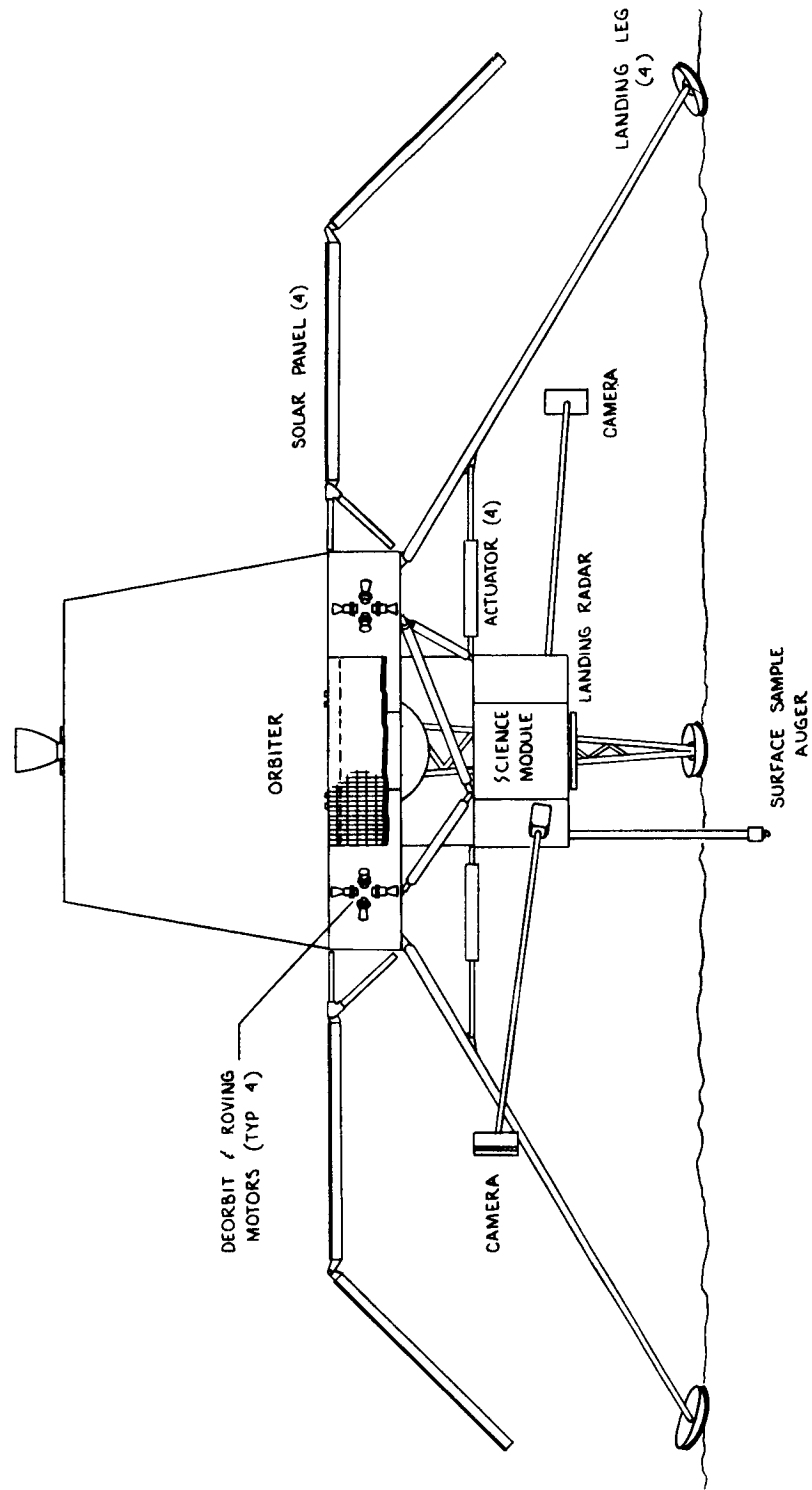


Figure IV-7 Phobos/Deimos Landed Orbiter on Surface

Table IV-5 Phobos/Deimos Landed Orbiter System Weight Summary (kgs)

Orbiter			
Structures & Mech Devices	274.9		
Communication	36.4		
Modulation/Demodulation	9.3		
Power	129.2		
Computer Command	20.2		
Flight Data	13.8		
Attitude Control	47.6		
Pyrotechnics	5.0		
Cabling	54.4		
Data Storage	22.3		
Propulsion - Inerts	304.1		
P/L - Orbiter Adapter	6.8		
Contingency (4%)	37.0		
Orbiter Dry Weight		961	(2130 lb)
Expendable Propellant	1927.8 (4250 lb)		
Orbiter Loaded Weight		2888.8	(6380 lb)
Landed Payload Allocation		498.9	(1100 lb)
Orbiter/Launch Vehicle Adapter	68.0		
Project Reserve	56.7		
LVMP	90.7		
Injected Payload Weight		3603.1	(7955 lb)

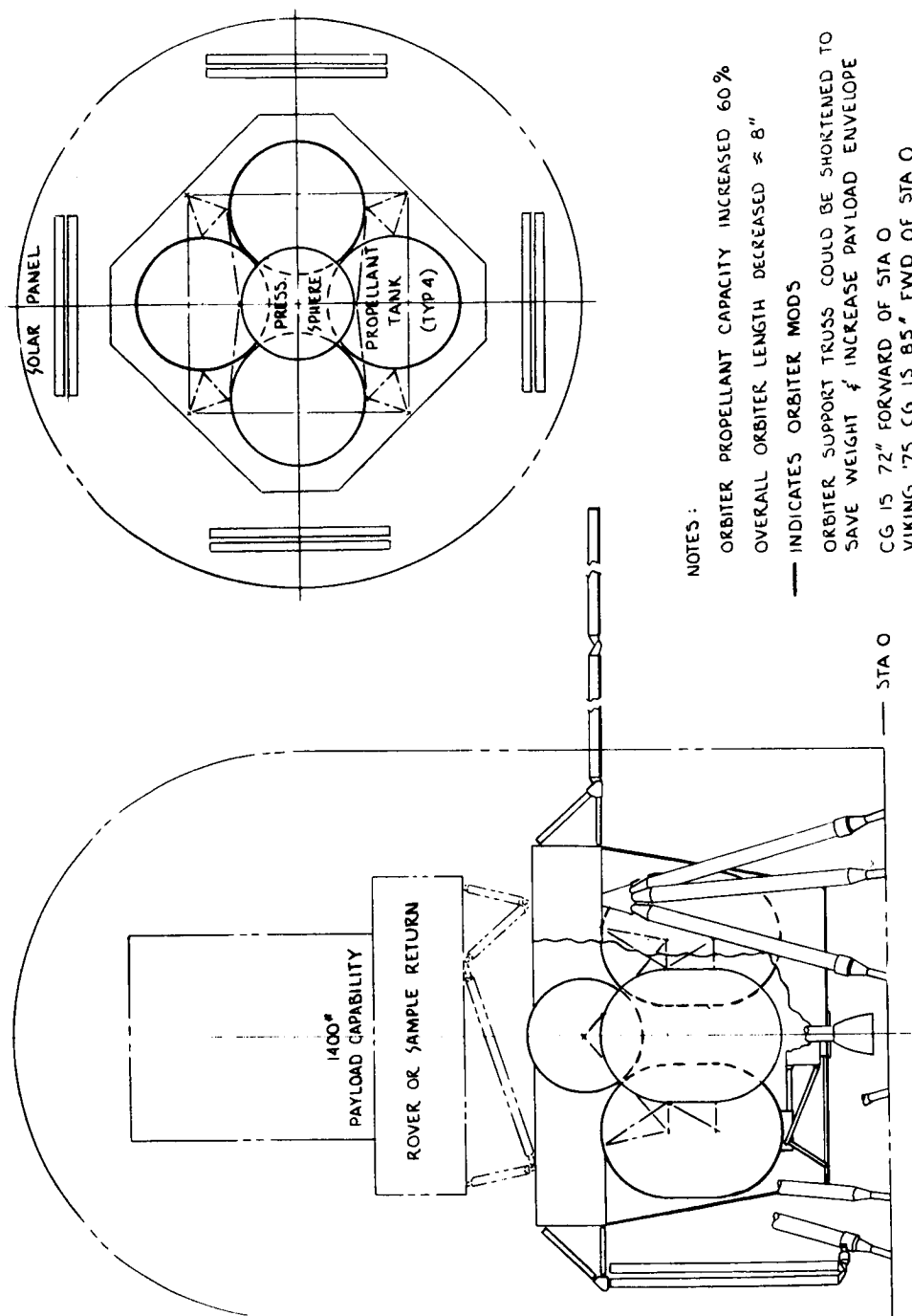


Figure IV-8 Phobos/Deimos Four Tank Concept

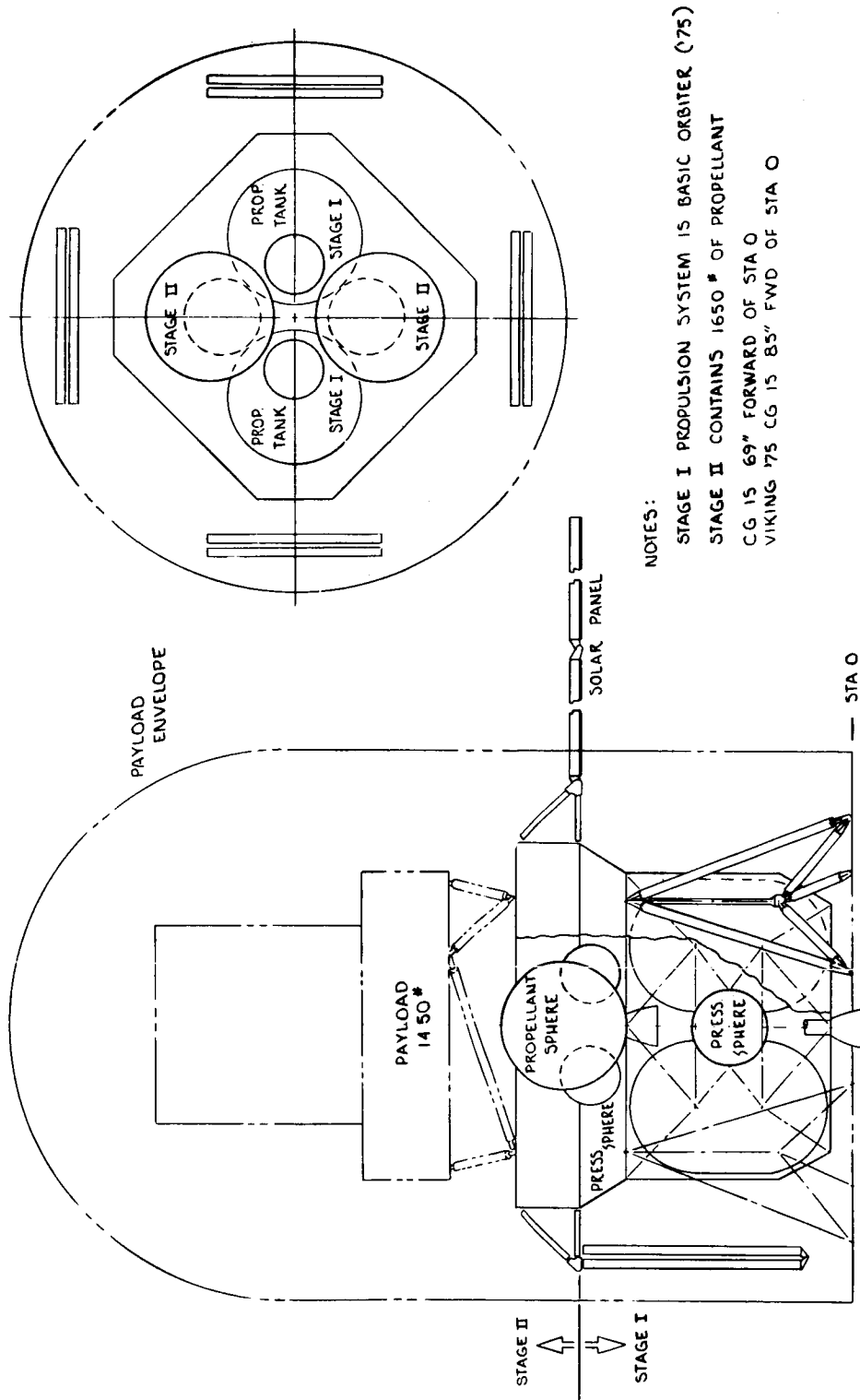


Figure IV-9 Phobos/Deimos Staged Concept

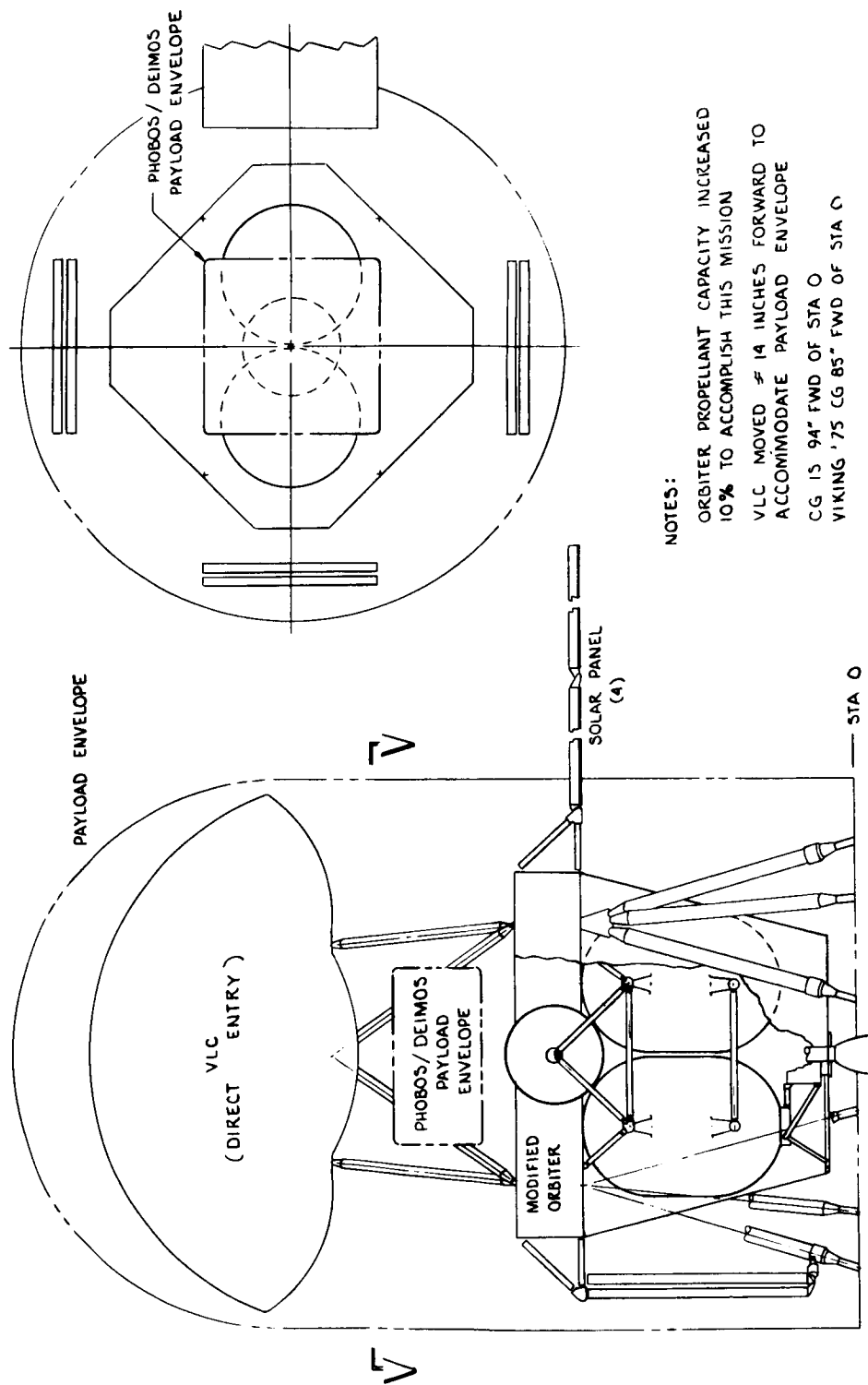


Figure IV-10 Combined Mars Lander and Phobos/Deimos Mission Concept

Table IV-6 Phobos/Deimos Four Tank System Weight Summary (kgs)

Orbiter			
Structures & Mech Devices	237.0		
Communication	46.1		
Modulation/Demodulation	9.3		
Power	129.2		
Computer Command	20.0		
Flight Data	13.8		
Attitude Control	55.0		
Pyrotechnics	5.0		
Cabling	54.4		
Data Storage	22.3		
Relay Telemetry	5.4		
Imaging & IR Spectrometer	44.9		
Propulsion - Inerts	372.4		
P/L - Orbiter Adapter	15.9		
Contingency (4%)	41.2	107L 9	(2363.1 lb)
Orbiter Dry Weight			
Expendable Propellant	2236.2		(4930 lb)
Orbiter Loaded Weight		3308.2	(7293.1 lb)
Separable Payload Allocation		635.0	(1400.0 lb)
Orbiter/Launch Vehicle Adapter			
Project Reserve	68.0		
LVMP	56.7		
	90.7		
Injected Payload Weight		4158.7	(9168.1 lb)

Table IV-7 Phobos/Deimos Staged Concept System Weight Summary (kgs)

Orbiter			
Structures & Mech Devices	238.0		
Communication	46.1		
Modulation/Demodulation	9.3		
Power	129.2		
Computer Command	20.0		
Flight Data	13.8		
Attitude Control	52.0		
Pyrotechnics	5.0		
Cabling	54.4		
Data Storage	22.3		
Relay Telemetry	5.4		
Imaging & IR Spectrometer	44.9		
Propulsion - Inerts	431.0		
First Stage	258.6		
Second Stage	172.4		
P/L - Orbiter Adapter	15.9		
Contingency (4%)	41.9		
Orbiter Dry Weight		1129.2	(2489.4 lb)
Expendable Propellant			
Orbiter Loaded Weight		3283.8	(7239.4 lb)
Separable Payload Allocation		657.7	(1450.0 lb)
Orbiter/Launch Vehicle Adapter			
Project Reserve	68.0		
LVMP	56.7		
Injected Payload Weight	90.7	4156.9	(9164.4 lb)

Table IV-8 Combined Mars Lander and Phobos/Deimos
Mission System Weight Summary (kgs)

ORBITER			
Structures & Mech Devices	244.0		
Communication	46.1		
Modulation/Demodulation	9.3		
Power	129.2		
Computer Command	20.0		
Flight Data	13.8		
Attitude Control	56.0		
Pyrotechnics	7.0		
Cabling	54.4		
Data Storage	22.3		
Relay Telemetry	5.4		
Imaging & IR Spectrometer	44.9		
Propulsion - Inerts	254.0		
P/L - Orbiter Adapter	22.2		
Contingency (4%)	37.0	965.6	(2130 lb)
ORBITER DRY WEIGHT			
Expendable Propellant	1550.0	2515.6	(5545 lb)
ORBITER LOADED WEIGHT			
DIRECT ENTRY MARS LANDER		1210.0	(2673 lb)
PHOBOS/DEIMOS LANDED PAYLOAD ALLOCATION		214.0	(471 lb)
Orbiter/Launch Vehicle Adapter	68.0		
Project Reserve	56.7		
LVMP	90.7		
INJECTED PAYLOAD WEIGHT		4155.0	(9164 lb)

section. The G&C subsystems for the separable lander configuration will be described in detail in this section, and the differences between this configuration and the landed orbiter configuration will be pointed out.

1. Cruise and Orbital Phases

a. Midcourse Corrections & Orbital Maneuvers - The Sun-Canopus acquisition maneuvers during the cruise phases, and the maneuvers during the midcourse corrections and orbital operations are similar to the Viking '75 and Mariner missions. For this reason, the execution of these maneuvers will not be discussed and only the rendezvous phase will be discussed in detail.

The S/C rendezvous with the satellite consists of an initial rendezvous phase, and a terminal rendezvous and landing phase. The initial rendezvous maneuver is executed like the other orbital maneuvers and injects the S/C from the observation orbit into a co-orbit with the satellite within a range of 100 km based on 3σ statistical errors (see Section III-B, Navigation Analysis).

b. Stationkeeping Orbit - By trimming the period of the co-orbit the spacecraft will be made to stationkeep with the satellite in a relative-motion pattern similar to an orbit about the satellite. This "pseudo orbit" will have a periapsis altitude of 100 km and a apoapsis altitude of 200 km based on maximum errors due to 3-sigma statistics. This relative motion will actually be caused by differences in eccentricity of the satellite and spacecraft orbits about Mars. The vehicle in this stationkeeping orbit will have the same orbital period as the satellite. Adequate time exists to track the vehicle in this orbit and trim the stationkeeping orbit until an accurate enough orbit is achieved. At the orbit periapsis and when the vehicle is within rendezvous radar range, the rendezvous radar data can

be used to refine the orbit if another orbital trim maneuver is needed to support science instrument viewing requirements for example.

2. Terminal Rendezvous and Landing Phase

a. Closing ΔV Phase - Figure IV-11 shows how the vehicle executes the terminal rendezvous and landing phase. Initially the spacecraft/lander is in a stationkeeping orbit and is locked on the Sun and Canopus. The vehicle is tracked for 13 hours or more, or one and one-half orbits, so the spacecraft orbit can be determined and the deorbit conditions (vehicle attitude and time of deorbit) calculated by the ground based computers. These data are telemetered to the spacecraft via the earth based antennas and stored in the onboard computer. The gyros are turned on and warmed up for an hour before the start of the de-orbit attitude maneuvers. The vehicle then does a roll, pitch, and roll maneuvers to the deorbit maneuver attitude.

After rendezvous radar acquisition and the time of separation discrete has been issued by the control computer, the lander is separated from the spacecraft by means of separation springs and unlatching mechanisms with a separation velocity of about one-third of a meter-per-second.

The lander is now in the closing ΔV phase where the RCS engines facing the top of the lander are fired continuously to impart a closing ΔV to the lander of 50 meters-per-second. A closing ΔV of this size will produce a rendezvous with the satellite that will be fairly optimum in terms of the propellant used. The vehicle attitudes are controlled by shutting off the appropriate RCS engine during this phase. The vehicle's attitudes are controlled to aim the radar boresight along the line-of-sight (LOS) vector and are controlled by nulling out these LOS errors. The line-of-sight vector is directed along a line

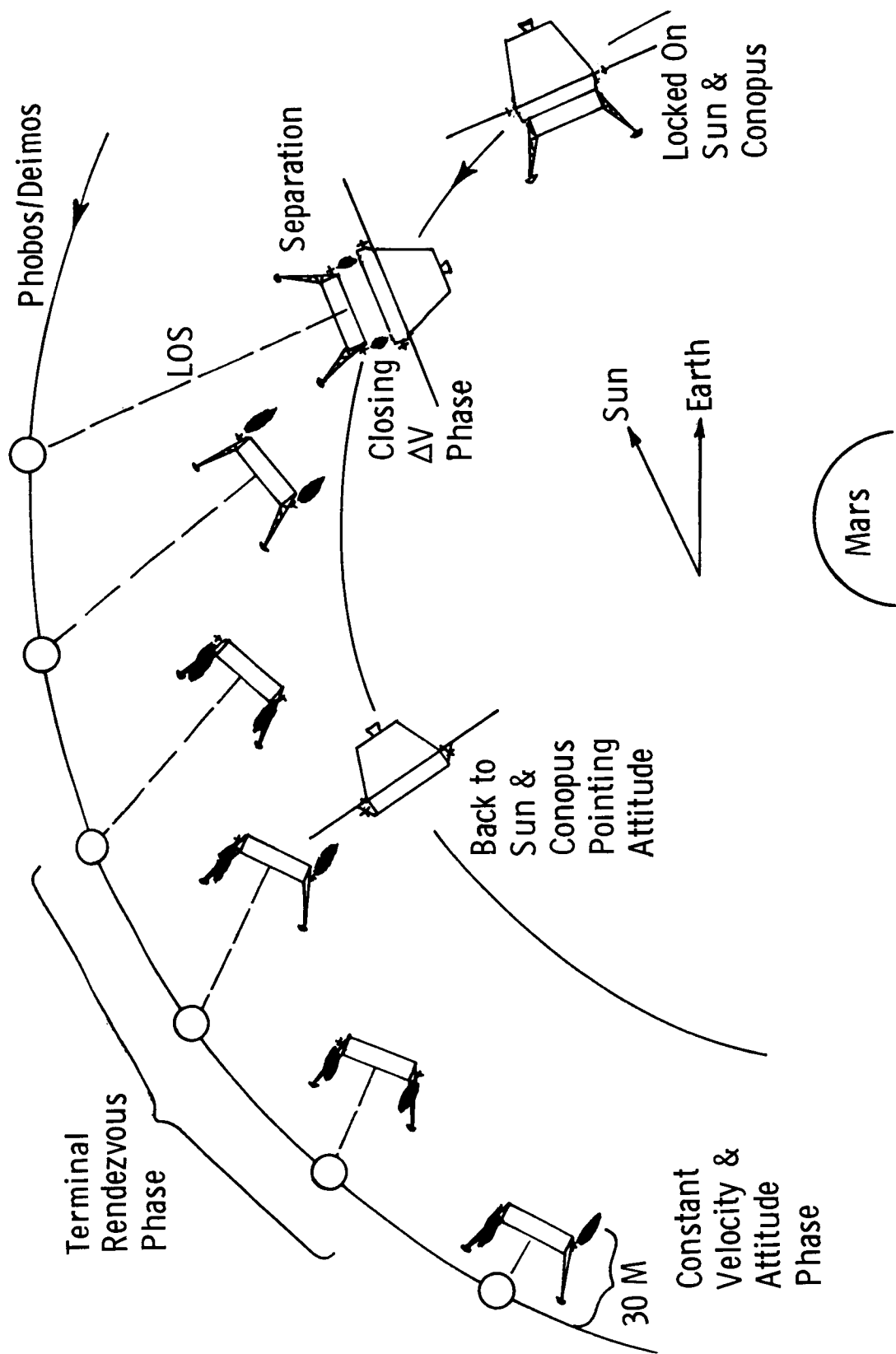


Figure IV-11 Terminal Rendezvous and Landing Phases

from the center of the spacecraft to the geometrical center of the satellite. In other words, the rendezvous radar boresight is controlled to point toward the center of the satellite. The vehicle attitudes are controlled this way during this phase and also during the terminal rendezvous phase.

b. Terminal Rendezvous Phase - When the lander achieves a velocity of 50 meters-per-second as indicated by the axial accelerometer, the guidance, control and sequencing computer (GCSC) commands the vehicle into the terminal rendezvous phase. During this phase, the vehicle attitudes are controlled as in the previous phase, but the lander axial velocity or range rate is controlled by using optimum range vs range rate control curves, which will be described later. During this phase, the vehicle does a rendezvous to within 30 meters of the satellite.

c. Constant Velocity Phase - The vehicle is commanded into the constant velocity phase when it descends to within 30 meters of the surface as indicated by the rendezvous radar. During this phase, the vehicle, using inertial navigation, descends at a constant velocity of 1 ± 0.5 meters-per-second (3σ) with the same attitude it had going into this phase, i.e., perpendicular to the average surface within the rendezvous radar field of view. The rendezvous radar dynamics at lower attitudes will be described later. During landing and when the vehicle is descending the last few feet, the RCS engines facing upward are fired continuously to improve the landing stability. These engines are fired until the lander has settled into a firm landing and help to compensate for the low gravitational field, i.e., produce an artificial gravity. The vehicle's attitudes are controlled by shutting off the appropriate engine during this latter phase.

The lander's lateral velocity must be synchronized with the satellite surface to insure a safe landing, since the lander is

navigating relative to an inertial coordinate frame. Our assumption on satellite surface velocity, which has been strengthened by Mariner 9 results, is that the satellites spin in one-to-one synchronism with their orbits about Mars. This assumption results in a Phobos surface velocity, with respect to inertial space, of two to three meters-per-second. The actual satellite surface velocity can be determined before landing by using the rendezvous radar prior to the constant velocity phase or by using the orbiter TV imaging system prior to separation. At low altitudes, the rendezvous radar will tend to command the vehicle to follow local terrain features and this can be used to determine the satellite surface velocity. The Viking Orbiter (VO) TV imaging system pictures can be used to determine the surface velocities in some appropriate coordinate frame. The surface velocity that is determined can then be used to bias the velocities in the GCSC, so the vehicle lateral velocity will match that of the satellite surface.

c. G&C Mechanization - The suggested baseline G&C system is shown in Figure IV-12. This system is mechanized similar to the Viking Lander, except the rendezvous radar is used instead of the terminal descent and landing radar. This change is required because the Phobos lander needs an inertial navigation capability during the constant velocity phase and when one or more radar beams are lost.

Range and range rate are used in the axial control law to determine whether the engine thrust should be turned off or on. The axial control law is based on thrust-on and thrust-off control curves of the form shown below:

$$QV_R^2 / T/M - R_K = R$$

where

Q = control gains

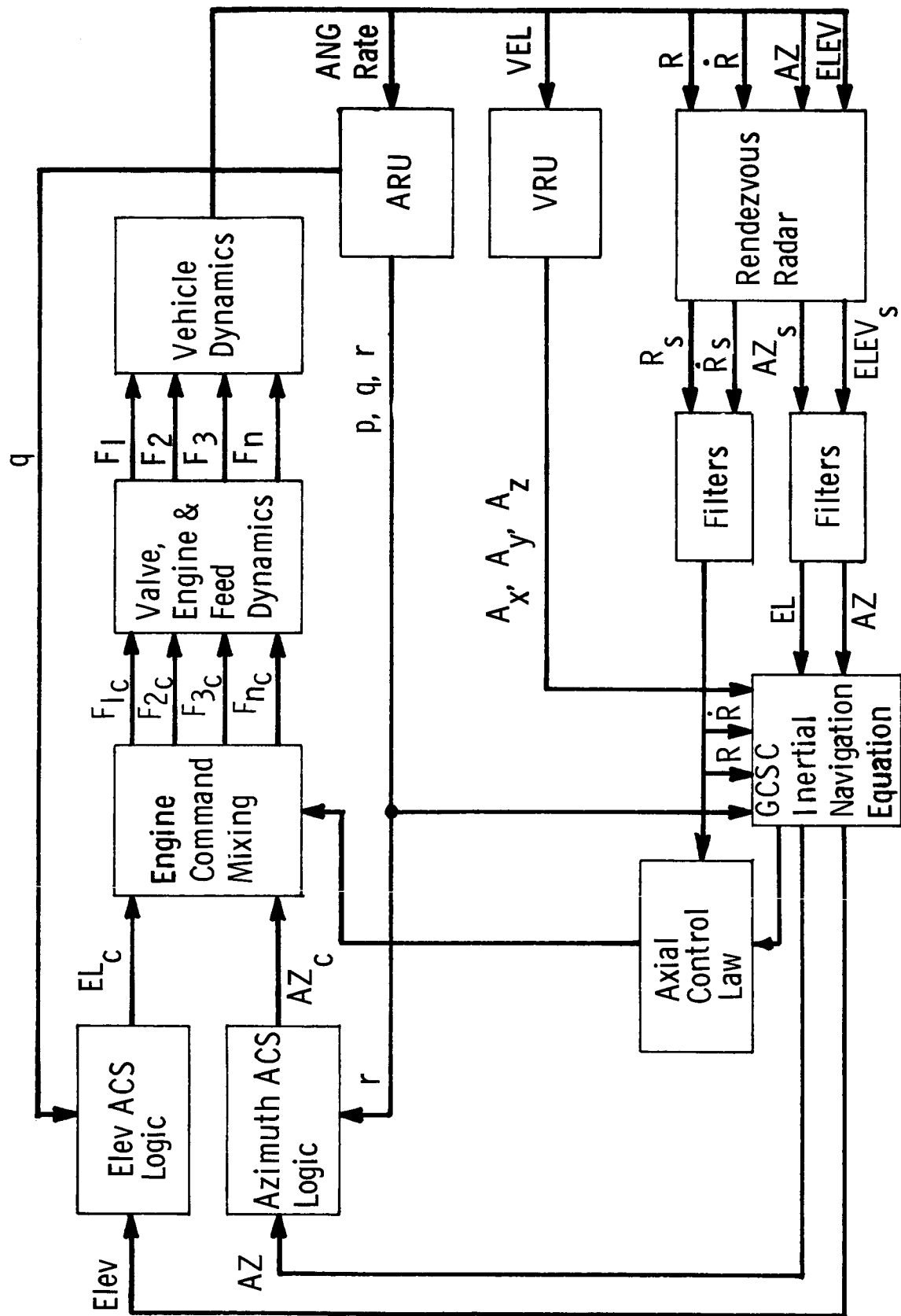


Figure IV-12 Rendezvous G&C System Mechanization

R_K = control constant that is the asymptote of the control curves

V_R = range rate

T/M = thrust-to-mass of the vehicle

R = range.

Figure IV-16 shows typical control curves for the separable lander configuration and shows the values of the various parameters. Control gain Q_1 is used in the thrust-on equation and Q_2 in the thrust-off equation, when the vehicle is above a certain altitude R_M . Below that altitude, P_1 and P_2 are used as control gains. The use of these curves will be described in a later section. The filters are used to eliminate the high frequency noise from the rendezvous radar output.

During the constant velocity phase and in the event of radar beam loss, the G&C mechanization gives the lander the capability of inertial navigation during these phases. The attitude reference unit (ARU) and velocity reference unit (VRU) are used to supply vehicle's attitude and position to the control algorithm. The body rates from the ARU are used for rate feedback in the attitude control system (ACS) logic as shown in Figure IV-12.

The symbols in this figure are defined below:

AZ, Elev	Azimuth and elevation attitude angles
AZ _C , EL _C	Azimuth and elevation attitude command angles
$F_{1_c}, F_{2_c}, \dots, F_{n_c}$	Engine thrust commands
F_1, F_2, \dots, F_n	Engine thrusts
p, q, r	Body attitude rates about x, y, and z axes respectively
A_x, A_y, A_z	Body accelerations along x, y, and z axes
R, \dot{R}	Vehicle range and range rate

R_s, \dot{R}_s Sensed range and range rate

$AZ_s, ELEV_s$ Sensed azimuth and elevation attitude angles

ACS logic is used in the elevation and azimuth channels, that is similar to that used in the Viking Lander. The vehicle can be controlled to 0.25 degrees in the small limit cycle mode and 5 command mixing, and the axial control laws are mechanized in the on-board computer.

4. Suggested Rendezvous Radar

The rendezvous radar selected for the baseline vehicle was mechanized using the Viking radar altimeter to save development costs and weight. A block diagram of the suggested rendezvous radar is shown in Figure IV-13. An estimated 10-15 percent modification of the present Viking radar altimeter is needed to add an interferometer tracking system to sense the line-of-sight (LOS) azimuth and elevation angles. This rendezvous radar mechanization is similar to that used on the Gemini vehicle and the technology is well understood.

The present Viking radar altimeter provides range and, since it has a second order tracker, range rate is also available. Four small lightweight antennas are needed to determine the vehicle LOS angles. Antennas which are wound in Archimedes spirals and printed on epoxy boards are suggested for the baseline vehicle because of the ease of getting phase shift in the channels and of the reduction in antenna weight. Two of these antennas are servoed by lightweight, accurate, instrument type servos, that shift the phase linearly with antenna rotation in those channels. Each of these servoed antennas has a digital encoder that indicates the angular rotation of the antennas. The other two antennas are the transmitter and the receiver reference antennas.

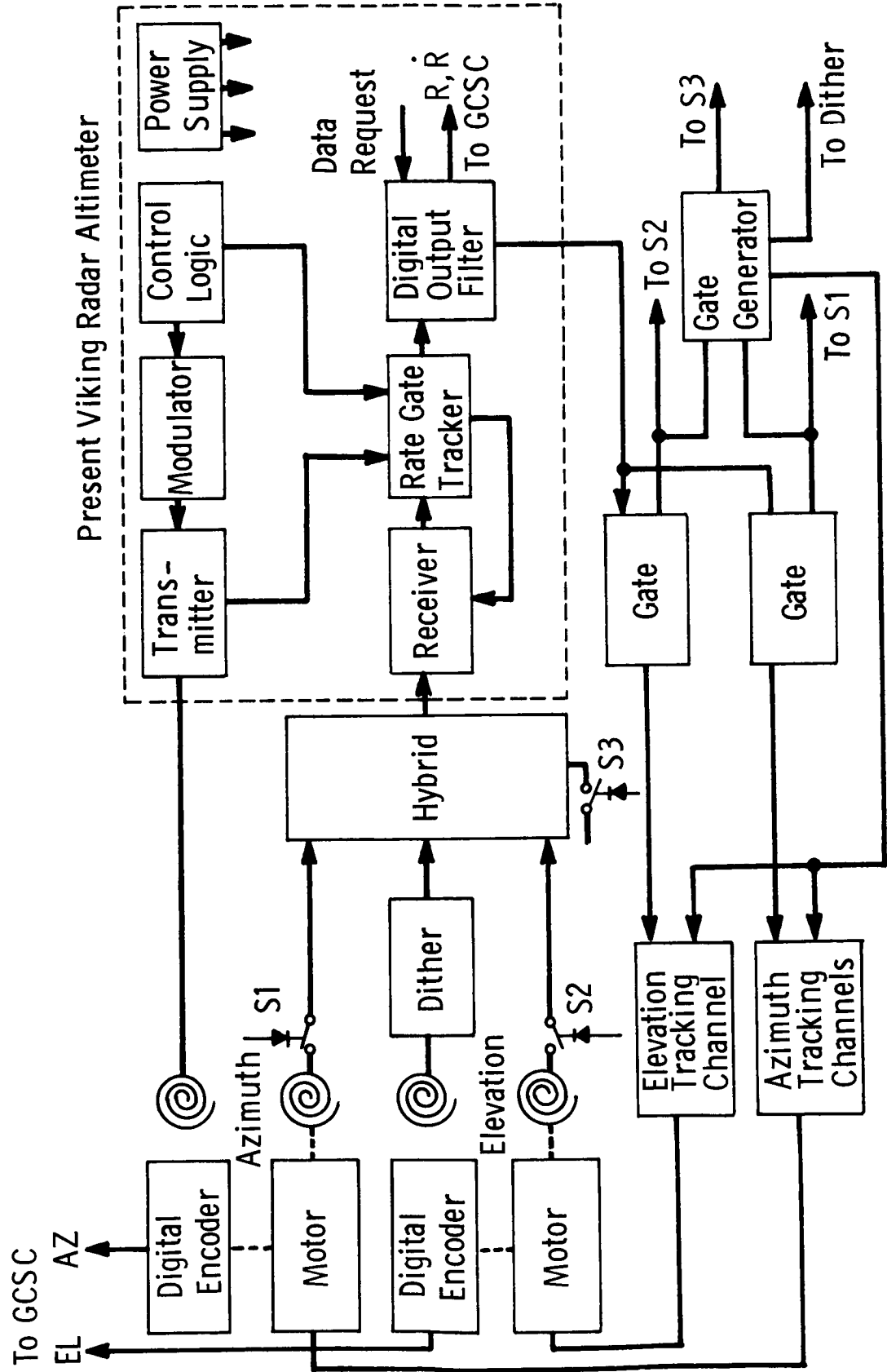


Figure IV-13 Suggested Rendezvous Radar

a. Interferometer Tracking System - Figure IV-14 shows how the antennas are mounted in the ground plane on the bottom of the lander. The elevation and azimuth antennas are servoed to shift phase in those channels. As shown by the block diagram included in this figure, the azimuth or elevation channel is compared to the receiver reference channel and this difference is used to null out the phase difference between these channels. The phase difference is related to the LOS angle by the equation:

$$\phi = \frac{2\pi D}{\lambda} \sin \theta$$

where

ϕ = phase difference

D = distance between antennas

λ = wave length

θ = LOS angle

When the phase difference between the two channels is zero, the shaft encoder angle is proportional to the LOS angle. Small parabolic antennas can be used instead of the spiral antennas if servo driven electronic phase shifters are used.

b. Landing Site Selection System - This type of rendezvous radar has the advantage of automatically choosing a favorable landing site. When the range to the satellite is such that the rendezvous radar field of view of 70 by 70 degrees is completely filled, the lander will descend controlling the vehicle's attitude, so the longitudinal axis is perpendicular to the average ground slope in the FOV as shown in Figure IV-15. Thus, for example, the lander will tend to align its longitudinal axis perpendicular to the average surface slope of a hill and a component of the thrust vector will move the lander to the bottom of the hill.

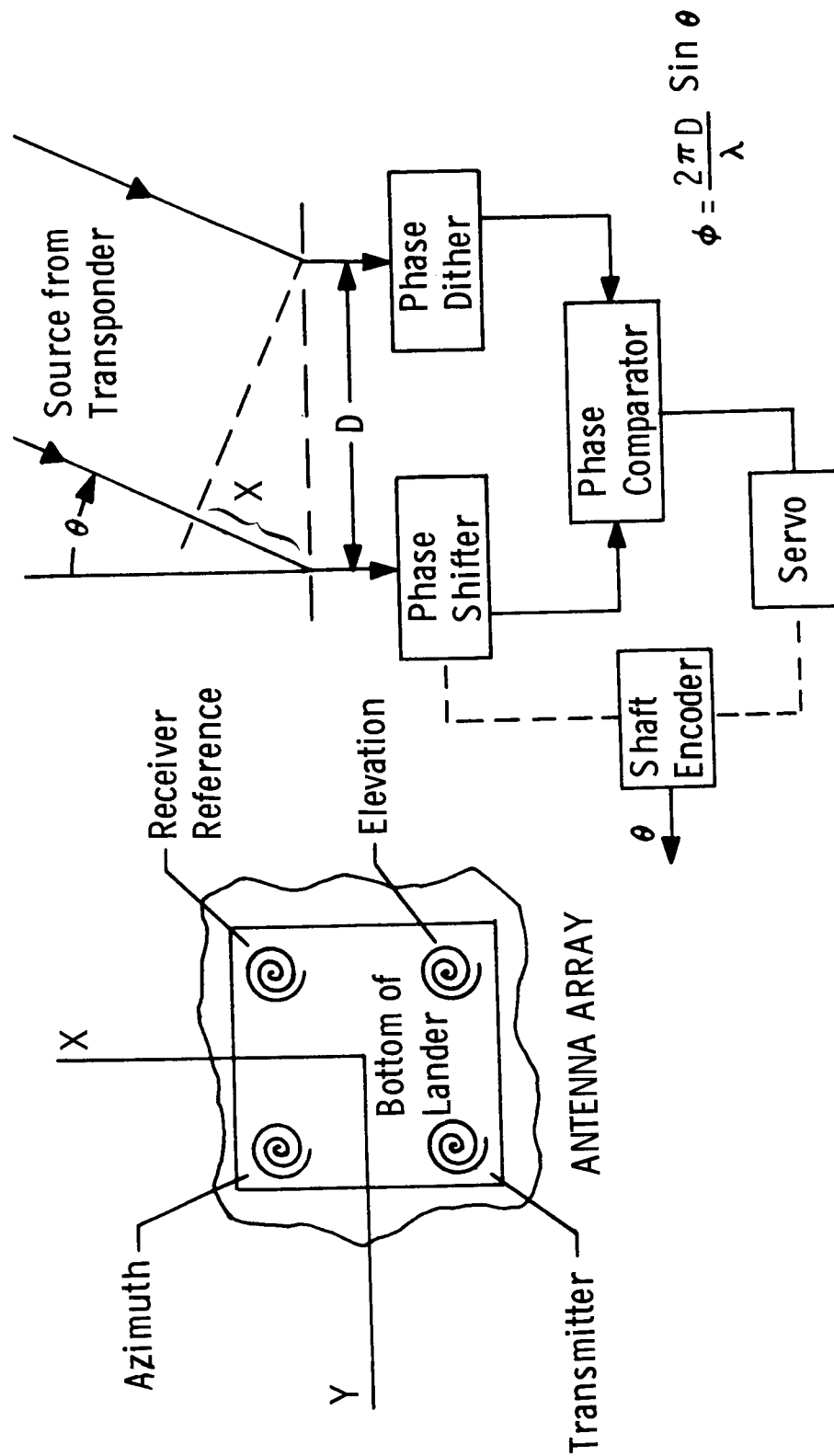


Figure IV-14 Interferometer Tracking System

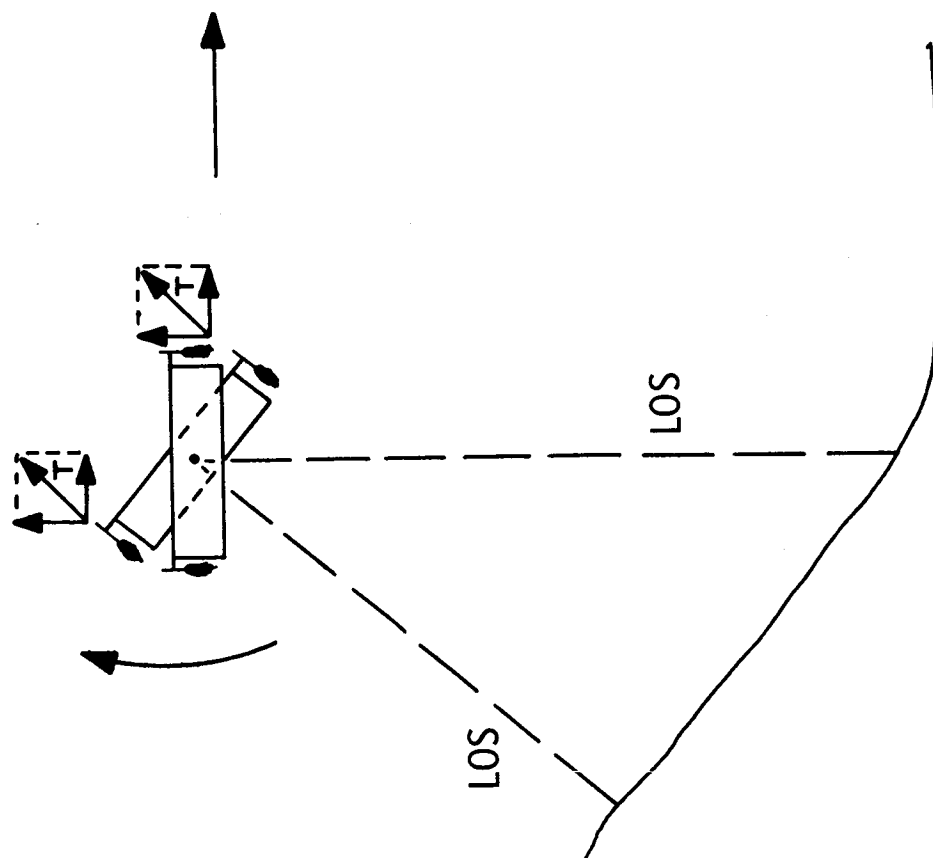


Figure IV-15 Landing Site Selection System

c. Rendezvous Radar Estimated Maximum Range - Table IV-9

shows the maximum range capability for suggested rendezvous radar as calculated by the radar range equation based on the estimated microwave gains and losses. A S-band radar frequency would have reasonable isolation from the telecommunication system frequencies. A pulse repetition frequency (PRF) of 256 hertz was selected. A pulse width of 6 microseconds should be adequate so that each received pulse is time shared to measure range and LOS angles. Time sharing eliminates the need for two receiving channels and keeps the information rate as high as possible.

A range of reflectivities from 3.5 to 9.0 can be expected as defined by the engineering model, which correlates to surfaces with reflectivities of talc powder texture to meteoric iron. A reflectivity of 3.5 was used because this would be the most pessimistic case. A radar cross section of Deimos was used because the satellite was smaller and would be the worst case. By using 5 kilowatts of peak transmitter output power (7.5 watts of average power) and the estimated losses as described in Table IV-9, a maximum acquisition range of the rendezvous radar would be 108 km as determined by this worst case analysis.

5. G&C Subsystem Weight and Power Requirements

The G&C subsystem weight and power requirements are shown in Table IV-10. The suggested rendezvous radar weighs 10.5 kilograms and consumes 60 watts of input power. This estimate of input power assumes 12.5 percent power efficiency. The Apollo rendezvous radar (RR) consumes 75 watts and the Gemini RR consumes 16 watts for cooperative rendezvous from 653 km (405 n mi) and 403 km (250 n mi) respectively. A non-cooperative rendezvous consumes considerably more power.

The weight of the suggested rendezvous radar is about the same weight as the Gemini system and much lighter than the manned and sophisticated Apollo radar, which weighs 32.8 kg (72 lbs).

Table IV-9 Rendezvous Radar Maximum Range

Freq = 1 GHZ PRF = 256 HZ Pulse Width = 6(10 ⁻⁶)Sec		3.5 ≤ ε ≤ 9.0(Used 3.5) Deimos Swerling Model V	
$R^4 = \frac{G^2 \lambda^2 \sigma L P_t}{(S/N)_{Req} (4 \pi)^3 KTB(NF)}$			
	NUM	DEN	
Antenna Gain (G) Wave Length (λ) Radar Cross Section (σ)-Deimos Losses (L) Transmitter Power (Pt) (S/N) _{3Req} (4 π) ³ KT B NF	+23.0 db - 4.0 +83.0 -10.0 +37.0	+ 8.0 db +33.0 -204.0 +62.0 +9.0	
Numerator & Denominator Total		- 93.0	
Total		222 db	

Table IV-10 G&C Subsystem Hardware for a Phobos/Deimos Mission

<u>Lander</u>	<u>Weight</u>	<u>Power</u>
Rendezvous Radar	10.45 Kg (23 lbs)	60 Watts
Guidance, Control & Sequencing Computer	20.2 Kg (45 lbs)	50 (3.5) Watts
Attitude Reference Unit	7.6 Kg (17 lbs)	100 (59) Watts
Velocity Reference Unit	2.27 Kg (5 lbs)	35 (10) Watts
Valve Drive Amplifiers	3.16 Kg (7 lbs)	120 (0.9) Watts

Orbiter

No Change For The Lander/Orbiter Configuration

The Viking lander guidance, control and sequencing computer (GCSC) was selected because a computer of this capability is needed for the science and the landing operations. Since the rendezvous radar and the GCSC were selected from the Viking lander, the selection of the other components of the G&C subsystem from this vehicle would simplify the integration and interface problems. For this reason, the ARU, VRU and RCS engines were selected from the Viking lander.

6. Landed Orbiter Configuration

The landed orbiter configuration would still require a GCSC or equivalent for the landed operations but the VO control computer and sequencer (CC&S) would be adequate for the other phases of flight. The rendezvous radar would have to be added to the VO system. Viking lander RCS engines would be added to the orbiter body to execute the terminal rendezvous maneuvers. The VO inertial reference unit (IRU) can be used if the inertial navigation capability is not required. If this capability is required, two additional accelerometers must be added to the present VO system, or the present Viking lander VRU can be used. In other words, either the same G&C components can be used on this configuration as was used on the separable lander (all Viking lander components) or a combination of Viking lander and Viking Orbiter components can be used.

7. Discussion of the Terminal Rendezvous Simulation

The terminal rendezvous phase was studied in detail using a digital computer program; which is a six degree of freedom, 3-body simulation of the vehicle in non-coplanar orbits and has the option of studying a number of rendezvous guidance schemes. The gravitational attraction between all three bodies--Mars, satellite and lander--were included in the equations of motion.

A number of rendezvous guidance schemes were tried but the

proportional navigation rendezvous appeared to be the best rendezvous scheme in terms of simplicity of the vehicle control algorithms and execution of a near optimum rendezvous. Similar rendezvous guidance schemes were used by Apollo, Gemini, and the Russian orbital space station.

In this scheme, the vehicle attitudes are controlled to null out the line-of-site angle errors. The vehicle's thrust is commanded on or off by thrust-on or thrust-off curves as shown in Figure IV-16.

This figure shows a rendezvous for the separable lander with a 3σ position error of 100 km. The initial conditions at the start of the rendezvous were a 100 km range and 50 km/sec range rate produced by the closing ΔV phase. The lander also started the rendezvous phase with an initial condition of 11 km out of the satellite orbital plane.

This figure shows two sets of control curves; one set is used for ranges greater than 45,700 meters ($R_M = 45700$) and the other set is used when the range is smaller than this value. The control curves are asymptotic at 15300 meters ($R_K = 15300$) for the higher range curves and 20 meters for the lower range control curves. The equation that describes these control curves is shown on this figure and was described previously in this section. The control gains Q are Q_1 and Q_2 for the larger ranges, and P_1 and P_2 for the smaller ranges. Q_1 and P_1 are the control gains for the thrust-on control curves, and Q_2 and P_2 are for the thrust-off curves or the lower curves. The control curve equations are mechanized in the GCSC. Exhaustive studies were conducted to determine the control gains for a near optimum rendezvous. The separable lander control constants and gains determined by this study are shown below:

<u>Above 45700</u>	<u>Below 45700</u>
Q1 = 8	P1 = 12
QZ = 16	P2 = 24
RK = 15300	RK = 20
RM = 45700	RM = 45700

The dotted line shown in Figure IV-16 describes the range vs range rate trajectory during the rendezvous maneuvers. The vehicle coasts until its range and range-rate mates the thrust-on conditions, the RCS engines facing downward are then fired continuously to reduce the vehicle relative velocity. When the vehicle range rate is reduced to match the thrust-off conditions, the RCS engines are turned off and the vehicle coasts until the thrust-on conditions are again achieved.

These control curves were designed so the vehicle would execute a near optimum rendezvous. The vehicle required 4900 seconds to complete the terminal rendezvous phase and used 9.7 kilograms of propellant. This is only two more kilograms of propellant than would be required for the most optimum case where the rendezvous is executed as two impulsive maneuvers. Figure IV-17 shows how the vehicle executes the final phase of the rendezvous.

Figure IV-18 shows the rendezvous trajectory in a satellite centered coordinate system. This figure shows the thrust periods and the vehicle rendezvous trajectory to the satellite. Eight thrust periods were required to rendezvous with the satellite. The vehicle's rendezvous at close range is shown in the insert on the left of this figure.

The rendezvous time profile is shown in the next figure-- Figure IV-19. The curve, represented by a dashed line, shows how the range varies as a function of time and when the vehicle executes the thrusting phases. This figure also shows how the

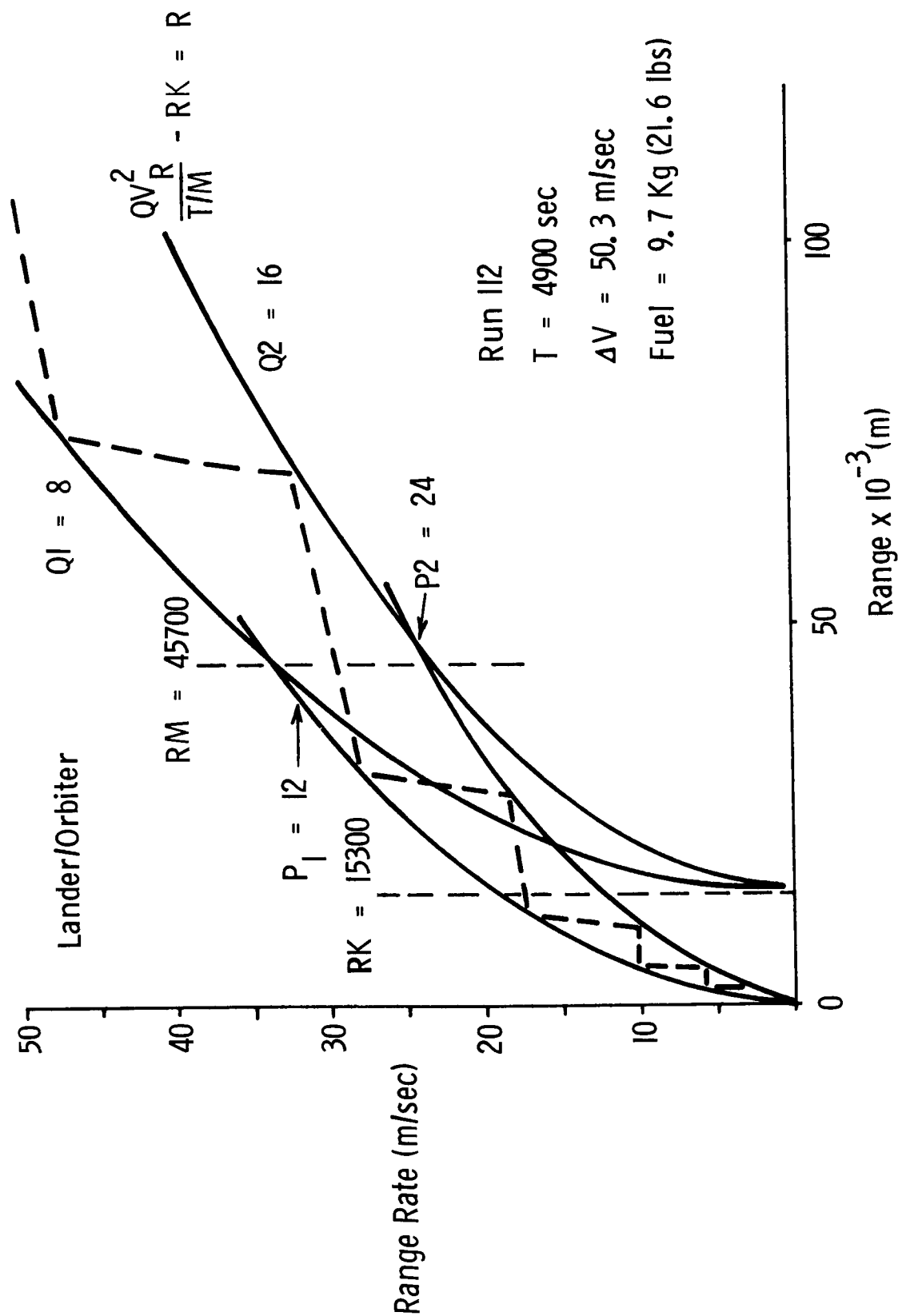


Figure IV-16 Typical Closure - Long Range

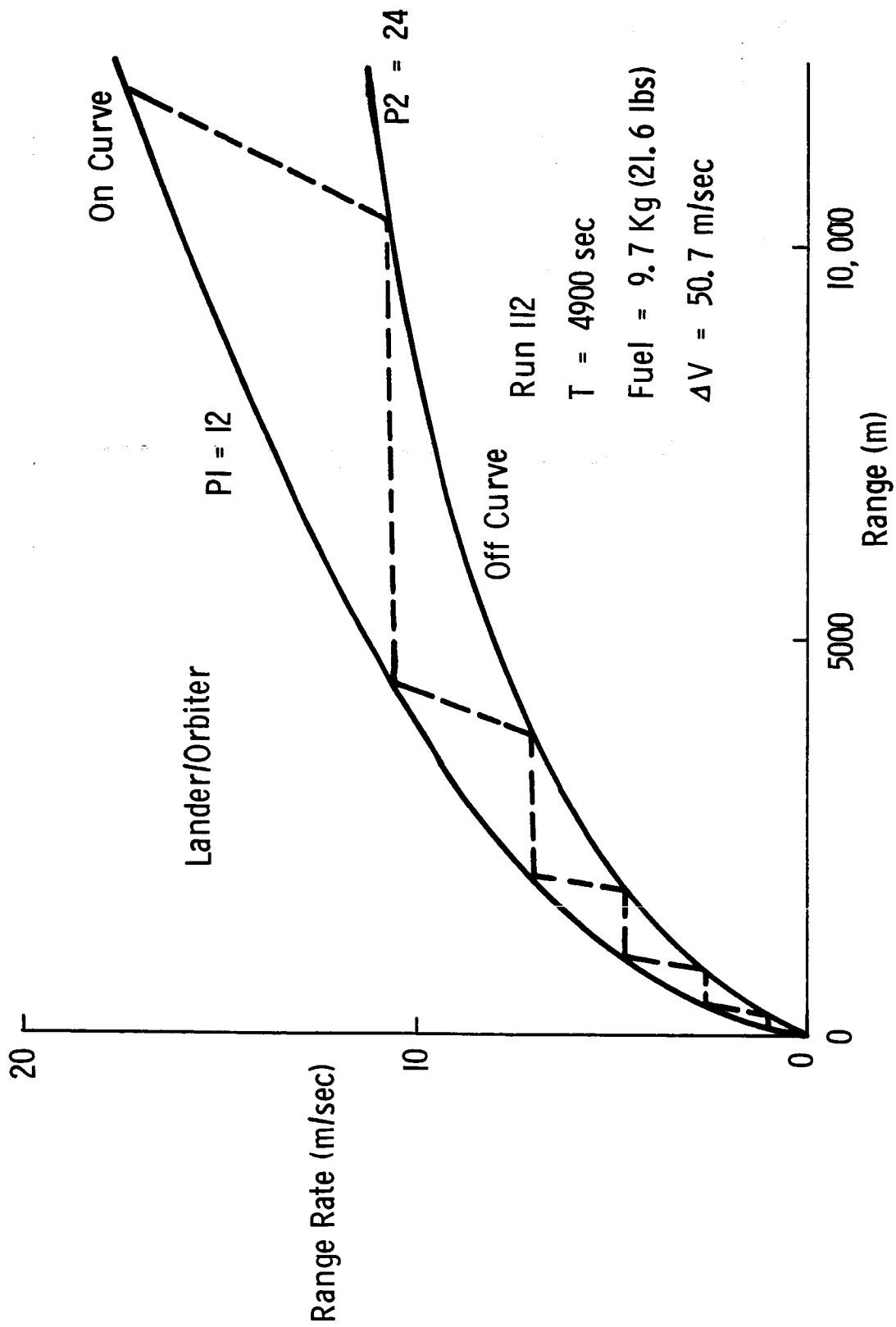
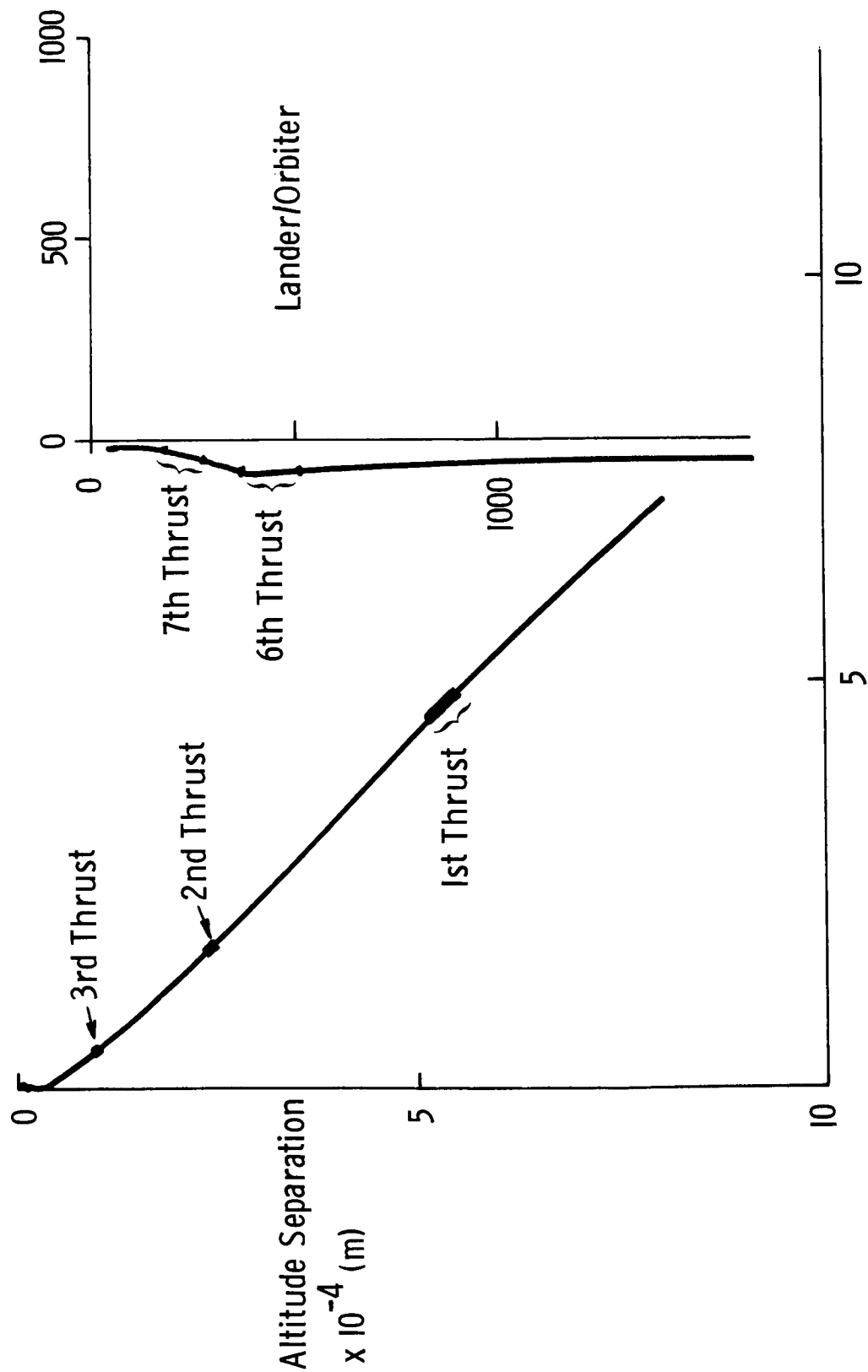


Figure IV-17 Typical Closure - Short Range



Downrange Separation $\times 10^{-4}$ (m)

Figure IV-18 Rendezvous Trajectory

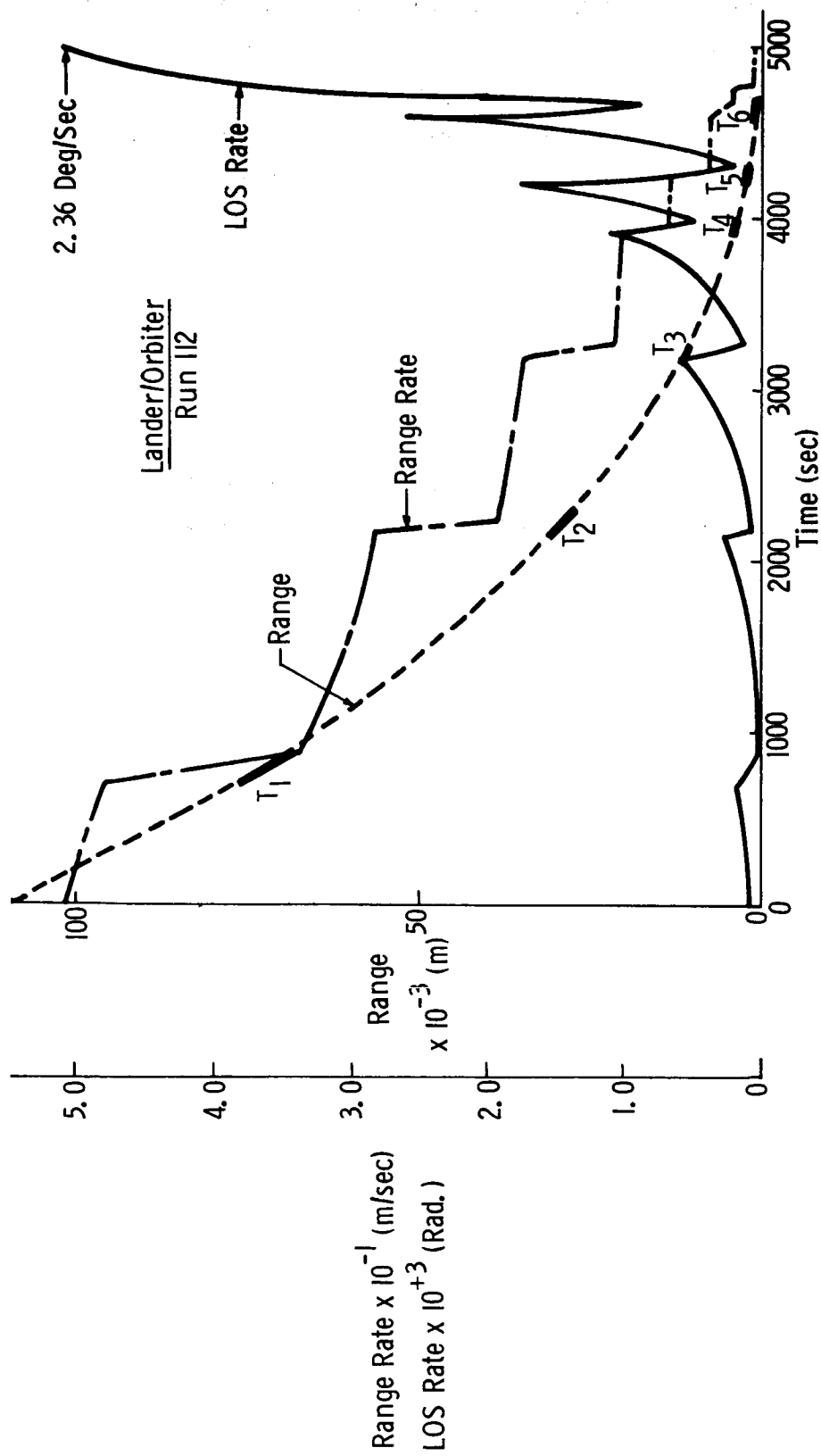


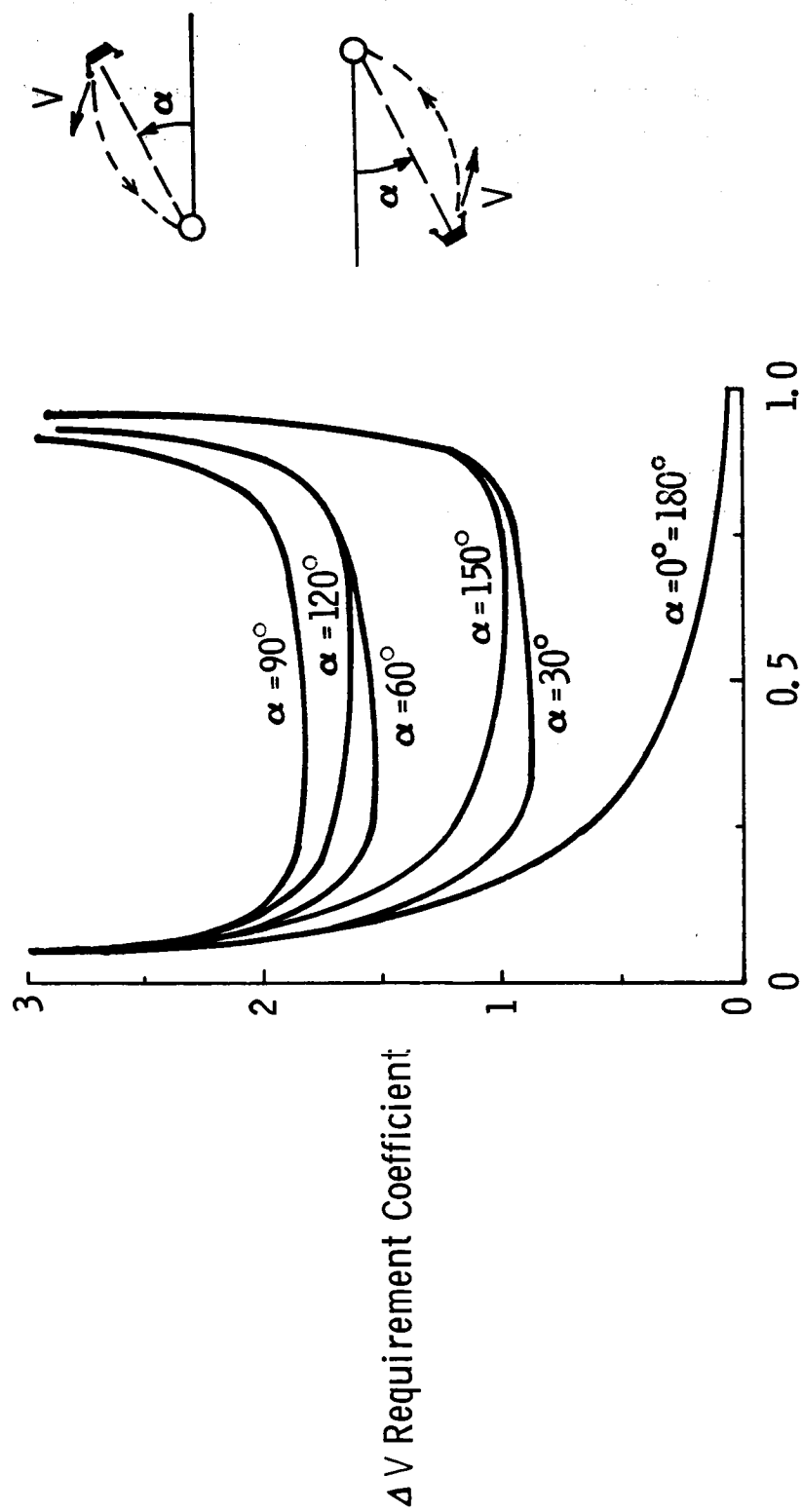
Figure IV-19 Rendezvous Time Profile

range rate and the total LOS rate varies during the rendezvous. The total LOS rate is the vector sum of the elevation and azimuth angle rates. The LOS rates get larger as the vehicle gets closer to the surface. If the rate could be kept small (less than one-milliradian) a more optimum rendezvous can be achieved. The smaller the LOS rates can be kept, the more optimum rendezvous can be achieved.

Figure IV-20 shows how the time of rendezvous affects the propellant efficiency. The ΔV requirement coefficient shown as the ordinate of the figure is proportional to the amount of propellant needed above the most optimum case. When $\alpha = 0$ or 180 degrees and the vehicle is essentially in the same orbit as the satellite, the most efficient rendezvous can be achieved. When $\alpha = 90$ degrees--the vehicle is in a larger or smaller orbit--the vehicle uses the most propellant. The reason these rendezvous are so inefficient is that a large closing ΔV is needed to catch the satellite which has to be taken out during the terminal rendezvous phase.

Navigation analyses of the baseline Phobos/Deimos mission indicates that the spacecraft will be delivered to the satellite such that α is between 135 and 180 degrees. The digital computer program results shown here are for $\alpha = 135$ degrees.

The time of rendezvous is also an important consideration in producing an efficient rendezvous. As can be seen in the last figure, fairly efficient rendezvous can be achieved from $1/4$ to $3/4$ of an orbital period. The rendezvous with Phobos as simulated by the digital computer took about a quarter of an orbital period, so a fairly optimum rendezvous was obtained. A slightly better rendezvous could be obtained if smaller RCS engines were used, so the time-of-rendezvous would be about a half of an orbital period.



Time to Rendezvous-Fraction of an Orbital Period

Figure IV-20 Rendezvous Propellant Efficiency

Figure IV-21 shows how the vehicle would rendezvous with the satellite from its out of orbit position. The vehicle's relative velocity vs relative range is shown for all three coordinates in the satellite centered inertial reference system. As can be seen, rendezvous from non-coplanar orbits can be easily achieved. Figure IV-22 shows how the vehicle executes the final portion of the rendezvous.

Figures IV-23 and IV-24 show the rendezvous trajectory for the landed orbiter configuration. The landed orbiter rendezvous takes 800 sec longer to rendezvous and 150 percent more propellant than the separable lander configuration. This rendezvous was very close to being an optimum trajectory (less than a pound more propellant was used than the most optimum case).

The same control curves were used for the landed orbiter configuration although different control gains and constants are needed in the control computer to mechanize these equations.

8. Summation of the Results

The proportional navigation scheme selected to control the vehicle during the terminal rendezvous phase appears to be easy algorithm to mechanize in the control computer and executes a near optimum rendezvous. For these reasons, this type of rendezvous algorithm is suggested for the baseline configuration.

Viking lander hardware can be used to mechanize the G&C subsystem to simplify the integration and interface problems and would be available in the time span for a Deimos/Phobos mission. Selection of a modified Viking lander radar altimeter would save development costs of a new lightweight rendezvous radar.

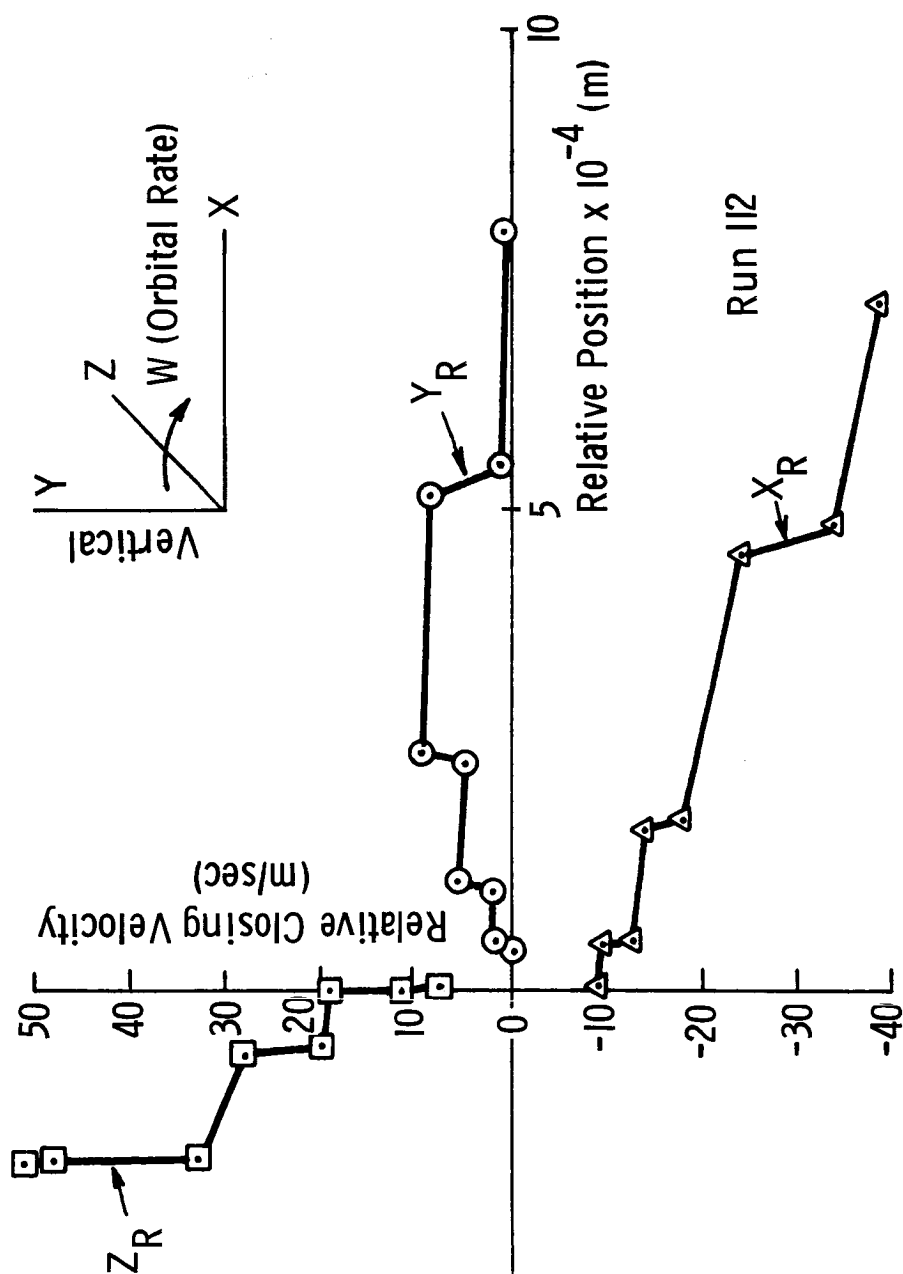


Figure IV-21 Relative Closing Velocity Vs Range - Long Range

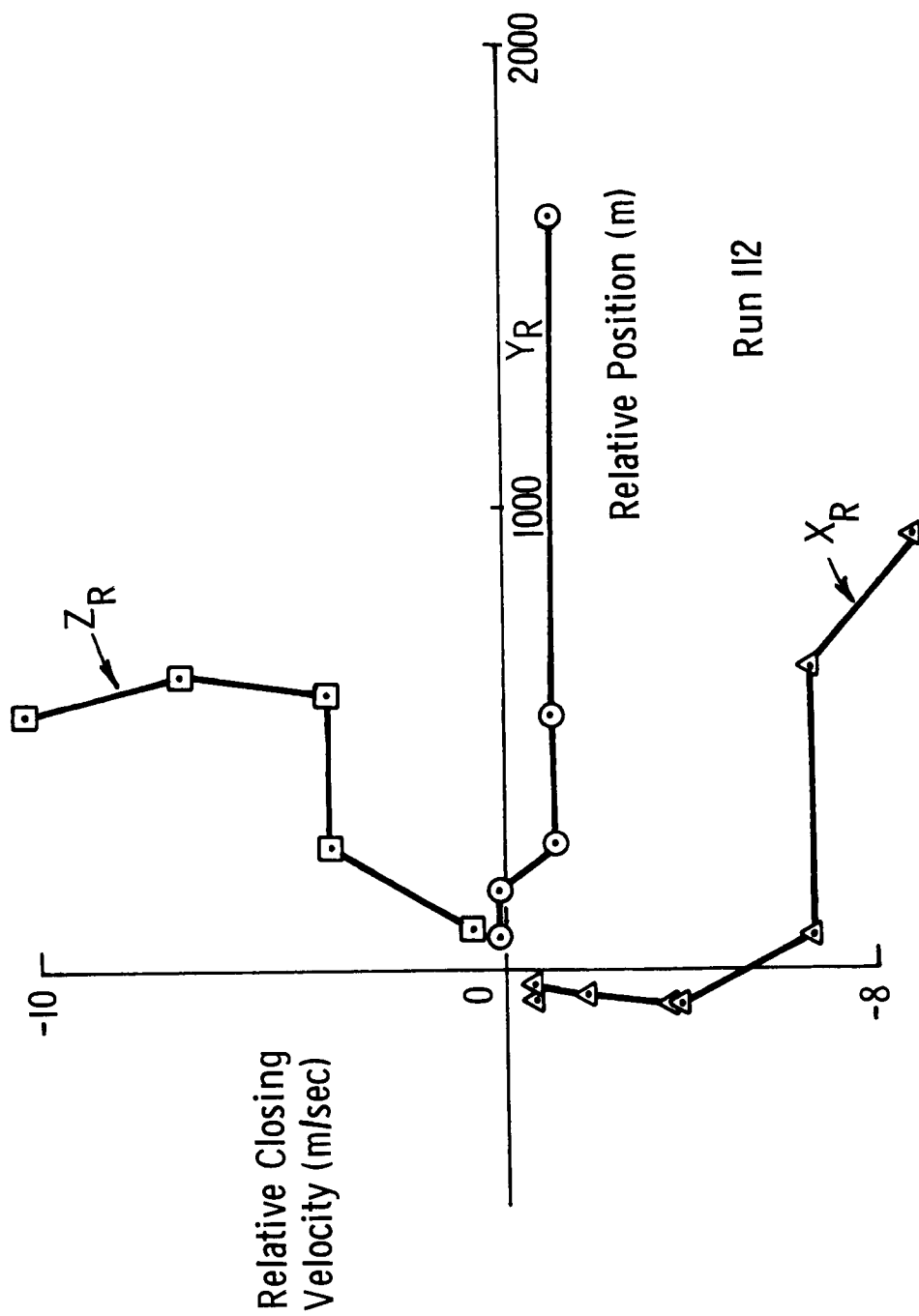


Figure IV-22 Relative Closing Velocity Vs Range - Short Range

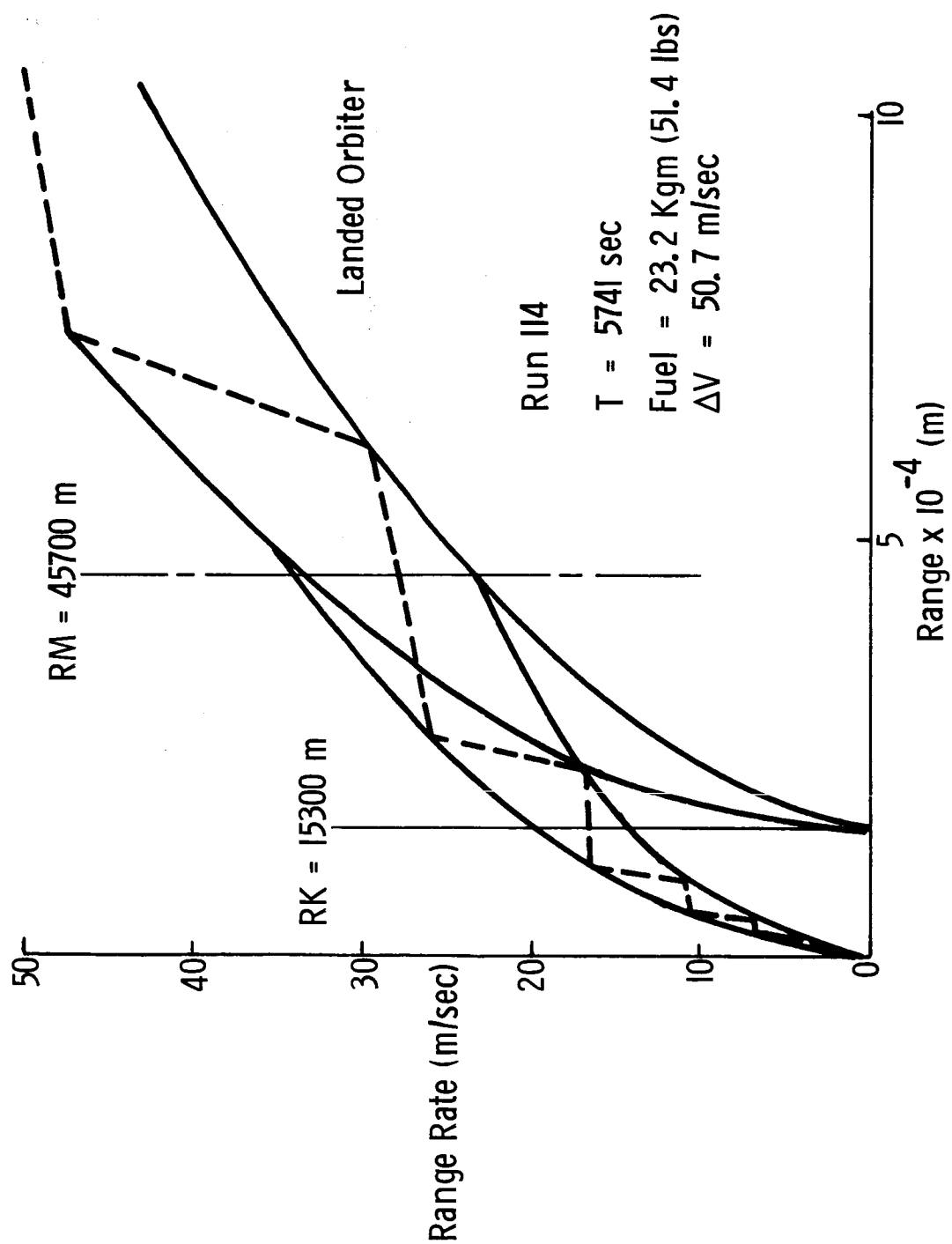


Figure IV-23 Typical Closure - Long Range

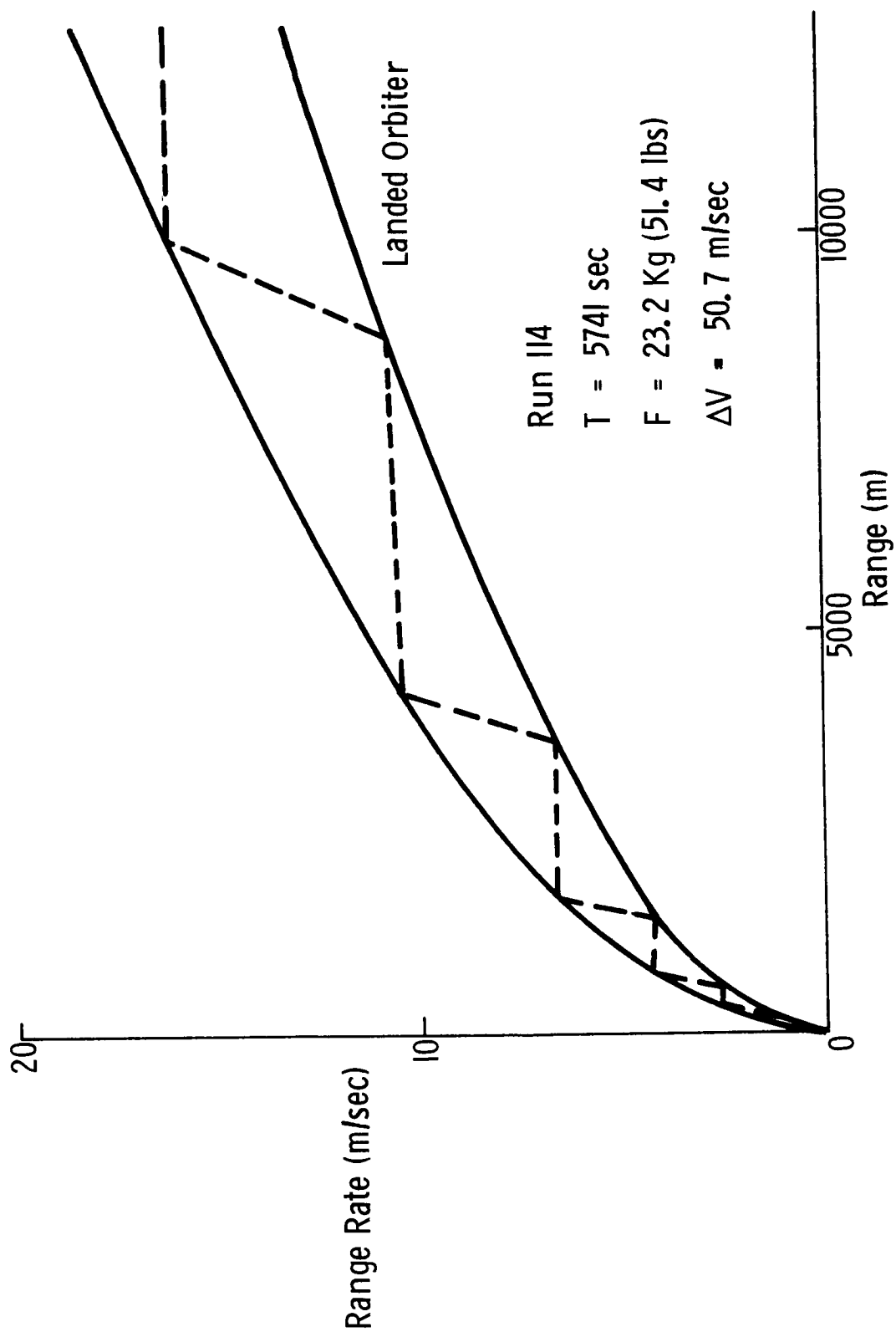


Figure IV-24 Typical Closure - Short Range

C. STRUCTURAL DESIGN

1. Design Approach

Structural design and systems installation of the spacecraft and the lander/orbiter/launch vehicle adapter trusses were studied in detail to define the necessary revisions and additions to the baseline Mars Viking configuration to perform the Phobos/Deimos rendezvous and landing missions.

The structural configuration selected for the baseline Phobos/Deimos spacecraft is a modified Viking '75 Orbiter, a separable lander/rover vehicle and associated truss adapters. All structural components utilize state-of-the-art processes and materials to minimize costs and to give high reliability.

The addition of the "growth" propulsion system module of the modified orbiter results in moving the upper surface of the orbiter less than 7.6 cm (3.0 inches) further forward relative to the Viking '75 Orbiter in its launch configuration. The composite CG of the Phobos/Deimos spacecraft is approximately 40.5 cm (16 inches) closer to the spacecraft-Centaur interface (Sta. 0) than the Mars Viking '75 spacecraft, resulting in somewhat lower design loading in the various spacecraft structural elements. All structural members were sized to meet Titan IIIE/Centaur launch and mission induced loading and dynamic requirements, with margins of safety sufficiently high to allow for mission induced transients excursions, and to allow for support of payloads weighing up to 657.7 kgs (1450 pounds).

a. Modified Orbiter - The orbiter structure, both the octagonally shaped bus and the truss which attaches the orbiter to the Centaur-spacecraft adapter were evaluated for their capability to accommodate the loads and moments introduced by the increased propellant loading and by the lander/rover vehicle.

The orbiter bus which is designed by loads encountered during launch consists of substantial upper and lower rings with short longerons between them. Shear capability is provided by the electronic subassemblies when they are bolted in place. Twelve electronic assemblies of the type used on MM '69 and MM '71 are housed within the eight electronic areas provided by the octagon shaped bus. Electronic sensors and experiments requiring defined fields of view are located outside of the electronic assembly compartment on the structure, solar panels or scan platform.

Outriggers are bolted to the longerons at the short side of the bus to provide support for the solar panels at their hinge line. Cable harnesses and attitude control plumbing are routed on the outriggers to the solar panels. The solar panels are 122 cm (48 inches) by 305 cm (120 inches) which gives a gross area of 14.8 m^2 (160 square feet). The cell surface is a single skin on transverse corrugations supported on beams. The panels are folded down and their tips are supported by the spacecraft adapter during launch. A damper assembly is required at this tiedown to attenuate vibration response of the panels.

The spacecraft is attached to the orbiter adapter truss at the four longerons in the middle of the long bays. The attachment is made to the adapter through pyrotechnically separable bolt and spring assemblies. The orbiter adapter truss is fabricated of aluminum alloy with each member being approximately 10.1 cm (4.0 inches) in diameter. This truss structure spans from the launch vehicle's 12-point truss adapter (Centaur-spacecraft adapter) to four separation points on the ring of the orbiter bus.

The propulsion module truss members, which have been increased in diameter and length to accommodate the increased propellant loading, tie into the orbiter lower ring structure at the same

points at which the adapter truss members attach, thus transferring loads to the adapter in a direct load path. The propulsion module is designed to be an entity, with truss members tying the tanks, pressure vessel and thrust plates together. Tabs are fabricated on the tanks to accommodate the truss member attachment fittings. Motor alignment is made by adjustment of the motor on the plate.

The propellant is housed in two propellant tanks. These tanks are fabricated of 6Al + 4V titanium alloy and are cylindrical with hemispherical domed ends measuring 104 cm (41 inches) in diameter by 150 cm (59 inches) in length. The current Viking Orbiter tanks measure 91.5 cm (36 inches) in diameter by 137 cm (54 inches) in length. The pressurant tank assembly consists of a single 74 cm (29 inch) diameter (corresponding Viking Orbiter tank diameter is 62.5 cm) titanium sphere.

Aside from the modifications required to be made to the propulsion module as cited above, the local "beef-up" of the orbiter lower ring structure to handle the increased weight of the propulsion module there are no other modifications required to be made to the basic structural components of the Viking '75 Orbiter.

b. Centaur-Spacecraft Adapter - The Centaur-spacecraft adapter truss which is supplied by GDC is designed to accommodate a wide range of spacecraft payloads. It consists of twelve aluminum truss members each 6.35 cm (2.5 inches) in diameter by .15 cm (.06 inch) in wall thickness, spanning from the attachment at the Centaur stage to the interface of the orbiter adapter truss.

A preliminary stress analysis was conducted to evaluate the capability of the Mars Viking Centaur-Spacecraft Adapter to accommodate the Phobos/Deimos loading conditions. This analysis indicated that the present adapter is adequate to sustain the loading imposed by the Phobos/Deimos mission.

c. Lander/Orbiter Adapter - The lander/orbiter adapter is a completely new design. The truss was increased approximately 10.2 cm (4.0 inches) in length when compared to the baseline Mars Viking adapter truss in order to provide sufficient clearance for the Multi-Hundred Watt RTG.

As shown in Figure IV-1 the adapter truss consists of 2024 aluminum alloy tabular members that attach at four points to the orbiter and at three points to the lander. Separation bolts and springs are installed on the upper end fitting of each of the three attachment points. The juncture of the adapter truss with the lander provides the separation plane of the adapter truss and the lander when the lander is separated from the orbiter. The adapter truss remains with the orbiter. Diagonal members provide restraint in a fixed position. A truss arrangement was employed not only from a structural point of view, but it is required to accommodate the strategy selected for navigation use in which the cameras on the scan platform must see out through the adapter. Thermal leakage from the orbiter bus through the truss is taken to be small, even with aluminum, but a material with a lower conductivity may be required.

Loads resulting from the launch phase of the mission design the adapter truss. The truss members are stepped column members with a maximum diameter of 8.5 cm (3.25 inch), tapering to a diameter of 3.2 cm (1.25 inch) at each end. Wall thickness is approximately .32 cm (.125 inches).

d. Lander/Rover - The baseline lander/rover vehicle is configured in much the same manner as the baseline Mars Viking Lander. As shown in Figure IV-2, the shape of the lander body is essentially a truncated triangle, approximately 316 cm (124 inches) across the points. The enclosed web box body structure is fabricated of aluminum alloy and consists of an upper equipment mounting

plate and side and end beams. The bottom surface consists of a thin metallic non-loading carrying structure which serves to complete the thermally enclosed box structure. Supporting subsystems are attached to the lander body by means of the equipment mounting plate. This mounting plate which is designed by launch loads was analyzed for the loads and g level imposed by the Phobos/Deimos mission. The external arrangement shown in Figure IV-4 illustrates the addition of the Multi-Hundred Watt RTG, rendezvous radar, terminal descent propellant tanks and the three-cluster motor assembly. As can be seen, these are located around the periphery of the lander in such a manner as to ensure that the CG of the lander is in the required location. The closed box lander configuration allows for an environmentally controlled compartment of approximately .91 meters³ (32 cubic feet) to protect thermally sensitive components.

To maintain adequate external equipment temperatures during the cruise and landed "night" phase of the mission, multilayer insulation is required to be added to selected critical components. In addition, heaters are required to maintain the externally mounted terminal descent propellant tanks at acceptable levels.

The three-legged landing gear configuration shown in Figure IV-2 has a ratio of leg spread radius to CG height of two to provide suitable landing stability. With a R/H ratio of 2.0 we have the capability to handle slopes of up to 25°. This same gear arrangement would provide approximately 45° of slope capability if the vehicle were landed on the Martian surface. For comparison purposes the present Mars Viking Lander is 100% stable for slopes up to 22° for Martian landings. The gear design as presented in Figure IV-2 is highly damped and very stiff to minimize the rebound effect. The stability analysis that was

conducted to evaluate the preliminary estimate of the landing stability utilized the method described in Appendix D.

The landing "g" loads experienced during the initial landing were approximately 0.5 Earth g's. Again, for comparison purposes the Mars Viking Lander experiences g levels of approximately 30.0 Earth g's when performing Martian landings.

Deployable items such as the cameras, gamma-ray spectrometer, and coarse age dating instrument are deployed by using a furlable boom identical to the one being developed for the surface sampler on Viking '75.

2. Dynamic Environment

A primary design objective for the Phase I study effort was to ensure that the primary structural elements have sufficient rigidity so as to avoid boost vehicle control-stability problems, excessive deflections and high structure responses. A preliminary dynamic assessment was conducted to assist in the design of the main structural elements to meet this objective.

The most critical acoustic environments exist during liftoff and time of maximum Q for the baseline Mars Viking. The acoustic level for the modified orbiter utilized for the Phobos/Deimos mission is of course identical to that experienced by the Viking '75 Orbiter. The acoustic level experienced by the lander/rover vehicle during the launch phase is predicted to be 143 dB. This is a 3 dB higher than the Mars Viking Lander value of 140 dB. This increased acoustic level experienced by the Phobos/Deimos lander/rover results from the absence of the bioshield, base cover and aeroshell, with their attendant acoustic attenuation characteristics.

Since it was highly desirable to make maximum utilization of Mars Viking Lander subsystem components in the design of the Phobos/Deimos lander/rover, a preliminary assessment was made as

to whether or not the present Viking subsystems could be employed without requalification in light of the increased acoustic levels to which the components would be subjected. The predicted random vibration induced by the acoustic generated excitation during liftoff was determined to be 4.2 grms for the Phobos/Deimos lander/rover compared to 3.0 grms for the baseline Mars Viking Lander. However, the qualification level to which all equipment and components must be qualified is 10 grms. Thus, even though the Phobos/Deimos level of 4.2 grms is still well below the qualification test level of 10 grms. Thus, no requalification of components is required due to the environment experienced for the Phobos/Deimos mission.

Perhaps the above statement requires some additional explanation. The rationale that no requalification of components is required is based on the current criteria that is used for the baseline Mars Viking. This criteria states that components on the lander structure, equipment mounting plate, and aeroshell must meet a 6.0 grms acceptance level test, and a 10 grms qualification test level. These levels were established by customer direction, based on his judgement that a minimum level of 6.0 grms is necessary to uncover manufacturing defects, and that a 4.5 dB margin shall be maintained between acceptance and qualification levels, resulting in the somewhat artificial 10 grms qualification test level. Thus, the maximum predicted vibration level of 4.2 grms for the Phobos/Deimos mission does not exceed 6.0 grms, and, therefore, this mission does not change the random vibration criteria.

The Phobos/Deimos mission imposes no increases in pyrotechnic shock magnitudes. High intensity, high frequency shock transients will be generated by the operation of linear charges and squib actuated pyrotechnic devices. The resulting design criteria for

the Phobos/Deimos mission will be within those used for the baseline Mars Viking mission.

Sustained accelerations will be applied to the Phobos/Deimos spacecraft during operation of the launch vehicle. The maximum design level accelerations are not different than those experienced by the baseline Mars '75 mission.

3. Alternate Spacecraft Configuration

An alternate configuration was investigated in which the entire orbiter delivery system is landed on the satellite surface instead of deploying a separable lander/rover payload. This section will address itself to a discussion of the configurational modifications required to adapt the modified orbiter of our baseline configuration to a landed orbiter role.

The additional structural modifications required to be made to the landed orbiter are confined to the octagonally shaped bus structure. The propulsion module modifications required for the landed orbiter concept.

Some of the more important modifications required are;

- 1) Four landing legs approximately 4.6 m (15 feet) in length are provided. A four-legged configuration was chosen instead of the three-legged concept employed for the lander/rover because the octagonal shape of the orbiter bus and the four solar panel arrangement tend to make a four-legged configuration more desirable. Although the landing stability is increased by approximately 5° (compared to a three-leg concept), the post-landing stability is reduced, since the loads can be imposed on two diagonally opposed legs. In addition, the weight attributed to the landing leg assembly is increased by some 9.0 kgs (20.0 pounds).

- 2) A terminal (final) descent propulsion system, similar to the terminal descent propulsion system used on the lander/rover is added to accomplish the landing phase of the mission. Four clusters of four thrusters each are mounted on the periphery of the orbiter bus (lander/rover required three clusters of four thrusters each) to supply the requisite closing ΔV . Propellant tanks are located within the bus structure.
- 3) The UHF and relay telemetry components have been removed, since a relay communication capability is no longer required.
- 4) A rendezvous radar has been added to the upper surface of the science module (see Figure IV-6).
- 5) A science module which houses the science complement for the landed orbiter mission is attached to the upper surface of the orbiter. As can be seen in Figure IV-7 the science module is facing the surface of the satellite when the landed orbiter is on the satellite's surface to facilitate the retrieval of science data.
- 6) Flip covers have been mounted over the existing Viking Orbiter temperature control louvers to de-activate the system during the landed "night" operations. Heaters have also been added as well as phase change material to selected components in order to equalize the diurnal variations.
- 7) Provisions have been made to enable the outboard panels of the solar array to be deployed so that they droop approximately 32° below the horizontal after the orbiter has settled on the surface of the satellite.

D. THERMAL CONTROL

The thermal control effort in support of the baseline Phobos/Deimos rendezvous and landing mission was directed towards two principal areas of study: prediction of the mission thermal environments, and thermal analyses of the proposed baseline and alternate vehicle configurations. The environmental studies included a parametric evaluation of diurnal ground temperature cycles of the Martian satellites, and an analysis of contamination hazards due to thermally stirred dust on their surfaces. The thermal design analyses were concentrated on the baseline and alternate landers, although adequate consideration was given to the thermal problems of the entire mission profile.

The level of detail of the analyses was that required for an adequate evaluation of mission feasibility.

1. Environmental Studies - Ground Temperature Profiles

The principal elements of the satellite thermal environments consist of the direct and reflected (albedo) solar fluxes and the infrared emission of the ground. For a given landing site, the first two of these can be predicted in a straightforward manner from known orbital parameters and albedo data; the infrared component, however, requires a parametric evaluation because of the unknown thermophysical properties of the satellite soils.

The predicted ground temperature profiles of Phobos and Deimos were determined from published data pertaining to Mars and the Moon, by the use of thermal similarity transformations. It may be shown that at comparable latitudes (and sun-spin axis angles) the thermal similarity of celestial bodies is guaranteed by the invariance of the following two parameters:

$$N_I = eT_R^4/a \quad \text{and} \quad N_{II} = (krc)^{1/2}/eT_P^3^{1/2}$$

where

e = emissivity, a = absorbtivity, k = conductivity,
 r = density and c = heat capacity of the soil; and
 T = surface temperature, R = distance from the sun,
 and P = period of rotation of the celestial body.

The results are shown in the form of a set of diurnal ground temperature profiles, with soil thermal inertia as a parameter on Figure IV-25. The thermal inertia, $(krc)^{1/2}$, ranges from "lunar-like" values to infinity (indicated by the dashed horizontal line on the figure). It is evident that the "lunar-like" soils are associated with wider extremes, and represent the worst-case conditions for the purposes of thermal feasibility studies.

2. Environmental Studies - Thermally Stirred Dust Atmosphere

Due to the low gravity on the surfaces of Phobos and Deimos, particulate matter (if present) may undergo thermal motions similar to the molecules of a gas. If such "atmospheres" of dust extend to sufficient heights to envelope the vehicle, they may cause contamination of thermal coatings and optical surfaces on the lander.

According to the tenets of statistical mechanics, at thermal equilibrium the dust particles will follow a Maxwellian velocity distribution, only their average speeds will be considerably lower than in the case of a molecular gas, because of the relatively large particle masses of the dust. For example, at 300°K, the root-mean-square speed of a 10^{-15} gram dust particle is 0.11 m/sec, as compared to 482 m/sec in the case of oxygen molecules. (Compare these with the escape velocities of Phobos and Deimos, which are of the order of 10 m/sec.)

The effect of gravity can be taken into account by the artifice of the "scale height." For an isothermal atmosphere, the scale height is defined as:

$$H = kT/Mg$$

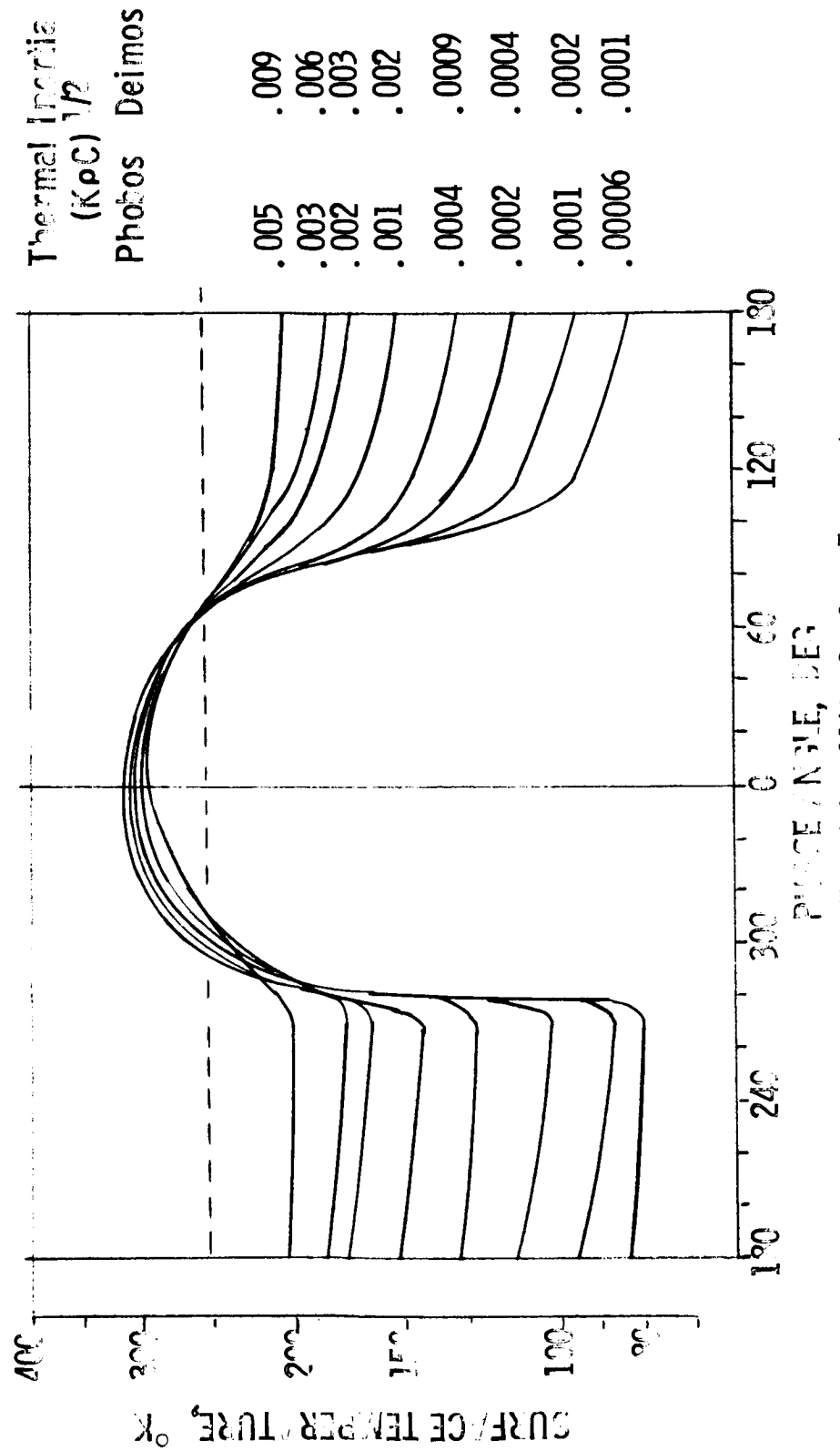


Figure IV-25 Predicted Satellite Surface Temperatures

where

k = Boltzmann's constant, T = temperature, M = particle mass, and g = acceleration of gravity. (For the dimensions of these parameters see Table IV-11). The scale height is numerically equal to the thickness of the atmosphere when "compressed" into a hypothetical uniform layer of constant density equal to the atmospheric density at ground level. The scale height also determines the rate of decrease of atmospheric density with height, according to the "barometric equation:"

$$n/n_0 = \exp(-Z/H)$$

where

n = particle number density at height Z , n_0 = particle number density at ground level. The following table was calculated from the above equation for illustrative purposes:

Z/H	=	1	10	100	200	225
n/n_0	=	0.368	4.54×10^{-5}	3.72×10^{-44}	1.38×10^{-87}	10^{-100}

Calculated representative scale heights for dust on Phobos and Deimos, for 300°K ground temperature, and a range of values of surface gravities and particle masses are shown on Table IV-11.

Since the characteristic height of a typical lander is in the order of 1 m, it is readily apparent that dust particles smaller than 10^{-14} g represent a potential contamination hazard on the satellites, whereas particles heavier than 10^{-13} grams will have little or no effect.

3. Thermal Design - Areas of Concern

The Phase I thermal analyses were concentrated on the landed phases of the mission, which presented the more challenging thermal requirements due to their unique environmental constraints. The

Table IV-11 Scale Height of Thermally Stirred Dust Atmospheres

	Phobos		Deimos	
	0.4	3.0	0.2	1.0
g, cm/sec ²				
Scale Height, H, m				
Particle Mass, g				
10 ⁻¹⁷	103.5	13.8	207.0	41.4
10 ⁻¹⁶	10.35	1.38	20.7	4.14
10 ⁻¹⁵	1.035	0.138	2.07	0.414
10 ⁻¹⁴	0.104	0.014	0.207	0.041
10 ⁻¹³	0.010	0.001	0.021	0.004
10 ⁻¹²	0.001	-	0.002	-

$$P = P_0 e^{-Z/H}$$

$$H = kT/Mg$$

P = Pressure, nt

P₀ = Pressure @ ground level, nt

Z = Altitude, m

H = Scale Height, m

k = Boltzmann's Constant

M = "Molecular" Mass, Kg

g = Acceleration of Gravity, m/sec²

interplanetary phases of the mission present no fundamentally new requirements as compared to Viking, although some significant differences in the respective vehicle configurations exist.

The potential thermal problem areas, and the proposed approaches to their solutions are summarized on Table IV-12.

Due to the absence of an aeroshell, base cover, and bio-shield, the Phobos/Deimos vehicles represent a more "open" thermal configuration than Viking; resulting in added insulation and heater requirements during the interplanetary phases of the mission. An estimated 100 watts (continuous) are required to keep the lander equipment compartment and the propulsion subsystem warm. The required heat energy may be supplied by the RTG (baseline configuration) or the orbiter (alternate configuration).

The relatively high waste heat dissipation of the TOPS (Multi-Hundred Watt) RTG creates some concern of local overheating. For example, with the baseline configuration as shown, local overheating may cause a 1 percent degradation in the efficiency of the orbiter solar panels. No significant degradation of thermal control louver performance was identified, however.

The thermal environment during landing on the Martian satellites is less severe than during landing on Mars itself, because of the absence of an entry atmosphere. Plume effects can be accounted for by the use of standard preventive measures.

The principal concern during the landed phases of the mission is the difficulty in obtaining a satisfactory coupling between the thermal management of the vehicle, and the relatively short diurnal cycles of the satellites. During daylight, the environment is characterized by the absence of a convenient heat sink, and the presence of significant external heat loads. It is also during the daylight hours when internal equipment heat dissipation is expected to be a maximum. During the night hours, on the other

Table IV-12 Thermal Control Areas of Concern

<u>Mission Phase</u>	<u>Potential Problem Areas</u>	<u>Approach/Comments</u>
Pre-Launch	RTG Overheating	Assume A/C available
Boost	Aero-Heating of External Surfaces & Coatings	200°F max temps anticipated with 280 sec shroud separation (acceptable)
Cruise	Equipment Compartment & Propulsion Subcooling	75w heater power available from RTG 25w additional power required from orbiter Potential utilization of TOPS RTG waste heat to be evaluated Insulation/heater mods required on orbiter
	Hot Spots Due To RTG Waste Heat	1% max (near Mars) degradation in orbiter solar panel efficiency; can be reduced to 1/2% by increasing distance between lander and orbiter by 1 ft No significant effect on lander and orbiter thermal control
Midcourse & Orbital Maneuvers	Overheating Due To Solar Transients (Same as Cruise)	No problems have been identified (Same as Cruise)
Post MOI Coast & Maneuvers	Plume Effects	High-temp insulation required on some surfaces; allow for effects of possible contamination of thermal control surfaces
Landing	Maintaining Vehicle Thermal Balance with Variable/Partial Solar Exposure	Max utilization of RTG electrical heat Study utilization of RTG waste heat Max utilization of solar heat (alternate configuration)
Landed Operations	Contamination by Dust	Scale height of possible "dust atmosphere" calculated; confirmation by experiment required

hand, external heat loads are entirely absent, and little or no heat is available from the equipment.

Under these conditions, there are obvious advantages associated with RTG power supplies, which represent a continuous energy source for thermal control purposes.

In view of the dust contamination hazards discussed above, the use of thermal-optical coatings whose performance is sensitive to dust, should be avoided, especially for long-duration missions.

4. Thermal Design - Baseline Configuration

Temperature control of the equipment compartment of the baseline lander is achieved by the use of insulation, penetration-heat leaks for the disposal of internally generated heat, solar-reflective external coatings to desensitize the vehicle from solar flux variations, and thermostatically-controlled heaters, powered by the available excess electrical energy from the TOPS RTG.

The calculated performance of the baseline thermal control subsystem is depicted on Table IV-13. The two environmental extremes considered are the "cold extreme," representative of maximum distance from the sun and reduced solar exposure during the day due to shadowing by crater walls and/or occultations by Mars. The "hot extreme" corresponds to the minimum solar distance during the mission, and unobstructed view of the sun during daytime.

The thermal budget shown on Table IV-13 is self-explanatory. The thermal control requirements of the mission can be met with adequate margins, when using this system. Note, however, that some 50 percent of the available electrical power from the RTG is used for thermal control purposes.

Table IV-13 Landed Thermal Performance, Baseline Configuration

	Cold Extreme	Hot Extreme
Distance From Sun, AU	1.53	1.396
Solar Exposure/Cycle, Hrs	2.75	3.827
Heat Budget, Watt-Hours/Diurnal Cycle		
Equipment Heat Dissipation, Day	206.3	287.0
Equipment Heat Dissipation, Night	80.9	63.1
Thermal Control Heaters, Max. Available	286.8	223.9
Max. Gain/Cycle	574	574
Heat Loss Through Penetrations (0.73 w/°F ΔT)	490	383
Heat Loss Through Insulation (MLI)	12	10
Total Loss/Diurnal Cycle	502	398
Margin on Heaters	72	176
Loss + Margin	574	574
Equipment Temperature Amplitude, °F	32	25

5. Thermal Design - Alternate Configuration

A schematic of the thermal control subsystem of the solar-powered alternate lander is shown on Figure IV-26. The equipment compartment is partially insulated, leaving its top surface available for a carefully designed radiation interface with the environment.

The major portion of the top surface (approximately 23 ft²) is covered with vacuum-deposited gold on Kapton, which represents a stable solar-absorber finish. Approximately 2 ft² of the top area consists of louver-controlled OSR radiator surface. Both the absorber and radiator are radiatively coupled with the equipment mounting plate.

The performance of this system for the hot and cold extremes previously discussed is depicted on Table IV-14. The requirement for a substantial solar energy absorber is indicated by the relatively small internal heat dissipation of this vehicle coupled with the large penetration heat leaks, characteristic of planetary science payloads.

The only performance margin available with this scheme is that provided for by the controlled emittance of the OSR radiator. A further disadvantage of this configuration lies in that the top surface of the lander cannot be used as a mounting platform for external equipment.

6. Conclusions

The conclusions of the Phase I thermal analyses are summarized on Table IV-15.

E. PROPULSION

The Phase I propulsion studies were concerned with the redesign and adaptation of the Mars Viking Orbiter primary and attitude control propulsion systems to meet the dictates of the

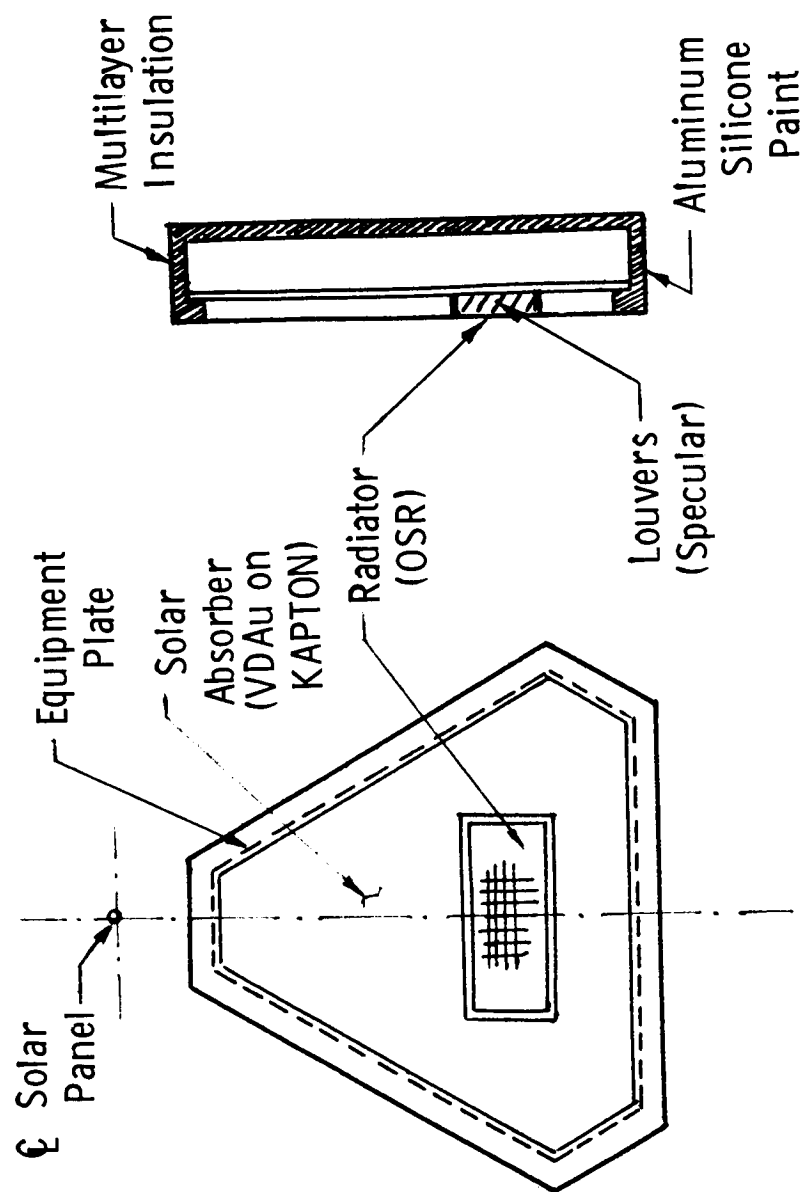


Figure IV-26 Thermal Control Schematic/Alternate Configuration

Table IV-14 Landed Thermal Performance/Alternate Configuration

	Cold Extreme	Hot Extreme
Distance From Sun, AU	1.53	1.396
Solar Exposure/Cycle, Hrs	2.75	3.827
Heat Budget, Watt-Hours/Diurnal Cycle		
Equipment Heat Dissipation, Day	154	154
Equipment Heat & Heaters, Night	98	61
Net Solar Absorbed by 23 Ft ² Absorber	315	504
Total Gain/Diurnal Cycle	<u>567</u>	<u>719</u>
Heat Loss Through Penetrations (0.73 w/°F ΔT)	490	383
Heat Loss Through Insulation (MLI)	10	8
Net Heat Emitted by 3 Ft ² Radiator*	67	328
Total Loss/Diurnal Cycle	<u>567</u>	<u>719</u>
Equipment Temperature Amplitude, °F	35	45

* Effective Emittance Controlled by Louvers

Note: Equipment Temperature Limits: 40 to 90°F and 0 to 100°F

Table IV-15 Phase I Conclusions - Thermal Analysis

<u>Environment:</u>	(1) Post MOI (Orbital)	: Less heat available than for Viking due to occultations and maneuvers
	(2) Landed	: Stabilized periodic exposure with moderate upper temperatures; on the average, a "cold" problem. Deimos more severe due to its longer period. Possibility of contamination & interference by thermally stirred dust atmospheres.
Thermal Design:	(1) RTG Lander/Rover Thermally Best Suited for the Mission	
		: RTG waste heat available during cruise & "night," provides flexibility for landing on any site, consistent with penetration heat leaks characteristic of landed science payloads.
	(2) Alternate Lander	: Heat budget extremely marginal, requires 100 watts from orbiter during cruise, solar panel thermal interface complicated, mission limited to sub-solar latitudes.
	(3) Landed Orbiter	: Extensive thermal modifications required to account for reduced power availability during landed operations and interference of ground radiation with louver performance.

Phobos/Deimos rendezvous and landing mission. A separable Phobos/Deimos lander propulsion system design was also generated and an Earth launch vehicle was selected.

1. Titan IIIIE/Centaur Launch Vehicle

The basic launch vehicle chosen for the Phobos/Deimos rendezvous and landing mission is a Martin Marietta/General Dynamics Titan IIIIE/Centaur. The Titan IIIC, Titan IIIF/Centaur and Shuttle/Centaur launch vehicles were also reviewed as possible candidates. The Titan IIIC launch vehicle did not have sufficient payload capacity for the mission and the performance capabilities of the Titan IIIF/Centaur and Shuttle/Centaur exceeded that required by a substantial margin. Therefore, the Titan IIIIE/Centaur is the smallest of these launch vehicles that will provide adequate mission capability. The Titan III and Centaur are currently being integrated and developed to launch the Viking spacecraft to Mars in 1975.

The Titan IIIIE/Centaur is a three-stage vehicle with two solid rocket motors (SRMs) and a standard Titan core. The SRMs, designated as Stage 0, are manufactured by United Technology Center and provide total vehicle thrust from liftoff to SRM separation. Each SRM consists of five center segments, forward and aft closures, nozzle, igniter, staging rockets, and thrust vector control (TVC) system. The center segments weigh about 35,800 kgs (79,000 pounds) when loaded with propellants. The nominal burn time of the SRMs is 117 seconds. TVC is achieved by injecting N_2O_4 into the exit nozzle; approximately 7650 kgs (16,850 pounds) of N_2O_4 is provided for this purpose. The SRMs deliver 1,050,000 kgs (2,307,000 pounds) of thrust to the vehicle and have a vacuum specific impulse capability of 266 seconds.

The core (Stages I and II) primary propulsion consists of gimballed pump feed engines that utilize nitrogen tetroxide as an

oxidizer and 50-50 mixture of hydrazine and unsymmetrical dimethylhydrazine as a fuel. These engines are manufactured by Aerojet-General Corporation. Stage I uses LR-87 engines with a nominal burn time of 146 seconds; this engine has two independent sub-assemblies mounted on a single engine truss assembly. The LR-87 engine thrust chambers have expansion ratios of 12:1 and deliver 301 seconds of vacuum specific impulse. These engines deliver 242,000 kgs (523,000 pounds) of thrust. The Stage II uses a single LR-91 engine. The LR-91 engine thrust chamber has an expansion ratio of 49:1 and is aligned with the centerline of the vehicle. This engine has a nominal burn time of 206 seconds and delivers 317 seconds of vacuum specific impulse. The Stage II engine uses exhaust products from the engine gas generator for vehicle roll control.

The Centaur is powered by two Pratt and Whitney RL-10 restartable engines rated at 6,800 kgs (15,000 pounds) thrust and 433 seconds of vacuum specific impulse. The RL-10 engines utilize the cryogenic propellants liquid hydrogen and liquid oxygen. Propellant is fed from each of the tanks to the engines by boost pumps driven by hydrogen peroxide turbines. Each engine contains integral "boot-strap" pumps driven by hydrogen propellant, which is also used for thrust chamber regenerative cooling. Centaur attitude control and propellant settling are provided by 6 pressure-fed monopropellant thrusters. For small corrections in yaw, pitch and roll attitude control, the system utilizes six individually controlled hydrogen peroxide reaction engines. These engines are mounted in clusters of three, 180 degrees apart on the periphery of the main propellant tanks at the interstage adapter separation plane. Each cluster contains one 2.7 kgs (6 pound) thrust engine for pitch control and two 1.59 kgs (3.5 pound) thrust engines for yaw and roll control.

In addition, four 22.6 kg (50 pound) thrust hydrogen peroxide engines are installed on the aft section of the vehicle, with thrust axes parallel with vehicle axis. These engines are used during retromaneuver for executing large attitude corrections if necessary.

2. Phobos/Deimos Orbiter Propulsion

The primary objective of the modified Phobos/Deimos orbiter propulsion subsystem is to provide the necessary thrust and attitude control forces required by the spacecraft to get to Phobos after separation from the Titan IIIE/Centaur boost vehicle. The primary propulsion system and attitude control system of the Viking spacecraft was selected during Phase I for application to the Phobos/Deimos orbiter.

a. Primary Propulsion - The Phobos orbiter employs a single propulsion subsystem module for all posigrade and retrograde velocity maneuvers including in transit trajectory corrections, orbit insertion at Mars encounter, and a series of orbital transfers culminating in the rendezvous with Phobos.

The principal propulsion system components for the baseline alternate spacecraft configurations generated in Phase I are identical to the Viking Orbiter system except for the size of the propellant tanks and pressurant sphere. The propulsion subsystem is functionally a pressure-fed multi-restart, fixed thrust, storable bi-propellant propulsion system, utilizing the propellants nitrogen tetroxide (N_2O_4) and monomethylhydrazine (MMH) at a weight mixture ratio of 1.550/F. The propulsion subsystem is designed to be an entity and includes all of the mechanical, structural, pneumatic, and hydraulic subassemblies required to provide a direct impulse from a mechanically-separable modular assembly. Principal components consist of a mounting structure, a high-pressure gas reservoir, a pneumatic pressure regulator, two propellant tanks with screens, and a rocket engine assembly

which is electromechanically gimballed in two planes and utilizes a direct acting, electrically operated, normally closed, linked, bi-propellant valve. The propulsion system schematic for the Phobos orbiter is presented in Figure IV-27.

The 136 kg (300 pound) thrust engine assembly is a Rocketdyne RS-2101 engine which demonstrated reliability on the Mariner 1971 spacecraft. To date, no serious hardware problems or anomalies have been encountered. Engine cooling is achieved by "intergen cooling" of the beryllium chamber and portions of the 60:1 expansion ratio L-605 (Haynes 25) nozzle extension. The RS-2101 operates at 117 psia chamber pressure and delivers 285 seconds of specific impulse; this value of specific impulse was used in computing propellant requirements for the Phobos/Deimos orbiter.

Thrust vector control consists of two-axes pivoted gimbaling with two push-pull linear electromechanical actuators. During the motor burn phases, attitude control is provided by the thrust vector control system and the roll channel of the attitude control system. The control system points the engine thrust vector through the spacecraft center of mass and maintains pitch and yaw attitude stability. Engine torque created by the interaction of the swirling exhaust gases on the engine nozzle extension is counteracted by the Phobos/Deimos orbiter roll control attitude thrusters.

The propellant tank assemblies consist of two equal volume propellant tanks. The propellant tanks have been increased 38% in volume over that of the Viking Orbiter tanks to meet mission propellant requirements. The Phobos/Deimos orbiter useable propellant load is 1928 kgs (4250 pounds). The tanks are titanium (Ti6Al-4V) and are cylindrical with hemispherical dome ends measuring 104 cm (41 inches) diameter by 149 cm (59 inches) long. The current Viking Orbiter tanks measure 91.5 cm (36 inches) in

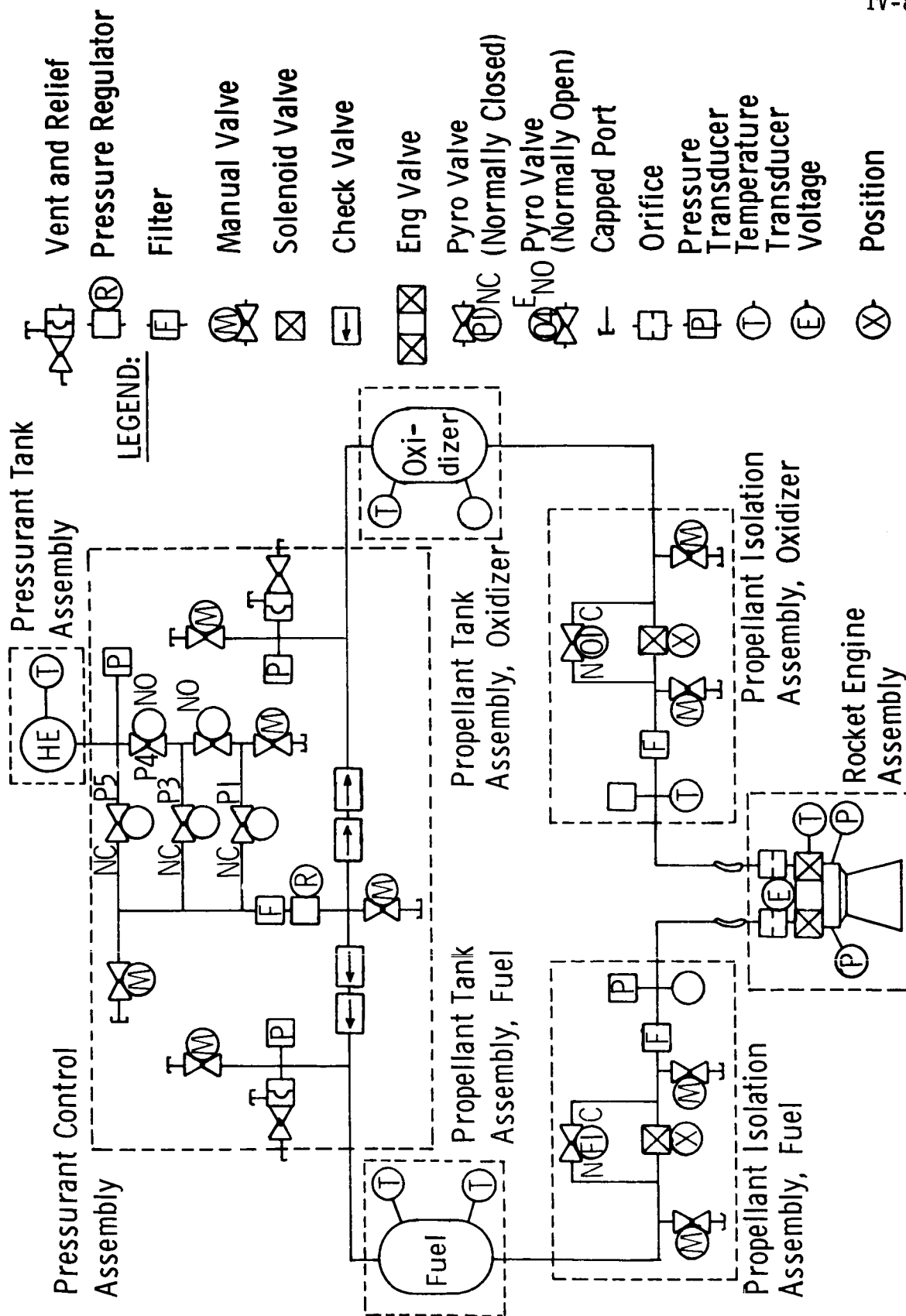


Figure IV-27 Phobos/Deimos Orbiter Propulsion System Schematic

diameter by 137 cm (54 inches) in length. The propellant tank operating pressure is 228 psia. The 38% increase in tank volume results in minor changes to the Viking spacecraft bus and still permits acceptable clearance within the launch vehicle payload fairing.

The pneumatic assembly consists of 2 subassemblies; a pressurant tank assembly and a pressurant control assembly. The pressurant tank assembly consists of a single 73.5 cm (29 inch) diameter (corresponding Viking Orbiter tank diameter is 61.9 cm (24.5 inches) titanium (Ti6Al-4V) sphere that is initially charged to 4000 psia with 14.2 pounds of helium. The pressurant control assembly includes gauged pyrotechnic valves, a single stage pressure regulator, flow filter, series check valves for propellant separation and propellant-fed line pressure relief provisions.

Listed in Table IV-16 is the propulsion system weight statement for the baseline Phobos/Deimos orbiter. The propellant load has been increased by 531 kgs (1170 lbs) over that of the 1975 Viking Orbiter. Table IV-17 lists the ΔV capability and general weights for the Phobos/Deimos orbiter.

b. Attitude Control Propulsion - During all phases of the mission, except during main motor burns, 3-axis control of the orbiter spacecraft attitude is provided by the attitude control system. This control system is made up of the reaction control system (cold N_2 gas system), gyros, celestial sensors, and associated electronics and logic. This control system performs the following functions:

- 1) Removal of initial spacecraft tumbling rates which occur at Centaur launch vehicle/spacecraft separation.
- 2) Acquisition of celestial references with capability for automatic reacquisitions as required.

Table IV-16 Phobos/Deimos Orbiter Propulsion System Weight Statement

Item	Viking '75 Orbiter Weight (KGS)	Baseline Phobos/Deimos Orbiter Weight (KGS)
Engine Assembly	8.2 (18.0)	8.2 (18.0)
Propellant Isolation Assembly	10.9 (24.0)	10.9 (24.0)
Pressure Control Assembly	15.9 (35.0)	15.9 (35.0)
Propellant Tank Assembly	94.5 (208.0)	130.1 (287.0)
Pressurant Tank Assembly	40.8 (90.0)	56.3 (124.0)
Command and Squib Harness	2.7 (6.0)	2.7 (6.0)
Contingency	11.3 (24.9)	14.5 (32.0)
Total Inert Weight	184.3 (405.9)	238.5 (526.0)
Pressurant	4.7 (10.3)	6.4 (14.2)
Propellant	1399.0 (3080.4)	1929.0 (4250.0)
Residual Propellant	18.3 (40.4)	24.3 (55.7)
Total Propulsion System Weight	1606.3 (3537.0)	2198.2 (4845.9)

Table IV-17 Phobos/Deimos ΔV Capability and Weight Sequence

ΔV Capability	2670 m/sec
Injected Phobos/Deimos Orbiter Weight	3160 kg (6954 lbs)
Useable Propellant	1930 kg (4250 lbs)
Dry Phobos Orbiter	970 kg (2130 lbs)

- 3) Maintenance of stable limit cycle behavior during periods of transit and orbital cruise.
- 4) Inertial hold capability for commanded turns and sun occultations,
- 5) Third axis (roll) control during the motor burn phase of spacecraft maneuvers.

The reaction control system consists of 2 high pressure gas tanks, 2 pneumatic regulators and pitch, yaw and roll electric solenoid valves and valve manifolds. A schematic of the Phobos/Deimos reaction control system and corresponding weight statement is presented in Figure IV-28 and Table IV-18.

Control torques about each of the 3 spacecraft axes are provided by thrust couples, that result in elimination of cross coupling between axes. The roll/yaw and pitch valve assemblies are mounted at the ends of the 4 solar panels. The thrusters utilize nitrogen gas from 4000 psia storage tanks that have been regulated to 15 psia via a pneumatic pressure regulator. The pitch/yaw and roll thrusters deliver .032 kg (.07 pounds) and .0052 (.014 pounds) thrust respectively.

The attitude control propulsion gas storage requirements for the Phobos Orbiter are based on launch vehicle separation rate removal, acquisition, searches, overrides, commanded turns (including unwinding), roll axis torque during burns, cruise attitude requirements and leakage. The cruise and discrete events requirements, along with a propellant summary, are listed in Table IV-19. The control requirements for the Phobos Orbiter are the same as those of the 1975 Viking Orbiter.

c. Separable Lander/Rover Propulsion - A terminal descent (Phobos rendezvous and landing) and attitude control propulsion system design was generated during Phase I as part of the baseline vehicle.

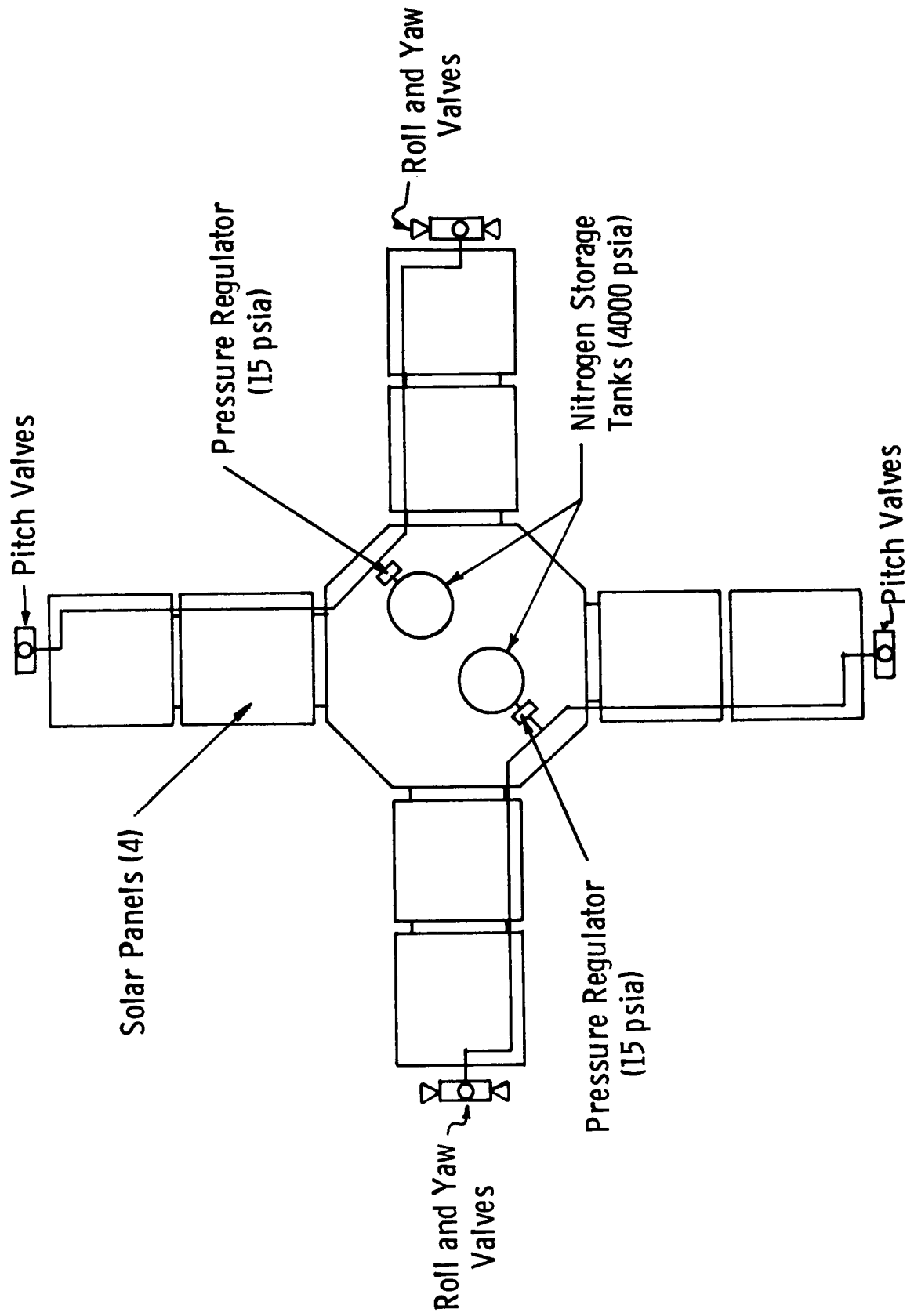


Figure IV-28 Phobos/Deimos Orbiter Attitude Control System

Table IV-18 Phobos/Deimos Orbiter Attitude Control
System Weight Statement

Item	Viking Orbiter		Modified Orbiter	
	Kg	lbs	Kg	lbs
Nitrogen	8.8	(19.3)	9.1	(20.0)
Nitrogen Tank	14.0	(30.8)	14.4	(31.9)
Fixed Gas System Hardware	10.7	(23.5)	10.5	(23.5)
Gas System Subtotal	33.5	(73.6)	34.0	(75.4)
Reaction Control Electronics	13.7	(30.3)	13.7	(30.3)
Reaction Control System Total	47.2	(103.9)	47.7	(105.7)

Table IV-19 Attitude Control System Requirements

CRUISE		DISCRETE EVENTS	
-	Limit Cycling	-	Initial Rate Reduction (3 deg/sec)
	Transit (325 Days)	-	Lander Separation Rate Reduction
	Orbital (115 Days)	-	Acquisitions (6)
-	Sun Occultations	-	Roll Searches (6)
-	Gravity Gradient	-	Roll Overrides (20)
-	Leakage	-	Command Turns (18)
		-	Main Engine Roll Control

PROPELLANT SUMMARY

Total Half System Propellant Requirement	3.0 Kg
RCS Sized for 3 Times Half System	9.1 Kg

For purposes of reliability and weight savings a monopropellant blow-down type propulsion system was chosen for these two configurations. The system consists of two titanium (Ti6Al-4V) hydrazine tanks, a gauged, normally-closed and normally-opened pyro-valved propellant filter and three quad-thruster/solenoid valve assemblies. The three engine assemblies are mounted in the same plane at equal angles on the outside of the lander bus (see Figure IV-2). These engines provide pitch, roll and yaw attitude control as well as rendezvous and landing thrust.

The thermally insulated propellant spheres are mounted around the periphery of the lander/rover body. A two-ply teflon polymeric bladder is used for tank propellant acquisition. The laminated construction consists of 5-mil polytetrafluorethylene (TFE) next to the hydrazine for strength and chemical compatibility and 5-mil polyfluorinated ethylene propylene (FEP) on the ullage or nitrogen side for permeation reduction and flexibility. Included in the propellant tank assembly are fill and drain provisions for the hydrazine propellant and nitrogen pressurant. The pyro-valve package consists of two normally-open and two normally-closed valves providing positive propellant isolation between rendezvous/landing burns and future surface maneuver burns. An in-line filter downstream of the pyro-valve package is provided to eliminate particulate matter from the thruster control valves. The thrusters and solenoid control valve assemblies are of the type to be used on the Mars Viking Lander for deorbit and terminal descent roll control. A schematic of the hydrazine thruster similar to the type recommended is illustrated in Figure IV-29. Shell 405 catalytic beds are used for spontaneous ignition of the hydrazine and the thrusters are capable of operating at chamber pressures up to 190 psia. A performance plot for the thrusters as a function of propellant feed

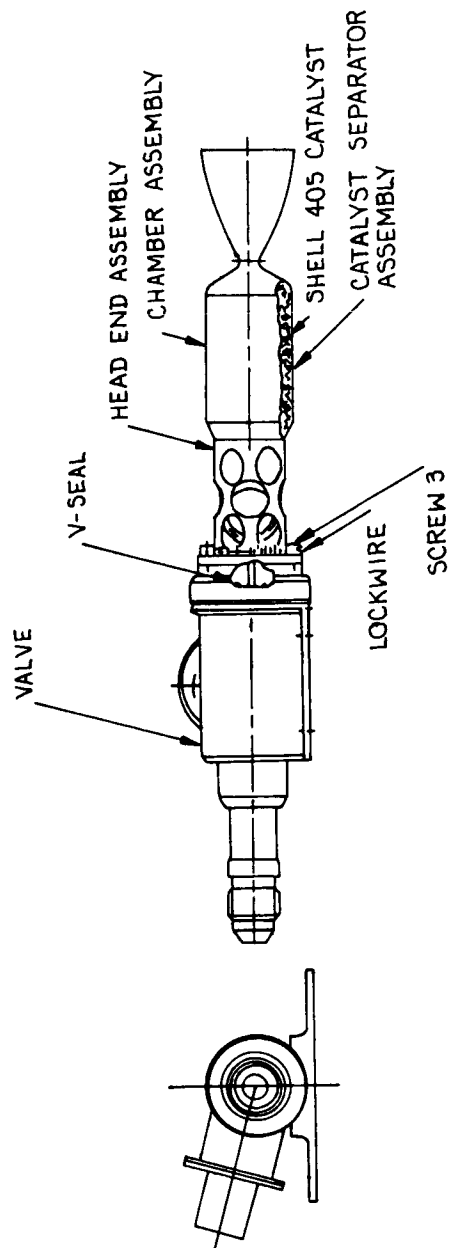


Figure IV-29 Thrust Chamber Assembly

pressure is presented in Figure IV-30. The resultant thrust variation for a propellant tank blow-down ratio of 2 to 1 (420 psia initial) is 4.25 kgs (9.25 pounds) to 2.54 kgs (5.6 pounds). A schematic of the lander/rover terminal descent propulsion system is shown in Figure IV-31. A weight statement for the lander propulsion system is presented in Table IV-20. Sufficient hydrazine has been allotted to provide for a ΔV capability of 50 meters/second for propulsive "hopping" after landing.

F. TELECOMMUNICATIONS

A number of communications links are required to adequately support the Phobos/Deimos mission. These include an uplink from Earth for transmission of commands and a downlink signal which is used for doppler tracking of the vehicle from Earth. The downlink signal also has subcarriers for telemetry transmission of science and engineering data, and command verification. The downlink can also be operated in the ranging mode where a wide-band pseudo-random noise modulation is employed to provide unambiguous turnaround ranging capability.

The communications links will be either direct S-band transmission to and from Earth or transmission to Earth via relay through an orbiter offset from the satellite surface. The link between the lander on the satellite surface and the orbiter will be at UHF and will utilize noncoherent frequency shift keyed (FSK) modulation. A nominal 1-watt output UHF transmitter and low gain antenna (HPBW = $\pm 65^\circ$) will be used on the lander. The orbiter communications subsystem will be identical to the Viking '75 configuration. It will consist of a UHF receiver and antenna and a 20-watt output S-band transmitter and high gain 58 inch diameter articulated parabolic antenna.

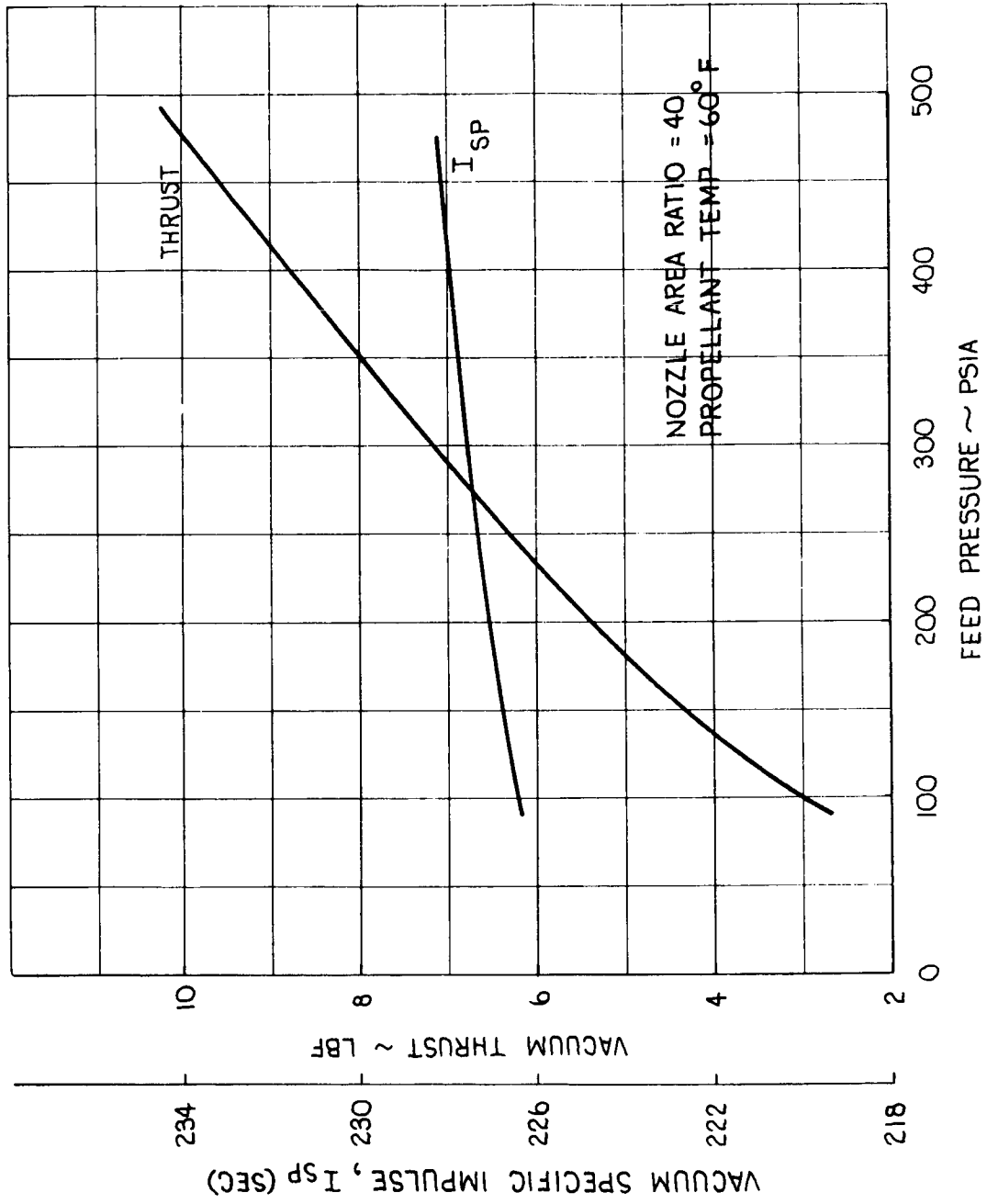


Figure IV-30 Performance of Lander Thruster

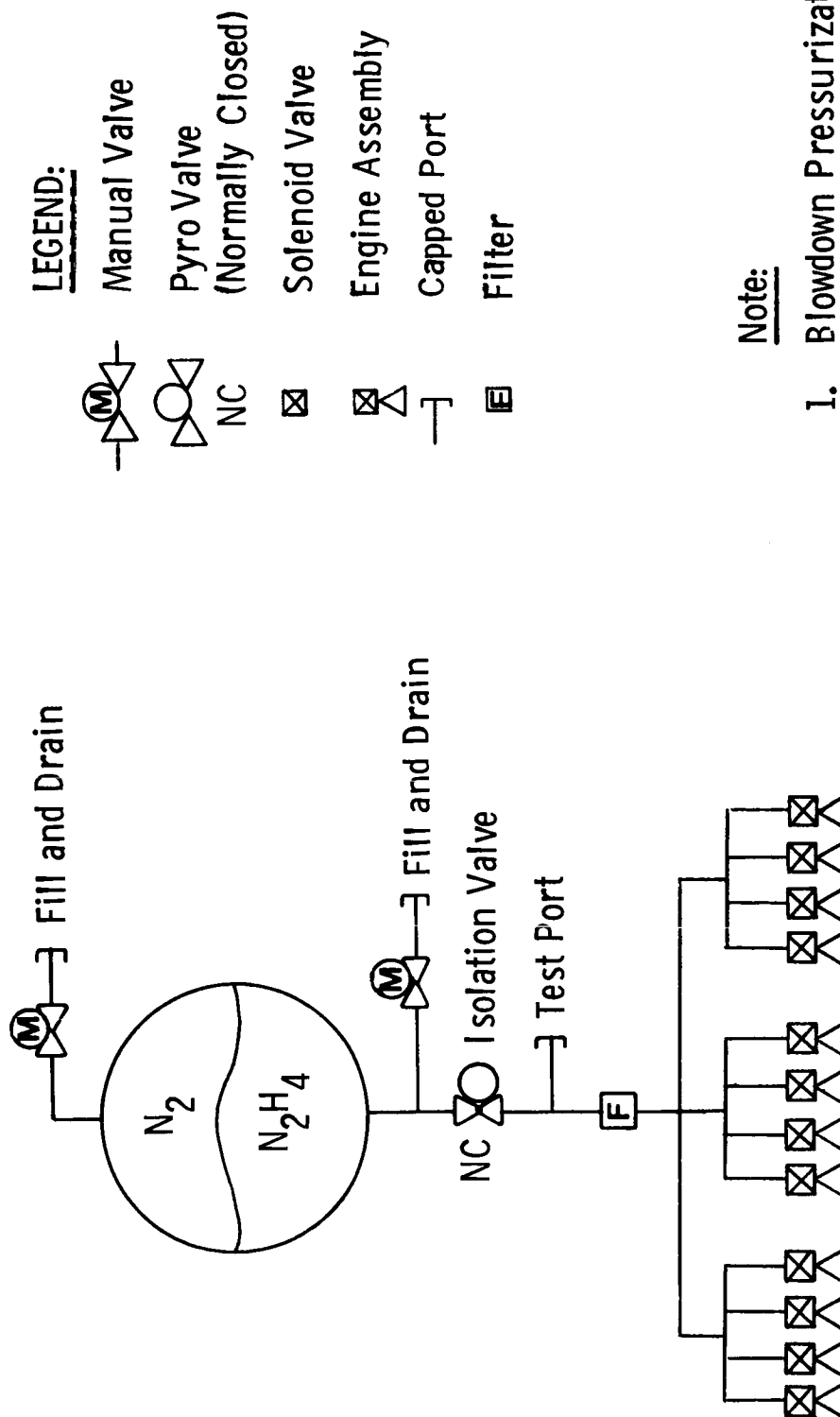


Figure IV-31 Lander/Rover Terminal Descent System Schematic

Table IV-20 Lander/Rover Terminal Descent Weight Statement

<u>Item</u>	<u>Weight (kg)</u>	<u>Weight (lbs)</u>
1. Engine Assemblies (12)	11.61	25.6
2. Filter	0.45	1.0
3. Isolation Valve	0.23	0.5
4. Fill and Drain Assemblies (2)	0.23	0.5
5. Propellant Tank Assembly	5.35	11.8
6. Plumbing, Wiring and Structure	5.63	12.4
7. Pressurant (N ₂)	1.18	2.6
8. Residual Propellant	<u>.91</u>	<u>2.0</u>
Total Inert Weight	25.59	56.4
9. Useable Propellant*	<u>30.40</u>	<u>67.0</u>
Total System Weight	55.99	123.4

* Sized for 50 mps ΔV Mobility Plus Rendezvous and Landing

The data rate capability for the lander to orbiter link will depend on the orbiter offset range from the satellite and is shown for a number of ranges in Table IV-21. For a lander to orbiter range of 350 km, the data rate allowable will be 16 kbps. For a two hour viewing time per orbit, the total data volume transferred between the lander and orbiter would be 115×10^6 bits.

The orbiter to Earth link has a maximum data transmission capability of 4 kbps at S-band. The orbiter data storage subsystem consists of two tape recorders with a storage capability of 640 megabits per recorder.

In Figure IV-32, the relative geometry of the orbital path around Phobos is shown. The viewing time between the satellite and the orbiter is two hours per orbital period of Phobos (7.65 hours).

Figure IV-33 shows the period of time in which the orbiter will be occulted from Earth view for both Phobos and Deimos. The average occultation for the Phobos mission between 10-3-80 to 1-3-81 is approximately one hour. Therefore, the average time available for transmission of data to Earth from the orbiter is 6.65 hours per revolution. At the allowable 4 kbps data rate, this amounts to a total data volume of 95.76 megabits per orbit.

To adequately define a communications subsystem for the baseline mission, a tradeoff comparison was made between the data volume obtainable via the direct to Earth link at both S-band and X-band and that obtainable via the relay link through the orbiter.

For the direct to Earth link a relatively high gain antenna would be required on the lander. This antenna would have to be pointed toward Earth and some articulation control provided to maintain sufficient signal strength.

The lander to Earth view times per orbit for Phobos vs date

Table IV-21 Relay Link Lander/Rover to Orbiter

2 Hour Transmission Time - Power Output = 1 Watt

Lander-Orbiter Range (Km)	Data Transmission Rate (KBPS)	Data Volume (Bits)
50	784	56.45×10^8
75	345	24.84×10^8
100	196	14.11×10^8
150	87.2	6.28×10^8
200	49.0	3.53×10^8
250	31.0	2.23×10^8
300	21.8	1.57×10^8
350	16.0	1.15×10^8
400	12.5	90×10^6
500	7.76	55.9×10^6
1000	1.94	13.97×10^6

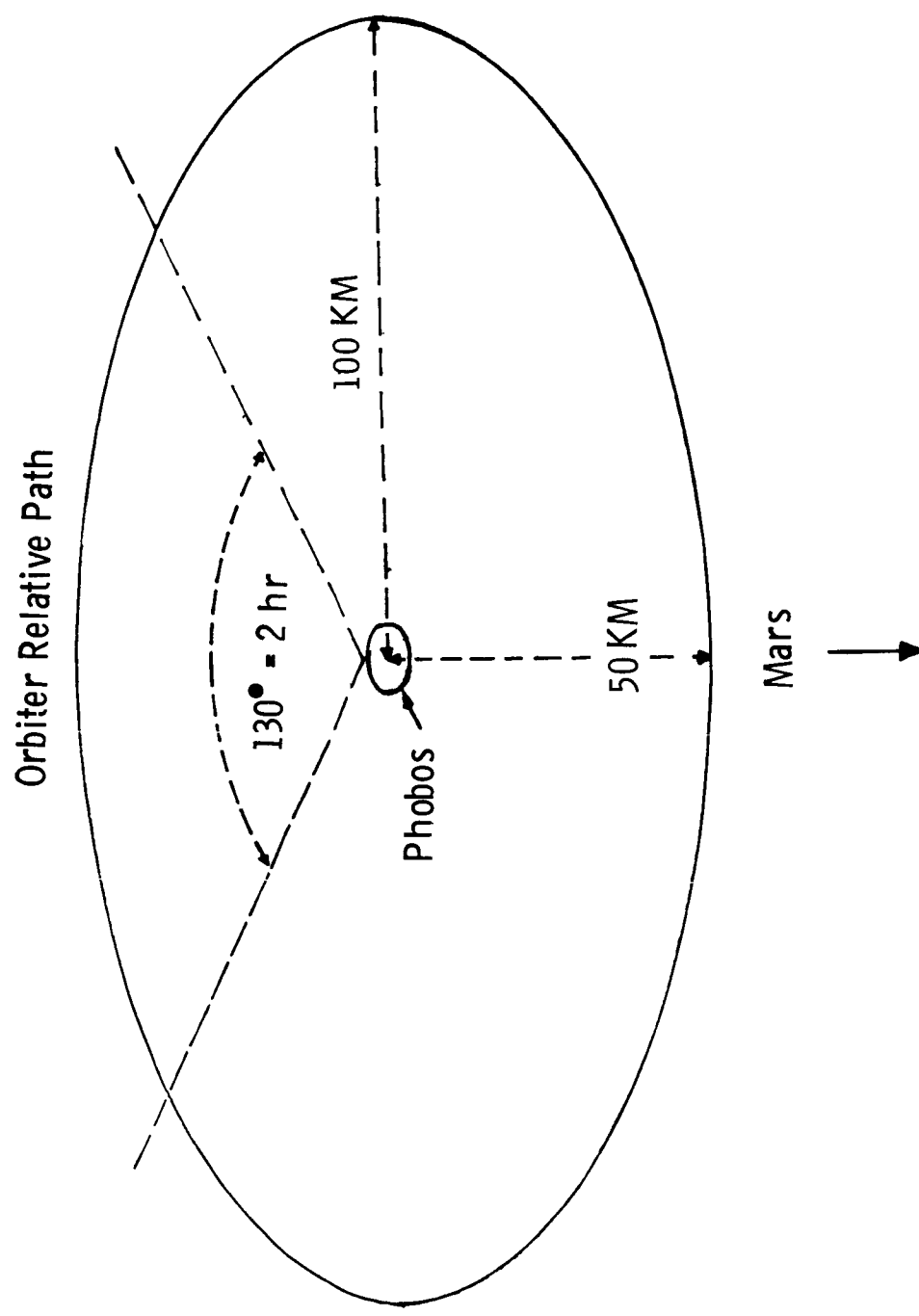


Figure IV-32 Lander to Orbiter - View Time

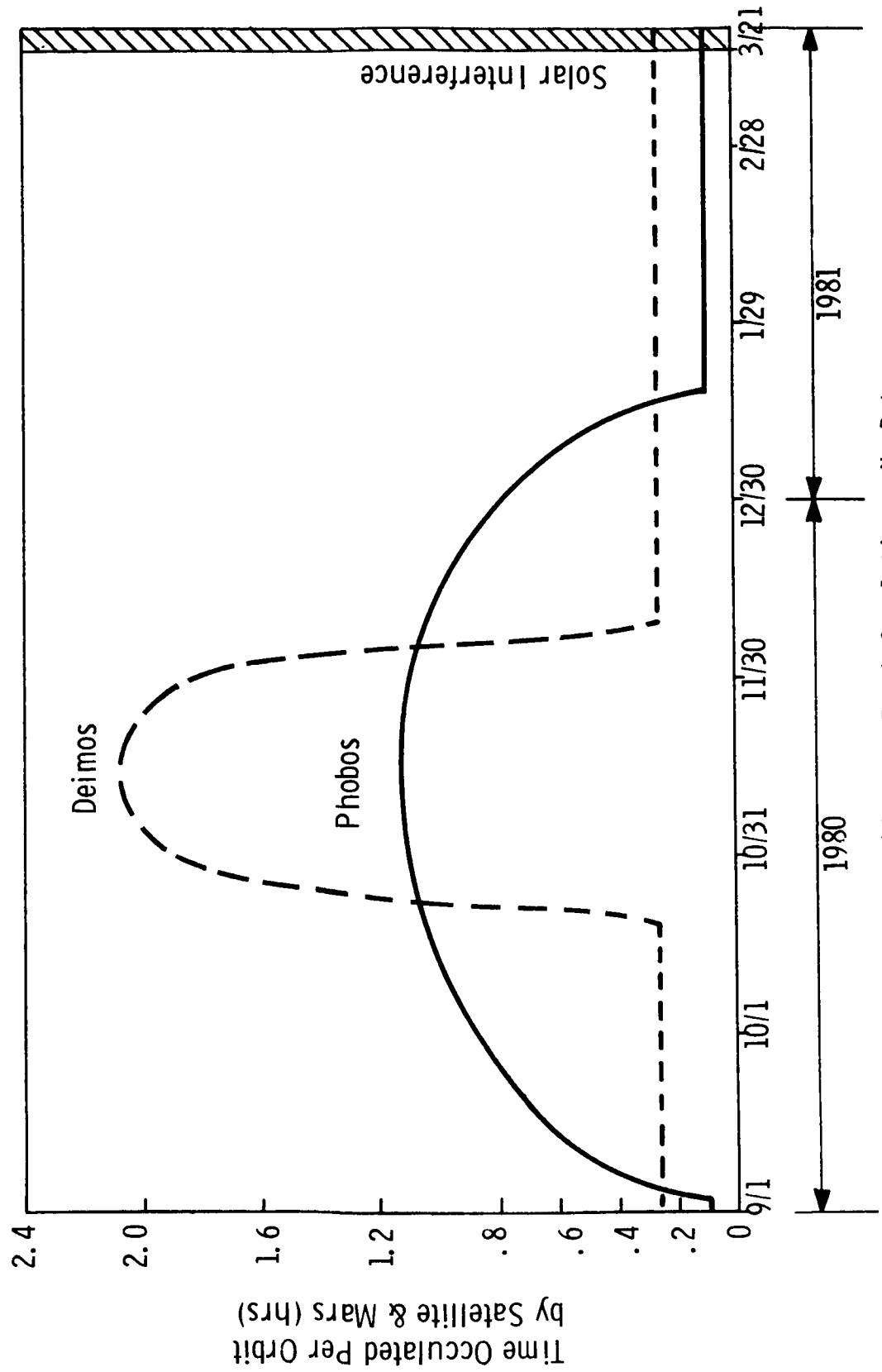


Figure IV-33 Orbiter to Earth Occultation - No Date

and as a function of landing site latitude is shown in Figure IV-34. For an equatorial latitude and for the mission dates considered, the average satellite to Earth view time is 2.7 hours per revolution.

If the Viking '75 S-band communications subsystem is considered for the lander to Earth direct link, the data transmission rate available is quite low, 250 bits per second. This subsystem consists of an S-band command receiver, a 20 watt output TWT amplifier and a steerable 30 inch diameter parabolic antenna. The 250 bps data transmission rate for a period of 2.7 hours of viewing time per revolution results in a total data volume per Phobos orbit period of 2.4 megabits. Since this does not represent a very large data volume capability, ways of increasing the capability were investigated.

If the link frequency utilized is X-band instead of S-band, a maximum increase in capability of 11.3 db is obtained for a given transmitter power output and fixed antenna aperture size ($20 \text{ LOG } 8500 \text{ MHz} / 2295 \text{ MHz} = 11.3 \text{ db}$). However, unlike S-band transmission which is impervious to weather conditions, local weather conditions at Earth (such as rainfall or heavy fog) can cause attenuation of X-band transmission. In addition, wind loading deformation effects on the large 210 ft DSN antenna must now be considered. The effects of local ground weather conditions on X-band propagation are shown in Figure IV-35. From the graph at the left of this figure, it is seen that for an average rainfall of 4.5 mm per hour and a wavelength (λ) of 3.5 cm, the attenuation due to oxygen absorption is 0.015 dB/km at X-band. The total attenuation would therefore be 0.045 dB/km. The weather and oxygen absorption are assumed to extend up to an altitude of 15 km. The total attenuation therefore for a vertical path or zenith would be 0.675 dB. Attenuation for angles other than zenith is obtained by multiplying the losses in the vertical direction by

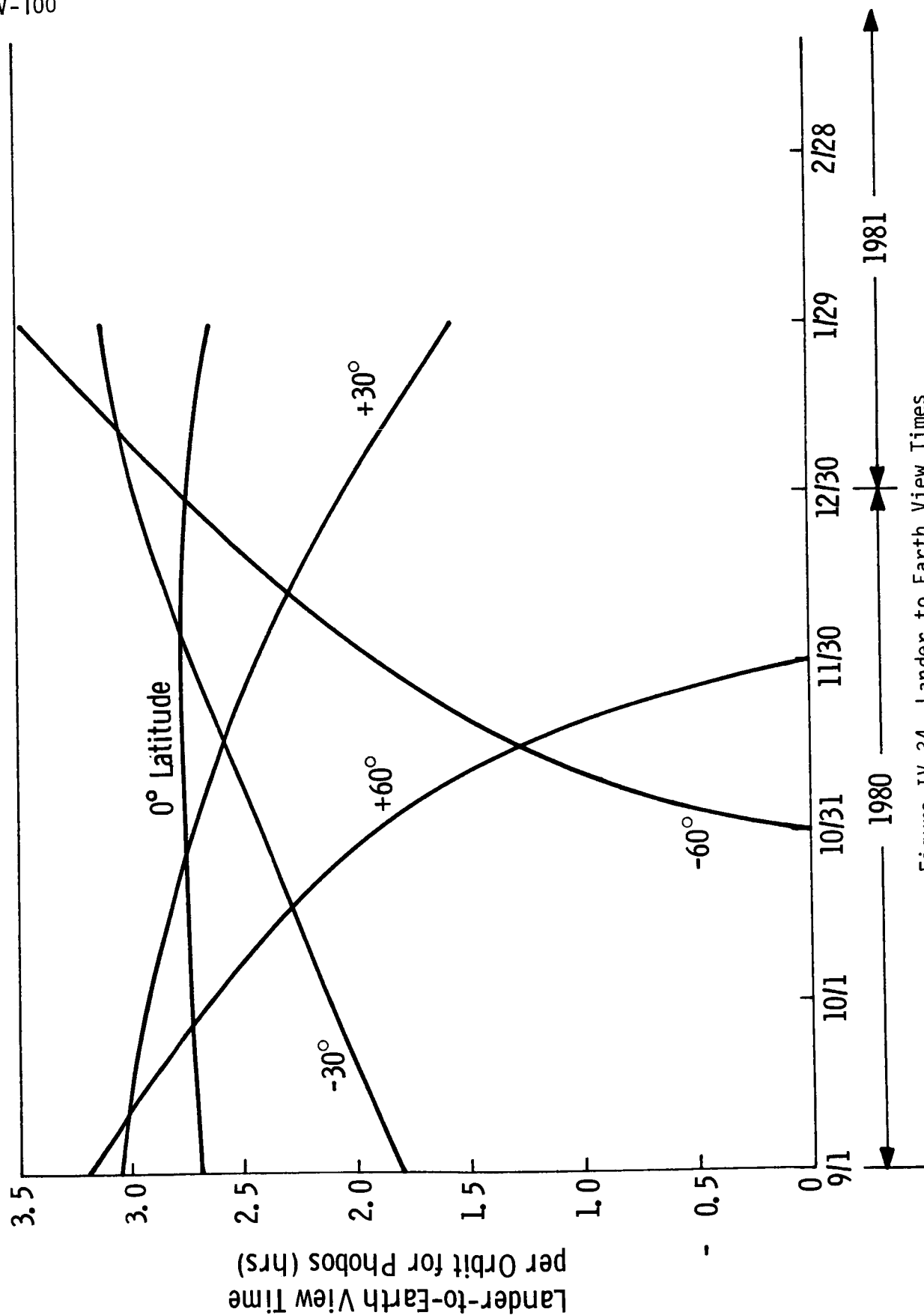
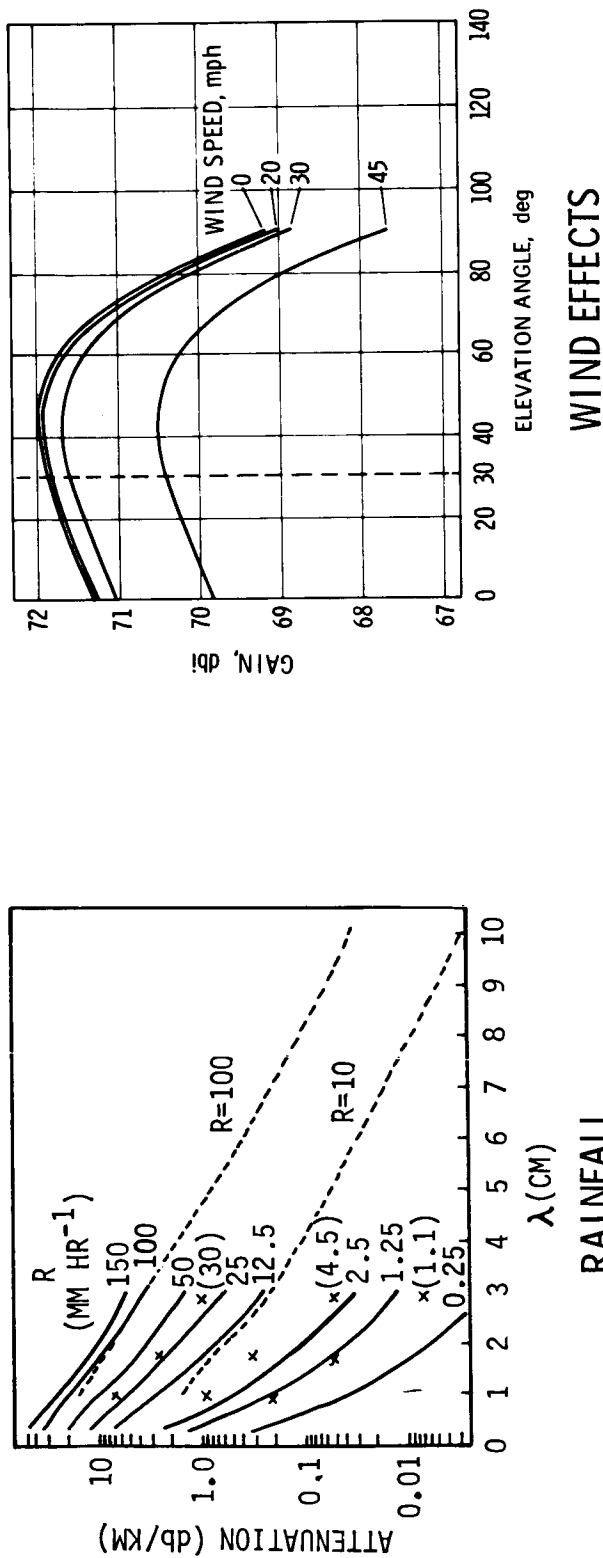


Figure IV-34 Lander to Earth View Times

Effects of Local Ground Weather Conditions on X-Band Propagation



Rainfall Attenuation - 1.5 db (4.5 mm/hr Rainfall)

Wind Effect on 210' Antenna - 1.5 db (Worst Case)

Total Degradation - 3.0 db (Worst Case)

Figure IV-35 Propagation of Anomalies of X-Band Transmission

by $1/\sin \theta$, where θ is the angle of elevation of the DSN antenna. Assuming an average elevation angle to be 30 degrees, the attenuation becomes $0.675 \times 1/\sin 30 \text{ degrees} = 1.5 \text{ dB}$.

The 210 foot DSN antenna gain as a function of elevation angle and wind effect is shown in the graph at the right of Figure IV-35. If the worst case wind velocity of 45 miles per hour is assumed, it is seen that the antenna gain is reduced by approximately 1.5 dB from the no wind condition.

Therefore, considering both the average rainfall and maximum winds occurring simultaneously, the total worst case attenuation would be 3 dB. This then reduces the theoretical advantage (11.3 dB) of X-band over S-band to around 8 dB. The data transmission rate capability at X-band would be approximately 2 kbps resulting in a data volume of 19.4 megabits per revolution.

The direct to Earth data rate and total volume could be doubled for both S-band and X-band by increasing the transmitter power output from 20 watts to 40 watts. In addition, the S-band antenna gain could be increased by 3 dB by increasing the antenna size from 30 inches to 42 inches, again doubling the allowable data rate.

When the data transfer capability of the direct link is compared to that of the relay link, it is seen that the relay link through the orbiter offers the more attractive communications option. This is particularly true, since the primary power requirement in the lander is reduced considerably with the use of 1 watt UHF transmitter instead of a 20 watt S-band transmitter. Also, the UHF antenna is a fixed wide beamwidth one which does not require steering as the S-band high gain antenna would. The data storage capacity afforded by the two high storage capacity recorders in the orbiter offer an opportunity for a much expanded science mission. This is particularly true for the transmission

and storage of high resolution imaging and TV data.

The S-band command receivers, decoders, and low gain antenna, however, will be retained in the lander to enable commands from Earth to be transmitted directly to the lander on the satellite surface. In addition, a command reception and verification capability will be provided from Earth via the orbiter to the lander.

G. POWER

Table IV-22 shows the various candidate primary power sources and secondary energy storage units that have been considered for use on Phobos/Deimos missions. For the baseline Phobos rendezvous and landing mission studied in Phase I, power subsystems were defined for:

1. Phobos/Deimos Orbiter Power

Shown in Table IV-23 are load listings for engineering and science for the orbiter together with determinations of total raw power requirements for major phases of the mission. The listings include loads imposed by the Phobos/Deimos Lander. Checkout prior to the landing operation is carried out using power from the orbiter. Plotted from comparison in Figure IV-36 are the raw power requirements together with the level of solar panel power available as taken from Table IV-24. Light areas indicate when power is available from the solar panels and shaded areas show periods when operation from the battery is necessary. The minimum margin of available power from the solar panels over that required is 11 percent.

2. Phobos/Deimos Lander/Rover Power

The Phobos/Deimos Lander/Rover must support the rendezvous and landing sequence after separation from the orbiter as well as

Table IV-22 Power Source Matrix

Vehicle	Primary Power Source						Secondary Source	
	Oriented Paddle Solar Array	Oriented Roll-up Solar Array	Omnidirectional Body Mounted Solar Array	RTG	Remotely Activated Ag-Zn Battery	Primary Fuel Cell	Ni-Cd Battery	Regenerative Fuel Cell
Orbiter	X	X					X	X
Lander	X		X	X			X	X
Orbiter/Lander	X	X	X	X			X	X
Lander/Rover	X		X	X			X	X
Rover	X		X	X			X	X
Sample Return (Satellite to Earth)		X	X	X				
Sample Return (Satellite to Orbiter)					X	X		
Sample Return (Orbiter to Earth)		X	X	X			X	X

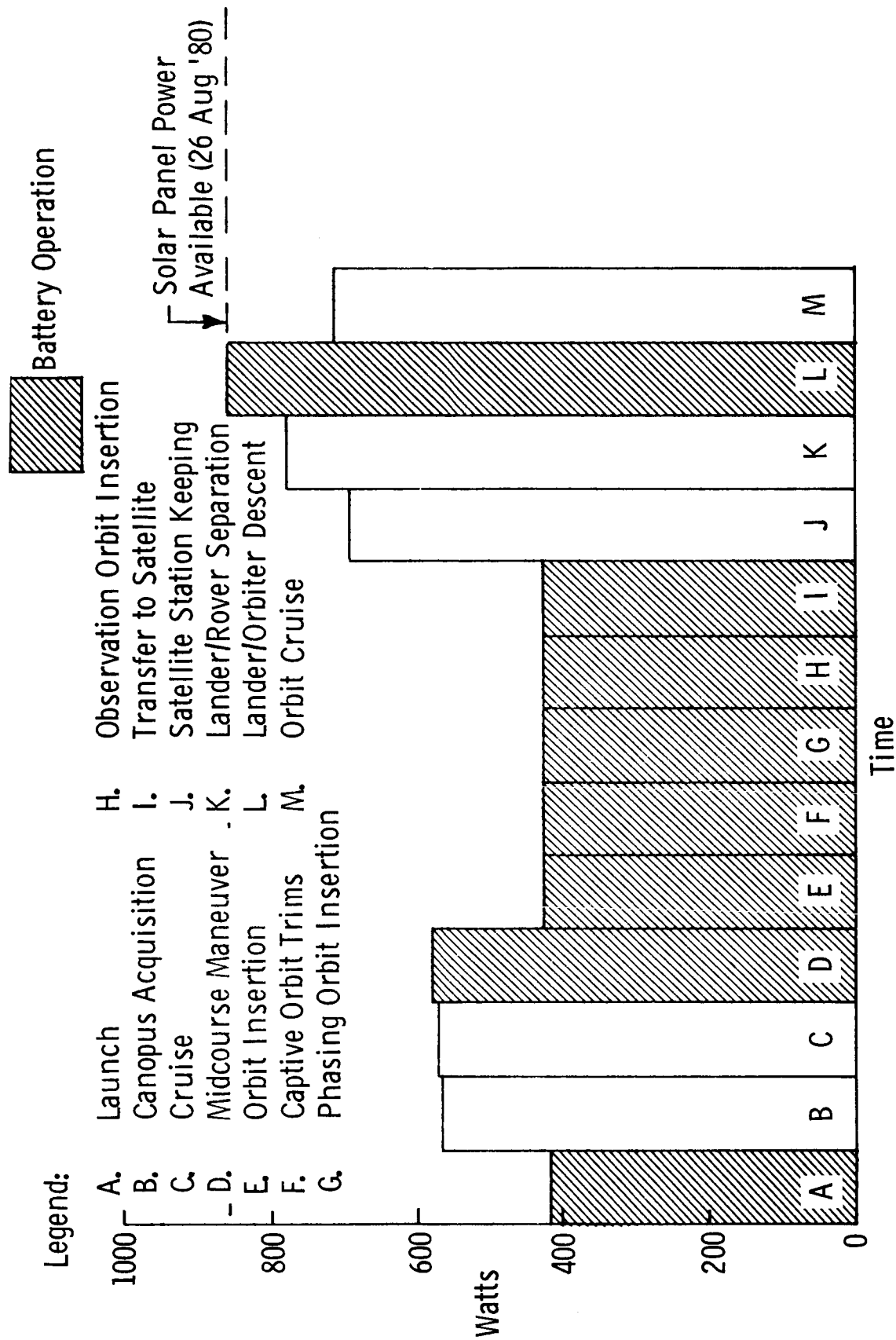


Figure IV-36 Orbiter Power Profile

Table IV-24 Orbiter Solar Panel Performance

	Arrival Date Aug 26 to Sep 20, 1980	90 Days Later Nov 26 to Dec 20, 1980
Distance From Sun	1. 53 to 1. 515 AU	1. 42 to 1. 396
Solar Intensity	59. 3 to 60. 7 mW/cm ²	69. 1 to 71. 5 mW/cm ²
Specific Power Near Earth (60°C) (No Rad Degradation)	10. 4 W/ft ²	10. 4 W/ft ²
At Mars	5. 35 W/ft ²	6. 0 W/ft ²
Total Power Available Near Earth	1664 Watts	1664 Watts
At Mars	856 Watts	960 Watts
Total Active Area	160 ft ²	160 ft ²

carry out science mission functions and data transmissions in Table IV-24. This tabulation includes operation of a rather ambitious science payload that uses the full 82 kg payload capability of the lander. By matching the power requirements shown in Table IV-25 to an assumed operational timeline, the power profile in Figure IV-37 is developed. The shaded area in the upper portion of the figure indicates when Sun is not available to a power system (4.90 hours) while the light portion (2.75 hours) indicates the presence of Sun. The total orbit time (7.65 hours) is the period of the satellite Phobos. The comparative short day time is caused by the assumption that the spacecraft has landed in a crater with a 30 degree side slope.

Power systems designed to serve the purposes of the lander/rover are shown in block diagram form in Figures IV-38 and IV-39. The RTG power source was chosen for the recommended baseline configuration and the solar array offered as an alternate. Each system includes provision of acceptance of power from the Viking Orbiter prior to separation.

When the lander/rover is operating on orbiter power, this power is regulated and isolation is maintained by redundant regulators. Isolated switches in the orbiter, controlled through the orbiter communications system, permit switching lander/rover loads as required. Redundant charge circuits are provided for conditioning and charging the batteries from orbiter power. The shunt regulator is designed to cause essentially constant current to be drawn from the power source (solar array or RTG) so as to maintain output voltage constant against input, ambient and load changes. The shunt regulator requires constant voltage and then dissipates the current difference between the power source current capability at that voltage and the load requirement.

Four eight ampere hour nickel cadmium batteries of the type

Table IV-25 Lander/Rover Power Summary (Watts)

EQUIPMENT NAME	Rendezvous Landing		Photography + Transmission		Sample Acquisition		Sample Analysis		Data Transmission		Photography + Transmission		Sample Acquisition		Sample Analysis		Age Dating + Transmission		Photography + Transmission		Location Transfer	
	1	2	3	4	5	6	7	8	9	10	11											
Experiments																						
Landed Imagery		18.0				18.0													18.0			
Dust Sampler			1.0																			
Drill Sampler																						
Integrated Geology		2.0	2.0	10.0	2.0	2.0	2.0	10.0									2.0		2.0			
Seismometer																						
Active Source Transmitter																						
Quasi-Microscope		3.0	3.0	3.0	3.0	3.0	3.0	3.0									3.0		3.0		5.0	
Gamma-Ray Spectrometer																	10.0					
Coarse Age Dating																						
Physical Properties																						
Subtotal		23.0	6.0	17.0	5.0	23.0	7.0	17.0									15.0		23.0		5.0	
Communications & Data Management																						
UHF Transmitter - 1 WRF	5.0	5.0			5.0	5.0											5.0		5.0			
S-Band Com Rec No. 1	6.5	6.5	6.5	6.5	6.5	6.5	6.5	6.5									6.5		6.5		6.5	
S-Band Com Rec No. 2																						
S-Band Com Def No. 1	1.5	1.5	1.5	1.5	1.5	1.5	1.5	1.5									1.5		1.5		1.5	
S-Band Com Def No. 2																						
Data Acq & Proc Unit	12.5	14.0	12.5	12.5	14.0	14.0	12.5	12.5									12.5		14.0		12.5	
Tape Recorder	10.5	10.5	10.5	10.5	10.5	10.5	10.5	10.5									10.5		10.5		10.5	
Core Storage																	2.5					
Subtotal	46.0	37.5	31.0	33.5	37.5	37.5	31.0	33.5									36.0		37.5		31.0	
Guidance, Navigation & Control																						
Guid, Control & Seq Comp	50.0	6.0	6.0	6.0	6.0	6.0	6.0	6.0									6.0		6.0		50.0	
Attitude Ref Unit	60.0																					
Velocity Ref Unit	10.0																					
Rendezvous Radar	60.0																					
Subtotal	180.0	6.0	6.0	6.0	6.0	6.0											6.0		6.0		50.0	
Reaction Control System	0.9																				0.9	
Electrical Losses	11.6	3.3	2.2	2.8	2.7	3.3	2.2	2.8									2.9		3.3		4.3	
TOTAL	238.5	69.8	45.2	59.3	50.9	69.8	46.2	59.3									59.9		69.8		91.2	

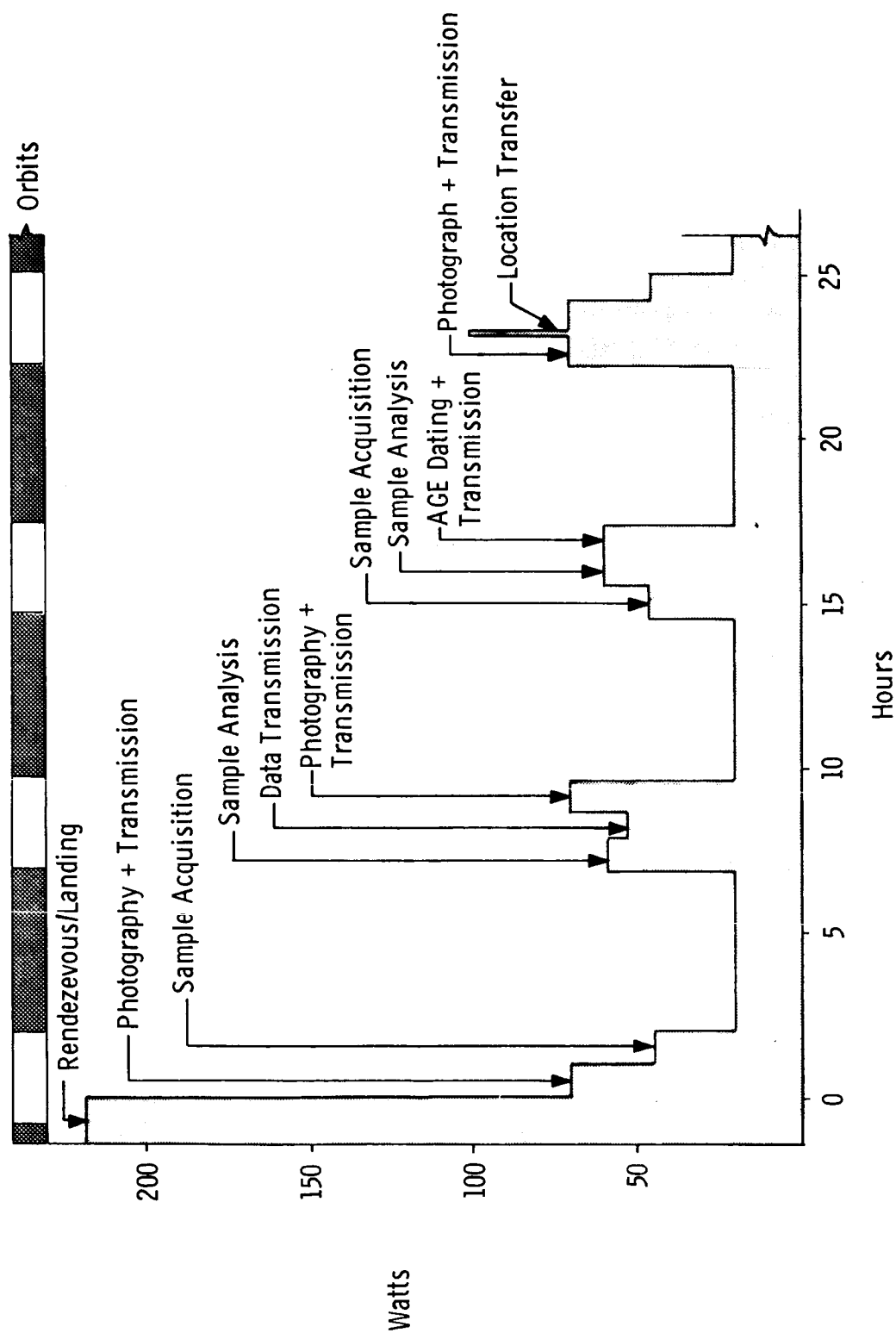


Figure IV-37 Lander/Rover Profile

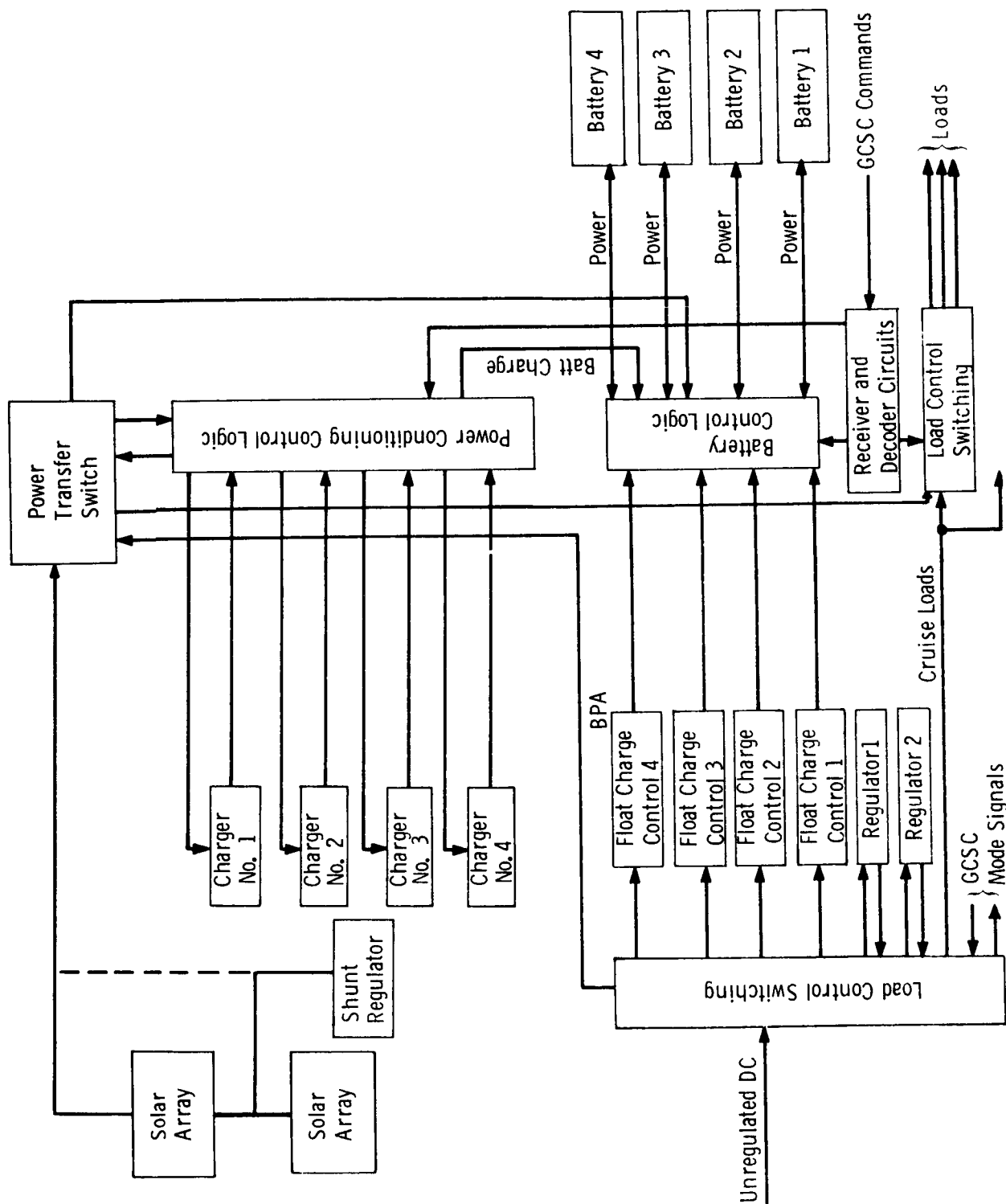


Figure IV-38 Solar Array Power System

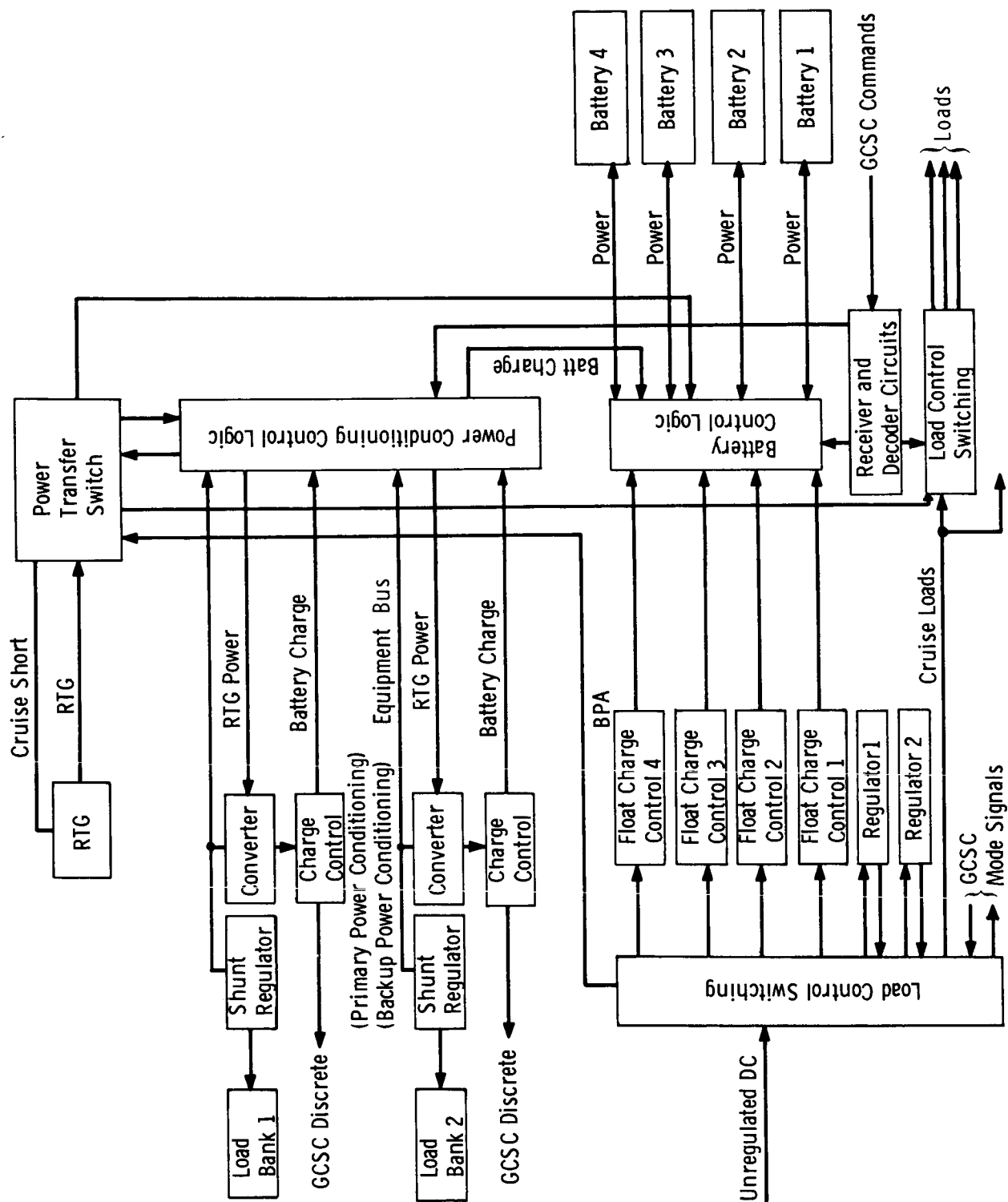


Figure IV-39 RTG Power System

used in the Viking '75 lander are utilized to provide the high peak power during landing and to provide power during night periods with the solar panel system. Three batteries are sufficient to provide power for the landing phase with one kept on standby. During this phase they are discharged by 12 ampere hours or to 50 percent of capacity. This is within the 75 percent limit established for the Viking '75 program.

Table IV-26 gives a weight breakdown for RTG and solar panel systems each of which are capable of meeting mission needs. The two power sources are shown on the lander in Figure IV-4 and Figure IV-5. The RTG is a derated version of one being developed by General Electric for the Atomic Energy Commission under the Multi-Hundred Watt Radioisotope Thermoelectric Generator Program (Ref. 3). It employs a silicon germanium converter heated by the radioisotope PU-238.

When the RTG is used, supplemental power is needed only during landing. As an alternative to the nickel cadmium batteries, a remotely activated silver zinc battery with a lower weight could be used for the RTG powered system.

In selecting the articulated 3.9 m^2 (42 ft^2) solar panel for the alternate lander configuration trade studies were performed to compare roll-up, articulated and body mounted arrays. The articulated panel shown in Figure IV-5 was chosen on the basis of weight, operational simplicity, and solar efficiency.

3. Landed Orbiter Power

An alternative to providing a separate vehicle for the landed operations is to use the orbiter in a landed mode. An examination was made of the power requirements for operation of the orbiter on the surface during periods when data transmission is taking place. This mode, as shown by the listings in Table IV-27, requires 330 watts of raw power.

Table IV-26 Power Source Tradeoffs

RTG	Solar Panel
Beginning of Mission: 137 Watts	Gross Capacity: 150 Watts
Derated Capacity: 100 Watts	Availability: 36% of Orbit
No Battery Needed for Landed Operation	Needs Battery for Keep-Alive Night Loads
Does Not Limit Time of Operations	Majority of Operations Limited to Sun Periods
Radiation (110 mrem at 1 meter) Can Affect Some Science Instruments	Solar Orientation Required for a 42 sq ft Panel
Weight:	Weight:
RTG	Solar Panel
Control Logic	Control Logic
Shunt Regulator & Load Bank	Shunt Regulator & Load Bank
Support Landing Battery	Support & Orientation Batteries
	Battery Chargers
45.2 kg (99 lb)	85.4 kg (188 lb)

Table IV-27 Landed Orbiter Loads - Transmitting Mode

	<u>Watts</u>		<u>Watts</u>
2.4 KHZ Inverter		Booster Regulator	147.5
Engineering Loads		Total 2.4 KHZ Inv Input	.885
Malfunction Det Sys	6.7	Total B/R Input	166.5
Flight Data System	29.2	Unregulated Power	
Power Distribution	13.0	Total B/R Input	166.5
Radio Freq Sys (ex TWT)	27.5	Battery Charging	60.0
Articulated Control	35.3	Power Failure Sensors	1.5
Data Storage Sys	17.1	TWT System	92.0
Total Engineering Loads	128.8	Total Unregulated Power	320.0
Science Loads		PSL Eff	.97
Seismometer	2.0	Total Raw Power	330.0
Gamma Ray Spectr	3.0		
Total Science Loads	5.0		
Total 2.4 KHZ Inverter Load	133.8		
2.4 KHZ Inv Eff	.906		
Total 2.4 KHZ Inverter Input	147.5		

The orbiter solar array consists of eight solar cell panels with a total area of 160 sq ft. In the landed configuration the outer four panels are inclined downward at an angle of 32 degrees. Output of the panels is computed on the basis of a Sun distance of 1.53 AU and a landed panel temperature of 55.5°C. The resulting output of the array as a function of Sun angle from the zenith is given in Figure IV-40. Also shown is the power required by the orbiter to carry out data transmission. This shows that available power permits data transmission to be carried out to Sun angles of 47.5 degrees from the zenith. This is equivalent to 2.2 hours per Phobos day.

H. ROVER CONCEPTS

By adding mobility to a Phobos/Deimos landing mission access can be gained to virtually any point on the satellite surfaces during a 90-day lander mission, making it possible to analyze both large and small scale surface variations. It should also be noted that the best landing sites (smooth areas) will not, in all likelihood, correspond to the best science sites.

In addition to providing access to surface variations and escape from landing site contamination, mobility can be used to follow a path that will provide maximum communication windows as the Earth/Mars/Phobos/Deimos/Orbiter geometry changes during the mission.

Even for less sophisticated, stationary lander missions, separable mobile science may be desirable or necessary to lessen the influences of landing site contamination and lander interferences.

During Phase I, the anticipated rover operating environment was summarized using the Phobos/Deimos engineering model developed early in the study. This information is summarized in

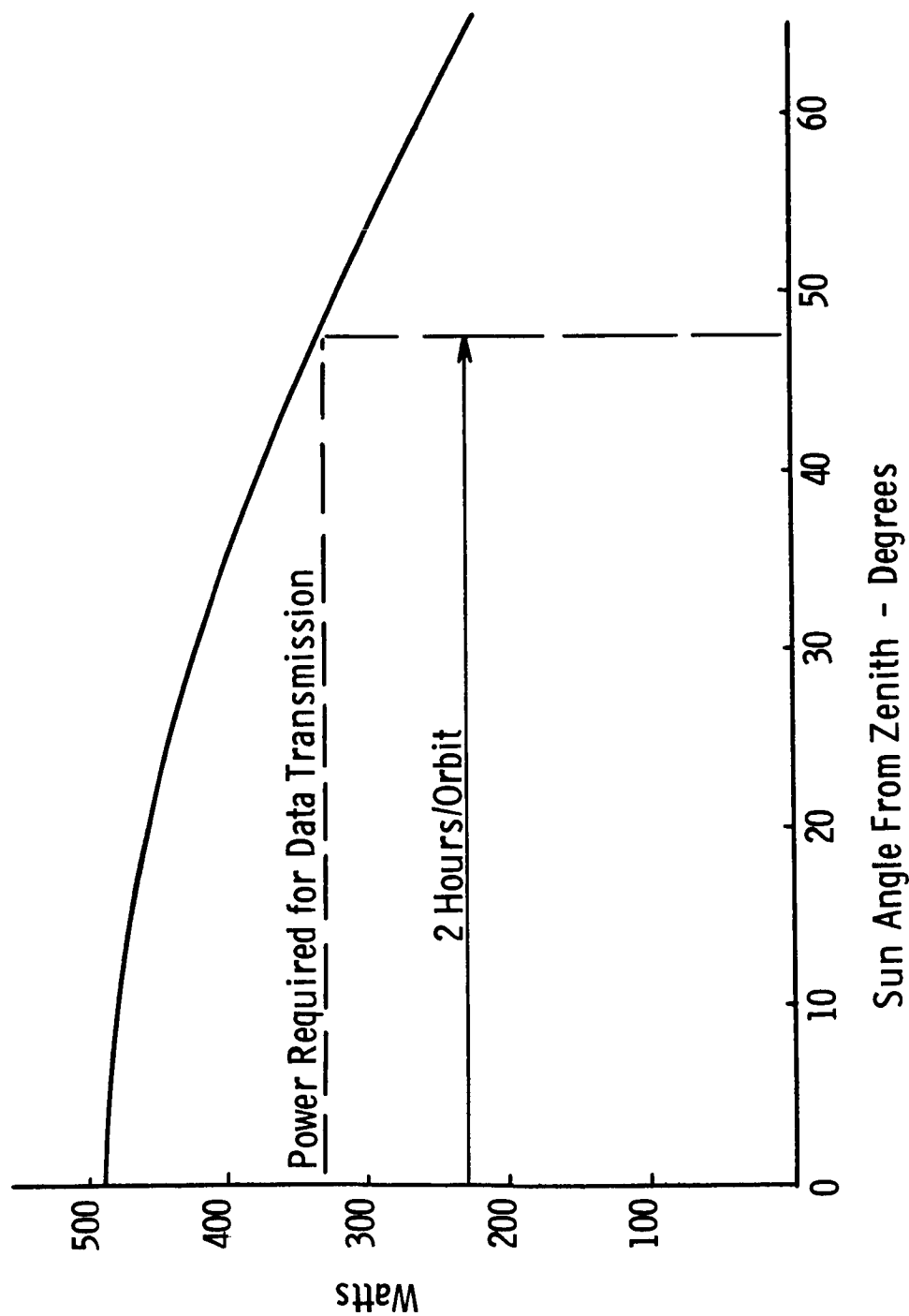


Figure IV-40 Solar Panel Output - Landed Orbiter

Table IV-28. The data returned from Mariner 9, while not conclusive enough to establish definite surface characteristics, has tended to confirm these assumptions. Perhaps the most significant Mariner 9 data, from the rover's viewpoint, was the definition of the large-scale topography of the Martian moons. The magnitude of the large-scale cratering can be used to derive estimates of small-scale characteristics, these being the features the rover must accommodate.

The Phase I rover concept analyses then, examined the options available for mobility on Phobos or Deimos. The sorting procedure indicated wheeled, flying, and boom-deployed systems should be considered. Tracked and walking systems were rejected due to susceptibility to dust and control complexity.

Preliminary analyses of the mobility performance and dynamics of wheeled systems (see Figure IV-41) produced a set of surface transport constraints and characteristics. These are presented in Table IV-29. Operating velocities (V_{Xop}) were calculated to keep vertical c.g. oscillations at or below one meter when contacting obstacles on a horizontal surface. The minimum hazard sensing range equals the distance required to stop in an emergency (e.g., a deep crevice in the vehicle's path).

Flying rover ΔV requirements were determined as functions of flight time (T), trajectory peak altitude (H) relative to starting point, and gravitational acceleration. These data are presented in Figure IV-42. Knowing traverse distance desired and obstacle height along the path, flight sequences and associated ΔV requirements can be calculated using the data in Figure IV-42. An example of a flying rover configuration is presented in Figure IV-43. On this, and other flying systems, cameras, antennas, solar arrays, and other flexible structures would have to be stowed during flying operations to prevent damage during landing.

Table IV-28 Rover Operating Environment

- Gravitational Acceleration at Surface:
Phobos: 0.4 to 3 cm/sec²
Deimos: 0.2 to 1 cm/sec²
- Craters (Minimum):

Diameter (KM)	Number of Craters with Larged Diameter	
	Phobos	Deimos
0.1	68	14
1	3	0.8
10	0.2	0.05
- Major Deformities Preserved
 - Craters
 - Low Velocity Ejecta
- Terrain could be Jagged and Irregular with Steep Slopes on all Scales of Observation
- Dust (Baseline Assumption): Thin Layer, Loosely Compacted
- Surface Coefficient of Friction: $\mu = 0.5$
- Interplanetary Vacuum
- Temperature Range: -150°C to +40°C
- Synchronous Rotation (Same Side always Faces Mars)

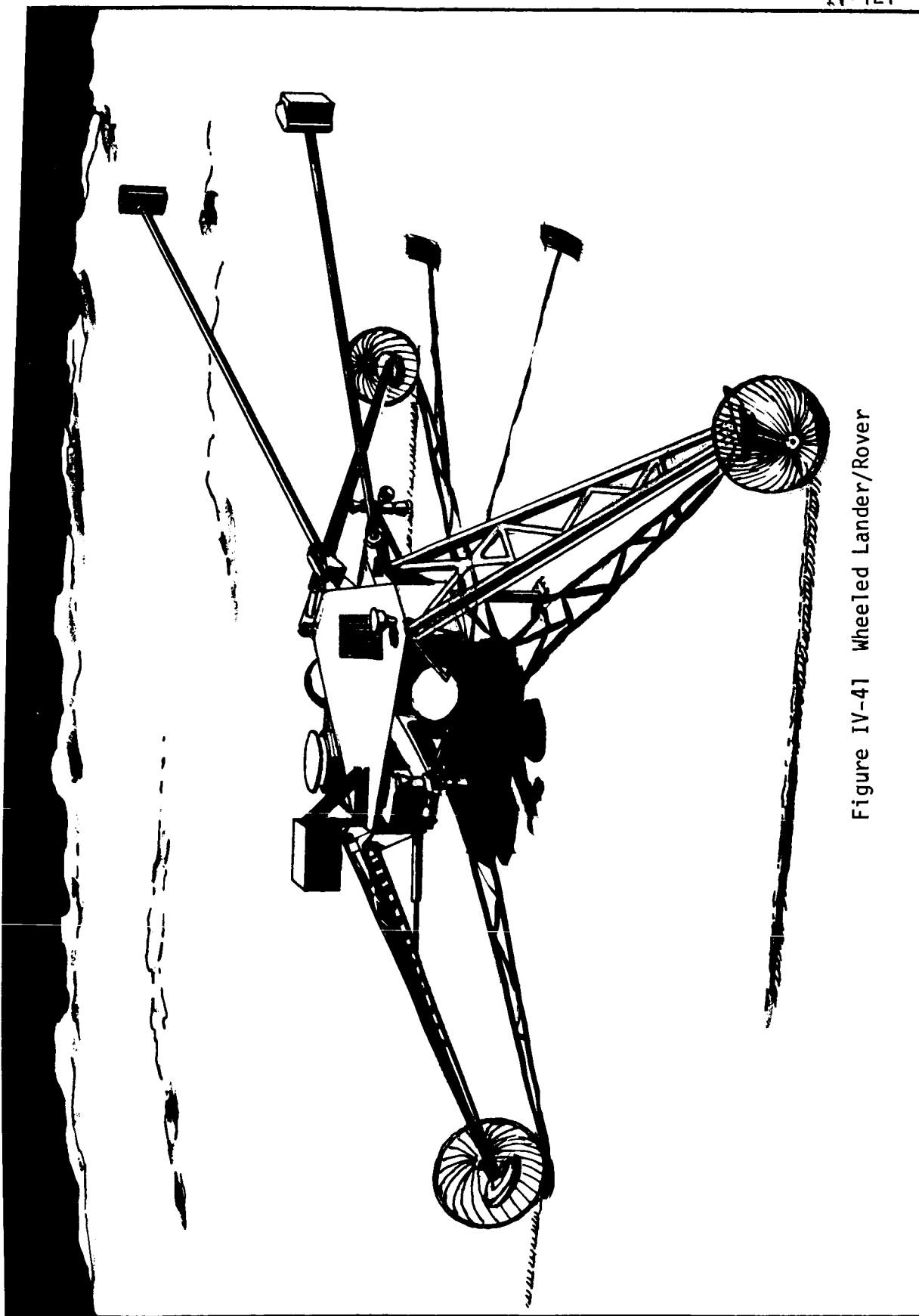
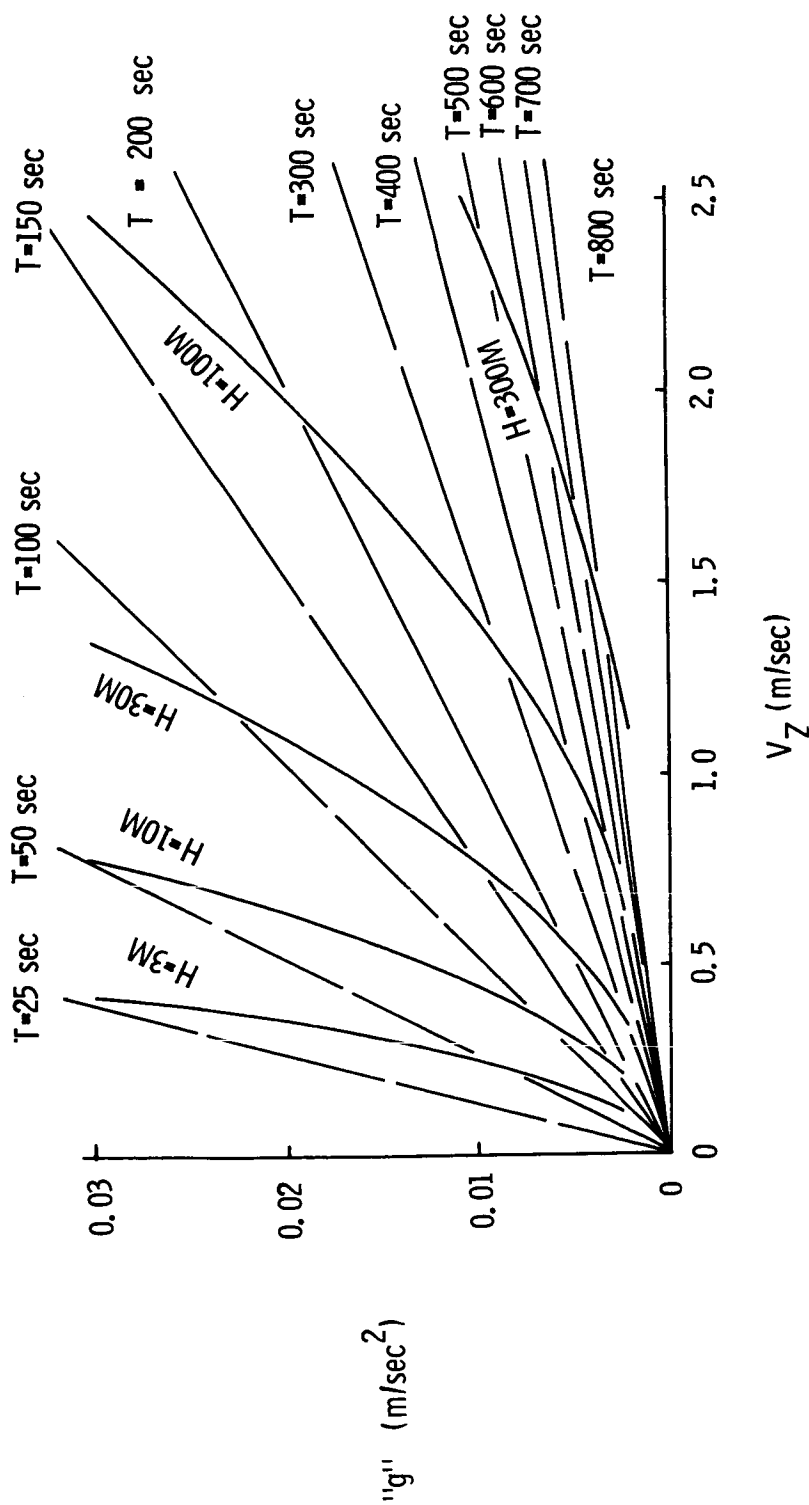


Figure IV-41 Wheeled Lander/Rover

Table IV-29 Surface Transport Constraints/Characteristics

	Phobos	Deimos
Gravitational Acceleration	0.4→3 cm/sec ²	0.2→1 cm/sec ²
Translational Acceleration ($\mu = 0.5$)	0.2→1.5 cm/sec ²	0.1→0.5 cm/sec ²
Maximum Horizontal Velocity (V_{Xmax})	9→24 cm/sec	6→14 cm/sec
Operating Horizontal Velocity (V_{Xop})	3→8 cm/sec	2→5 cm/sec
Time Required to Reach V_{Xop}	15→5.3 sec	21→9.6 sec
Distance Required to Reach V_{Xop}	22 cm	22 cm
(= Minimum Hazard Sensing Range)		
Maximum Drivemotor Input Power	3 w	1 w
(450 KG Rover, Maximum Acceleration or Slope, Total for All Motors)		
Slope Capability		
Step Obstacle Height	≤ Surface Material Internal Angle of Friction	
Crevice Width	Functions of Vehicle Configuration and Surface Material Internal Angle of Friction	
Ground Clearance	Function of Vehicle Configuration	



- Sequence:
- 1) Input V_Z Sufficient to Clear Terrain Obstacles
 - 2) Input V_X Sufficient to Reach Destination Before T Elapses
 - 3) Input $-V_X$ to Stop V_X at Destination
 - 4) Input Retro V_Z to Reduce Landing V_Z to Permissible Level
 - 5) Maintain Attitude Control Throughout

Figure IV-42 ΔV , Altitude and Flight Duration - Phobos/Deimos Rovers

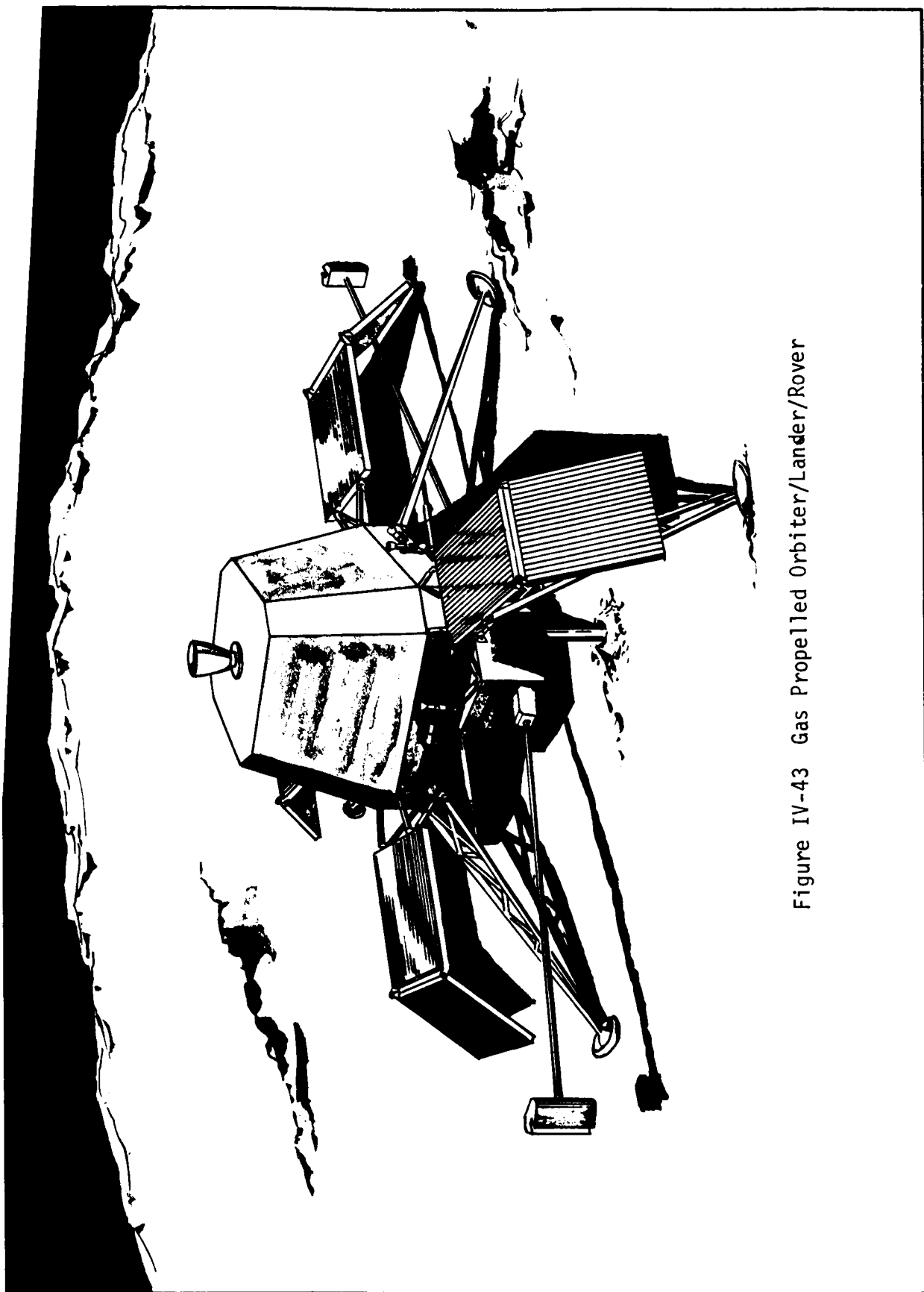


Figure IV-43 Gas Propelled Orbiter/Lander/Rover

The final science mobility mode considered in Phase I was a tubular boom deployment from a stationary lander. As shown in Figure IV-44, such systems can provide access to nearby surface, structures and a reduction in lander-originated interferences.

The initial mobility-mode sorting and analyses conducted in Phase I indicate that wheeled, flying, and deployable boom mobility systems can be developed to operate satisfactorily and take advantage of the unique, low gravity environments of Phobos and Deimos. Lightweight, low power wheeled systems can operate at velocities (0.2 km per hour) high enough to cover significant traverse distances in a 90-day mission. Flying systems offer low ΔV requirements for significant ballistic ranges and a capability to cross significant terrain barriers. Tubular booms take advantage of the low gravity conditions that permit significant reach with relatively low deflections and base-joint loads.

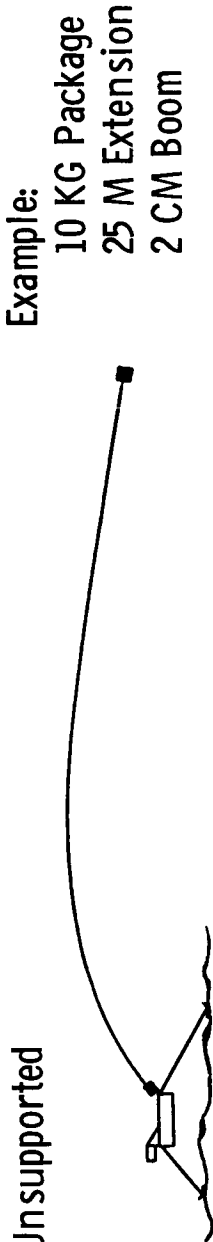
As a result of these analyses, it is recommended that Phase II mobility studies analyze these system concepts in greater detail, particularly with regard to system dynamics and mobility subsystem weight requirements.

Typical Extendable Tubular Boom Characteristics

Tube Diameter (CM)	Wall Thickness (MM)	Allowable Base Joint Load (NT-M)
1	0.05	2
2	0.10	8
3	0.15	18

Deployment Concepts

- Unsupported



- Supported

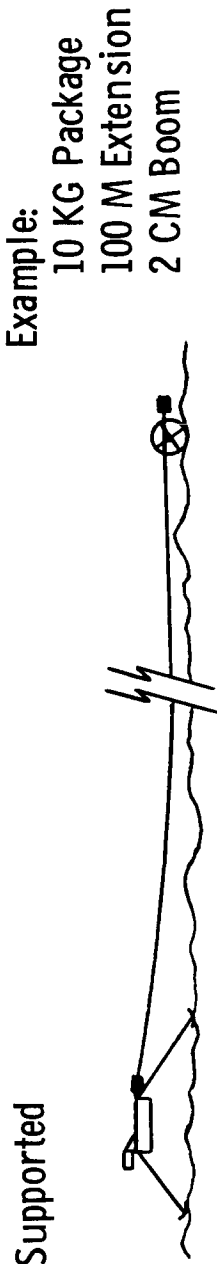


Figure IV-44 Boom Deployed Instruments

V. Program Costs

V. PROGRAM COSTS

The cost summary shown in Table V-1 reflects the estimated funding requirements for the Phobos/Deimos baseline mission.

The ground rules and assumptions that were used in developing these costs are:

- 1) One flight and one spare flight spacecraft are to be developed;
- 2) Costs are in FY '72 dollars;
- 3) Titan IIIIE/Centaur launch vehicle;
- 4) One contractor will have overall system responsibility for the design, development, fabrication and qualification of the Phobos/Deimos mission;
- 5) Sterilization is not required;
- 6) No interference with other Viking programs;
- 7) Use modified Viking '75 ground equipment.

Spacecraft costs were estimated in the following fourteen categories for labor, material, subcontract and ODC:

Management
Mission analysis
Systems integration
Power
Electronics
Guidance and control
Propulsion
Structures
Assembly and test
Ground equipment
Launch operations
Flight operations
Mission data
Parts, materials, and processes

Table V-1 Baseline Mission Cost Summary - Phase I

<u>COST SUMMARY (FY 72 DOLLARS)</u>		
<u>SPACECRAFT</u>		241
Management & Technical Support	72	
Mission Analysis and Systems Engr. & Integ.	20	
Subsystem Development & Qualification	110	
System Assembly & Test	18	
Launch & Flight Operations	21	
<u>SCIENCE INSTRUMENTS</u>		66
<u>OTHER NASA</u>		77
<u>LAUNCH VEHICLES</u>		<u>22</u>
		406
	<u>TOTAL</u>	
	<u>FUNDING BY FISCAL YEAR</u>	
75	<u>76</u>	<u>77</u>
		<u>78</u>
		<u>79</u>
23	78	102
		86
		48
		<u>81</u>
		<u>TOTAL</u>
		406

Science costs were estimated for each science instrument as defined for the Phase I baseline mission.

The category of Other NASA Costs includes:

- Government furnished equipment
- Science investigator teams
- Technical and management support
- Support contractor
- Contractor award fee
- Headquarters tax

Table V-2 presents similar cost data for the alternate landed orbiter mission and a 90 kg science payload. It differs from the baseline mission in that it eliminates the separable Phobos lander/rover and reduces the science from 125 kg to 90 kg. Also, two launches are provided. Costs are in FY '72 dollars.

Table V-2 Alternate Mission Cost Summary - Phase I

	(\$ in Millions)				
Spacecraft (Landed Orbiter)					198
Science					30
Other NASA Costs					52
					<u>280</u>
Launch Vehicles (2)					44
					<u>324</u>
TOTAL					<u><u>324</u></u>
	Funding by Fiscal Year				
	<u>1976</u>	<u>1977</u>	<u>1978</u>	<u>1979</u>	<u>1980</u>
	18	62	82	69	38
					<u>1981</u>
					29
					<u>1982</u>
					26
					<u>Total</u>
					324

VI. Program Schedule

VI. PROGRAM SCHEDULE

The schedule shown in Figure VI-1 depicts the key milestones and span times for the Phase I Phobos/Deimos Satellite Rendezvous and Landing Mission, from long lead activities, and full go-ahead through detail engineering, test and launch.

The basic assumptions and ground rules used in the development of this schedule are:

- 1) The target launch date is 9 October 1979 with a nominal launch window of 30 days;
- 2) Two flight and one spare configuration systems are to be developed;
- 3) One contractor will have overall systems responsibility for the design, development, fabrication and qualification of the Phobos/Deimos mission.

The approach to scheduling program activities was to arrange them so that adequacy of the design is confirmed as early as possible to allow time for unpredicted development problems. The schedule of program development activities is keyed on the early start of science development and mission analysis, some twelve months before full go-ahead. Subsystem areas that will pace the system development are the multi-hundred watt RTG proposed for the lander/rover and the growth of the orbiter propulsion system.

The basic philosophy used in developing the schedule is to make maximum use of the Mars Viking subsystem and system technology, and hardware development. The schedule as structured in Figure VI-1 takes maximum advantage of the Mars Viking subcontract buys.

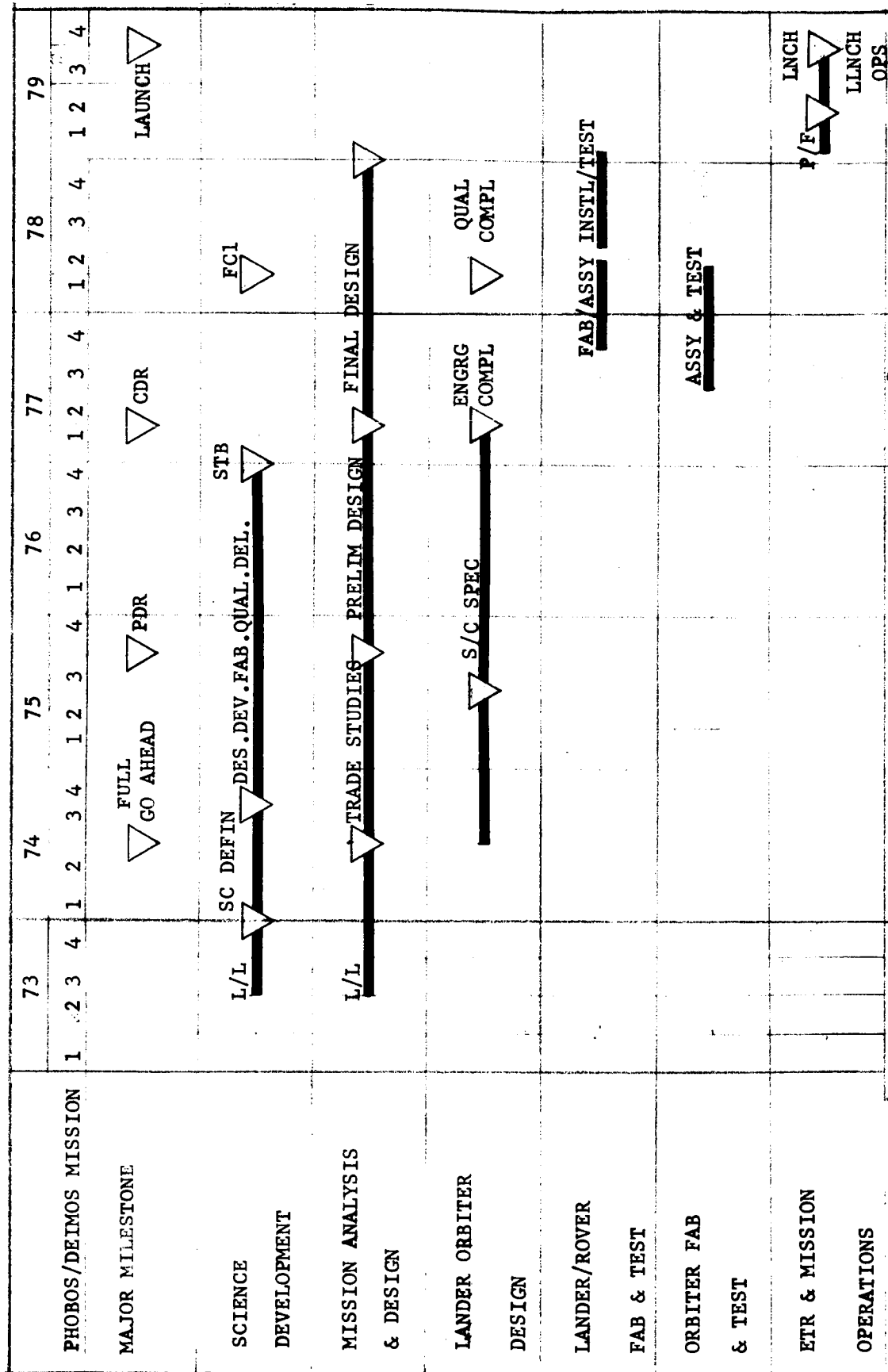


Figure VI-1 Phase I Program Schedule

VII. Conclusions

VII. CONCLUSIONS

The principal conclusions drawn from the Phase I study effort are summarized in this section. Results indicate that the Phobos/Deimos satellite rendezvous and landing mission is technically feasible in the 1979-1981 time period using the Titan IIIE/Centaur launch vehicle and Mars Viking hardware and technology. No high-risk technology problems were identified in the subsystem mechanizations selected for the baseline concept or the alternate system.

The modifications and changes required to be made to the Mars Viking Orbiter to accomplish the baseline mission are minimal and easy to accomplish. The most significant changes are as follows:

- 1) The propulsion system propellant capacity has increased by 38% to accommodate the additional propellant to accomplish the Phobos/Deimos mission.
- 2) Minor increase in the orbiter's cold gas attitude control system to handle the increased mass and inertia of the spacecraft.
- 3) Modified the scan platform by substituting an IR spectrometer in lieu of the IR thermal mapper and the Mars atmospheric water detector.

Although the lander/rover vehicle is a completely new machine, it utilizes Mars Viking developed hardware with the lone exception being the addition of a rendezvous radar, components of which are currently available off-the-shelf. Actually the only "new" subsystem is the basic structure. Here again, maximum use is made of existing Mars Viking technology.

Modification of the Mars Viking Orbiter to accomplish the alternate landed orbiter mission is somewhat more extensive but still falls into the category of a modified system rather than a new one.

The key conclusion that was reached during this study was the fact that the baseline Phobos/Deimos spacecraft that was defined, with the modifications delineated above, is compatible with a 1979 launch date with no interference with the present Mars Viking program. A launch date in this time period also allows procurement of subsystem hardware that will be current technology.

Table VII-1 indicates the areas where further study would be of benefit and also the areas where new technology would enhance the mission. These items are briefly described in the following paragraphs.

Table VII-1 Recommendations for Further Study
and Technology Requirements

<u>Further Study</u>
Navigation Analysis for Unmanned Orbital Maneuvers and Rendezvous
Mobility and Navigation Mechanization for Planetary Lander Missions
Thermal Control Techniques for Combined Cruise and Landing Missions
Landed Orbiter Power, Propulsion and Structural Analysis
Isolation of Science Data from RTG Radiation
Adaptive Science Payloads for Satellite Lander Missions
<u>Technology Requirements</u>
Light-weight, Low-Power Rendezvous Radar Subsystems
Satellite Sampling and Tie-Down Techniques
Universal Space Storable Propellant Propulsion Module

A. NAVIGATION ANALYSES FOR UNMANNED ORBITAL MANEUVERS AND RENDEZVOUS

Missions to Phobos and Deimos and return require orbital maneuvers at Mars and automatic uncooperative rendezvous sequences. Supporting research and technology (SRT) work in the following areas would improve the predicted navigation accuracies for these mission operations and increase confidence in mission success:

- 1) Software for real time Kalman/Schmidt (with propagation down-weighting) navigation filter. This basic filter is used in all mission phases.
- 2) Capability of obtaining TV data (for navigation purposes) at the rate of one equivalent star/satellite "image" per 10 minutes.
- 3) Earth based astronomical sightings on Phobos and Deimos prior to Mars encounter. (This guarantees the ephemeris accuracy assumed in the study.)

B. MOBILITY AND NAVIGATION MECHANIZATION FOR PLANETARY LANDER MISSIONS

Landed planetary missions benefit significantly from the ability to explore large areas of the surface by means of mobility. Concepts for wheeled and flying (hopping) mobility were developed for Phobos/Deimos landed missions in contract NAS1-10873. SRT activity in accordance with the following outline would extend the work already done and provide increased confidence in mobile landed mission concepts.

- 1) Update Phobos/Deimos engineering model using Mariner 9 data.

- 2) Define typical traverse missions.
- 3) Determine navigation requirements for these missions.
- 4) Establish feasibility of rover navigation system developed in Phase II of contract:
 - a) Develop camera system requirements model;
 - b) Camera systems tradeoff study;
 - c) Analyze errors associated with using Inertial Measurement Unit (IMU) as gravitometer in low gravity non-spherical body environment;
 - d) Develop automatic steering philosophy compatible with adaptive science operations.
- 5) Establish feasibility of rover hazard detection system:
 - a) Develop hazard detection requirements from revised engineering model and typical traverse;
 - b) Tactile and remote detector tradeoff study;
 - c) Evaluate potential adaptive science relationships between hazard detection and science sensors.
- 6) Define hazard avoidance algorithms.
- 7) Further refinement of unmanned roving vehicle digital simulation to permit evaluation of mobility subsystem concepts in light of the revised engineering model.

C. THERMAL CONTROL TECHNIQUES FOR COMBINED CRUISE AND LANDING MISSIONS

The Phobos/Deimos sample return mission imposes several rather severe thermal control design constraints. Probably the principal constraint is the widely different thermal requirements occurring during landed operations as compared to the cruise

phase(s). Compounding this constraint is the available "thermal view" of natural heat sinks and sources that are a result of the necessity of "staging" during cruise and on the surface. These requirements are satisfied by modifying the existing Viking Orbiter temperature control louver system. The modifications proposed (Sun-oriented OSRs and louver flip covers) are presently state-of-the-art but will require a considerable amount of development effort before they can be considered flight qualified.

Another major thermal control constraint is the diurnal cycle effects on the satellite's surface. The constraint is satisfied by mounting subsystem equipment to supporting members via a phase change material. Again, this concept is state-of-the-art but requires some amount of development effort.

D. LANDED ORBITER POWER, PROPULSION AND STRUCTURAL ANALYSIS

Modifying the Viking Orbiter to accommodate its landing role requires that additional detailed analysis be performed in the areas of power, propulsion and structural analysis.

The solar array must be deployed during the cruise phase of the mission, then retracted or supported during the terminal descent phase and again redeployed during landed operations. Additional studies need to be accomplished to adequately evaluate how this is best performed.

In the propulsion area, further studies should be made to establish more accurately the maximum allowable "stretch" of the propulsion subsystem and to evaluate the detail changes that result from this growth.

Detail structural analysis should be performed to determine the component structural impact associated with landing a vehicle designed primarily to act as an orbiting cruise machine.

E. ISOLATION OF SCIENCE DATA FROM RTG RADIATION

Many of the science instruments that would serve as valuable tools in the geological and geochemical investigation of Phobos and Deimos are degraded by the radiation environment of an RTG. Since it may be desirable to use an RTG power source on missions carrying these instruments, SRT work is recommended to investigate the interfering effects, develop shielding methods, and determine schemes for separating data from radiation noise. The following potential Phobos/Deimos mission instruments are vulnerable to RTG radiation.

<u>Instrument</u>	<u>Effect</u>
Integrated Geology Alpha Backscatter Spectrometer	Unknown but probably significant
X-Ray Fluorescence Spectrometer	Reduces accuracy for certain elements
X-Ray Diffraction	Severe, may require deployment
Gamma-Ray Spectrometer	Very severe: requires spectrometer to be an independent subsystem with power and T/M for deployment and remote data acquisition
Course Age Dating	Depends on technique employed: could cause severe interference for K/Ar dating

F. ADAPTIVE SCIENCE PAYLOADS FOR SATELLITE LANDER MISSIONS

In developing science strategies for satellite landing missions, emphasis should be on returning the most valuable scientific data for a given payload cost and weight. For missions to bodies about which very little is known, such as Phobos and

Deimos, it becomes difficult to establish, before arrival, the most effective sequence of investigations, priorities for measurement and selection of data to be returned. For this reason, an approach to science mission design is suggested that provides flexibility in instrument design, in sequence programming, and in data processing. This flexibility would be used either by controllers at Earth or by an on-board computer to allow the mission to respond to initial findings and reprogram subsequent investigations accordingly.

SRT work is recommended to develop and experiment with specific adaptive instrument techniques and to design candidate adaptive science payloads that can be compared with equivalent (in cost and weight) conventional payloads for science value. The specific adaptive instrument techniques might include application of rovers (mobility), pattern recognition schemes, selection of "interesting" (i.e. different) surface samples, meteorological and seismic "phenomena" detectors, etc.

G. LIGHTWEIGHT, LOW-POWER RENDEZVOUS RADAR SUBSYSTEM

A modified Viking Lander radar altimeter was suggested for the Deimos/Phobos rendezvous radar. A lightweight radar was mechanized from the radar altimeter that could perform the required rendezvous and landing (docking) functions without the costs of developing a new rendezvous radar. An estimated 10-15 percent modification of the Viking radar electronics would be needed. SRT effort would be needed to develop the suggested antenna system and integrate it into the radar altimeter. Additional SRT to develop this concept into a proven non-cooperative rendezvous radar and test it would build confidence in mission feasibility and reduce future development risks.

H. SATELLITE SAMPLING AND TIE-DOWN TECHNIQUES

The very low gravity field of both Phobos and Deimos ($\sim .001$ Earth g's) and the relatively unknown composition of these satellites result in problems in staying attached to the surface, particularly when attempting to drill into the surface to obtain a core sample. Additional technology studies are required to be performed to reduce possible future development risks.

I. SPACE STORABLE PROPELLANT PROPULSION SYSTEMS

A study of the application of the space storable propellant's fluorine/hydrazine to the Phobos sample return mission indicated the possibility of increasing landed payload weights as much as 25% over that of conventional earth storable propulsion systems application. This increase in spacecraft performance could be realized with the development of a safe and reliable space storable propellant propulsion module.

It is felt that the technologies associated with space storable propellant propulsion systems that have been accumulated by such companies as Rocketdyne, Pratt & Whitney and Aerojet are sufficient for the successful development of a pressure-fed or pump-fed propulsion module. However, recently neither the funds nor the interest have been available. There are certain propulsion subsystem development requirements that must be resolved before an integrated flight qualified multi-start long burn duration propulsion module can be successfully developed. A compilation of these requirements include:

- 1) Demonstrate propellant tank and component materials compatibility;

- 2) Demonstrate leak-free fluorinated oxidizer storage and pressurization systems;
- 3) Demonstrate multi-start and stable engines;
- 4) Develop safe fluorinated oxidizer management techniques;
- 5) Develop efficient propellant thermal control systems for deep space missions;
- 6) Develop reliable fluorinated oxidizer leak detectors.

The problems of developing an integrated space storable (fluorine/hydrazine) propulsion module are currently being resolved at the Jet Propulsion Laboratory. It is anticipated that a flight weight propulsion module of the 600 pound thrust class will be available in the latter half of 1973.

Appendix A

APPENDIX A

PHOBOS/DEIMOS ENGINEERING MODEL

PHOBOS/DEIMOS ENGINEERING MODEL

- I. INTERPLANETARY ENVIRONMENT - See Mars Engineering Model (MEM)
 - A. Gas Properties
 - B. Magnetic Field
 - C. Solar Radiation
 - D. Cosmic Radiation
 - E. Meteoroids
- II. NEAR-MARS ENVIRONMENT - (300 km to Satellite Orbit)
 - A. Gas Properties - See Mars Engineering Model. For worst case drag on spacecraft, use Maximum Density Model, Table II-3.
 - B. Magnetic Field - See MEM
 - C. Thermal Radiation - See MEM
 - D. Cosmic Radiation - Same as I-D above
 - E. Trapped Radiation - See MEM
 - F. Meteoroids - See MEM
- III. PHOBOS AND DEIMOS ENVIRONMENTS
 - A. Atmosphere - Phobos and Deimos are much too small to hold atmospheric vapors gravitationally. They are likewise too small to support a significant steady-state outgasing rate. The Martian atmosphere is also completely negligible at the altitudes of Deimos and Phobos (see MEM, Table II-3). The gas properties are therefore approximated by that of the interplanetary environment, I-A.
 - B. Surface Environment
 1. Atmospheric Properties - Same as A. above.
 2. Solar Energy - Same as II-C above. Martian albedo radiation should be calculated for Phobos from the equation given in MEM II-C-2 using the following values of f, depending upon the phase angles (Sun-Mars Center-spacecraft),

<u>f for Deimos</u>	<u>f for Phobos</u>	<u>phase angle</u>
0.02	0.05	0°
0.015	0.04	30°
0.01	0.02	60°
0.005	0.015	80°

It is to be noted that even for the most extreme case (Phobos, phase angle of 0°), the albedo radiation from Mars is less than 1% of that received directly from the Sun.

Thermal radiation emitted by the Martian surface and impinging upon the satellites is given in II-C-3 of the MEM. Use $(R/r) = 0.36$ for Phobos and 0.14 for Deimos.

3. Cosmic Radiation - Same as I-D above, except that on the surface, the satellite produces 2π shielding, reducing the interplanetary cosmic ray flux by one-half.
4. Surface Radiation
 - a. Natural Radioactivity - Alpha, beta, and/or gamma rays emitted by rather long-lived radioisotopes of potassium, uranium, and thorium are the "natural radioactivity" of planetary material. Concentrations of these radioisotopes above the average values in the Earth's crust (which is highly enriched compared to the bulk planet composition) are very unlikely. Possible values include the following:

	CONCENTRATION (PPM)		
	<u>Chondritic Meteorites</u>	<u>Lunar Samples</u>	<u>Earth's Crust (Average)</u>
Potassium	845	1,700	25,900
Uranium	0.01	0.6	1.8
Thorium	0.04	2.8	7.2
	Ref. 2	Ref. 3	Ref. 4

These levels of natural radiation produce a dose-rate less than 25μ R/hour.

- b. Induced Radioactivity - The radioactivity induced in surface material via interaction with cosmic rays depends upon the exact chemical composition of the material and the surface turnover and/or loss rate. Lunar samples provide a satisfactory baseline model (Ref. 5). It is unlikely that the dose-rate from induced radioactivity at the surface will exceed 100μ R/hour.

5. Meteoroid Influx - When the spacecraft is very near the surfaces of Deimos or Phobos, the cometary meteoroid flux will be reduced by one-half due to satellite shielding. The asteroidal meteoroid flux, which is nearly unidirectional with the spacecraft will be at its full flux except for that part of the time when the satellite directly shields the spacecraft. Meteoroid fluxes are given in Section I-E.
6. Magnetic Field - Use the interplanetary magnetic field as given in Section I-B.

C. Surface Properties

1. General Statement - Deimos and Phobos are so small that they appear as objects of the 11th or 12th magnitude; and the brilliance of Mars, renders observation very difficult. Today, 94 years after their discovery, we know little more about these satellites other than their orbital elements.
2. Albedo - The diameters of the satellites of Mars cannot be determined directly from ground observations, but have been inferred by measuring their brightness and assuming an albedo the same as that of Mars. Porter suggested in 1960 (Ref. 6) that the satellites probably have a lower albedo than the planet. This was shown to be the case for Phobos, at least, during the Mariner 7 flyby in 1969. Although seen at poor resolution, Phobos was determined to be irregularly shaped (18 x 22 km), with the elongation along its orbital plane (Ref. 7). The cross-sectional area was larger than predicted, and the geometric albedo was found to be only 0.065, lower than that known for any other body in the solar system.
3. Topography - Phobos and Deimos are much too small to have achieved a spherical, equilibrium figure via gravitational forces. The absence of weathering will allow deformities produced by meteoroid impacts to be maintained over long periods of time, and the weak gravitational forces will have but little influence on the rearrangement of fragments and fine particles. Thus, slopes can be very steep on all scales of observation. The terrain could be

very jagged and irregular, and for analysis, one could consider the rough flank of the lunar crater Censorinus as revealed by Lunar Orbiter V photographs.

Cratering of the surfaces of Phobos and Deimos may be estimated from the crater densities observed on certain regions of Mars (Ref. 8). Based on these results and the approximate surface areas of the satellites, the minimum number of craters greater than various diameters to be found on each satellite are given in Table 1.

<u>Crater Diameter</u>	<u>Minimum Number of Craters with Larger Diameter</u>	
	<u>Phobos</u>	<u>Deimos</u>
0.1 km	68	14
1 km	3	0.8
10 km	0.2	0.05

Craters may be somewhat more difficult to identify on these small bodies because crater rims are formed mostly by ejected material, most of which would escape from Phobos and Deimos.

4. Properties of Near-Surface Materials

- a. Composition - J. Salisbury has conducted laboratory studies to simulate the low albedo of Phobos, using a particle-size distribution based on lunar results. He concludes (Ref. 9) that Phobos must contain a much higher percentage of opaques than silicates, and may be not unlike stony-iron meteorites containing 20% or more iron. Indeed, his data are consistent with the assumption that Phobos is an iron meteorite with no stony component. This conclusion hinges upon the assumption that the surface of Phobos contains dust (see next Section).

The question of the composition of Phobos and Deimos hinges upon their origin. If they are solid fragments derived from the Martian surface, they will reflect that particular composition (taken by the MEM to be basalt). If captured asteroids, their composition could be that of any of a number of different types of meteorites: irons, stones, or stony

irons. They could even have a composition like that of carbonaceous chondrites, which are very fragile under stress. Even if the base material is not meteoroid-like, it is possible that considerable meteoroid-like material is embedded in the surface. Sagan and Pollack estimate that the total micrometeorite infall on Mars has been sufficient to cover that planet to a depth of from 2 to 200 meters (Ref. 10). The satellites of Mars would have been subjected to the same amount of bombardment. Synchronous rotation does not appreciably shield one face of the satellite since Mars blots out only 0.5% and 3% of 4π steradians for Deimos and Phobos, respectively.

- b. Strength and Bearing Capacity of Soil - The bearing strength of the surface material on these satellites could range all the way from extremely poor (very loosely compacted rubble) to excellent (bar rock or iron). It could even vary between these extremes from place to place on the satellite. Even if the satellite surface were not affected by meteoroid bombardment, it could be very easily crumbled if it has a high organic content, such as occurs in carbonaceous chondrite meteorites. For further discussion, see Section 5 below.
- c. Soil Water and Permafrost - Due to the high vacuum of space and the heating of the near-surface material by the sun, the surface is most probably quite free of water and other volatiles, as is the Earth's moon.
- d. Thermal Properties - Baseline thermal parameters for the surface material were selected for a range of thermal inertia values (as shown on Figure IV-25) including lunar-like and meteorite soils.
- e. Dielectric Constant - The dielectric constant for these satellites may be near that of the moon, 2.5 to 3.5. On the other hand, the surface materials may be mainly iron, and hence conductive.

- f. Radar Properties - The radar signatures of Deimos and Phobos are unknown at present. Again, for purposes of modeling, two extreme cases can be taken as (1) the lunar surface, and (2) a conductive surface such as provided by iron meteoritic material.
 - g. Optical Properties - The surface spectrophotometric functions are also unknown at present for the Martian satellites. Indeed, their determination will be one of the science objectives. The geometric albedo in the visible for Phobos has been determined by Mariner 7 to be 0.065 (Ref. 7).
5. Soil Models - Soil is defined as the loose, unconsolidated material of all sizes (dust to boulders) which covers the solid portion (bedrock) of a body. In the case of very small bodies such as Phobos, Deimos and the asteroids, Smith has argued for complete absence of soil (Ref. 7), while Dollfus suggests patches of soil in some places and bare bedrock in others (Ref. 11), and Veverka has evidence that such bodies are completely dust covered, but believes this extends only to a depth of one centimeter or so (Ref. 12).

Smith as pointed out (Ref. 7) that the very low escape velocity of approximately 0.01 km/sec for Phobos, compared with meteoroid encounter velocities of about 2.1 km/sec (orbital velocity of Phobos) and perhaps velocities of 24 km/sec (orbital velocity of Mars), will result in a net mass loss from Phobos each time an impact occurs, since an impacting meteoroid usually sets in motion an amount of mass at least 1000 times its own mass. Smith thereby concludes the surface of Phobos is dust free, but Salisbury and Gault (Ref. 9 and 13) contest this conclusion on the grounds that there is always a low-velocity component of the material set in motion. Furthermore, even though most of the material easily escapes Phobos, only a small fraction can escape Mars orbit. Consequently, most of the debris is injected into co-orbit with Phobos and may later be swept up. Gault states the problem is not amenable to calculation due to lack of knowledge of the bulk composition of Deimos and Phobos (Ref. 13).

The physical properties of the surface material are important to two aspects of the proposed missions: (1) landing, takeoff, and roving, and (2) sample acquisition. In the former case, one must consider that soil, if present, would be very loosely compacted due to the low g forces present. Lack of moisture will reduce cohesion to very low values, but enhance electrostatic effects. Landing maneuvers could raise a dust cloud, producing site alteration and perhaps covering solar cells and thermal control surfaces. Landing impact could cause significant compaction of surface material. Roving may be very difficult in the usual sense because of the poorly compacted soil and the low g field. For these aspects of the mission, the model recommended is the lunar soil model, given in Section III-C-5 of the MEM.

In terms of sample acquisition, many possible models must be considered and the sampling systems designed to handle, if possible, all contingencies. The models recommended include:

- Soils: (1) lunar soil (see MEM, III-C-5)
- (2) lag gravel (see MEM, III-C-5)
- (3) loess (see MEM, III-C-5)
- (4) powdered iron
- Bedrock: (1) hard rock (see MEM, III-C-5)
- (2) iron meteorite
- (3) carbonaceous chondrite meteorite

IV. ORBITAL, PHYSICAL, AND ASTRODYNAMICAL DATA

A. Orbit and Rotation

1. Orbital Parameters - The following data on orbital characteristics are intended to serve as a guide to the orbits of Deimos and Phobos. The values given may not necessarily be the most modern ones available in every case. For calculations of location of the satellites as a function of time, it is recommended that the MARSAT subroutine be used (Ref. 14). Note that because of the nearness of the satellites to their primary, the oblateness of Mars causes the orbital planes to wobble and the lines of apsides to rotate.

	<u>Phobos</u>	<u>Deimos</u>	<u>Ref.</u>
Period	7h 39m 13.85s	30h 17m 54.87s	(15)
Distance from center of Mars (km)	9365	23,525	(1)
Eccentricity	0.0210	0.0028	(16)
Inclination to Mars equator (degrees)	1.12 to 1.14	0.85 to 2.69	(16)
Rate of regression of ascending node (deg/Julian year)	158.5	6.54	(16)

Uncertainties in these orbital parameters have been given by Wilkins (Ref. 23).

2. Rotation - Although some textbooks (Ref. 17 and 18) state that Phobos and/or Deimos have spin periods that are synchronous with the rotation rate of Mars (just as with the Moon and the Earth), these statements are apparently not regarded as firmly established by the scientific community. On the other hand, many satellites of the planets are known to be synchronous (Ref. 19). Fish states that this is quite probably true for Phobos because of tidal effects (Ref. 20); and Alfven and Arrhenius comment (Ref. 21), "As far as is known, all satellites have synchronous rotation."

Cook and Clark argue that regardless of initial spin state, Phobos and Deimos will assume one of a family of possible resonant spin states (Ref. 22). Veverka has made calculations of damping times for Phobos to achieve resonance from non-resonance states and finds that these times are always short on a solar system time scale (Ref. 12). He also believes that the satellites must be trapped in the simplest kind of resonant state (one spin revolution for one orbit revolution) because of the near-circularity of their orbits. Mariner 9 preliminary results indicate that Phobos and Deimos are in synchronous rotation about Mars.

It is therefore recommended that for design purposes, it be assumed that Phobos spins with a period of 7.65 hours and Deimos with a period of 30.3 hours. Of possible practical significance is the fact that with this spin period, the tangential velocity at the "equator" of Phobos will be 2.5 meters/sec at the 22 km

dimension (see Section on size below). For Deimos, it would be the order of 0.25 meters/sec.

B. Physical Properties

1. Size - The sizes of Deimos and Phobos have been estimated from their visual magnitudes being 10 and 19 km in diameter, respectively (Ref. 1). However, Mariner 9 obtained photographs of Deimos and Phobos indicating dimensions of 12 x 13.5 km for Deimos and 21 x 25 km for Phobos when viewed in the orbital plane. (Ref. 7). Thus, Phobos is larger than previously thought. Indeed, since it is probably in resonant rotation, the third axis should be longer than either of the other two axes since it should lie along the direction of gravity-gradient stabilization.
2. Mass and Density - Neither of these quantities have been determined for the Martian satellites. The density of nearly all rocks and rock-forming minerals is between 3.0 and 4.0 g/cm³. In powdered form, densities could be as low as 1.0. Iron meteorites have densities in the neighborhood of 8.0. The most likely density for Phobos and Deimos is 3.5, but could range from 1 to 8.

The density uncertainties, combined with volume uncertainties, allow masses for the satellites which vary by an order of magnitude:

$$\text{mass of Phobos} = 0.4 \text{ to } 4 \times 10^{16} \text{ kg}$$

$$\text{mass of Deimos} = 0.4 \text{ to } 4 \times 10^{15} \text{ kg}$$

From these values, one can calculate

	<u>Phobos</u>	<u>Deimos</u>
Escape velocity at surface (m/sec)	8.6 to 24	4.3 to 10
Gravitational accel. at surface (cm/sec ²)	0.4 to 3	0.2 to 1

C. Astrodynamical Data

The currently recommended ephemerides are those generated by the subroutine MARSAT (Ref. 14).

V. REFERENCES

1. "Mars Engineering Model," NASA, Langley Research Center, Report No. M75-125-1, dated 8 December 1970.
2. G. J. Wasserburg, G.J.F. McDonald, F. Hoyle, and W. A. Fowler, *Science* 143 (1964) 465.
3. G. H. Morrison, et al, *Science* 167 (1970) 505.
4. B. Mason, Principles of Geochemistry, J. Wiley and Sons, N. Y. (1966).
5. R. W. Perkins, L. A. Rancitelli, J. A. Cooper, J. H. Kaye, and N. A. Wogman, *Science* 167 (1970) 577.
6. J. G. Porter, *J. Brit. Astron. Assoc.* 70 (1960) 33.
7. B. A. Smith, *Science* 168 (1970) 829.
8. B. C. Murray, L. A. Soderblom, R. P. Sharp, and J. A. Cutts, *J. Geophys. Res.* 76 (1971) 313.
9. J. Salisbury, to be published in *J. Geophys. Res.*
10. J. B. Pollack and C. Sagan, *Space Science Reviews* 9 (1969) 243.
11. A Dollfus, presented at the Asteroid Symposium, Tucson, Arizona, Jan. 1971.
12. J. Veverka, private communication, June, 1971.
13. D. E. Gault, private communication, June, 1971.
14. MARSAT, a subroutine of PLASAT, was written by P. Roberts, JPL.
15. The American Ephemeris and Nautical Almanac, Wash., D.C., U. S. Government Printing Office, 1969.
16. C. M. Michaux, *Handbook of the Physical Properties of the Planet Mars*, NASA SP-3030, Washington, D. C., 1967.
17. I. M. Levitt, A Space Traveler's Guide to Mars, H. Holt and Co., N.Y., 1956.
18. L. Rudaux and G. deVaucouleurs, Larousse Encyclopedia of Astronomy, Prometheus Press, New York, 1967.
19. P. Goldreich and S. Peale, *Astron. J.* 72 (1967) 662.
20. F. F. Fish, *Icarus*, 12 (1965) 442.
21. H. Alfven and G. Arrhenius, *Astrophys and Space Sci.*, 8 (1970) 338, and 9 (1970) 3.
22. W. S. Cook and B. C. Clark, Martin Marietta Corp., AVSN-56, 1971.
23. G. A. Wilkins, in Mantles of the Earth and Terrestrial Planets, ed. by S. K. Runcorn, Interscience Publ., New York, 1967.

Appendix B

APPENDIX B

TRACK PROGRAM DESCRIPTION

TRACK PROGRAM DESCRIPTION

The TRACK program was originally designed and programmed by T. Gamber on the Viking Project. Modifications have been made to incorporate the additional requirements of a Phobos/Deimos mission. The program calculates the launch and encounter performance requirements using conic heliocentric trajectories for a Mars mission as a function of launch and encounter date. The C3 and DLA constraints for the trans-Mars injection for each launch date are used in a 29-term polynomial to determine the launch vehicle's capability. The program then calculates the impulsive ΔV requirements for the specified Mars orbit insertion maneuver which is a function of the arrival VHE and desired orbit periapsis and apoapsis.

The plane change ΔV is then calculated and added to the MOI ΔV requirements. The additional ΔV requirements for the mission are also added to this accumulated ΔV . These include allocations for the midcourse maneuvers, the maneuvers from the capture orbit to the desired final conditions, navigation uncertainty requirements and gravity and steering losses. The ΔV capability of the allocated propellant loads (5 values are used for each launch/encounter date) are calculated and if this capability is less than the calculated requirements, the spacecraft initial weight is reduced to the point where the propellant now has the exact required ΔV capability. If the ΔV capability is in excess of the requirement, the excess portion is printed out.

The program now prints out the total weight after the ΔV requirements are satisfied and also calculates the propulsion system weight and subtracts this value from the total weight.

The program also calculates and prints out the ZAE angle, the geocentric declination of Mars at encounter, the VHE magnitude and equatorial declination, and plane change data. This data allows the selection of a launch and encounter space and propellant load which yield a maximum usable spacecraft weight after the required ΔV expenditures.

Appendix C

APPENDIX C

VEAMCOP PROGRAM DOCUMENTATION - RENDEZVOUS VERSION

VEAMCOP PROGRAM DOCUMENTATION - RENDEZVOUS VERSIONReferences

1. "Langley Orbit Insertion Programs," E. D. Vogt, March 18, 1970.
2. "Generation of a Computer Program from VEAMCOP which approximates the VITAP Optimization Subroutine Using Taylor Series," J. Sabo, August 28, 1970.
3. Final Report for RA909.
4. Final Report for TOS 48910: STEAP II Documentation for Natural Satellite Observation Option.
5. Space Trajectories Error Analysis Programs - Version II.
6. "VEAMCOP - Rendezvous Program Listing," Memorandum 1.
7. "A Monte Carlo Error Analysis Program for Near-Mars, Finite Burn, Orbital Transfer Maneuvers," by Richard N. Green, Lawrence H. Hoffmann, and George R. Young, NASA TN-6598, February 1972.

The purpose of VEAMCOP is to simulate the Mars orbital insertion burn followed by a rendezvous with Deimos for the Deimos/Phobos mission. Originally, VEAMCOP was used for Viking '75 statistical ΔV studies (Ref. 7): The rendezvous involves six maneuvers where the ΔV is calculated for each case and minimum distance between the satellite and spacecraft is calculated at the final maneuver. The original VEAMCOP program was designed to calculate the MOI burn and associated trim maneuvers for the Viking '75 mission. This program was modified for the rendezvous sequence by removing the trim procedures and inserting the rendezvous subroutine (REND). The documentation contains flow sequence of the main program, complete description of new subroutines, any modifications of existing programs, and references to currently documented programs. For the program listing of VEAMCOP, refer to Reference 6.

The effect of various error sources may be simulated through data inputs. Such errors include:

1. Encounter knowledge and control represented as the semi-minor axes of the B-plane ellipse and the ellipse orientation angle (SIGK, PSIK, SIGC, PSIC).
2. Execution: 1 σ errors on the controls (CONT).
3. Ephemeris: 1 σ errors on the Kepler elements (SIGD).

The DSN & TV knowledge matrices are entered as DSN1, DSN2, DSN3, TV1, and TV2. The matrix of eigenvectors for each is calculated by JACOBI and stored in the original covariance matrix. The corresponding vectors of eigenvalues are EVDSN1, EVDSN2, EVDSN3, EVTV1, and EVTV2. The resultant eigenvectors and eigenvalues were checked by calculating $X'CX=D$ where

X = matrix of eigenvectors

C = original covariance matrix

D = diagonalized matrix where the diagonals are the eigenvalues.

The original program is capable of MOI optimization through second order Taylor series expansion of the burn controls as a function of the estimated approach hyperbola. The input 1σ knowledge and control B-plane uncertainties are employed to calculate uncertainties along and perpendicular to the B-vector. Four B-vector perturbations (along and perpendicular to the B-vector. Four B-vector perturbations (along and perpendicular to the B-vector in the \pm direction) are calculated, and these vectors are mapped backward (by calling BTC) to obtain the corresponding conic elements. Thus, four sets of conic elements are calculated. The largest of each Kepler element is determined and the perturbation vector of the Kepler elements (DEL) is calculated by the formula

$$\delta K = K_E = K_R$$

where

K_E = the maximum conic elements from above

K_R = nominal conic

Following targeting of the nominal state, the partials with respect to the approach conic elements are calculated based on the perturbation conic vector (δK). The partials are

GRAD = vector of first order partials of Taylor series expansion

HMX = matrix of second order partials of Taylor series expansion

and are calculated by subroutine TAYLOR.

During the Monte Carlo simulation, the partials are used to calculate the delta controls by the formula

$$\delta C = \text{GRAD} \cdot \delta K + \delta K^T \cdot \text{HMX} \cdot \delta K.$$

The B-plane errors along and perpendicular to the B-vector are sampled to calculate the actual and estimate B-vector (BACT and BEST). The actual and estimated approach hyperbolic states are calculated uniquely from the estimated and actual B-vectors respectively. The perturbation vector of the Kepler elements, δK , is determined on each cycle by

$$\delta K = K_E - K_R$$

where

K_E = estimate conic state

K_R = nominal conic state

Either TAYSER or VITAP is employed to solve for the minimum ΔV MOI controls. The controls are represented by the equation

$$C = \delta C + C_R$$

where C_R = nominal controls.

The MOI burn is simulated by XSER13, and the actual final conic (XIN(7) - XIN(12)) is calculated by CARCON. It is this actual final conic that is used as input to the rendezvous program.

To alleviate computer running time, the partials depicted by IPOPT, KOPT, and NOPT (ref. 2) can be punched out during the first run of the program by setting IPFLG=1. For all remaining runs set IPFLG=0 and IRFLG=1, and use the punched partials as input following the NAMELIST data.

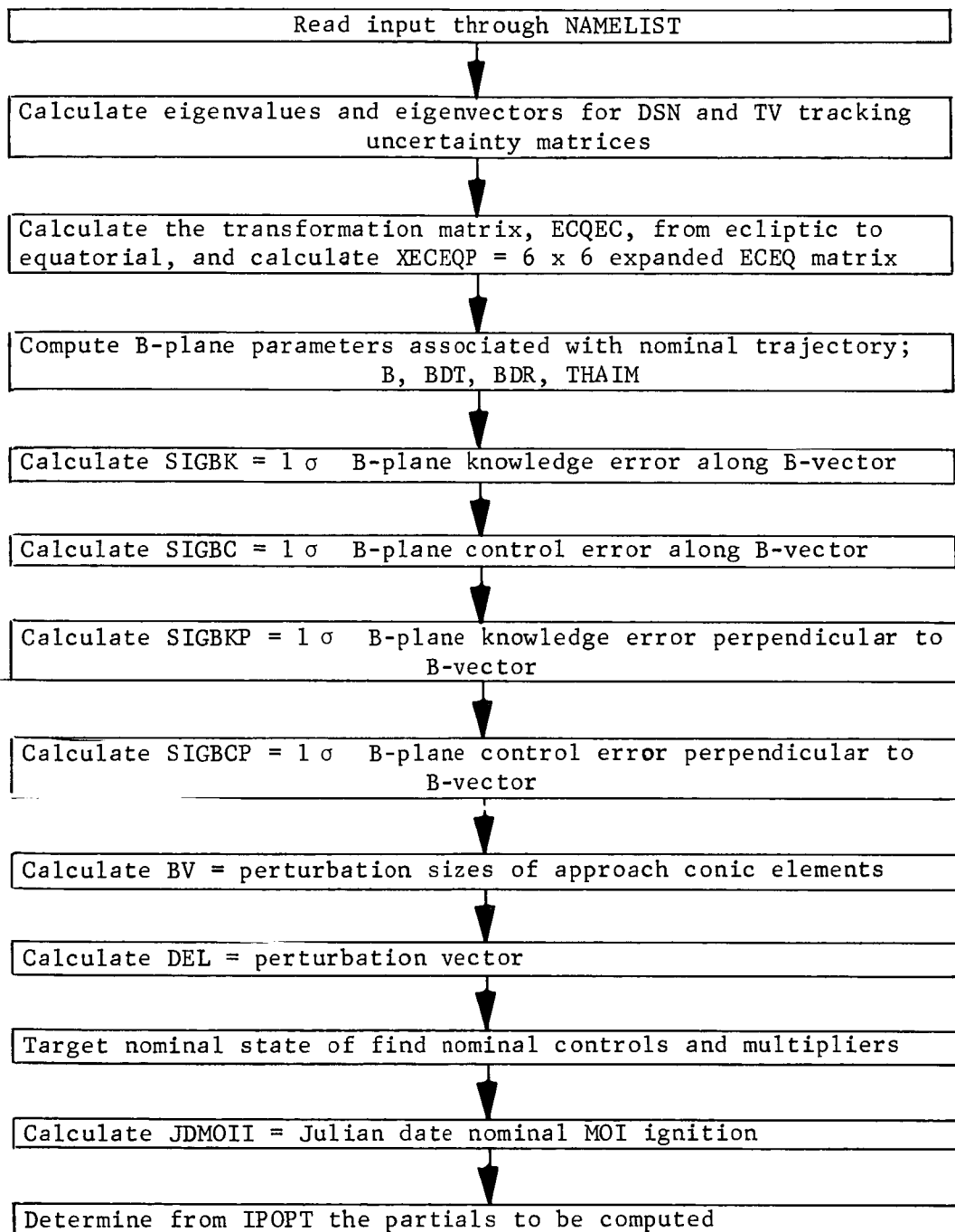
The program calculates the nominal MOI and the nominal rendezvous. The nominal rendezvous mission is simulated by assuming all errors are zero. The Monte Carlo simulation involves perturbation of MOI and rendezvous errors through random sampling of the errors. Consequently, for each Monte Carlo case, new statistics are kept in order to calculate the statistical ΔV and minimum distance between spacecraft and satellite and rendezvous, and other statistics.

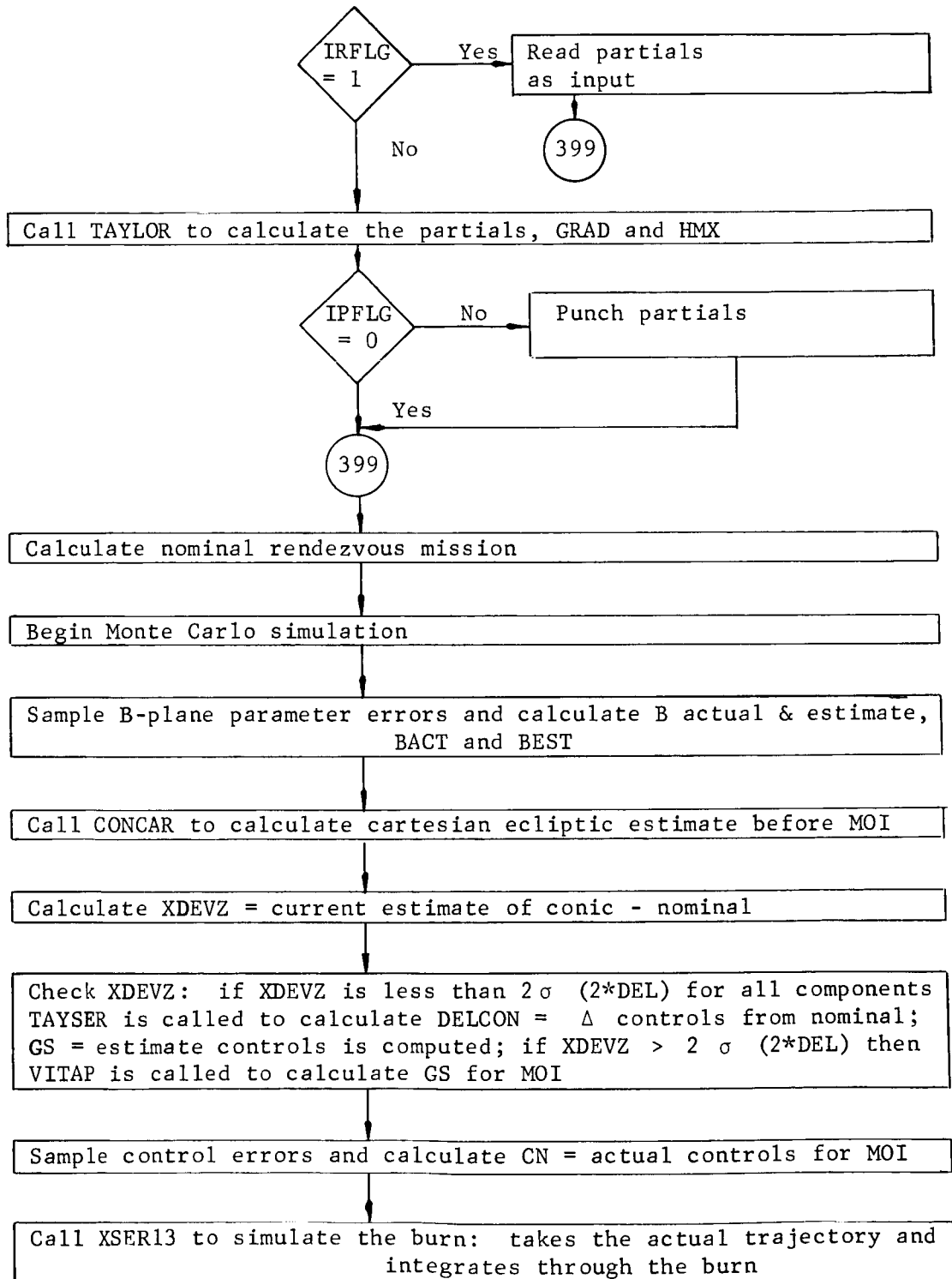
Program VEAMCOP

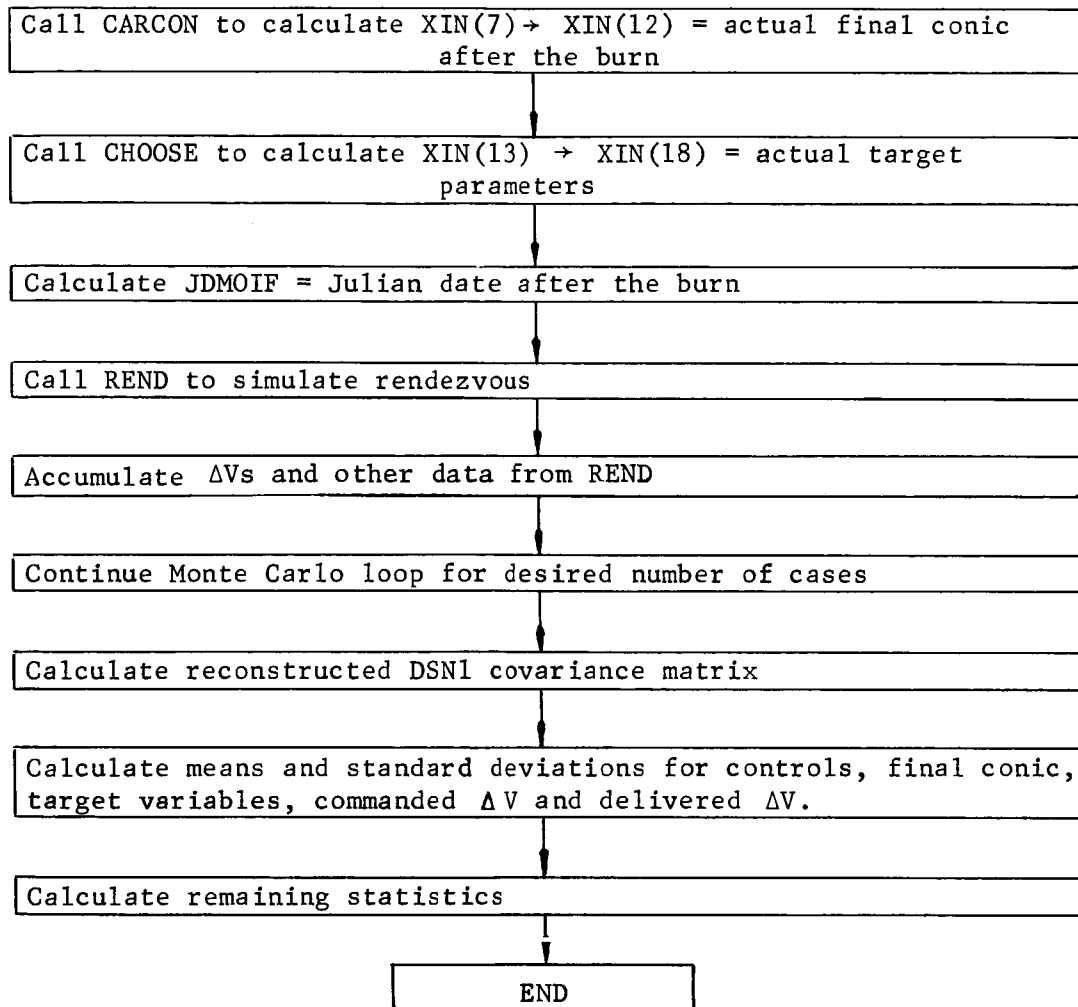
Data for VEAMCOP is defined through NAMELIST CASE. A description of the data is given in refs. 1 and 2. Data not included are:

SRANN = start for random number generator

MAXVIT = not used
 DJD = Julian date of encounter
 IPFLG = flag for punching partials
 = 1 punch partials
 = 0 do not punch partials
 IRFLG = flag for reading partials
 = 1 read partials as input
 = 0 calculate partials
 SIGD = 1 σ ephemeris errors (Kepler elements $a, e, i, \omega, \Omega, TA$)
 SIGC = 1 σ control ellipse semi-major and semi-minor axes
 PSIC = control ellipse orientation angle = angle between \vec{T} and
 major axis of error ellipse defining uncertainty in the
 B-plane aim point
 SIGK = 1 σ knowledge ellipse semi-major and semi-minor axes
 PSIK = knowledge ellipse orientation angle
 DSN1, DSN2, DSN3, TV1, TV2 - DSN & TV in-orbit tracking knowledge
 matrices
 MFLAGI = flag denoting DSN tracking
 = 1 DSN tracking
 = 0 no DSN tracking
 LFLAGI = flag denoting TV tracking
 = 1 TV tracking
 = 0 no TV tracking

Flow Diagram





The following subroutines are documented in ref. 3:

ACTB

AMXBM

ANG

ASER3

BTC

CARCON

CHOOSE

CONCAR

CONF

GPFI

HYT

INTER

INV

LATLING

MTXMY

SCAD

STATX

TAYLOR

TAYSER

TCONIC

TINVS

TRIM

VITAP

XSER13

XSER14

Subroutines Documented in STEAP

The following subroutines are documented in Space Trajectories Error Analyses Programs Version II, Ref. 5

CAREL

ELCAR

EULMX

JACOBI

PECEQ

Minor changes were made to CAREL and ELCAR which affected only the calling sequence. These changes are described here. For information pertaining to EULMX, JACOBI, and PECEQ refer to the STEAP documentation.

Subroutines Documented, Ref. 4

MARSAT

UNORM

UXV

VCOMB

VCROSS

VRTAX

VTRANS

Subroutine CARELInputGM = μ Mars

R = vector of cartesian coordinates

Output

TFP = time flight to periapsis

ORB = conic elements corresponding to R

PP = unit vector from planet to periapsis on ellipse and in direction of periapsis

QQ = vector perpendicular to PP and in the orbit plane

WW = vector perpendicular to plane of orbit and defined by

$$| \vec{r} \times \vec{v} |$$
Calling Sequence

Call CAREL (GM, R, TFP, ORB, PP, QQ, WW)

Discussion

The purpose of CAREL is to transform coordinates to conic elements. Further documentation can be found in

Space Trajectories Error Analysis Programs, Version IIVolumes I and II, ref. 5Subroutine CPROPInputGM = μ Mars

TI = initial Julian date

XX = cartesian state at time specified by TI

TF = final Julian date

Output

XEST = cartesian state propagated from TI to TF

IOUT = error flag

Calling Sequence

Call CPROP (GM, TI, XX, TF, XEST, IOUT)

Discussion

CPROP is a conic propagator which, given a state at an initial time, propagates it forward to a final time.

Subroutine DTDTA

Input

ORB = orbital elements of vehicle or satellite

TA1 = initial true anomaly

TA2 = final true anomaly

GM = μ Mars

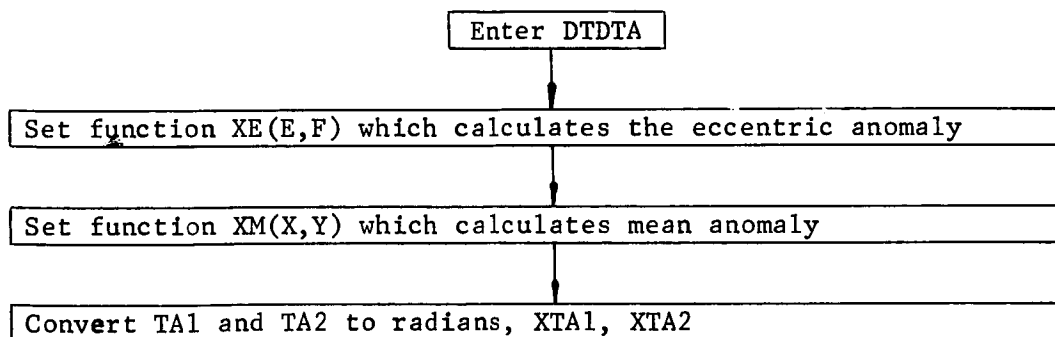
Output

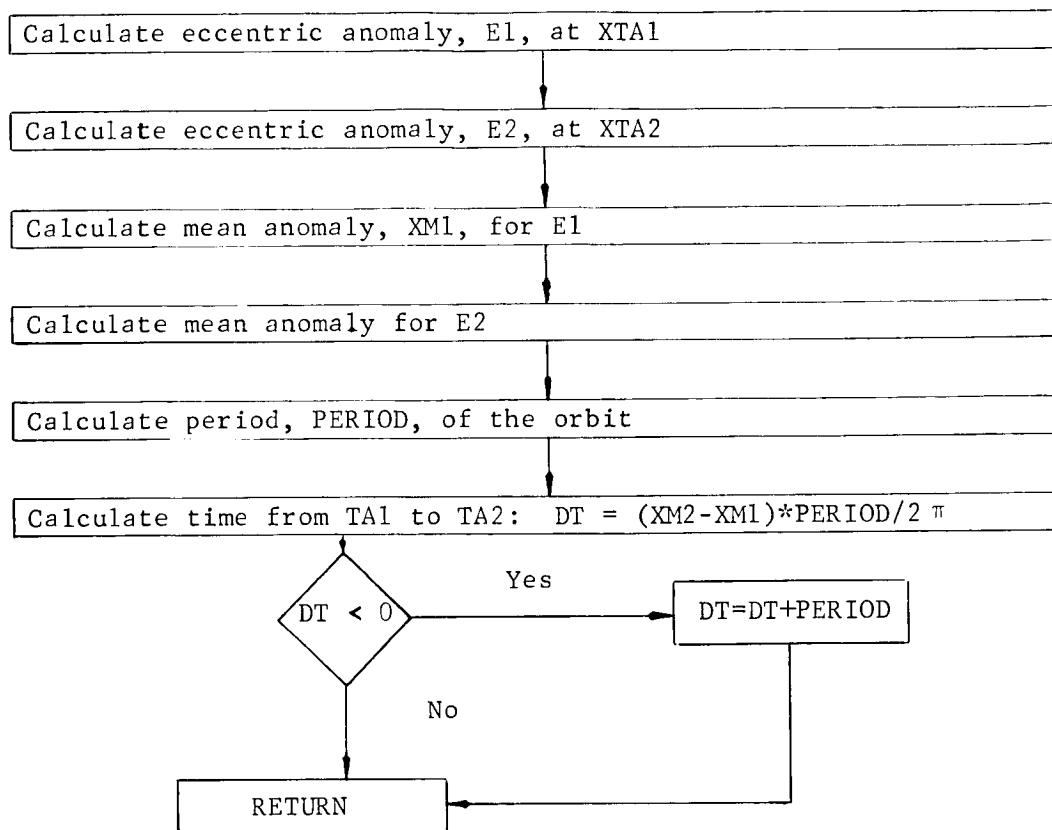
DT = amount of time from TA1 to TA2 on the orbit specified
by ORB

Calling Sequence

Call DTDTA (ORB, TA1, TA2, DT, GM)

Flow Diagram





Subroutine ELCAR

Input

GM = μ Mars

ORB = orbital elements

Output

R = cartesian coordinates associated with ORB

RM = magnitude of position

VM = magnitude of velocity

TFP = time of flight to periapsis

Calling Sequence

Call ELCAR (GM, ORB, R, RM, VM, TFP)

Discussion

The purpose of ELCAR is to transform orbital elements to cartesian coordinates. Further documentation can be found in

Space Trajectories Error Analysis Programs, Version II
Volumes I and II. Ref. 5

Subroutine HOHDVInput

X = cartesian state vector

RAP = orbit period

GM = μ Mars

Output

MDV = ΔV magnitude

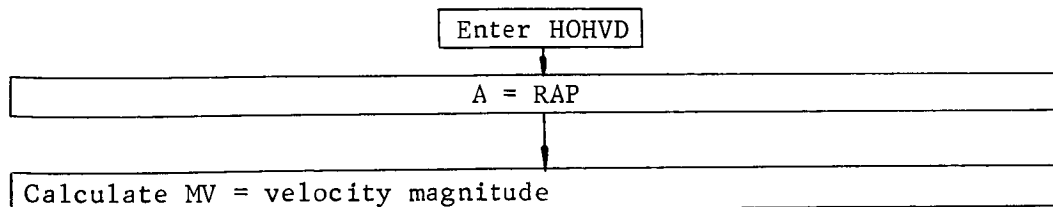
DV = components of the ΔV

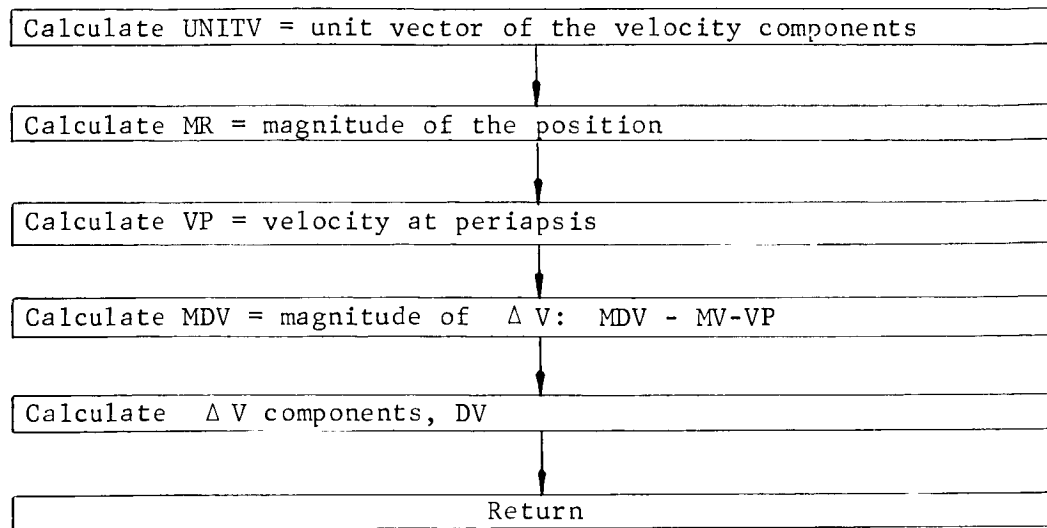
Calling Sequence

Call HOHDV (X, RAP, MDV, DV, GM)

Discussion

The purpose of HOHDV is to calculate the commanded ΔV vector and magnitude for a Hohmann transfer maneuver given the estimated state of the vehicle and the desired period of the final orbit

Flow Diagram



Subroutine MISS

Input

DTA = degree increment

TAl = initial true anomaly for starting the incremental search

XACT = actual state vector of the vehicle

DJ = Julian date of vehicle location

XACTF = Actual state vector of the satellite

DJ270 = Julian date of satellite location

GM = μ Mars

Output

RMIN = minimum distance between spacecraft and satellite at closest approach

TAMIN = true anomaly at RMIN

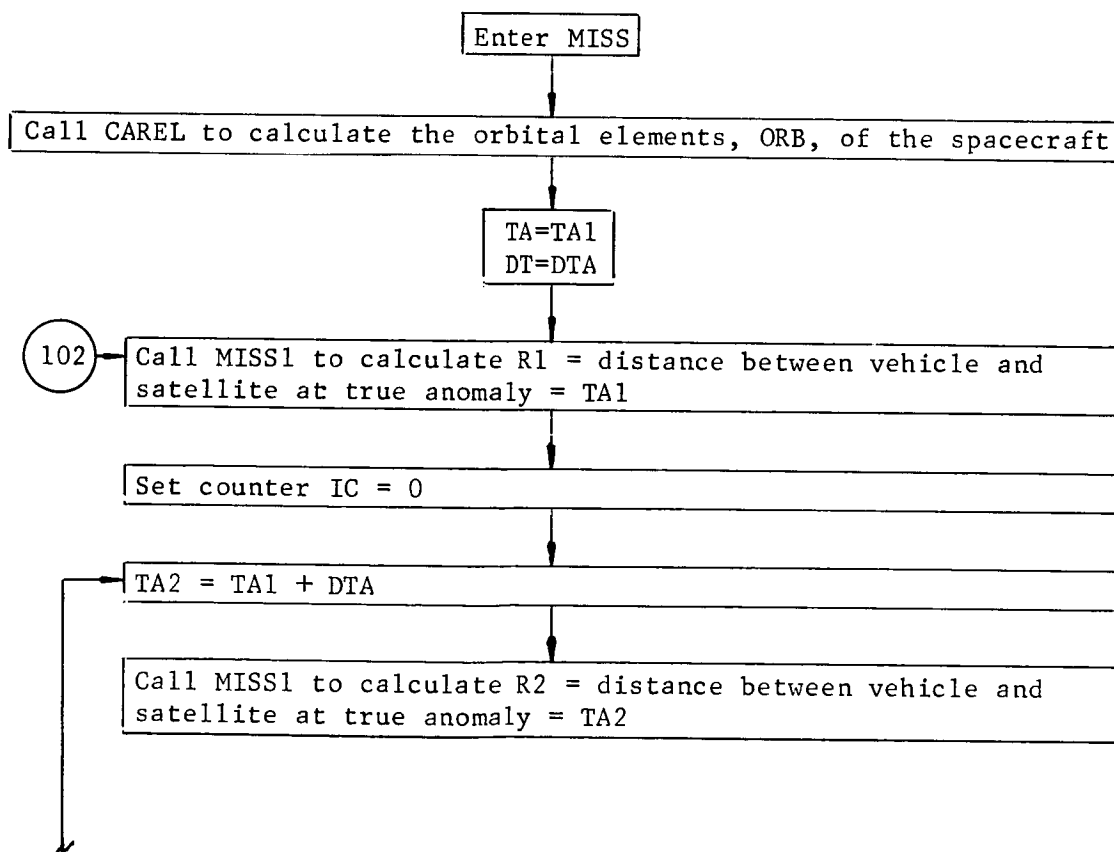
DJDCA = Julian date at closest approach

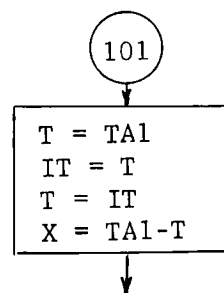
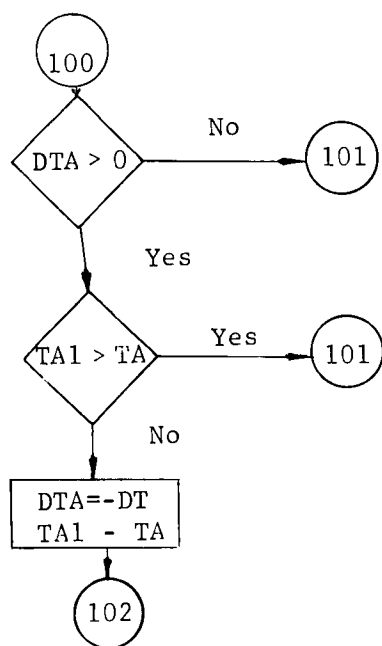
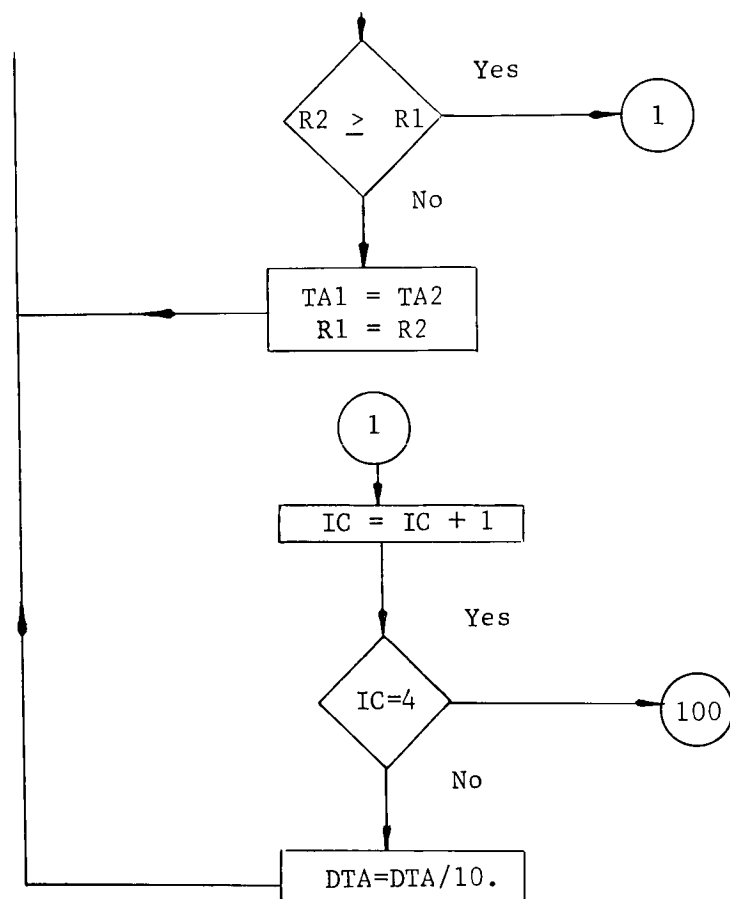
Calling Sequence

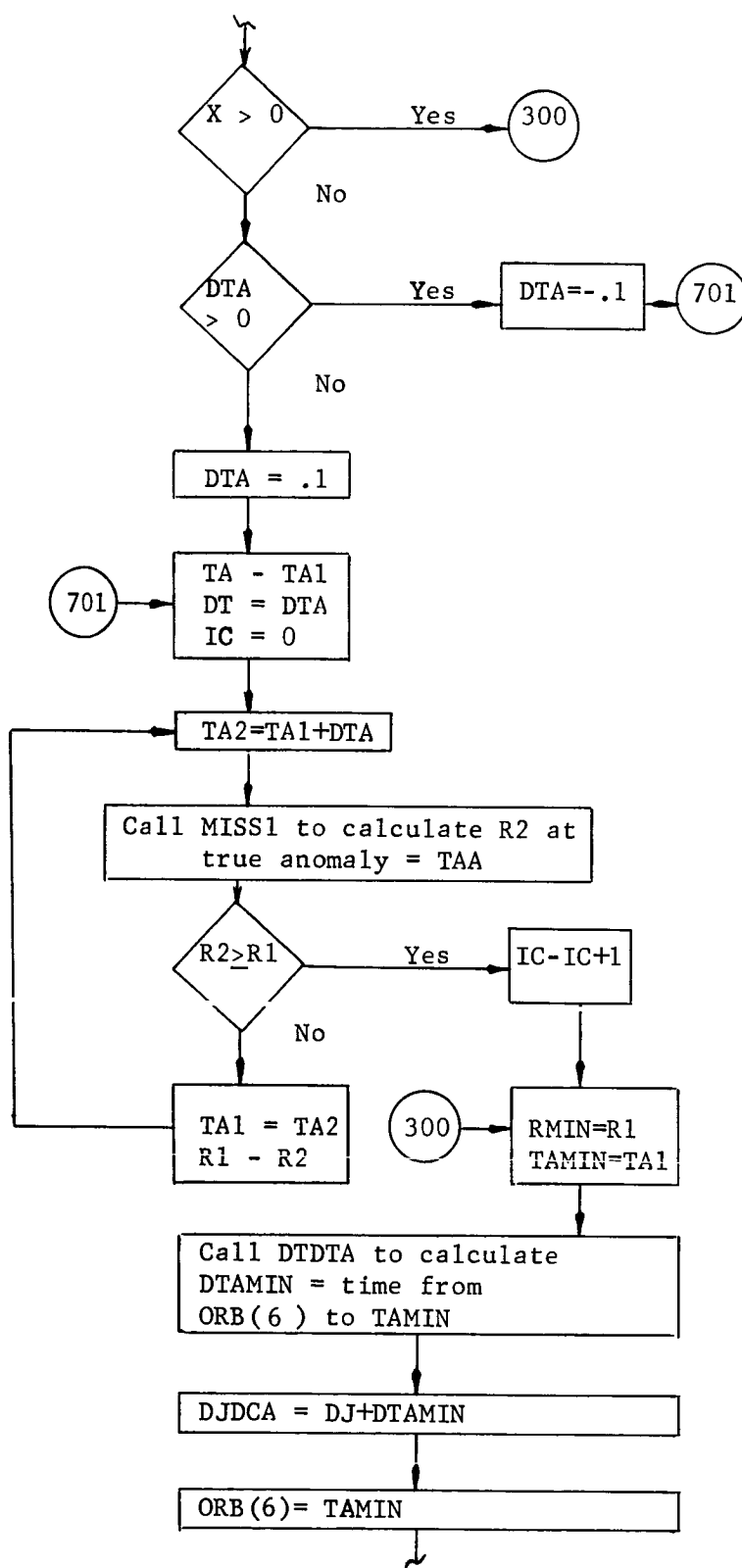
Call MISS (DTA, TA1, XACT, DJ, RMIN, TAMIN, XACTF,
DJ270, DJDCA, GM)

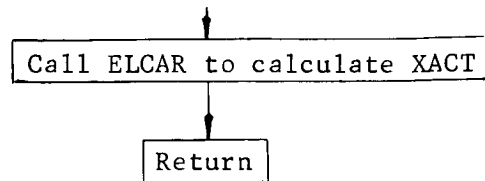
Discussion

The purpose of MISS is to calculate the minimum distance between the spacecraft and satellite at closest approach through an iterative scheme. The accuracy of the answer depends upon the true anomaly degree increment, DTA. For this program DTA was set equal to 1 implying that the increments will be 1., .1, .01, and .001. TA1 is the initial guess for the true anomaly at closest approach. Since the true anomaly should be near 180° but could vary $\pm 10^\circ$, 170° was chosen as the guess.

Subroutine MISSFlow Diagram







Subroutine PLASAT

Input

JD = Julian date

IS = satellite number

= 1 denotes Phobos

= 2 denotes Deimos

IP = Planet number

= 5 denotes Mars

ECEQ = transformation matrix from ecliptic to equatorial

IFLAG = flag denoting ecliptic or equatorial system

= 0 leave cartesian coordinates in ecliptic

= 1 transform coordinates to equatorial

Output

R - cartesian state of the satellite

ORB = Satellite orbital elements

Calling Sequence

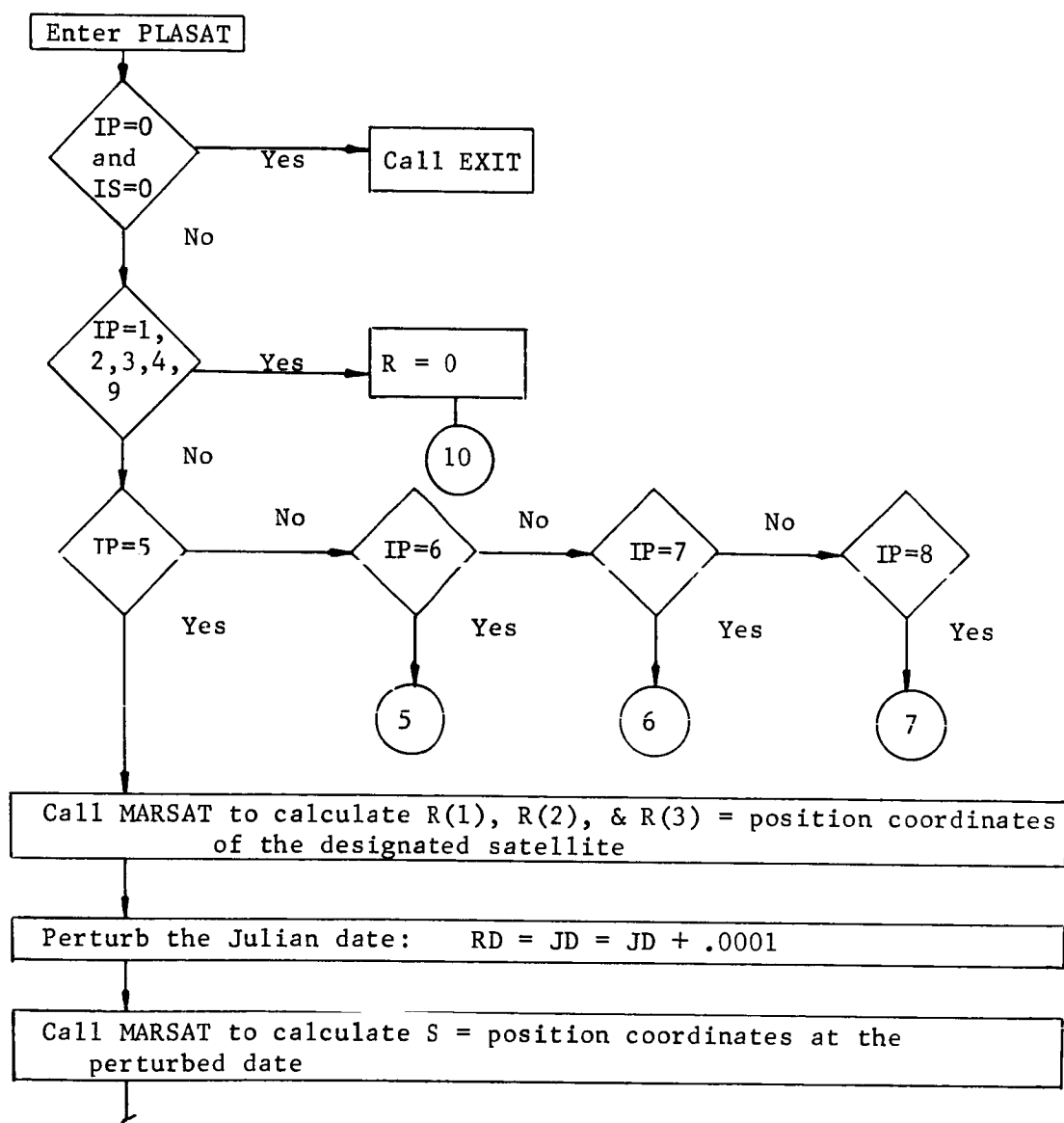
Call PLASAT (R, JD, IS, IP, ORB, ECEQ, IFLAG)

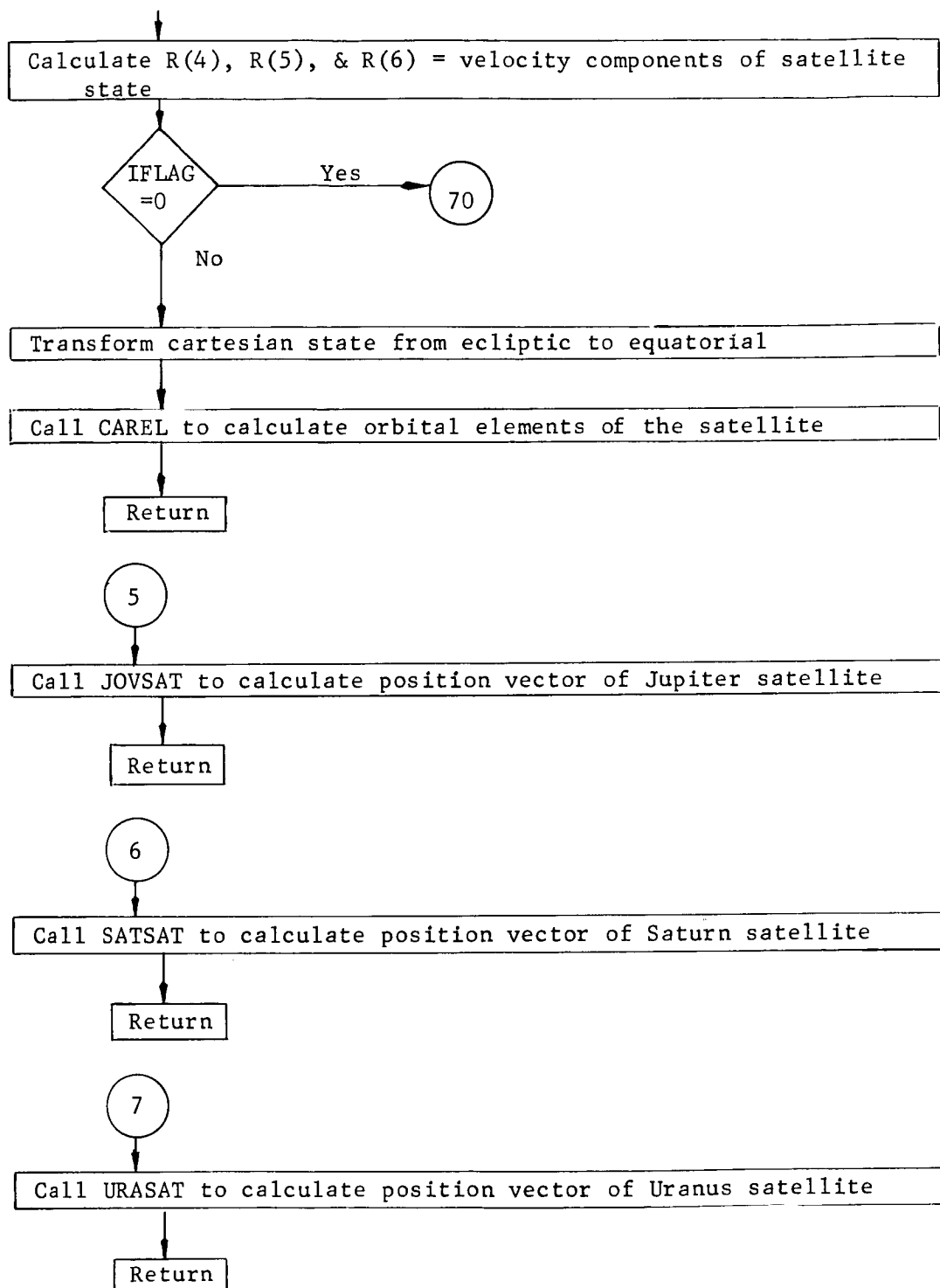
Discussion

The purpose of PLASAT is to calculate the cartesian state and orbital elements of a specific satellite for a given outer planet.

For the purposes of this program, only the Martian satellites are considered and specifically Deimos. Modifications were made to the subroutine to compute the velocity components of the satellite state, to transform the state from ecliptic to equatorial, and to calculate the satellite orbital elements. Since other planet satellites are not considered, these modifications were not made for Jupiter, Uranus, and Saturn. Also, the subroutines, JOVSAT, SATSAT and URASAT are not included in the program.

Flow Diagram





Subroutine PRIMEInput

A = 6 x 6 matrix

Output

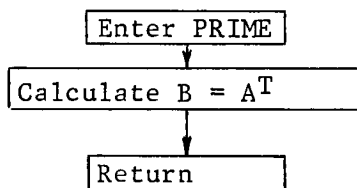
B = transpose of A

Calling Sequence

Call PRIME (A, B)

Discussion

The purpose of PRIME is to calculate the transpose of a matrix.

Flow diagramSubroutine RANDOMInput

COV: 6 x 6 matrix of eigenvectors

C : 6 dimensions vector of eigenvalues

Output

X: 6 dimension vector of random errors obtained by the sampling procedure

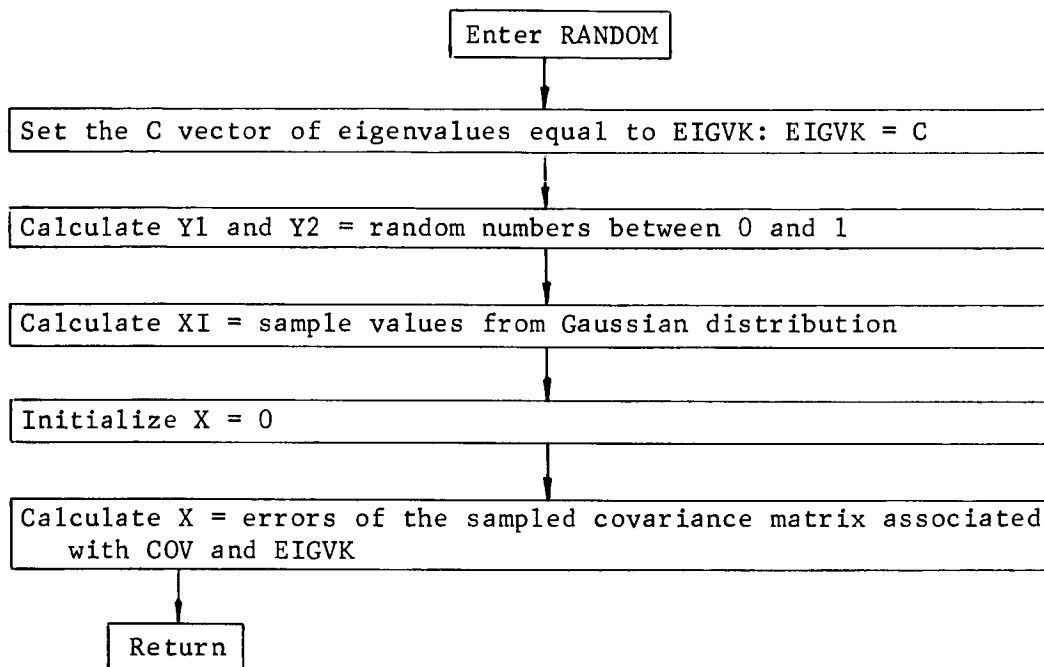
Calling Sequence

Call RANDOM (COV, X, C)

Discussion

The purpose of RANDOM is to sample a 6 x 6 covariance matrix. The sampling process is based on the eigenvectors and eigenvalues of the covariance matrix. For simplicity, the eigenvalues and matrix of eigenvectors are calculated in the main program and are passed to REND through common.

Flow Diagram



Subroutine REND

Input

CACTO(6): Actual Kepler elements of the spacecraft orbit at the time of MOI burn completion.

DJMOIF: Julian date of the MOI burn termination.

SIGD(6): One sigma errors for orbital elements of Deimos (a, e, i, ω , Ω , TA)

CONT(10): One sigma execution errors

MFLAG: Flag denoting DSN tracking
 =1 DSN tracking with DSN error
 =0 Perfect DSN tracking

LFLAG: flag denoting TV tracking
 =1 TV tracking with errors
 =0 perfect TV tracking

SMARS: gravitational constant of Mars

Output

DV(6): vector containing the magnitudes of delta V for the six maneuvers performed in the subroutine.

RMIN: minimum distance spacecraft missed the satellite at rendezvous

Calling Sequence

Call REND (CACTO, DJMOIF, DV, RMIN, SIGD, CONT, MFLAG, LFLAG, SMARS)

Common Blocks

Most of the inputs to REND are made through the following labeled common blocks:

1. SAVE - XINI is the resultant error vector from sampling the DSN1 matrix (XIN1 = PXEST). The purpose of saving this vector is for reconstruction of the covariance matrix performed in the main program (see page 1, flow diagram).
2. ROT - ECEQ is the matrix of transformations of cartesian coordinates from ecliptic to equatorial. XECEQP is the expanded 6 x 6 matrix of ECEQ.
3. BK - The variables are supplied by the calling program
4. TRACK - DSN1, DSN2, DSN3, TV1, TV2 are the matrices of eigenvectors associated with the DSN and TV tracking covariances inputed in the main program. These matrices along with the vectors, EVDSN1, EVDSN2, EVDSN3, EVTV1, EVTV2, of eigenvalues are used by RANDOM for random sampling of covariances.

Discussion

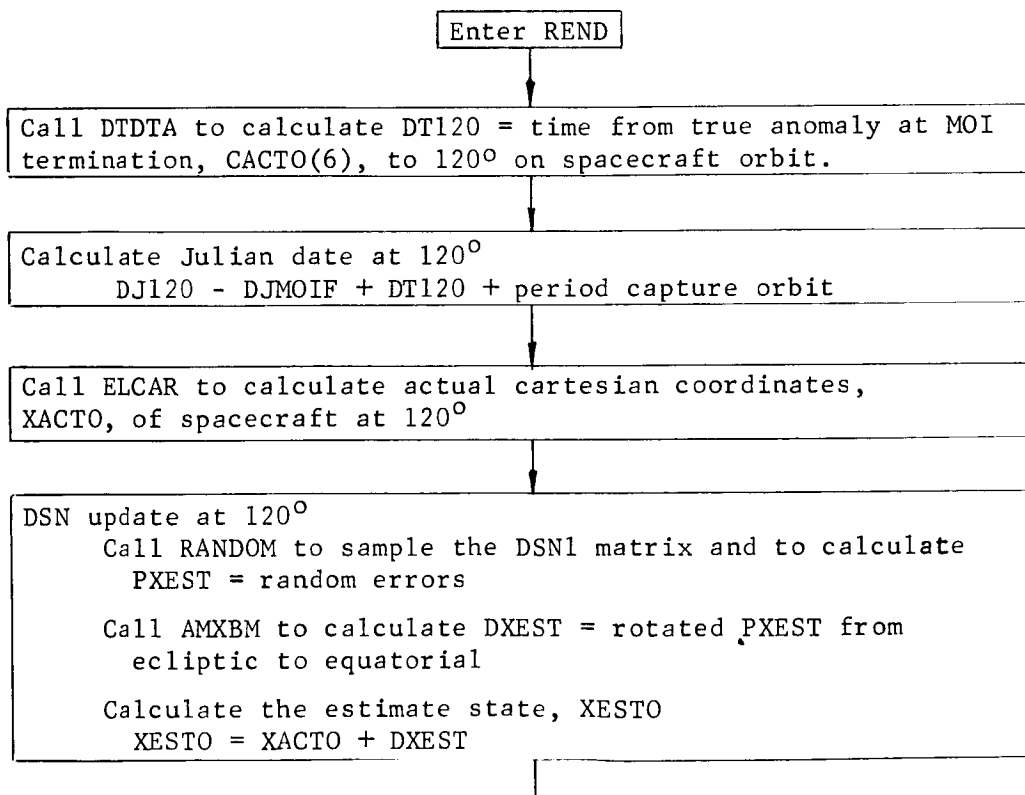
The purpose of REND is to simulate six maneuvers for the

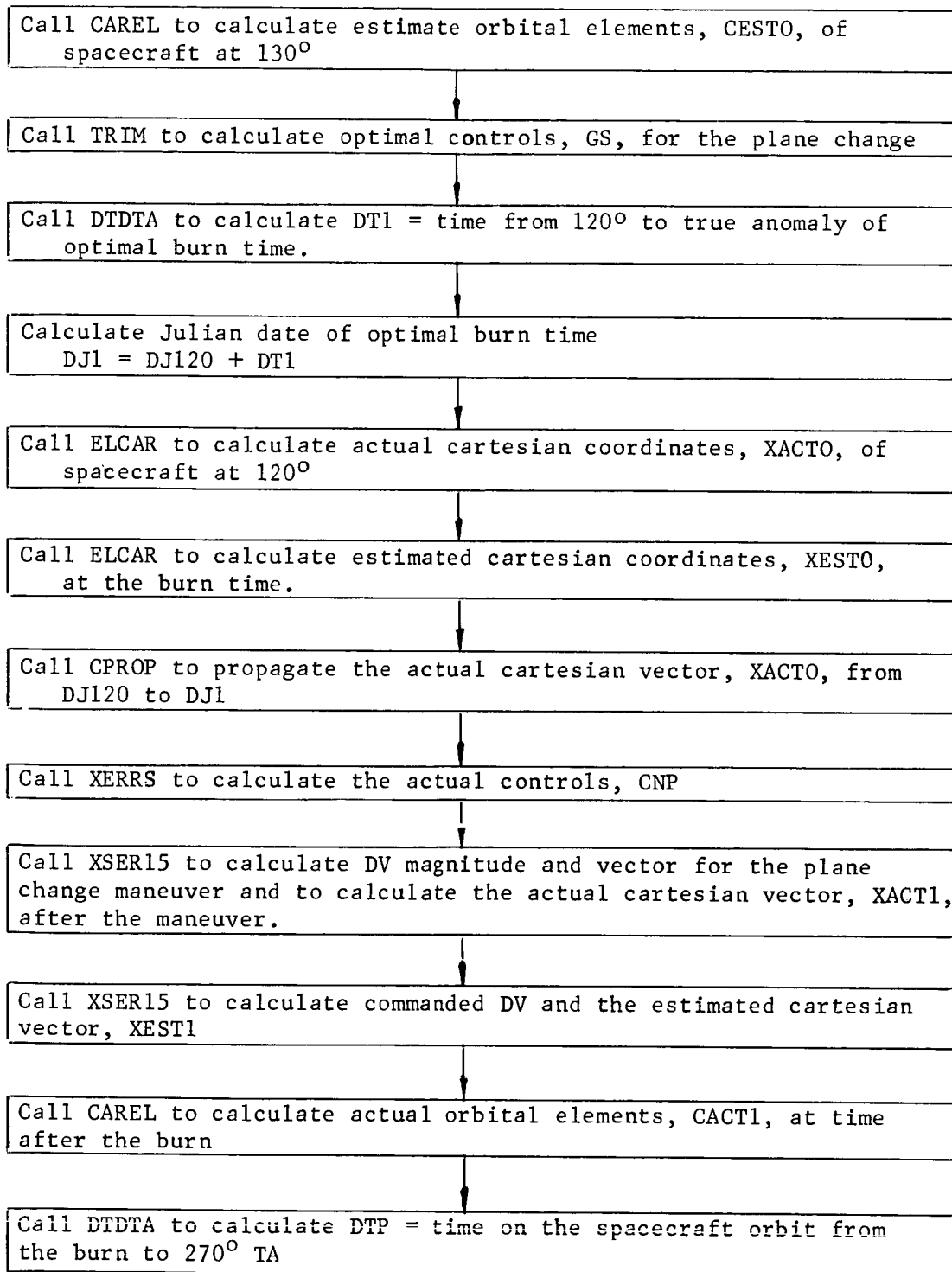
rendezvous calculating the commanded and actual ΔV s for each maneuver, and at the final maneuver to calculate the minimum distance between the spacecraft and Deimos.

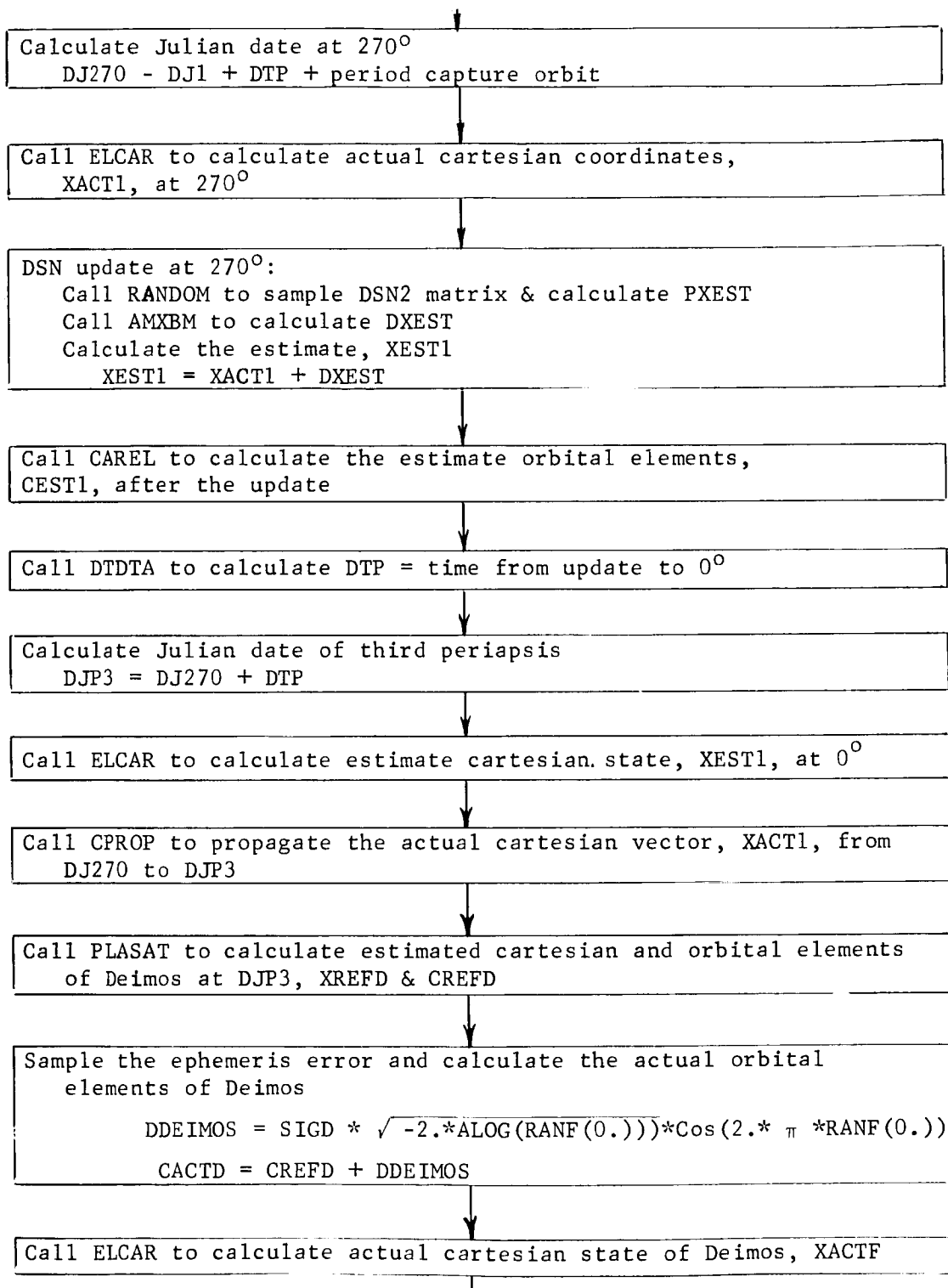
The six maneuvers are:

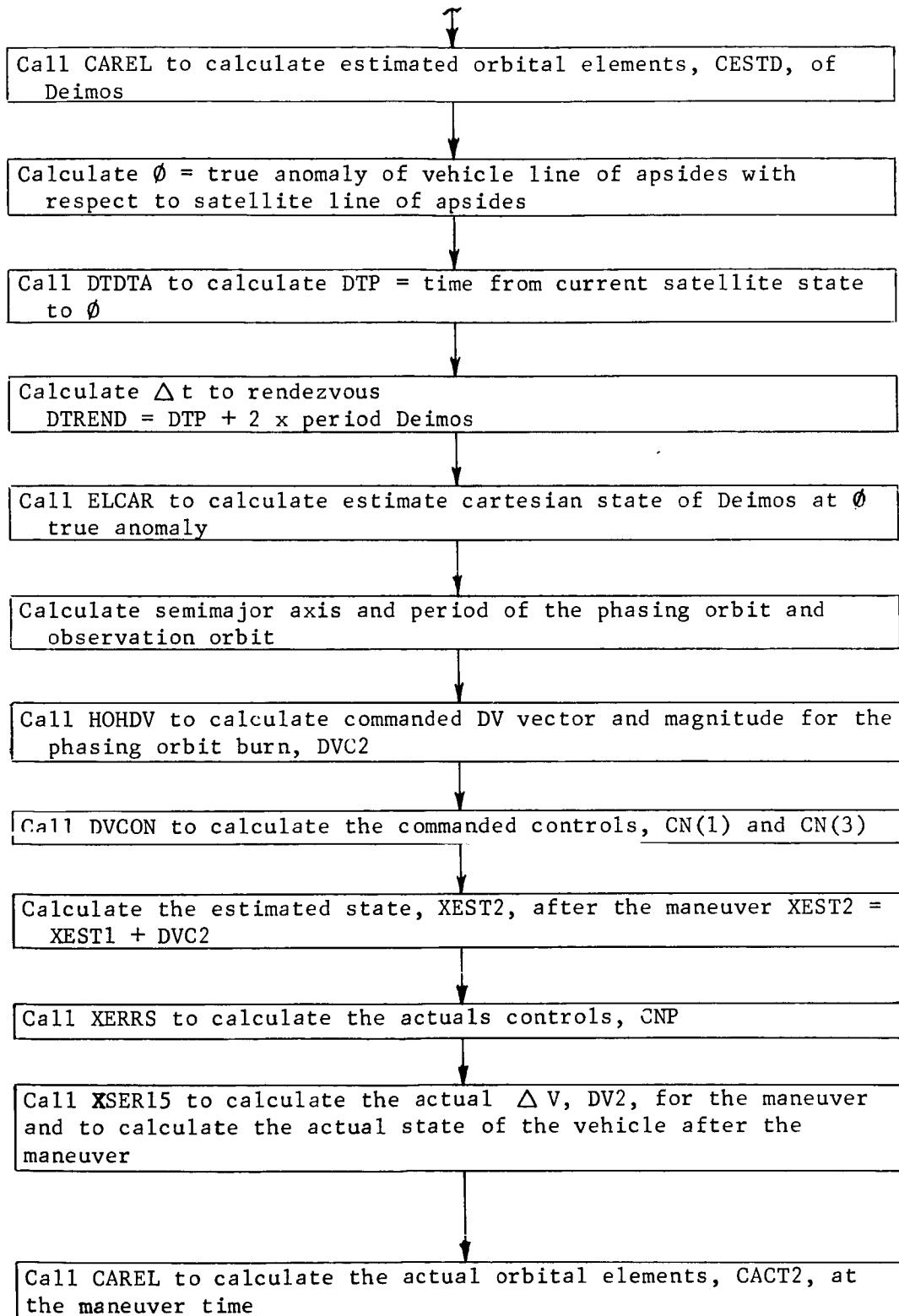
1. Plane change to change inclination of capture orbit
2. Phasing orbit maneuver to drop from capture orbit to phasing orbit
3. Observation orbit maneuver to burn into the observation orbit
4. Lambert Transfer
5. Midcourse correction
6. Plane change to match Deimos

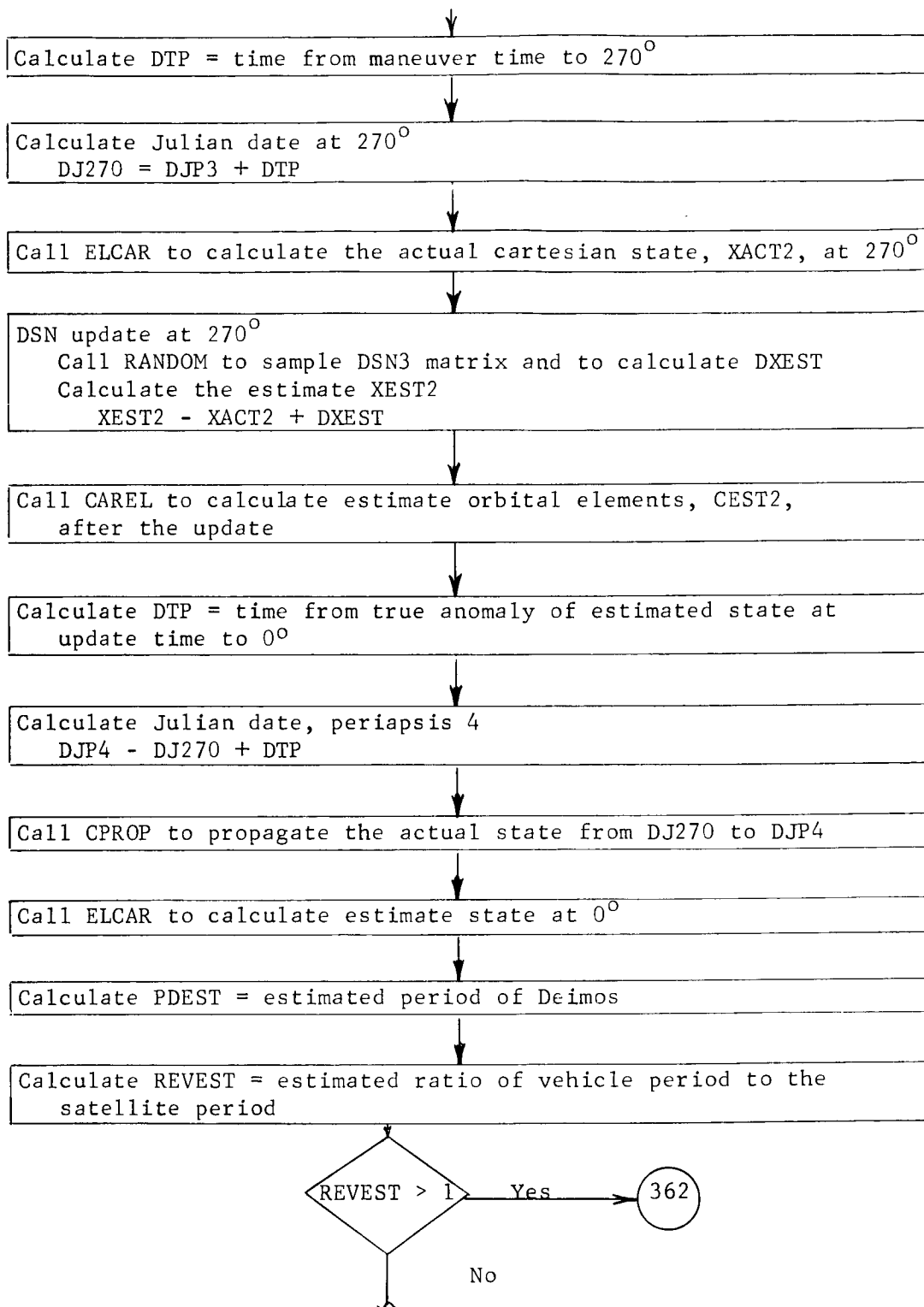
Flow Diagram

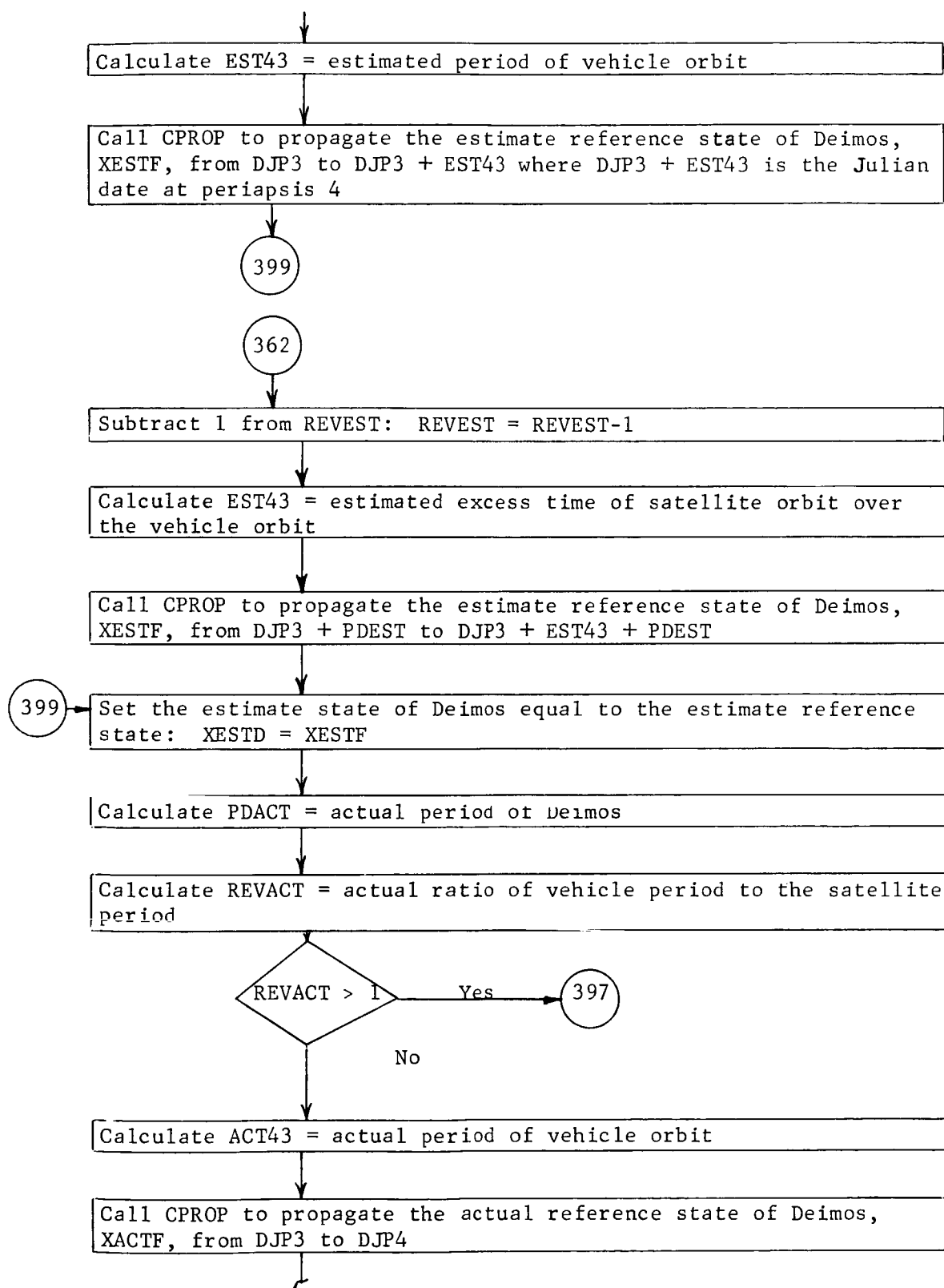


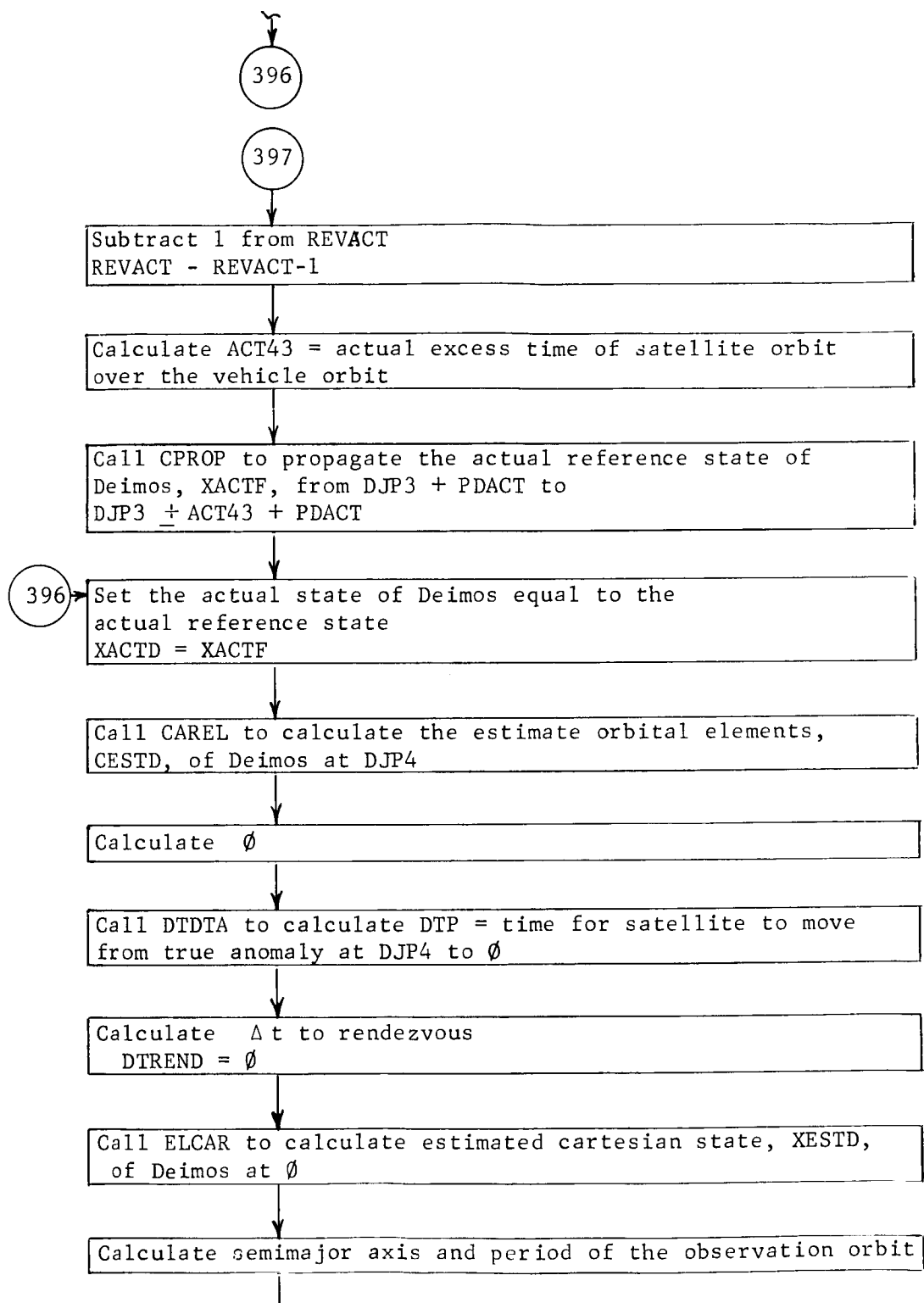


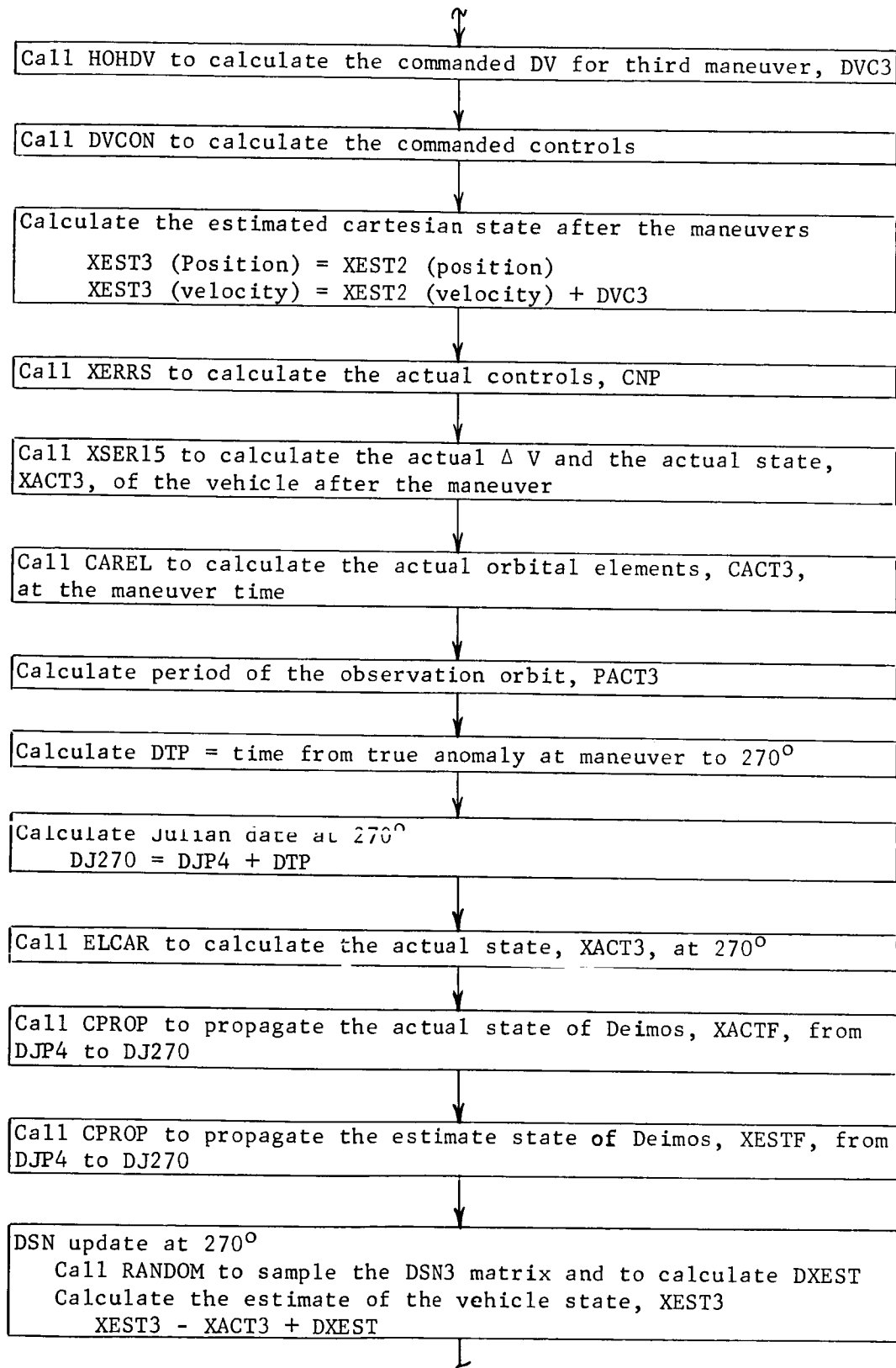


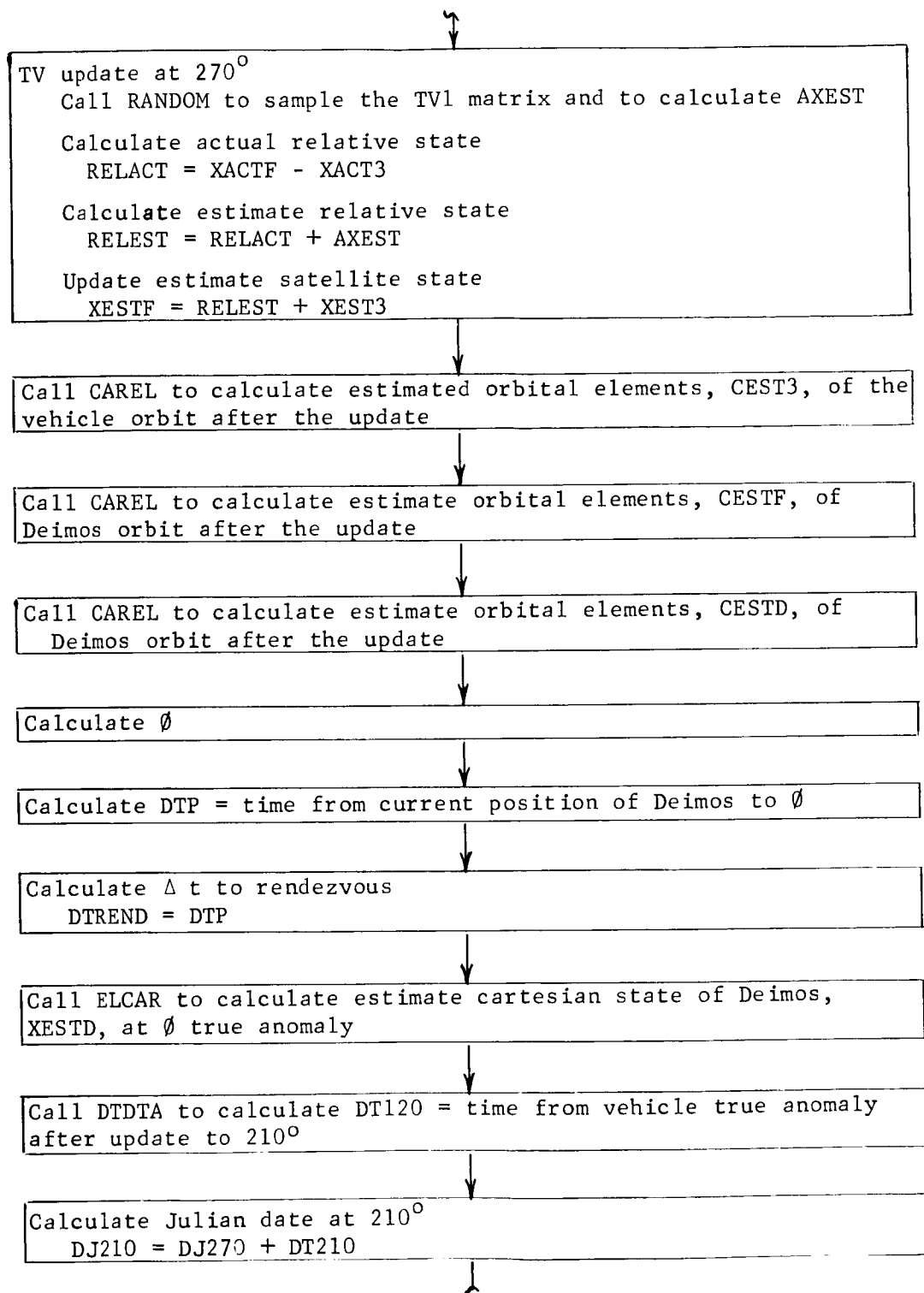


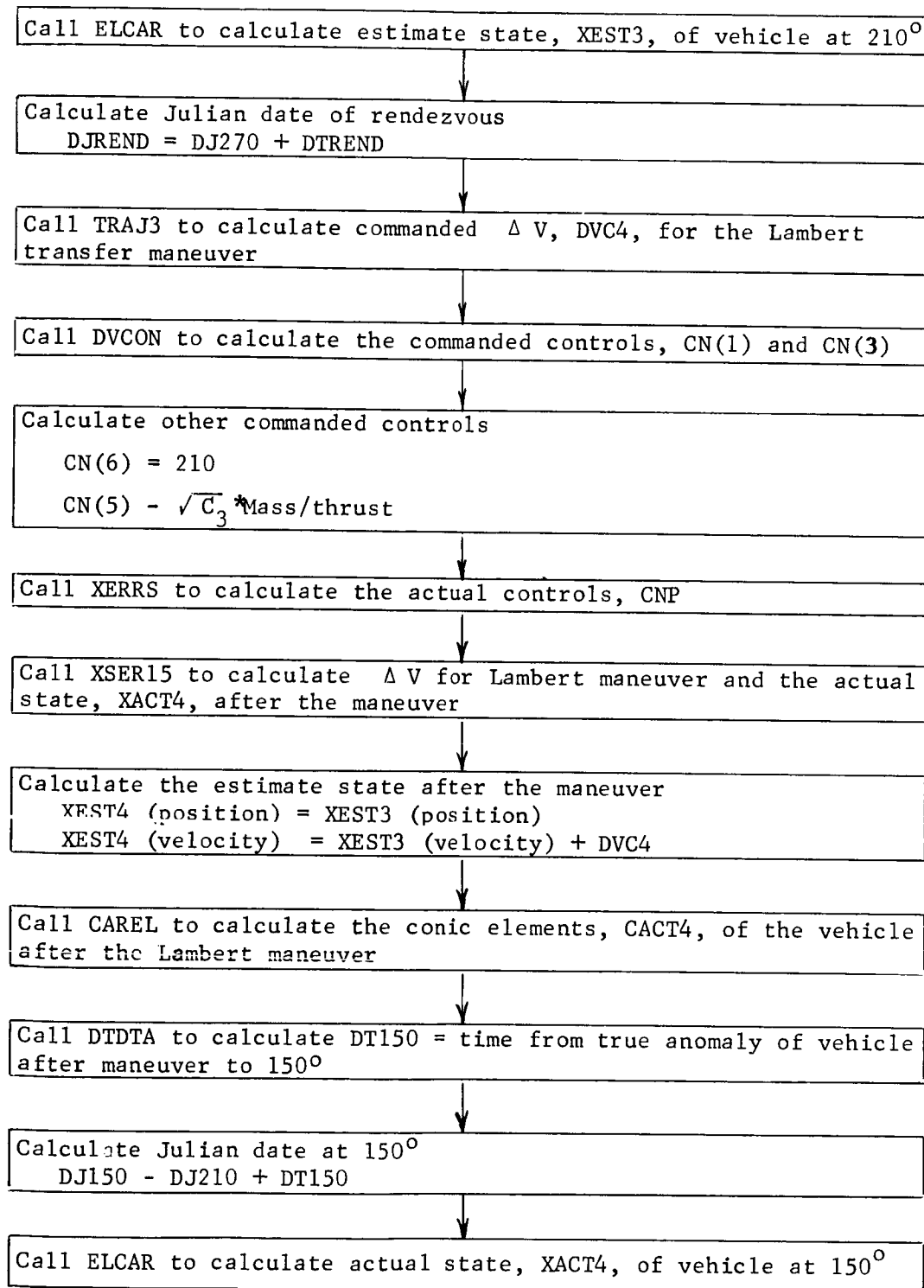


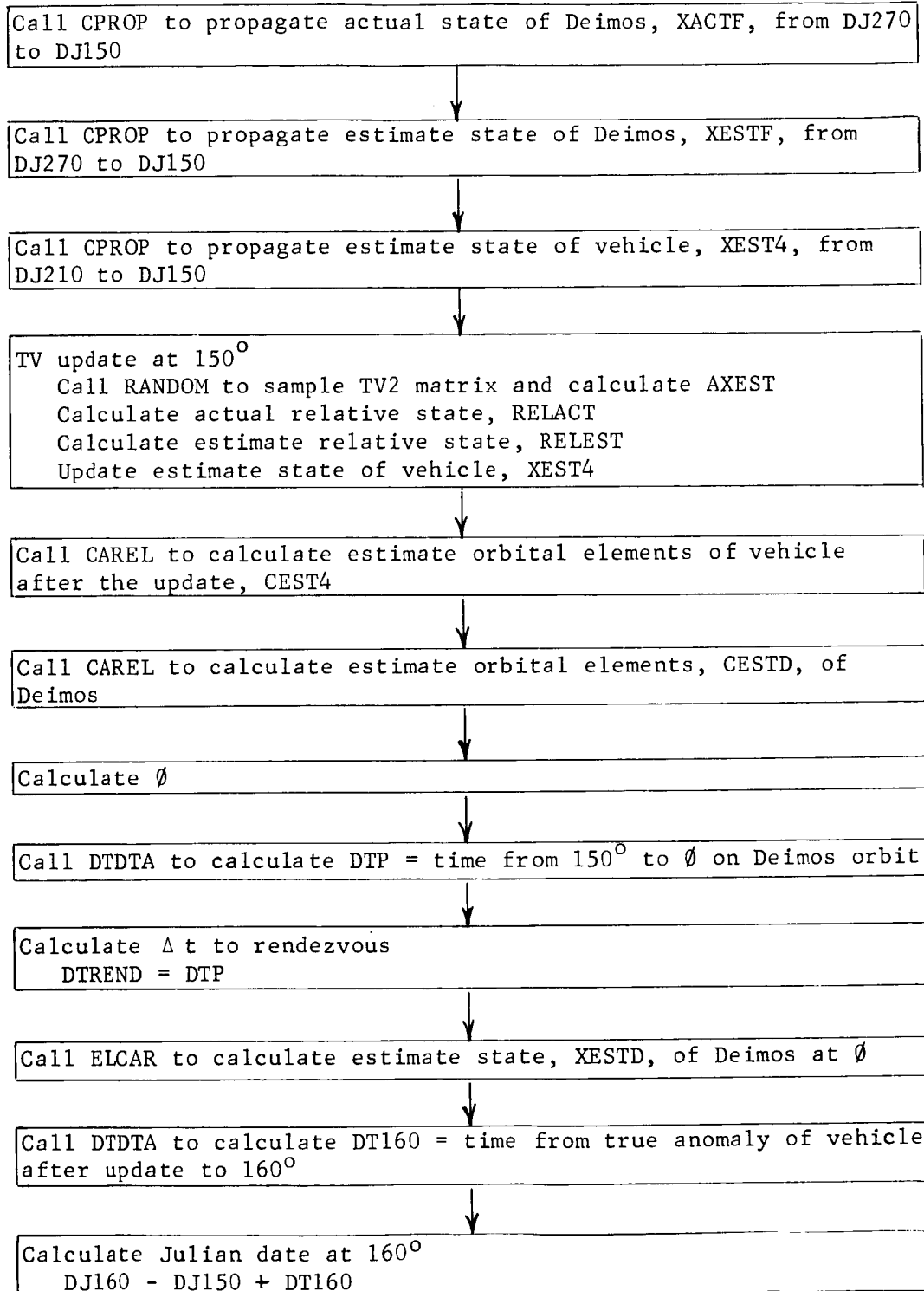


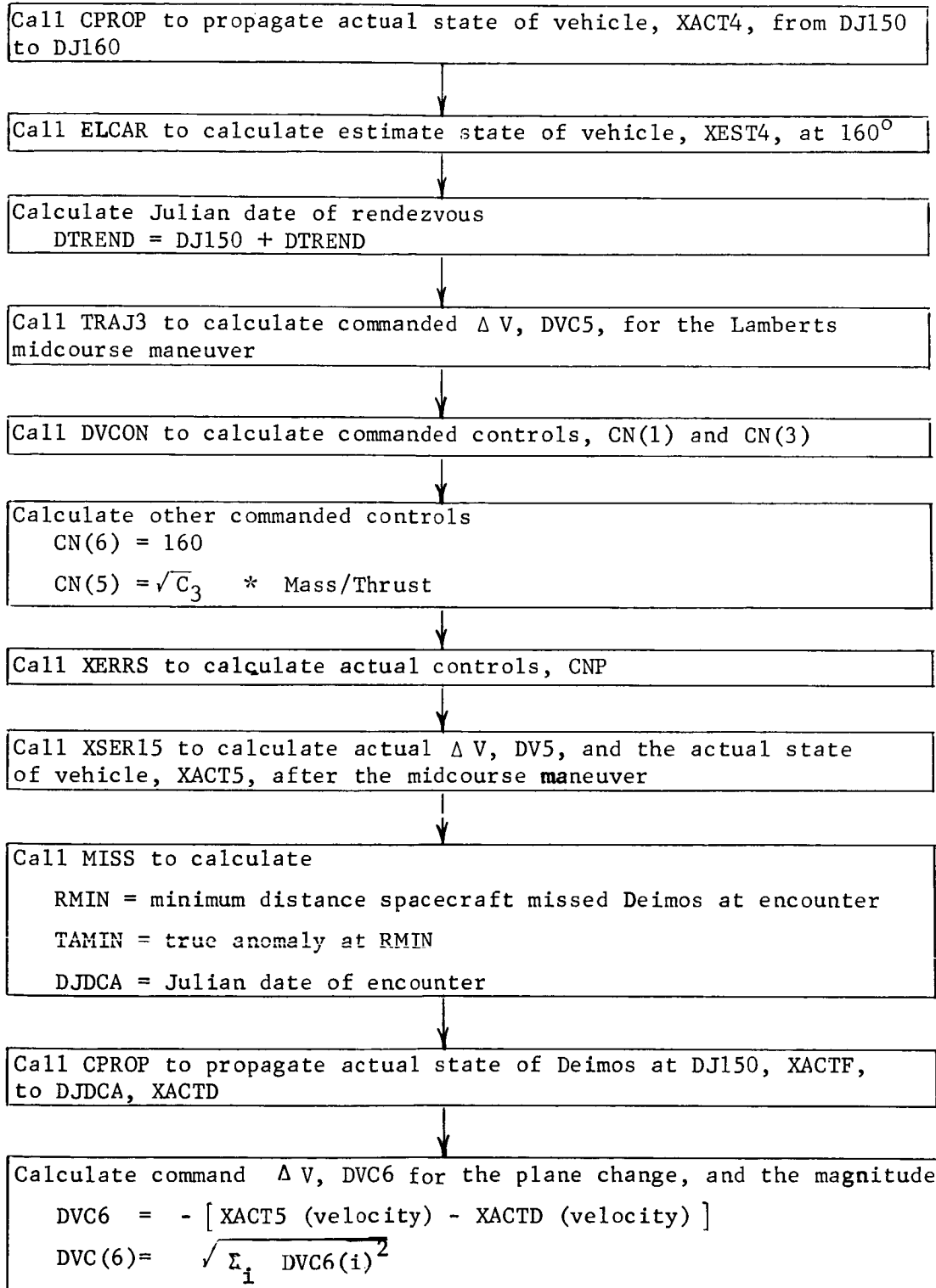


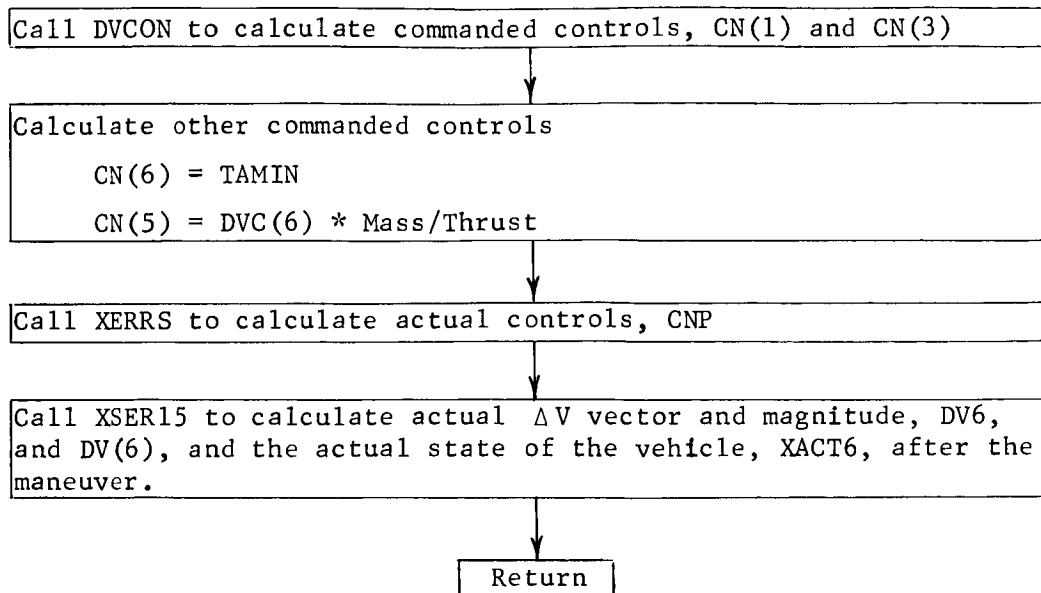












Subroutine XERRS

Input

GGs - set of commanded controls

CONTR - one σ errors on the controls

MASS = mass

THR = thrust

I = maneuver number

Output

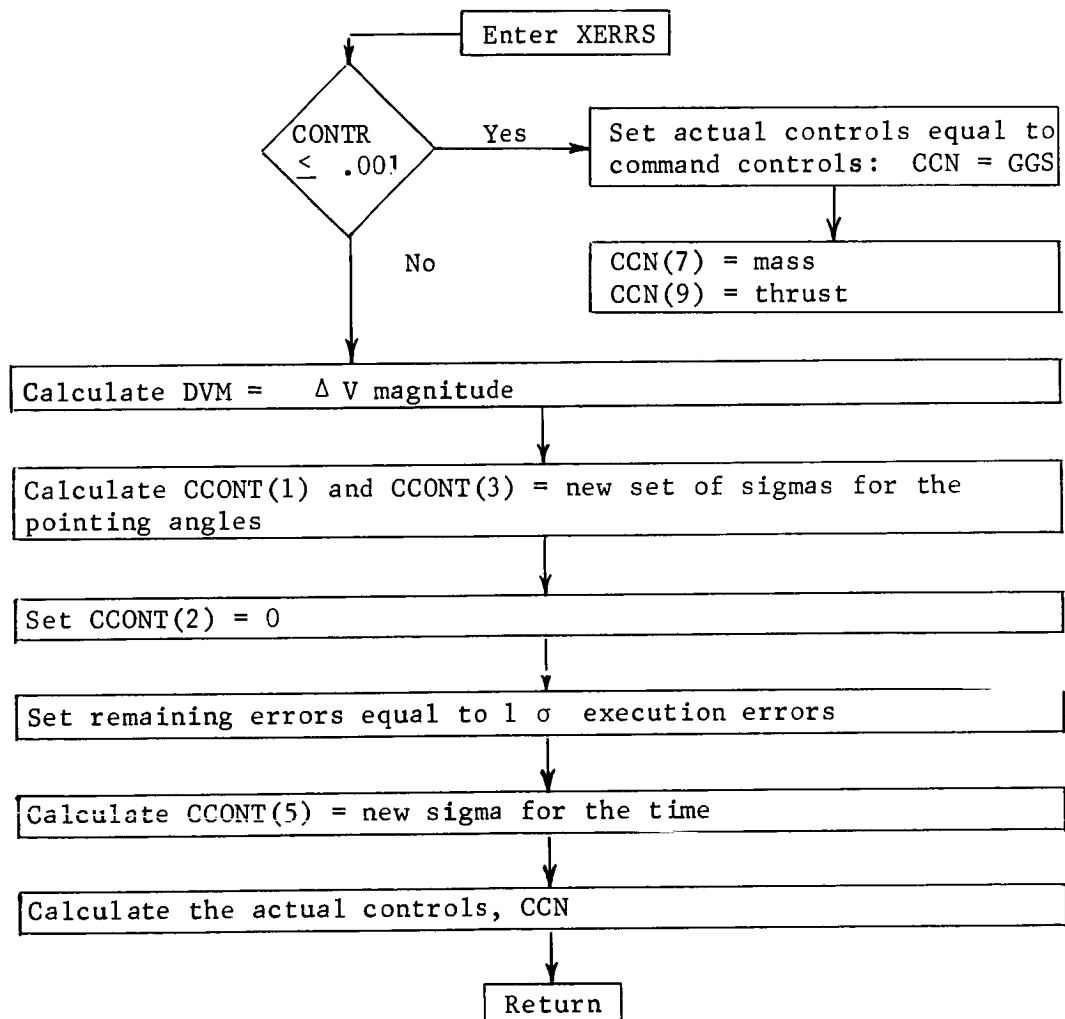
CCN = set of actual controls

Calling sequence

Call XERRS (GGs, CONTR, MASS, THR, CCN, I)

Discussion

The purpose of XERRS is to calculate actual controls given a set of commanded controls and the execution errors. The program takes the 1σ execution errors of MOI, calculates a new set of 1σ errors, samples these new execution errors and then calculates the actual controls. If there is no execution error, the actual controls are equal to the commanded controls.



Subroutine XSER15Inputs

XI = 6 dimensioned state vector before a maneuver

CN = set of controls

Output

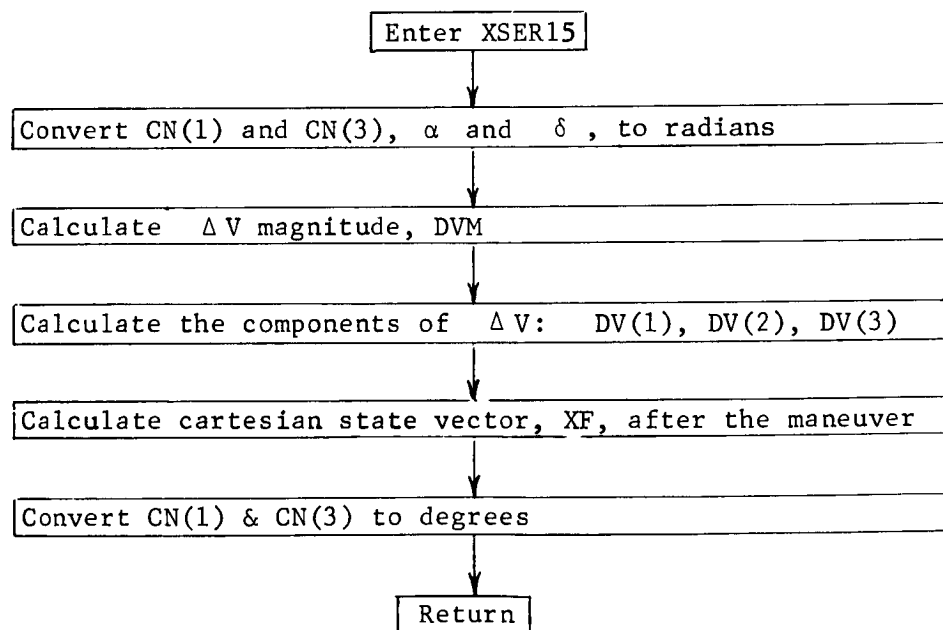
XF = 6 dimensional state vector after a maneuver

DVM = delta V magnitude

DV = three-dimensional delta V components

Calling Sequence

Call XSER15 (XI, CN, XF, DVM, DV)

Flow Diagram

Appendix D

APPENDIX D

LANDING STABILITY COMPUTER PROGRAM METHODOLOGY

LANDING STABILITY COMPUTER PROGRAM METHODOLOGY

With the large number of variables involved in a six-degree-of-freedom computer program, vector notation becomes a necessity. With the use of more than one coordinate system, transforming these vectors between coordinate systems necessitates the use of matrices and matrix multiplication.

The equations of motion are simple in the linear mode but become complex when applied to rotations. The solution for this problem is to work with the coordinate transform matrix directly rather than indirectly through position angles.

The fundamental geometry can be further complicated by the initial conditions being given by position angles and ground slopes. The conversions from these to the initial position transform matrix are worked out by brute force.

A. EQUATIONS OF MOTION

The equation for linear momentum is

$$\bar{F} = m \bar{a}$$

where \bar{a} is the acceleration at the center of gravity and \bar{F} is applied anywhere on the body.

The moments on the body can be found from the forces and their moment arms by

$$\bar{M} = \bar{r} \times \bar{F}$$

where \bar{M} , \bar{r} , and \bar{F} are all in the same coordinate system.

The equation for angular momentum is

$$\bar{M} = \dot{\bar{L}} = \dot{L}_x \bar{i} + \dot{L}_y \bar{j} + \dot{L}_z \bar{k} + (\bar{\omega} \times \bar{L})$$

where the components of \bar{L} are fixed in the body. If the fixed axes are principal axes, the equations reduce to

$$M_x = I_{xx} w_x - (I_{yy} - I_{zz}) w_y w_z$$

$$M_y = I_{yy} w_y - (I_{zz} - I_{xx}) w_z w_x$$

$$M_z = I_{zz} w_z - (I_{xx} - I_{yy}) w_x w_y$$

where all components are measured along the fixed principal axes of the body.

The linear accelerations can be integrated to give velocity and displacements.

$$\bar{v}_{t_1} = \bar{v}_{t_0} + \int_{t_0}^{t_1} \bar{a} dt$$

$$\bar{r}_{t_1} = \bar{r}_{t_0} + \int_{t_0}^{t_1} \bar{v} dt$$

The angular accelerations can be integrated to give angular velocities.

$$\bar{w}_{t_1} = \bar{w}_{t_0} + \int_{t_0}^{t_1} \dot{\bar{w}} dt$$

B. FINITE TIME ITERATION

In the case of a physical dynamics problem, the accelerations are determined by forces and moments which are functions of position and velocity. If the accelerations and their derivatives are rational functions, an approximation can be made over a small time period such as:

$$\int_{t_0}^t \ddot{x} dt = \ddot{x}_{t_0} (t - t_0)$$

If we set the time increment, $(t - t_0)$, at a value small enough to eliminate the effects of the slope and curvature of \ddot{x} , the approximation approaches the equality. If $dt (= t - t_0)$ is a small finite time,

$$\dot{x}_t + dt = \dot{x}_t + (\ddot{x}_t) dt$$

and

$$x_t + dt = x_t + (\dot{x}_t) dt + 1/2(\ddot{x}_t) dt^2$$

In the case of translational degrees of freedom, the time is incremented when the new velocities and positions are found. These are used in physical equations to determine a new set of forces, and therefore linear accelerations. The process is repeated for the total time of the dynamic input.

In the case of the rotational degrees of freedom, however, the approximation is mathematically invalid. The equations for pitch, roll, and yaw velocities are:

$$\dot{\theta}_p = w_y \cos \theta_R - w_z \sin \theta_R$$

$$\dot{\theta}_y = (w_y \sin \theta_R + w_z \cos \theta_R) \sec \theta_p$$

$$\dot{\theta}_R = w_x + (w_y \sin \theta_R + w_z \cos \theta_R) \tan \theta_p$$

$\dot{\theta}_y$ and $\dot{\theta}_R$ approach infinity as θ_p approaches 90° . Their slopes and curvatures approach infinity even faster. The approximation,

$$\int_{t_0}^t \theta dt = \theta_{t_0} (t - t_0)$$

is no longer valid since θ is changing radically with time. In any case, the computer is limited to size of numbers and the process breaks down. This problem is avoided by using transform matrices to define angular position.

C. TRANSFORMS

In order to solve the general case in rigid body dynamics, a number of different coordinate systems are used. There is a system fixed on the body and a system parallel to a reference system. It will be necessary to find components of a vector in one system from the components in the other system, or "transform" the vector. For instance, if the moments of a body are found in an absolute system, the moments in the body axis must be found in order to solve for the angular acceleration.

If we have a vector \bar{u} in a coordinate system as shown in Figure D-1 its components are $u \cos \alpha$, $u \cos \beta$, and $u \cos \gamma$, where α , β , and γ are the angles that define u in the x, y, z coordinate system.

If three vectors are used, each one has three direction cosines to the coordinate system. Where \bar{i} , \bar{j} , and \bar{k} are the unit vectors on the x, y, and z axes,

$$\bar{u} = u \cos \alpha_u \bar{i} + u \cos \beta_u \bar{j} + u \cos \gamma_u \bar{k}$$

$$\bar{v} = v \cos \alpha_v \bar{i} + v \cos \beta_v \bar{j} + v \cos \gamma_v \bar{k}$$

$$\bar{w} = w \cos \alpha_w \bar{i} + w \cos \beta_w \bar{j} + w \cos \gamma_w \bar{k}$$

are the equations for the three vectors shown in Figure D-2.

Rearranging the equations into vector and matrix form, they become

$$\bar{V} = \begin{Bmatrix} u_x + v_x + w_x \\ u_y + v_y + w_y \\ u_z + v_z + w_z \end{Bmatrix} = \begin{bmatrix} \cos \alpha_u & \cos \alpha_v & \cos \alpha_w \\ \cos \beta_u & \cos \beta_v & \cos \beta_w \\ \cos \gamma_u & \cos \gamma_v & \cos \gamma_w \end{bmatrix} \begin{Bmatrix} u \\ v \\ w \end{Bmatrix}$$

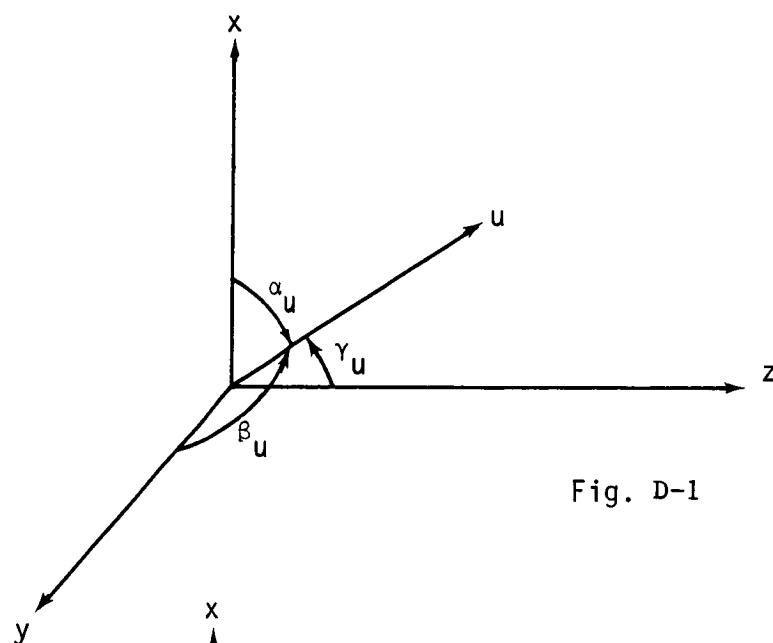


Fig. D-1

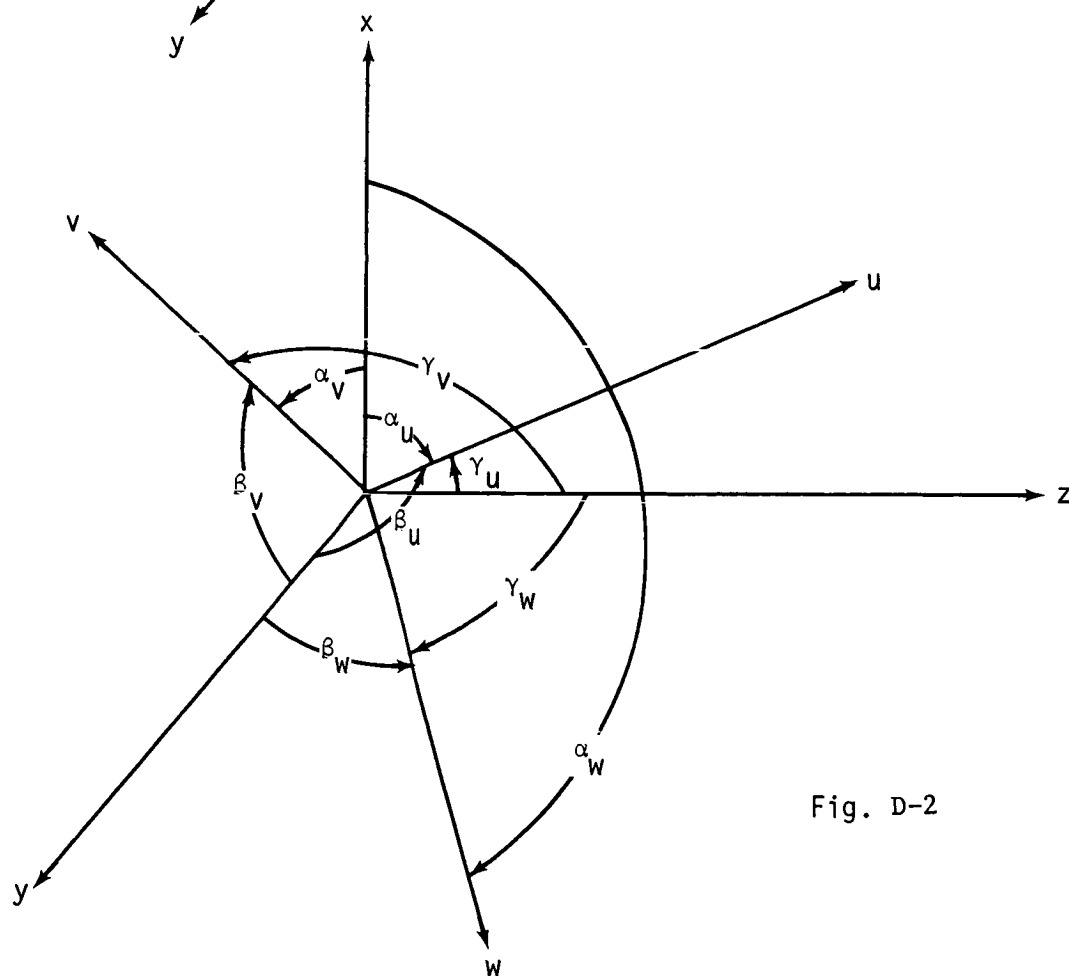


Fig. D-2

Vector \bar{V} is equal to $\bar{u} + \bar{v} + \bar{w}$ and has three components v_x , v_y , and v_z . If u , v , and w are vectors along a second coordinate system, the components of \bar{V} in this system are u , v , and w . The matrix in the equation transforms \bar{V} from the second system to the x , y , z system.

The matrix used to transform the u , v , and w components into x , y , and z components is called the "transform matrix" A and is used in the general equation

$$V_{\text{body}} = [A] \cdot V_{\text{reference}}$$

where V_{body} is the same vector as $V_{\text{reference}}$, but the components are measured relative to a different coordinate system. Since the matrix A is orthonormal then:

$$V_{\text{reference}} = [A]^T \cdot V_{\text{body}}$$

Since these transforms are general, they can be used for all forms of vectors in the solution - displacement vectors, velocity vectors, angular velocity vectors, etc.

D. TRANSFORM MATRIX MOTION

The changes in the transform matrix A due to rotation of the body are best expressed as rotations of unit vectors placed on the body axes. Unit vectors placed on the principal body axes are expressed in fixed coordinates as:

$$\bar{x} = A_{11}\bar{i} + A_{12}\bar{j} + A_{13}\bar{k}$$

$$\bar{y} = A_{21}\bar{i} + A_{22}\bar{j} + A_{23}\bar{k}$$

$$\bar{z} = A_{31}\bar{i} + A_{32}\bar{j} + A_{33}\bar{k}$$

The motion, or time derivative, of the vector \bar{x} for instance is:

$$\begin{aligned}\frac{d\bar{x}}{dt} &= \bar{\omega} \times \bar{x} \\ &= (w_y A_{13} - w_z A_{12})\bar{i} \\ &\quad + (w_z A_{11} - w_x A_{13})\bar{j} \\ &\quad + (w_x A_{12} - w_y A_{11})\bar{k}\end{aligned}$$

w_x , w_y , and w_z are the angular velocities in fixed coordinates.

Using time iteration:

$$\bar{x}_{t+dt} = \bar{x}_t + \frac{d\bar{x}}{dt} dt$$

The components of \bar{x}_{t+dt} are the new elements A_{11} , A_{12} , and A_{13} . For instance:

$$A_{11t+dt} = A_{11t} + (w_y A_{13} - w_z A_{12})dt$$

The process is repeated for the \bar{y} and \bar{z} unit vectors to complete the new matrix. To eliminate errors, the vectors are normalized to unit length and made orthogonal by taking their mutual cross products. The final solution is the new "transform matrix".

$$\begin{bmatrix} A \end{bmatrix}_{t+dt}$$

Appendix E

APPENDIX E

TERMINAL RENDEZVOUS DIGITAL COMPUTER PROGRAM

TERMINAL RENDEZVOUS DIGITAL COMPUTER PROGRAM

A digital computer program, RENDZ, was developed to simulate the terminal rendezvous phase.

This program is a three degree-of-freedom (three translation coordinates) simulation with perfect dynamical control of the vehicle's altitudes. The vehicle and satellite orbits are defined by their initial conditions and Mars' gravitational field. The program has the capability of using one type of rendezvous scheme (Type II Guidance) for the initial rendezvous maneuver, and another type for the terminal rendezvous maneuver (Type I Guidance).

The Type II guidance uses approximate guidance equations to execute an impulsive maneuver so the vehicle will intercept the satellite using approximate intercept equations. This type of rendezvous scheme requires target ephemeris data, and the angles between LOS vector and the spacecraft velocity vector. Up to two corrective thrust periods are used to bring the relative position of the spacecraft to within the range of the rendezvous radar after which Type I rendezvous is used for the final closure.

The terminal rendezvous maneuver is accomplished by causing the relative velocity and position between the satellite and the spacecraft to converge to zero between the two optimum switching curves. A new set of optimum switching curves are required for each spacecraft design. A different set of switching curves are used below the altitude R_M to optimize the vehicle rendezvous performance at both high and low altitudes.

Each set of switching curves consists of thrust-on and thrust-off parabola that are selected for a near optimum rendezvous. These control curves are mechanized in the control

computer and are implemented to control the thrust of the vehicle. The vehicle's altitudes are controlled to null out the LOS angle error in each channel as sensed by the rendezvous radar.

The flow block diagram of the digital computer mechanization of rendezvous program (RENDZ) is shown in Figure IV-12. The symbols used on this figure are defined below.

DRM	Range rate used in computer
DT	Time increment
IGFLG	Type of guidance flag
K	Phase flag
L	Range flag
M	Type of guidance flag
N	Engine thrust flag
NØN	Number of engine thrusts
Q1, Q2	Control gain
RB	Gain change altitude
RM	Range at start of Type I guidance
RR	Range
RRM	Range used in computer
TA	Thrust-to-mass
TG	Vehicle thrust
T/M	Vehicle average thrust-to-mass
TWX, TWY, TWZ	Vehicle thrust
VINT	Accumulated velocity
VRM	Relative velocity in computer
VM	Vehicle velocity
VTØT	Total vehicle velocity
W2	Vehicle total LOS rate
W2M	Total LOS rate stored in computer
W	Vehicle weight
WFR	Engines total weight flow rate

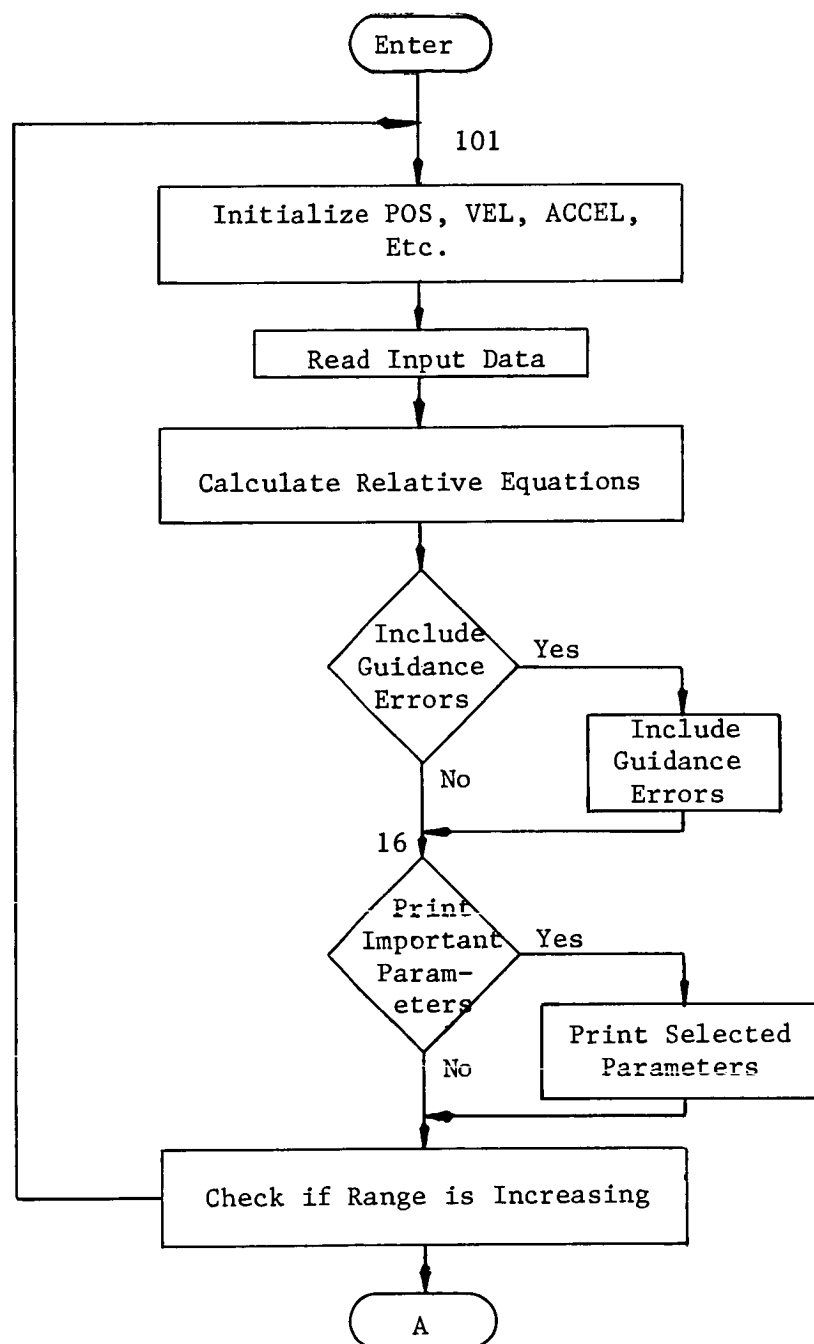


Figure 1 RENZ Digital Computer Flow Diagram

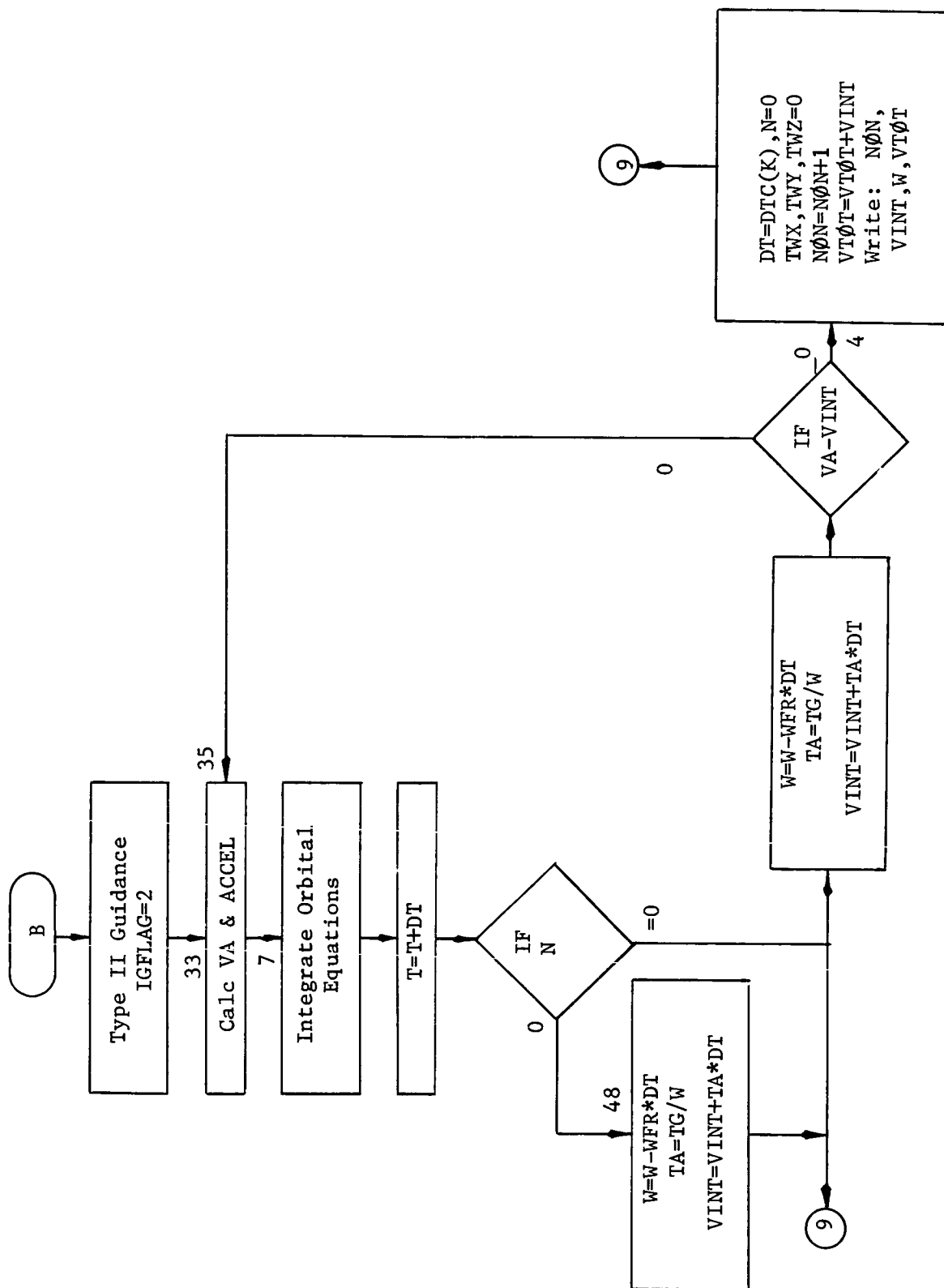


Figure 1 (concluded)